SAPIENZA
UNIVERSITÀ DI ROMA

Design and thermal-hydraulic transient analysis of primary cooling systems for tokamak fusion reactors

Facoltà di Ingegneria civile e Industriale
Dottorato di ricerca in Energia e Ambiente
Scuola di Dottorato in Scienze e Tecnologie per l'Innovazione industriale
XXXIV Ciclo

Candidate
Cristiano Ciurluini
ID: 1553838

Thesis Advisor
Fabio Giannetti

Co-Supervisors
Gianfranco Caruso
Alessandro Del Nevo

February 2022

(page left intentionally blank)

To Elisa,

my heart.

To my family, Fabio, Maria, Umberto e Anita,

the stars in my sky.

To Nuela, Florida, Checco e Licio,

since strong roots give marvellous leaves.

To ‘Gruppo Zozzo’,

more than friends, a way of life.

Thanks to all of you

Acknowledgements

Normally, in a scientific document, acknowledgments section is expected to be brief and formal. Although, these three years have been such an amazing journey for me that I don't succeed in being brief and on point. In addition, I can't think of a better way to start the description of my work but thanking all the people that helped and supported me in this long period.

First of all, my supervisor Prof. Fabio Giannetti. He transmitted me the interest, if not the passion, for this fascinating field that is the thermal-hydraulics. And even more, he supported me at every hour of the day and every day of the week. Since the very beginning of my master's degree thesis, far back in 2017, we have always shared the same office, working side by side. For me, this has been and is still today a great honor and pleasure.

I wish to thank also Prof. Gianfranco Caruso. His scientific and human guide has inspired me throughout these years and it has been fundamental to realize this work.

My research activity has been closely related with the one carried out at the ENEA research centre of Brasimone. There, I only found very valuable and helpful people. Among them, special thanks go to Ing. Alessandro Del Nevo and Ing. Amelia Tincani. Their advice and support have been very precious to me during these years.

A great thank is also due to my reviewers, Prof. Antonio Cammi and Prof. Songlin Liu. Their suggestions have enhanced the quality of this manuscript. Probably this mention is not enough to reward their efforts, but it is definitely very well deserved.

During these three years, the 'headquarter' of my research activity was in an office located at the second floor of Baleani palace in Rome. There, I met and collaborated with a bunch of brilliant and very talented young scientists. I'm very proud to define them my colleagues and, even more, my friends. Everyday life in an office could seem very boring looking from the outside. But if you have the chance to meet the right people, and with 'right' I mean 'gifted with enough degree of funny craziness', it can turn out as the most exciting adventure of your life. For all the fun and the friendship, the experience and the support, I'm very glad to thank Matteo, Vincenzo, Alessandro, Simone, Lorenzo e Luca.

Let me dedicate this work to my friends and my family. Paraphrasing a famous sentence by Winston Churchill, 'Never was so much owed by a single to so many'. That' s nothing more to say.

Finally, thank you Elisa. For everything.

This work has been carried out within the framework of the EUROfusion Consortium and has received funding from the Euratom research and training programme 2014-2018 and 2019-2020 under grant agreement No 633053. The views and opinions expressed herein do not necessarily reflect those of the European Commission.

Abstract

The PhD activity discussed in this document was conducted between 2018 and 2021. It profited from a collaboration between the Department of Astronautical, Electrical and Energy Engineering (DIAEE) of Sapienza University of Rome and the Experimental Engineering Division of ENEA at Brasimone. Within the framework of EUROfusion Consortium research activity, the R&D efforts focused on the investigation of one principal blanket option for the European DEMOnstration Power Plant (EU-DEMO): the Water-Cooled Lead-Lithium (WCLL). For this concept, ENEA and its Italian related partners are the principal investigators. During last years, DIAEE played an important role in the conceptualization of the WCLL Breeding Blanket (BB) and its related primary cooling systems. In addition, an extended transient analysis was carried out to assess their thermal-hydraulic performances in both normal operations and accidental conditions. Such work was carried out involving research activities related to both International Thermonuclear Experimental Reactor (ITER) and EU-DEMO fusion power plant.

This document is articulated in seven sections. The first one defines the PhD activity framework. In order to perform system-level transient analysis of tokamak reactors, a modified version of the thermal-hydraulic code RELAP5/Mod3.3 was developed at DIAEE in collaboration with ENEA. The aim is enhancing the code modelling capabilities with respect to fusion power plants. Section 2 is dedicated to discuss the implemented features. Sections 3 and 4 refer to the research activity involving DEMO WCLL. In **§** 3 the pre-conceptual design of the blanket component and related primary cooling circuits is described in detail. Their thermal-hydraulic model, developed for calculation purposes, is treated in **§** 4. The same section also reports the outcomes of the transient analysis. In the same way, **§** 5 and 6 are related to ITER WCLL-Test Blanket System (TBS) research activity. The TBS conceptual design, in particular the one of Water Cooling System (WCS) circuit whose DIAEE is responsible for, is described in **§** 5. To perform the system thermal-hydraulic assessment a dedicated model was developed. Its detailed description is provided in **§** 6, together with a full comment of the calculation results. Finally, **§** 7 focuses on the main conclusions and future perspectives of the work done.

The first issue to be addressed was the development of a suitable code to perform the computational activity. System thermal-hydraulic codes are the reference numerical tools adopted for the nuclear reactor transient analysis. Most of them, such as RELAP5, were developed and validated to perform best-estimate transient simulations of Light Water Reactors (LWR). Once validated against experimental data coming from more than one-hundred facilities, they have been used throughout decades to perform the licensing of LWRs. Simulation results allowed to characterize the reactor transient behavior in the full range of operative and accidental conditions. The same approach to reactor transient analysis was envisaged also for fusion power plants. Although, existing system codes lack of some specific features required to properly simulate the fusion reactor performances. For this, during the last years, a modified version of the system code RELAP5/Mod3.3 was developed at DIAEE, including some new upgrades needed to address the modelling issues arising from the simulation of tokamak fusion reactors. New implementations consist in: **i)** lead-lithium (PbLi) and HITEC© working fluids, with their thermophysical properties; **ii)** new heat transfer correlations for liquid metals and molten salts; **iii)** helicoidally tubes dedicated heat transfer correlations and two-phase flow maps. The effectiveness of the new features introduced was verified throughout the three years of research activity by performing transient simulations involving tokamak reactors.

Referring to the helicoidally geometry, the new two-phase flow maps were also tested against experimental data coming from OSU-MASLWR (Oregon State University - Multi Application Small Light Water Reactor) facility. In particular, a power manoeuvring test (named ICSP Test SP3) was

selected for benchmarking purposes. Several power steps of the Fuel Pin Simulator, standing for the reactor core, was reproduced, from 80 to 320 kW. The aim of the experiment was to investigate the primary system natural circulation and secondary system superheating for a variety of core power levels and feedwater flow rates. The effects of the code modifications on the simulation outcomes were clearly visible at higher power levels when the heat transfer within the HCSG plays a more important role. Indeed, above a certain power threshold, nearly 200 kW, the default version showed limited capabilities to reproduce the test. On the contrary, the trends related to the modified version fit quite well the experimental data.

Regarding the DEMO WCLL, in this document, it was presented the outcome of the pre-conceptual design developed during the just finished Horizon 2020 research programme. The design activity performed at DIAEE which the candidate took part to was mainly related to the BB Primary Heat Transfer System (PHTS) layout. The main system function is to remove the heat produced in the blanket components, delivering such thermal power to the Power Conversion System (PCS) to be converted into electricity. The BB PHTS is divided in two independent cooling systems, foreseen for the heat removal from the Breeder Zone (BZ) and the First Wall (FW). Both the BZ and the FW PHTSs consist of two cooling loops based on proven technologies extrapolated from Pressurized Water Reactors (PWR). Each primary system comprises the in-vacuum vessel cooling circuit, the ex-vacuum vessel equipment (pumps, heat exchangers/steam generators and a pressurizer), and the correspondent connecting lines. The BB PHTS is conceived in order to avoid a loop segregation. The BZ/FW PHTS cold legs feed the cold ring, which accomplishes the distribution of the cold water to each in- vacuum vessel cooling circuit (one per each sector). Primary coolant removes power from the blanket components and is collected in the hot ring that delivers water to the hot legs. In case of pump trip in a single PHTS loop, the other cooling loop guarantees the power removal from the whole system after the plasma shutdown. With the aim of the design improvement, system-level transient analyses were run involving the WCLL blanket component and related PHTS. The DIAEE version of RELAP5/Mod3.3 was used for this purpose. Such activity was related to EUROfusion Consortium Work Packages Breeding Blanket (WPBB) and Balance of Plant (WPBoP).

Firstly, a full DEMO WCLL thermal-hydraulic model was prepared, considering the BoP Indirect Coupling Design option. Blanket was simulated using equivalent components characterized by lumped parameters. The BZ and FW PHTS circuits were modelled including all the components within and outside the vacuum vessel. PCS nodalization starts from the main feedwater line and arrives up to the Turbine Stop Valves. Thus, only the BZ Once Through Steam Generators (OTSG) secondary side was simulated. Regarding the Intermediate Heat Transfer System (IHTS), the same approach was adopted. Only the cold and hot legs upwards/downwards the FW Heat EXchangers (HEX) shell side were added to the input deck. PCS feedwater and IHTS molten salt conditions at the BZ OTSGs and FW HEXs secondary side inlet were provided by means of boundary conditions.

The model developed was tested against the design data by simulating the full plasma power state. Beginning of Life conditions were considered. Proportional-Integral (PI) controllers were implemented to: **i)** regulate the primary pump rotational velocity and set the required value of the system flow; **ii)** control the PCS feedwater and IHTS molten salt mass flows in order to obtain the required PHTS water temperature at blanket inlet (i.e. OTSG outlet, 295 °C). Simulation results were in good agreement with the nominal values, demonstrating the appropriateness of the nodalization scheme prepared and of the control system implemented. Blanket and PHTS thermal-hydraulic performances in this flat-top power state were fully characterized, including the calculation of the system pressure drops and heat losses.

Then, this steady-state calculation was used as initial condition to perform the DEMO WCLL transient analysis, including some operational and accidental transients. The DEMO reactor

normal operations were simulated, including both pulse and dwell phases. Reference plasma ramp-down and ramp-up curves were adopted for simulations purposes. Primary pumps were kept running at nominal velocity for the whole transient, as for DEMO requirement. In addition, during dwell, PHTS circuits must be operated at the system average temperature (nearly 310 °C). Since no control strategies related to BZ OTSGs and FW HEXs were available, a preliminary management strategy for the PCS feedwater and IHTS molten salt mass flows were proposed and investigated. The BB PHTS parameters calculated by the code were analyzed to assess the circuit performances. The imposed trends proved to be effective in keeping the PHTS average temperature during dwell at the required value.

After, it was performed a benchmark exercise involving DEMO reactor power fluctuations. System code results were compared with the more detailed ones obtained with ANSYS CFX. The aim was to evaluate the effectiveness of the thermal-hydraulic model developed for the blanket component, prepared using equivalent components characterized by lumped parameters. BZ and FW PHTS water temperatures at blanket outlet were selected as figures of merit. Their trends showed a good agreement between the simulation outcomes obtained with the system code and the Finite Element Method (FEM). Results obtained from this benchmark exercise also indicated an effective way to perform simulations involving components, such as the breeding blanket, characterized by complex geometries and heat transfer phenomena. System code and 3D calculations can be externally coupled in an iterative process where CFX provides more accurate parameters to refine the RELAP5 model and the latter is used to update the inlet conditions for finite volume model computation.

Finally, the blanket primary cooling system response during accidental conditions was investigated. The selected transients to be studied belong to the category of “Decrease in reactor coolant system flow rate”. This transient analysis was aimed at understanding the thermal-hydraulic response of the blanket component and related primary circuits. In this way, it was possible to evaluate the appropriateness of their pre-conceptual design and the eventual need of mitigation actions to withstand such accidental scenarios. Different faults that could result in a decrease of the BB PHTS primary flow were postulated and investigated. In particular: **i)** partial and complete loss of forced primary coolant flow; **ii)** primary pump shaft seizure (or locked rotor); **iii)** inadvertent operation of a loop isolation valve.

Firstly, the most limiting of the above primary flow decrease event was chosen. It consisted in the complete loss of forced circulation in both FW and BZ PHTS. In this ‘worst case’ scenario, even if very unlikely, a sensitivity was performed on the flywheel to be added to the PHTS main coolant pumps in order to keep the system temperatures within acceptable ranges. The proper moment of inertia values to be applied to BZ and FW primary pumps were selected according to the simulation outcomes. Later, they were also used in all the following transient calculations.

The initiating events mentioned above were all simulated when interesting either BZ or FW system components (i.e. pumps and loop isolation valves). Calculations were replicated also considering the influence of loss of off-site power, assumed to occur in combination with the PIE. An actuation logic, involving some components of the DEMO reactor, was proposed and preliminary investigated. It was inspired by the one used for Generation III + nuclear power plants.

Results highlighted how the type of circulation (natural or forced) characterizing each cooling system is the main element influencing the correspondent thermal-hydraulic performances. If forced circulation is available, the following behavior can be observed in BZ and FW systems.

- Few seconds after the start of transient, the temperature spikes at blanket outlet characterizing the trend of both BZ and FW PHTS water are significantly smoothed.
- In FW system, the availability of forced circulation in both primary and secondary (only for the first 10 s) circuits limits the pressure increase and avoids the intervention of the pressurizer Pilot-Operated Relief Valve (PORV) in the short term.
- The OTSGs cooling capability lasts less. The presence of forced circulation in the primary cooling system enhances the steam generator heat transfer coefficient, increasing the thermal power transferred to the PCS. This reduces the time between two subsequent steam line Safety Relief Valves (SRV) openings and speeds up the evacuation of the water mass present in the OTSGs secondary side. Once terminated, the steam generators are no more able to provide any cooling function to the BZ PHTS.
- For more or less two hours from PIE occurrence, the system pressure is controlled by the pressurizer sprays. The first PORV intervention in the long term is significantly delayed.
- The temperature slope characterizing both BZ and FW systems (thermally coupled) is higher since pumping power is added to the power balance. This is valid until the pump trip is triggered in each system.

Summarizing, forced circulation improves the BZ and FW performances in the short term, smoothing the temperature spikes, but reduces the ones in the mid-long term. In fact, it shortens the cooling interval provided to the BZ PHTS by the steam generators and increases the temperature slope experienced by BZ and FW systems, reducing the reactor grace time. The best management strategy for PHTS pumps is to use, at the start of transient, the forced circulation they provide, in order to avoid excessive temperatures in the blanket, and then stop them, to increase the reactor grace time.

In all the transient simulations, BZ and FW systems experienced a positive temperature drift in the mid-long term. It is due to the unbalance between decay heat produced in the blanket and system heat losses, with the former overwhelming the latter. The temperature slope is higher if the forced circulation is still active. In these cases, it must be added another source term to the power balance, represented by the pumping power. In the calculations performed, no Decay Heat Removal (DHR) system was implemented in the input deck and the power surplus is managed by the pressurizer PORV. Power in excess produces a pressure increase and when this parameter reaches the PORV opening setpoint, PHTS water mass is discharged with its associated enthalpy content. This is the way adopted by BZ and FW system to dissipate the power surplus. In the future developments of this research activity, the impact of the DHR system will be also evaluated.

In conclusion, simulation outcomes highlighted the appropriateness of the current PHTS design and of the management strategy chosen for the selected accidental scenarios.

During the third ITER council (2008), it was established the so-called ITER Test Blanket Module (TBM) program. Its objective is to provide the first experimental data on the performance of the breeding blankets in the integrated fusion nuclear environment. More recently, in 2018, the WCLL option was inserted among the selected blanket concepts to be investigated. From this time, an intense research activity was conducted within the EUROfusion Work Package Plant level system engineering, design integration and physics integration (WPPMI) in order to perform the pre-conceptual and conceptual design phases of ITER WCLL Test Blanket System. The overall work (i.e. TBS) was divided in ‘Part A’, related to TBM set and ‘Part B’, referring to its related ancillary systems. For the latter, R&D effort was led by ENEA and involved many European research institutions and universities, including DIAEE of Sapienza University of Rome. The work was

supervised also by Fusion for Energy, the EU organization managing Europe's contribution to ITER reactor. By the fall of 2020, both design phases were concluded, and the system successfully underwent its Conceptual Design Review. Among the TBM ancillary systems, the most relevant is the Water Cooling System, acting as primary cooling circuit of the TBM module. The design and thermal-hydraulic characterization of this circuit was up to DIAEE.

The TBS conceptual design was presented in this document. A special focus was given to the WCS layout whose DIAEE is responsible for (i.e. the candidate took part to). The Water Cooling System was designed to implement the following main functions: **i)** provide suitable operating parameters to the water flow cooling the TBM in any operational state; **ii)** transfer thermal power from WCLL-TBM to CCWS; **iii)** provide confinement for water and radioactive products; **iv)** ensure the implementation of the WCLL-TBS safety functions. In addition, ITER WCLL-TBM must be DEMO relevant. Such relevancy refers to the water thermodynamic conditions at the TBM (15.5 MPa, 295-328 °C) since the experimental program will deal with the test of this blanket reference concept. The reduced thermal power produced in the TBM set (near 700 kW) with respect to DEMO blanket (1923 MW), allows to use a single water-cooling system for both the FW and the BZ. The correspondent WCS primary flow was computed considering the TBM power balance. The ultimate heat sink for the WCLL-TBM WCS is the ITER Component Cooling Water System (CCWS). With the aim to include an additional barrier between the contaminated primary water and the CCWS coolant, the WCLL-WCS was split in a primary and a secondary loop. In such a way, the CCWS radioactive inventory is kept below the limit in any operative and accidental scenario (note that CCWS is a non-nuclear system). To simplify the WCLL-WCS management, liquid only condition was selected for the secondary coolant instead of the two-phase fluid, as in DEMO PCS. It is worth to emphasize that electricity generation is not a purpose of ITER and, thus, steam production is not required. CCWS provides water coolant at low pressure and temperature (0.8 MPa at 31 °C), and requires that return temperature must be limited to 41 °C. Hence, there is a considerable difference between the average TBM temperature and the average CCWS temperature. To avoid an excessive temperature excursion (i.e. thermal stresses) between the two sides of a single heat exchanger, an economizer was installed in the middle of the WCS primary loop, leading to the typical "eight" shape of this circuit. Therefore, a total of three heat exchangers were considered for the whole WCS, namely: HX-0001 (economizer), HX-0002 (intermediate heat exchanger between primary and secondary loops) and HX-0003 (heat sink delivering power to CCWS). Each heat exchanger was provided with a bypass line allowing the regulation of the exchanged power by tuning the shell side mass flow. Finally, an electrical heater was added to the WCS primary loop in order to compensate the power unbalance in the system. Most of the WCS equipment is installed in the TCWS Vault, at level four of the tokamak building. The rest of the components, including the TBM, is placed in the level one Port Cell #16. Both locations are linked by means of connection pipes hosted in a vertical shaft.

To support the WCS design a preliminary transient analysis was performed. For this purpose, a full thermal-hydraulic model of the system was developed by using the DIAEE version of RELAP5/Mod3.3. Since this circuit is directly connected to PbLi loop within the TBM, also these two systems were included in the overall TBS model. A preliminary control system was implemented for both WCS and PbLi loop. All the main circuit parameters (pressure, temperatures, and mass flows) are controlled in order to ensure system stability in any operative scenario and to provide water coolant and breeder at TBM with the required inlet conditions.

Firstly, full plasma power state was simulated at both Beginning of Life (BOL) and End of Life (EOL) conditions. Such calculations were needed to test and evaluate the appropriateness of the model prepared. Simulation outcomes demonstrated that control systems corresponding to WCS and PbLi loop are able to ensure the required values at TBM inlet in both the operative scenarios. For

WCS, the main differences between BOL and EOL conditions were highlighted, mainly regarding the operation of the temperature control system (i.e., the mass flow through the heat exchangers bypass). WCS and PbLi loop performances in this flat-top states were fully characterized, including the calculation of pressure and temperature fields, as well as the system power balance. In addition, an insight into the TBM behavior during full plasma power condition was given. Its operation does not change from BOL to EOL since it is provided with water coolant and liquid metal at constant thermodynamic conditions and flow rate. It is important to note that a full thermal-hydraulic characterization of the component was out of the scope of the research activity carried out by DIAEE. Nevertheless, TBM box contains part of the WCS circuit and constitutes the system source term. Furthermore, thermal coupling between WCS and PbLi loop occurs inside the module. For this, it was mandatory to properly simulate the heat transfer phenomena taking place within the component. The results obtained with the system code were compared with the more detailed ones available in literature (produced by using FEM methodologies). The latter were used to calibrate the component thermal-hydraulic model.

Then, the two steady-state calculations were used as initial condition to simulate operative scenarios and abnormal conditions. The Normal Operation State (NOS) was the first to be analyzed. The WCS and PbLi loop control systems were tested to demonstrate their effectiveness in ensuring stable operations against the pulsed regime characterizing the NOS. Both BOL and EOL conditions were considered in order to assess the change in WCS thermal-hydraulic performances with the system aging. The reference ITER pulsed plasma regime was adopted for simulation purposes. The system code results demonstrated the appropriateness of the WCS and PbLi loop control systems. They are able to ensure water coolant and PbLi at the TBM with nearly constant inlet thermodynamic conditions and flow rate. For water inlet temperature, oscillations were limited to +/- 3 °C, acceptable for WCS and TBM operation. Moreover, it was verified that in any part of the PbLi loop an adequate margin (16 °C) from the freezing point is maintained.

Finally, in order to assess and verify the WCS design, two abnormal scenarios were selected and investigated. The aim was to evaluate the system capabilities under degraded conditions and to verify if the standard control strategies without any external action are capable to maintain the TBM cooling function for an entire plasma pulse. This last condition allows to avoid the triggering of the Fast Plasma Shutdown System, demonstrating that a minor accident in the WCS does not interfere with the ITER global operation. The transients considered were: **i)** LOFA occurring in WCS secondary loop; **ii)** LOHS, i.e. loss of flow in the CCWS. The worst operative condition was supposed to be the EOL, since plugging and fouling limit the heat exchange. For this, NOS at EOL was imposed as initial condition for the transient calculations. In both scenarios, simulation outcomes highlighted that WCS primary loop is kept in safety conditions over the whole accidental evolution. In addition, the safety margin from the PbLi freezing is ensured by keeping the reference water temperature at the TBM inlet. The current WCS design and the control systems implemented proved to be effective to withstand the selected accidental scenarios.

Table of Contents

List of Figures

List of Tables

List of Abbreviations

AC	*Alternating Current*
ASME	*American Society of Mechanical Engineers*
ASTM	*American Society for Testing and Materials*
BB	*Breeder Blanket*
BC	*Boundary Condition*
BFP	*Baffle Plate*
BOL	*Beginning Of Life*
BoP	*Balance of Plant*
BP	*Back Plate*
BRC	*Breeding Cell*
BSS	*Back Supporting Structure*
BU	*Breeding Unit*
BZ	*Breeder Zone*
CAD	*Computer Aided Design*
CCWS	*Component Cooling Water System*
CEA	*Commissariat à l'énergie atomique et aux énergies alternatives*
CFD	*Computational Fluid Dynamics*
CHF	*Critical Heat Flux*
CL	*Cold Leg*
CP	*Connection Pipe*
CPS	*Coolant Purification System*
CR	*Cold Ring*
CT	*Cold Tank*
CTR	*Cold TRap*
CV	*Control Volume*
CVCS	*Chemical Volume Control System*
DCD	*Direct Coupling Option*
DEMO	*DEMOnstration Power Plant*
DHR	*Decay Heat Removal System*
DIAEE	*Dipartimento di Ingegneria Astronautica, Elettrica ed Energetica*
DIV	*Divertor*
DN	*Nominal Diameter*
DNBR	*Departure from Nucleate Boiling Ratio*
dpa	*displacement per atom*
DWT	*Double Walled Tube*
EFDA	*European Fusion Development Agreement*
ENEA	*Agenzia nazionale per le nuove tecnologie, l'energia e lo sviluppo economico sostenibile*
EOL	*End Of Life*
EPR	*European Pressurized Reactor*
ESS	*Energy Storage System*

EU	*European Union*
FBR	*Film Boiling Region*
FEM	*Finite Element Method*
FOM	*Figure Of Merit*
FP	*Feeding Pipe*
FPS	*Fuel Pin Simulator*
FPSS	*Fast Plasma Shutdown System*
FW	*First Wall*
HC	*Helium Cooled*
HCCR	*Helium Cooled Ceramic Reflector*
HCPB	*Helium Cooled Pebble Bed*
HCSG	*Helicoidally Coil Steam Generator*
HEX	*Heat EXchanger*
HF	*Heat Flux*
HL	*Hot Leg*
HR	*Hot Ring*
HRD	*Heating RoDs*
HS	*Heat Structure*
HT	*Hot Tank*
HTC	*Heat Transfer Coefficient*
HX	*Heat Exchanger*
IB	*Inboard Blanket*
ICD	*Indirect Coupling Option*
ID	*Inner Diameter*
IHTS	*Intermediate Heat Transfer System*
INL	*Idaho National Laboratory*
ITER	*International Thermonuclear Experimental Reactor*
JUN	*Junction*
LB	*Left Boundary*
LOCA	*Loss Of Coolant Accident*
LOFA	*Loss Of Flow Accident*
LOHS	*Loss Of Heat Sink*
LOSP	*Loss of Off-Site Power*
LR/SS	*Locked Rotor/Shaft Seizure*
LWR	*Light Water Reactor*
MASLWR	*Multi Application Small Light Water Reactor*
MCP	*Main Coolant Pump*
MHD	*Magnetohydrodynamic*
MoI	*Moment of Inertia*
MS	*Molten Salt*
NAS	*Neutron Activation System*
NBR	*Nucleate Boiling region*
NOS	*Normal Operation State*
NPP	*Nuclear Power Plant*

NWL	*Neutron Wall Load*
OB	*Outboard Blanket*
OD	*Outer Diameter*
OSU	*Oregon State University*
OTSG	*Once-Through Steam Generator*
PbLi	*Lead-Lithium*
PC	*Port Cell*
PCS	*Power Conversion System*
PF	*Pipe Forest*
PHTS	*Primary Heat Transfer System*
PI	*Proportional/Integral*
PIE	*Postulated Initiating Event*
PL	*Primary Loop*
PORV	*Pilot-Operated Relief Valve*
PRT	*Pressure Relief Tank*
PRZ	*Pressurizer*
PT	*Plasma Termination*
PWR	*Pressurized Water Reactor*
QST	*Quantum and radiological Science and Technology*
R&D	*Research And Development*
RAFM	*Reduced Activation Ferritic/Martensitic Steel*
RB	*Right Boundary*
RD	*Ramp Down*
RELAP	*Reactor Excursion Leak Analysis Program*
RP	*Radial-Poloidal*
RPV	*Reactor Pressure Vessel*
RT	*Radial-Toroidal*
RU	*Ramp Up*
§	*Section (of the current document)*
SC	*Side Caps*
SHR	*SuperHeated Region*
SL	*Secondary Loop*
SMS	*Single Module Segment*
SRV	*Safety Relief Valve*
STH	*System Thermal-Hydraulic*
SW	*Side Wall*
TAS	*Tritium Accountancy System*
TBM	*Test Balnket Module*
TBR	*Tritium Breeding Ratio*
TBS	*Test Blanket System*
TCR	*Tokamak Cooling Room*
TES	*Tritium Extraction System*
TEU	*Tritium Extraction Unit*
TH	*Thermal-Hydraulics*

TSV	*Turbine Stop Valve*
TT	*Turbine Trip*
UNS	*Unified Numbering System*
VS	*Vertical Shaft*
VV	*Vacuum Vessel*
W	*Tungsten*
WC	*Water Cooled*
WCCB	*Water Cooled Ceramic Breeder*
WCLL	*Water Cooled Lead Lithium*
WCS	*Water Cooling System*
WPBB	*Work Package Breeding Blanket*
WPBoP	*Work Package Balance Of Plant*
WPPMI	*Work Package Plant level system engineering, design integration and physics integration*
WPSAE	*Work Package Safety and Environment*

1 INTRODUCTION

1.1 Why nuclear fusion?

In the last years, the sensibility towards climate change topic is growing all around the world. Recently, new movements, such as 'Fridays for Future' of Greta Thunberg, were born next to the old ones (Greenpeace, etc.), focusing people attention on the need of decarbonizing global economy in the upcoming decades. The formal commitment of world governments to develop policies leading to climate-neutrality before the end of the century is represented by the signature of the Paris agreement. This Agreement is the first-ever universal, legally binding global climate change agreement, adopted at the Paris climate conference (COP21) in December 2015, [1]. Its main goal is limiting global warming well below 2 °C, pursuing efforts to stop the temperature increase at 1.5 °C. This challenging purpose requires that policies headed to a significant reduction of the CO_2 emissions must be put in action immediately, starting from the current decade. The issue of progressively substituting the fossil fuels forces humanity to invest more and more in the research for alternative energy sources that can prove their long-term sustainability and security. Renewable energy sources, such as photovoltaic and wind, still provide some concerns about the required reliability. Nuclear fission cannot be seen as a long-term solution to the power generation problem due to the production of long lived radioactive waste. In this framework, nuclear fusion is becoming more and more considered as the most probable solution to the energy problem, ensuring sustainability and security of supply. Its most attractive features are:

- fuels are widely available and virtually unlimited, namely deuterium, naturally present in seawater, and tritium, that can be bred directly in the tokamak blanket from lithium, abundantly occurring in earth's crust and seawater;
- no production of greenhouse gases;
- intrinsically safe, as no chain-reaction is possible;
- environmentally responsible - with a proper choice of materials for the plasma chamber radioactivity decays in a few tens of years and at around 100 years after the reactor shutdown all the materials can be recycled in a new reactor.

1.2 Nuclear fusion

Nuclear fusion is basically the process that powers the stars. It is a nuclear reaction where two or more atomic nuclei combine to form a heavier one whose mass is less than the sum of the masses of the reactants. This mass reduction is due to the binding energy between reactant nuclei. It produces a significant energy release according to the famous Einstein equation $E = mc^2$. Between the known fusion reactions, the most promising and technologically investigated is the $D - T$ one, shown below:

$$ {}_1^2D + {}_1^3T \rightarrow {}_2^4He(3.5\ MeV) + n(14.1\ MeV) \tag{1.1} $$

The previous was chosen since it is the best compromise between energy efficiency, likelihood of interaction (large cross section) at lower temperature (i.e. engineering feasibility) and fuel availability (i.e. cost).

Nuclear reactions are ruled by the so-called Lawson Criterion, [2], (also known as "triple product"). It determines the conditions needed to reach ignition, defined as the state when the

heating generated by the nuclear reactions is able to maintain the temperature of the plasma against all losses. This synthetic law derives from the energy balance for a steady-state plasma. In the case of the $D-T$ reaction the Lawson Criterion states that:

$$nT\tau_E = 10^{21}\ keV \cdot s^{-1} \cdot m^{-3} \tag{1.2}$$

where n is the nuclear plasma density [m^{-3}], T the plasma temperature in keV and τ_E the confinement time [s^{-1}], measuring the rate at which the confined plasma loses energy to its environment. According to Lawson Criterion, given a plasma temperature, for example $T = 10\ keV \approx 11 * 10^6\ K$, that is the reference for engineering nuclear fusion facility, ignition conditions can be achieved either by dense plasmas (10^{30} m^{-3}) with low τ_E (10^{-10} s^{-1}), or by less dense plasmas with a higher τ_E, (respectively equals to 10^{20} m^{-3} and 1 s^{-1}). These two-philosophies gave birth to different nuclear fusion reactor technologies. The first and more world-wide spread is based on magnetic confinement. It attempts to use the electrical conductivity of the plasma to contain it through interaction with magnetic fields. In the last years, European Union (EU) has been focusing its R&D efforts on this fusion technology, [3][4]. Instead, inertial confinement has been more investigated in USA, developed principally in some facilities such as the National Ignition Facility (NIF) at the Lawrence Livermore National Laboratory (California, [5]). Inertial confinement relies on small solid fuel shells that are bombarded (one at a time) by high-power lasers. In this process, the capsule and its deuterium–tritium fuel is compressed to high density and temperature, reaching the ignition condition.

1.3 Overview of a fusion reactor based on tokamak technology

At the high temperatures needed for fusion reaction, matter is subject to another change of state becoming plasma. In a plasma, the electrostatic forces binding electrons and nuclei are overcome and they become two distinct populations of negatively charged electrons and positively charged ions. For this reason, plasma is able to conduct currents and interact with magnetic fields, allowing its own confinement by means of properly-designed magnetic coils. A tokamak (Russian acronym for *toroidalnaya kamera i magnitnaya katiushka*, "toroidal chamber and magnetic coil") is a fusion device using strong magnetic fields to confine the plasma within a chamber with an approximate toroidal shape. The first tokamaks were developed in the former Soviet Union in the 60s, [6]. The modern Tokamak design consists of the fundamental parts listed below:

- *The magnetic system*: in case of spatially uniform magnetic field, like the one produced within an ideal solenoid, the plasma ions and electrons move along helicoidally trajectories around the straight magnetic field lines. It is called *Larmor motion* and limits plasma particles in the transversal direction. To achieve axial confinement, the best approach is closing the solenoid, creating a torus. In such a way, ions and electrons are subjected to a toroidal magnetic field ($B\tau$) generated by external coils wrapping around the plasma. In a real tokamak, $B\tau$ is not perfectly uniform in the poloidal section and particle motion is the composition of their usual *Larmor motion* plus a transverse drift phenomenon due to the magnetic gradients ($\vec{B} \times \overrightarrow{\nabla B}$). Furthermore, there is charge separation due to interaction between electrical and magnetic fields ($\vec{E} \times \vec{B}$) which provokes particle losses. To overcome these problems, it is necessary to introduce a poloidal magnetic field (Bp) which allows to twist the magnetic field lines, creating the so-called *magnetic surfaces*. It is typical in a tokamak design that Bp is directly generated by the toroidal current ($I\tau$) flowing along the confined plasma itself. To induce $I\tau$ in a tokamak a system of transformers are used. The primary transformer winding consists in the central solenoid. The latter induces a current in the plasma acting as secondary

transformer winding. Due to the time dependence of Bp, tokamaks are pulsed regime machines. This solution creates some difficulties in the managing of the fusion reactor Balance of Plant (BoP) system, above all for the steam turbine. Typically, $B\tau$ is of several Tesla (up to 12-13), conversely, $Bp \approx 0.1\, B\tau$. To control plasma shape and position, tokamak design foresees extra coils for finely tuning Bp. They are realised as ring coils coaxial with the plasma. First tokamaks were characterized by a circular poloidal section. Although, theoretical studies and experimental tests highlighted that D-shaped plasmas are more stable, [6]. The external coils can be made out of either an ordinary metal material (e.g. copper) or with superconductive alloys (for example Nb_3Sn or NbTi). This second option is the more attractive and investigated.

- *The blanket*: see **§** 1.3.1.

- *The divertor*: it is the device performing the online removal of waste material from the plasma, [6][7]. This allows to keep under control the build-up of fusion products in the fuel, and to remove impurities from the plasma. The design option mostly investigated foresees its location in the bottom part of the plasma chamber. There, poloidal magnetic field lines lead plasma impurities to be collected and pumped away by vacuum pumps. The divertor main functions are: **i)** reduce the heat flux on the first wall by redirecting much of the charged particle beams to its external surfaces; **ii)** remove helium ashes from the plasma outer layers, avoiding the dilution of fuel ion density; **iii)** prevent impurity atoms sputtered by the first wall from entering the plasma.

- *The vacuum system*: the Vacuum Vessel (VV) is situated inside the magnet system and the cryostat and hosts the blanket and the plasma facing components. The vacuum vessel is classified as a Safety Important Component (SIC) since it provides the confinement and decay heat removal functions. It consists in a large torus-shaped, double-wall structure with shielding material and coolant between the inner and outer shells. The inner vessel surface is in contact with the blanket and represents a reliable first confinement barrier. The space between shells is filled with plates made of ferromagnetic material to provide neutron shielding and to reduce toroidal field ripple. The vacuum vessel is divided into several sectors in toroidal direction, joined by welding using splice plates. The vessel is supported by gravity supports from the floor. The VV has upper, equatorial, and lower port structures used for equipment installation, utility feedthroughs, vacuum pumping, and access inside the vessel for maintenance. An ultra-high vacuum is needed in fusion devices to keep the fuel mixture of deuterium and tritium very pure. Prior to operation, the air is first pumped out of the chamber until a pressure of 10^{-5} Pa or lower is obtained, [6][7]. This function is deputized to the vacuum system, composed by the vacuum pumps, the vacuum ducts (connecting the pumps with the plasma chamber) and the volumes used to stack or recycle the VV exhausted gas of any kind.

- *The cryogenic system*: most superconducting applications work at nearly 4 K, that is the liquid helium boiling point. Cryogenic system is realized with the purpose of maintaining that temperature during tokamak operations, typically by using liquid helium as cryogenic fluid. Liquid nitrogen, whose boiling point is at almost 77 K, may also be needed for high temperature superconductors (Nb_3Sn or NbTi), and staged cooling of helium system. The cooling of the large magnet system from room temperature to working conditions may even take many days. The most important issues linked with this very low temperature are the insulation of the cryogenic environment and the embrittlement of the metallic material in these operative conditions. The cryostat is a large, stainless steel structure surrounding the vacuum vessel and the superconducting magnets, providing a supercool,

vacuum environment. It is made up of a single wall cylindrical construction, reinforced by horizontal and vertical ribs. The cryostat has many openings, that give access to the vacuum vessel for cooling systems, magnet feeders, auxiliary heating, diagnostics, and the remote handling system which removes blanket and divertor parts at the end of their operating cycles. Large bellows are located between the cryostat and the vacuum vessel to compensate differential thermal contraction and expansion between the two structures. The cryostat is completely surrounded by a concrete layer known as the bioshield.

- *The plasma heating system*: in order to ignite the nuclear fusion reaction, plasma must be heated to very high temperatures. The first contribute to plasma heating is provided by the toroidal current, $I\tau$, that, once induced, flows along plasma producing the so-called Ohmic heating due to the Joule effect. At low temperatures, this mechanism is quite effective. Although, since plasma resistance decreases with the trend $T^{-1.5}$, it is useless at high temperatures. Hence, other heating systems are required to reach the temperature needed for ignition. Neutral beam injection systems and radio-frequency heating systems are typically used for this purpose. The former injects into the plasma neutral particles with high kinetic energy. Once reached the plasma they are ionized and then transfer their kinetic energy to the charged particles by collision. Radio-frequency heating involves electromagnetic waves produced by some antennas and then addressed to the plasma. By properly selecting the wave frequency it is possible to couple these waves with plasma typical frequencies, allowing their absorption.

A schematic view of a modern tokamak reactor with all its main components is shown in Figure 1.1, [8].

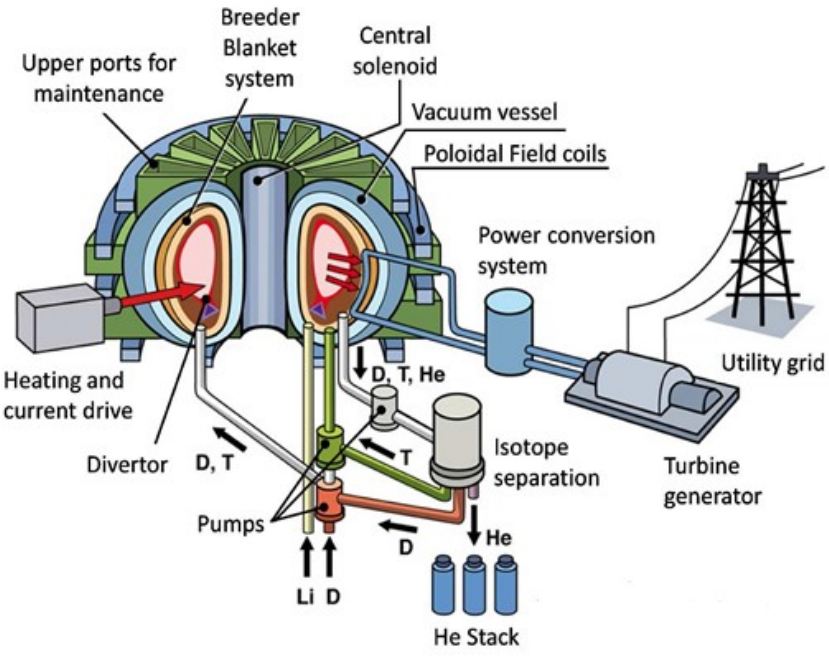

Figure 1.1 – Schematic view of a modern tokamak reactor with all its main components [8].

1.3.1 Blanket.

D-T is the reference nuclear reaction considered for tokamaks. Deuterium is naturally present in seawater, accounting for the 0.0153% of the total hydrogen. It is readily extractable, with a process similar to the one already used for Uranium, thus constituting essentially infinite fuel source, [7]. Conversely, since undergoing beta decay with a half-life of 12.5 yr, tritium is not enough present in nature. The most viable option to overcome this problem is producing the needed quantity of this isotope directly *in situ*. Achieving tritium self-sufficiency is a critical issue in the development of a fusion power plant operating with a DT fuel cycle, [7]. A feasible solution to generate tritium within the tokamak consists in exploiting the nuclear reactions involving the high energy neutrons out coming the plasma and the lithium contained in the blanket surrounding the plasma chamber.

$$ {}^{6}_{3}Li + n(14.1\ MeV) \rightarrow {}^{4}_{2}He + {}^{3}_{1}T + 4.78\ MeV \tag{1.3} $$

$$ {}^{7}_{3}Li + n \rightarrow {}^{4}_{2}He + {}^{3}_{1}T + n - 2.47\ MeV \tag{1.4} $$

Blanket is usually constituted of a compound of lithium and a neutron multiplier material, enhancing the breeding. An additional production of neutrons is needed because of the capture and absorption reactions in structural materials and the leakage through ports and divertor. All these losses lower the total neutron population of nearly 30%, [7]. Materials commonly used as neutron multiplier are Beryllium and Lead.

The total energy generated by D-T fusion reaction (equation 1.1) is divided in two fractions. The 80% is given to the neutron produced $(14\ MeV)$. It directly reaches the blanket without interacting with the charged particles constituting the plasma. The nuclear reactions here occurring (equations 1.3 and 1.4) represents a volumetric heat source for this component. They convert the neutron kinetic energy into heat that can be extracted by a suitable cooling system. For the blanket coolant, several options are currently under study.

The residual 20% of energy produced by D-T reaction, together with the one externally supplied to the plasma for heating purposes, ultimately leave the plasma chamber in the form of charged particles, atoms and radiative energy. They represent a surface heat load incident on the plasma facing components, namely the First Wall (FW) and the divertor. While the former is a wall distributed along the poloidal coordinate, covering the overall blanket, the latter is situated at the bottom of the plasma chamber with specific goals to be accomplished (see **§** 1.3). Their design strongly depends on the distribution of the entire heat load among them, i.e. on the magnitude of the heat flux insisting on their external surface. This distribution is still object of investigation.

Since the blanket is located between the plasma and the magnet system, it acts also as neutron shield to prevent their damage. This is of capital importance above all if the magnets are realized in superconductive alloys because when heated by radiative bombing, these materials lose their superconductive properties.

In conclusion, the breeding blanket is one of the key reactor components, accomplishing the functions of cooling device, tritium breeder and neutron shield. A schematic view of the blanket radial placement with respect to other tokamak components is shown in Figure 1.2.

The two main breeding blanket concepts selected to be investigated in the upcoming European R&D activities are: Water-Cooled Lead-Lithium (WCLL) and Helium-Cooled Pebble Bed (HCPB), [9]. WCLL option foresees the usage of water at typical Pressurized Water Reactor (PWR) thermodynamic conditions (295–328 °C and 15.5 MPa) as coolant. The blanket relies on liquid lead-lithium as breeder, neutron multiplier and tritium carrier. Instead, the current HCPB design is

based on the use of Li_4SiO_4 as tritium breeder, beryllium as neutron multiplier and helium (300°-500 °C and 8 MPa) as coolant. In both cases, Reduced-Activation Ferritic/Martensitic (RAFM) steel, also known as EUROFER-97, is selected as structural material and an armour, consisting of a thin tungsten layer, is assumed to cover the first wall.

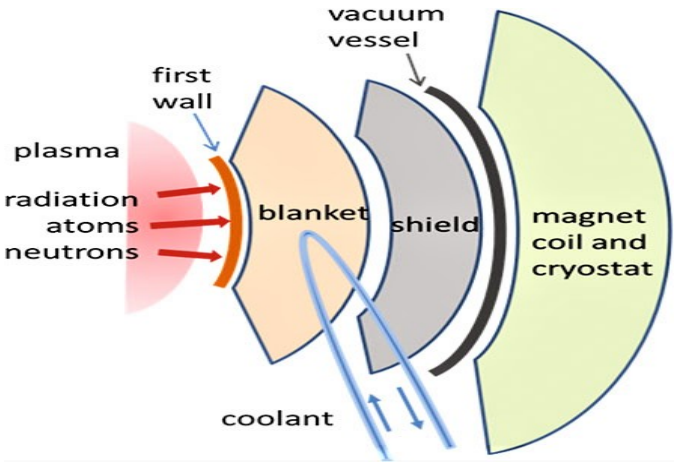

Figure 1.2 - Blanket radial position with respect to other tokamak components.

1.4 National and international framework of research activity in the field of nuclear fusion

In 2012 the European Fusion Development Agreement (EFDA) has published a roadmap which outlines the way to supply fusion electricity by 2050. In the near term, it foresees the construction of the International Thermonuclear Experimental Reactor (ITER) located in the southern France (Cadarache). ITER will be the first fusion device to generate net energy, to maintain fusion reaction for long periods, and to test the integrated technologies, materials, and physics regimes needed for the commercial production of fusion-based electricity, [10]. ITER reactor must be followed by the European DEMOnstration Power Plant (EU-DEMO) as the remaining crucial step towards the exploitation of fusion energy source. The reactor should demonstrate the capability of producing few hundred MWs of net electricity while operating with a closed-tritium fuel cycle, [11]. More in detail, the *Roadmap to the realization of fusion energy*, [3], is articulated in eight priority missions which have to be accomplished:

1) Demonstrate plasma regimes of operation (based on the tokamak configuration);
2) Demonstrate a heat exhaust system capable of withstanding the large load of DEMO;
3) Develop materials that withstand large 14 MeV neutron fluence without degrading their physical properties;
4) Ensure tritium self-sufficiency through technological solution for the breeding blanket; which will have to be made consistently with the choice of the components for the transformation of the high-grade heat into electricity (the so-called Balance of Plant).
5) Implement the intrinsic safety features of fusion into the design of DEMO following the experience gained with ITER;

6) Combining all the fusion technologies into an integrated DEMO design; e.g. exploiting a complete Balance of Plant including the heat transfer and associated electrical generation systems;
7) Ensure the economic potential of fusion by reducing the DEMO capital costs and developing long-term technologies;
8) Bring the stellarator line to maturity.

The roadmap is a living document, reviewed regularly in response to the physics, technology and budgetary developments. Although, in its latest version, [4], all the aforementioned goals have been confirmed. A schematic view of the *Roadmap to Fusion Energy* is shown in Figure 1.3.

EUROfusion Consortium, [11], has the task to coordinate all the research activities aimed at the realization of DEMO fusion reactor. It is funded by the EURATOM research and training programme, accordingly to the *Roadmap to Fusion Energy*. The Consortium was established in 2014, with an agreement signed by thirty members (research organizations and universities) from twenty-six European Union countries plus Switzerland. The signatory for Italy is ENEA, playing the role of national programme leading actor and coordinator. Among the ENEA related partners there are many major universities (e.g. Sapienza University of Rome, UNIPI, UNIPA, UNITO, etc.), university consortia (e.g. CREATE), research institutions (e.g. INFN, CNR, etc.) and industries (e.g. Ansaldo Nucleare).

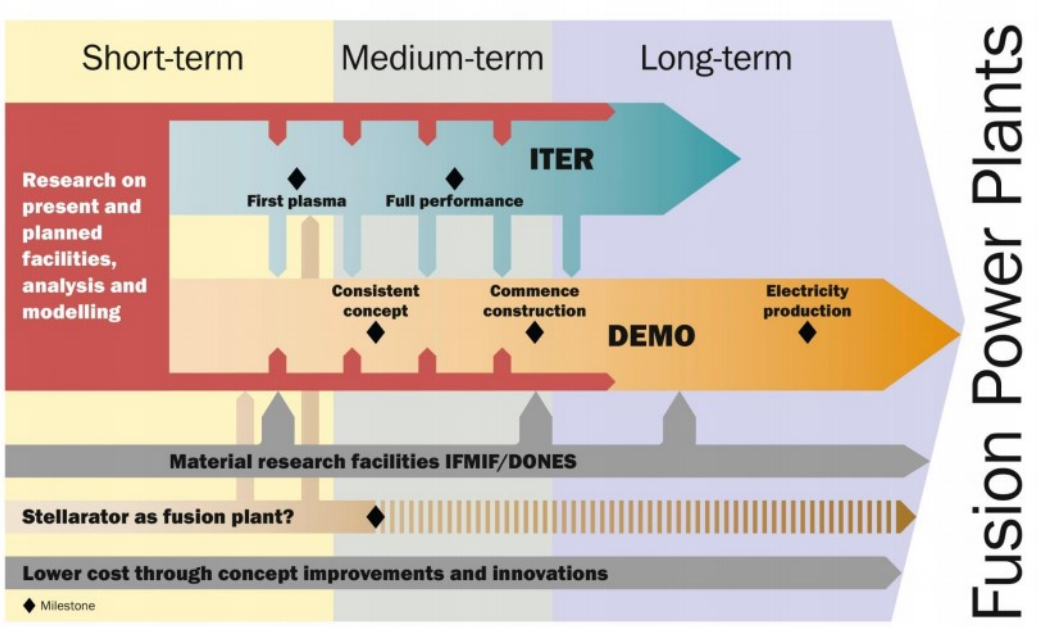

Figure 1.3 – *Roadmap to the realization of fusion energy*, [4].

1.5 System-level thermal-hydraulic transient analysis of a fusion reactor: state-of-the-art

System Thermal-Hydraulic (STH) codes are the reference numerical tools adopted for the nuclear reactor transient analysis, [12]. Most of them, such as RELAP (Reactor Excursion and Leak Analysis Program, [13]), CATHARE (Code for Analysis of Thermal-hydraulics during an Accident of Reactor and safety Evaluation, [14]) or TRACE (TRAC/RELAP Advanced Computational Engine, [15]), were developed and validated to perform best-estimate transient simulations of Light Water Reactors

(LWRs). Once validated against experimental data coming from more than one-hundred facilities, they have been used throughout decades to perform the licensing of LWRs. Simulation results allowed to characterize the reactor transient behavior in the full range of operative and accidental conditions.

The same approach to reactor transient analysis was envisaged also for fusion power plants. In the last years, a large experience was matured in the simulation of transients involving fusion reactors. Due to its criticality, attention was given to the study of breeding blanket component and its related primary cooling system.

Referring to EU-DEMO WCLL blanket, both the in-vessel [16] and ex-vessel [17] Loss Of Coolant Accidents (LOCA) were investigated with MELCOR code, [18]. The main simulation purpose was assessing the hydrogen production and the radiological source term mobilization in order to demonstrate the consistency of the EU-DEMO design with the safety and environmental criteria. MELCOR code was also used for a parametrical study in support of the reactor Vacuum Vessel Pressure Suppression System design, as described in [19].

For what concerns the EU-DEMO HCPB blanket, RELAP5-3D code, [20], was properly integrated with a computational fluid-dynamic code in order to investigate the thermal-hydraulic performances of the primary circuits during an Ex-Vessel LOCA scenario, [21]. With the same code, multiple Loss of Flow Accident (LOFA) scenarios were also studied [22]. LOCA transients were also simulated with MELCOR code, [23]. The activity goal was to perform a parametric study on the break size and to assess its impact on some reactor relevant parameters, such as containment pressure and FW component maximum temperature.

System codes were largely adopted also in the framework of research activities related to China Fusion Engineering Test Reactor (CFETR) and Korean DEMO (K-DEMO) Reactor. CFETR design foresees a Water-Cooled Ceramic Breeder (WCCB) blanket concept. RELAP5/Mod3.3 code was employed for transient analysis involving LOFA, [24], and Loss of Heat Sink (LOHS), [25], scenarios. The calculations allowed an in-depth evaluation of the WCCB blanket behavior. As initial conditions, different fusion power modes were considered.

One of the blanket concepts proposed for K-DEMO reactor is the water-cooled multiple-layer breeding blanket. It consists of a sandwich of multiple layers of breeder (Li_4SiO_4) and multiplier ($Be_{12}Ti$) mixtures, cooling channels, and structural materials. They are stacked in the radial direction, parallel to the first wall. MELCOR was adopted to investigate the reactor response after a vacuum vessel rupture, mainly focusing on hydrogen production and dust explosions, [26].

System codes also allow to study operational transients and to conceptually design the machine control system. This is a relevant design issue for fusion reactors where a plasma pulsed operating regime is foreseen (including both pulse and dwell phases). Similar studies were conducted for all the aforementioned fusion reactor concepts: EU-DEMO HCPB, [21], with RELAP5-3D; CFETR, [27], with RELAP5/Mod3.3; K-DEMO, [28], with Multi-dimensional Analysis of Reactor Safety (MARS-KS) [29].

1.6 Description of the PhD research activity

The work discussed in this PhD thesis was conducted in the framework of EUROfusion Consortium research activity, within a collaboration between DIAEE (Department of Astronautic, Electrical and Energy Engineering) of Sapienza University of Rome and the Experimental Engineering Division

(FSN-ING) of ENEA (Agenzia nazionale per le nuove tecnologie, l'energia e lo sviluppo economico sostenibile), in particular with its research center at Brasimone. As stated in **§** 1.3.1, in the last years, EUROfusion Consortium has been focusing its R&D efforts in the investigation of two principal candidate options for EU-DEMO blanket: the Water-Cooled Lead-Lithium and the Helium-Cooled Pebble Bed. ENEA, together with its Italian related partners, has been the principal investigator of the WCLL concept. DIAEE has played an important role in the conceptualization of the blanket, its related primary cooling system and in the assessment of their thermal-hydraulic performances in both normal operations and accidental conditions. This PhD thesis will concentrate on the best-estimate system-level analysis performed with a modified version of the Thermal-Hydraulic (TH) code RELAP5/Mod3.3. EUROfusion Consortium distributed its research activity in different Working Packages. The current study addressed tasks belonging to both Work Package Breeding Blanket (WPBB) and Work Package Balance of Plant (WPBoP). Simulations were performed with the goal of the design improvement. Calculation outcomes were used to evaluate the appropriateness of the blanket cooling circuit design and the eventual need of mitigation actions in selected accidental scenarios.

During the third ITER council (2008), it was established the so-called ITER Test Blanket Module (TBM) program, [30]. Its objective is to provide the first experimental data on the performance of the breeding blankets in the integrated fusion nuclear environment, [31]. Initially it foresaw the test of six mock-ups. In 2018, the R&D strategy was strongly revised and the number of tested TBMs lowered to four. Also the selected blanket concepts were changed, with the insertion of WCLL option next to the previously chosen HCPB, Helium Cooled Ceramic Reflector (HCCR) and Water Cooled Ceramic Breeder (WCCB), [32]. From 2018, an intense design activity was performed within the EUROfusion Work Package Plant level system engineering, design integration and physics integration (WPPMI). The R&D effort was led by ENEA and involved many European research institutions and universities. The entire work was supervised also by Fusion for Energy (F4E), that is European Union organization managing Europe's contribution to ITER reactor, [33]. By the fall of 2020, the pre-conceptual and conceptual design of the WCLL Test Blanket System (TBS) were performed. TBS consists of the TBM and the related ancillary systems. Among them, the most relevant is the Water Cooling System (WCS), acting as primary cooling circuit of the TBM set. The design and thermal-hydraulic characterization of this circuit is up to DIAEE. The work done within this framework will be presented in this PhD Thesis.

In conclusion, these three years of research activity were focused on the conceptualization and thermal-hydraulic assessment of the primary cooling system for the WCLL blanket option, involving both ITER and DEMO fusion reactors.

1.7 Document outline

This document is articulated in seven sections. The first one defines the PhD activity framework, while **§** 7 focuses on the main conclusions and future perspectives of the work done.

Section 2 highlights the main characteristics of the best-estimate thermal-hydraulic system code RELAP5/Mod3.3. A modified version was developed at DIAEE with the aim of enhancing the code modelling capabilities with respect to fusion reactors. The new implemented features are also presented in this section.

Sections 3 and 4 refer to the research activity involving DEMO WCLL. In **§** 3 the pre-conceptual design of the blanket component and related primary cooling circuits is described in detail. Their thermal-hydraulic model, developed for calculation purposes, is treated in **§** 4. Annexes A1 and A2

provide information about material properties used and further details on the blanket nodalization adopted. **§** 4 also reports and discusses the outcomes of the transient analysis.

In the same way, **§** 5 and 6 are related to ITER WCLL-TBS research activity. The TBS conceptual design, in particular the one of WCS circuit whose DIAEE is responsible for, is described in **§** 5. To perform the system thermal-hydraulic assessment a dedicated model was developed. Its detailed description is provided in **§** 6, together with a full comment of the calculation results. An insight into the simulation outcomes obtained during the pre-conceptual design phase is provided by annex A3.

2 RELAP5/MOD3.3

2.1 The code

The RELAP5 series of code, [13][34][35][36], was developed at the Idaho National Laboratory (INL) under the sponsorship of the U.S. Department of Energy and the U.S. Nuclear Regulatory Commission. Specific code applications included transient simulations related to LWR systems such as loss of coolant, anticipated transients without scram, and operational transients such as loss of feedwater, loss of offsite power, station blackout, and turbine trip. RELAP5/Mod3.3 is a highly generic code that, in addition to calculating the behavior of a reactor coolant system during a transient, can be used for simulation of a wide variety of hydraulic and thermal transients in both nuclear and nonnuclear systems involving mixtures of vapor, liquid, noncondensable gases, and nonvolatile solute. The code was used for space reactor simulations, gas cooled reactor applications and fast breeder reactor modelling.

The RELAP5/Mod3.3 code is based on a nonhomogeneous and nonequilibrium model for the two-phase system that is solved by a fast, partially implicit numerical scheme to permit economical calculation of system transients. The RELAP5/Mod3.3 development effort from the outset was to produce a code that included important first-order effects necessary for accurate prediction of system transients but that was sufficiently simple and cost effective so that parametric or sensitivity studies were possible.

The code includes many generic component models from which general systems can be simulated. The component models include: pumps, valves, pipes, heat releasing or absorbing structures, reactor kinetics, electric heaters, jet pumps, turbines, compressors, separators, annuli, pressurizers, feedwater heaters, ECC mixers, accumulators, and control system components. In addition, special process models are included for effects such as form loss, flow at an abrupt area change, branching, choked flow, boron tracking, and noncondensable gas transport.

The hydrodynamic model and the associated numerical scheme are based on the use of fluid control volumes (CVs) and junctions (JUNs) to model the exact reactor geometry. The control volumes can be viewed as stream tubes having inlet and outlet junctions. The control volume has a direction associated with it that is positive from the inlet to the outlet. Velocities are located at the junctions and are associated with mass and energy flow between control volumes. Control volumes are connected in series, using junctions to represent a flow path.

Heat exchange is also modelled in a one-dimensional sense, using a finite difference mesh to calculate temperatures and heat flux vectors. The heat conductors can be connected to hydrodynamic volumes to simulate a heat flow path normal to the fluid flow path. The heat conductor or heat structure (HS) is thermally connected to the hydrodynamic volume through a heat flux that is calculated using heat transfer correlations. Electrical or nuclear heating of the heat structure can also be modelled as either a surface heat flux or as a volumetric heat source. The heat structures are used to simulate pipe walls, heater elements, nuclear fuel pins, and heat exchanger surfaces.

2.2 The DIAEE modified version

During the last years, DIAEE, in collaboration with ENEA, upgraded the standard version of the code including some new features needed to address the modelling issues arising from the simulation of ITER and DEMO fusion reactors, [37]. New implementations consist in:

- Lead-lithium and HITEC© working fluids, with their thermophysical properties;
- New heat transfer correlations;
- Helicoidally tubes dedicated heat transfer correlations and two-phase flow maps.

2.2.1 Addition of new working fluids

Within the code, the available set of working fluids was extended by adding lead-lithium (PbLi) and HITEC©, [38]. The latter is a molten salt already adopted for solar applications and now selected as fluid for the intermediate circuit of DEMO reactor (see **§** 3.6). It is a mixture of the nitrate salts $NaNO_3$, $NaNO_2$ and KNO_3 with a molar composition of 7:49:44 and a weight composition of 7:40:53, [38]. RELAP5/Mod3.3 computes thermal properties by calling a dedicated subroutine for each property. These subroutines work in a quite simple way. They are called by higher-order subroutines, such as the ones calculating pressure drops, heat transfer, etc. They receive arguments from the calling subroutine (basically the temperature), apply the specific correlation for the property computation and return its value to the calling subroutine. The main thermal properties to be implemented to add a working fluid in RELAP5 code are: density, heat capacity, viscosity, thermal conductivity and surface tension. The correlations considered for them are the reference ones selected in the framework of EUROfusion research project after a wide literature review. For PbLi and HITEC©, chosen expressions were derived from [39] and [38], respectively. They are reported in Table 2.1 and Table 2.2.

Table 2.1 – PbLi thermal properties implemented in DIAEE version of RELAP5/MOD3.3 code, [39].

Parameter	Unit	Function	Range T [°C]
Density	kgm^{-3}	10520.35 – 1.19051 · **T**, [K]	235-607
Specific Heat	$Jkg^{-1}K^{-1}$	1950 – 9.116 x 10^{-3} · **T**, [K]	235-527
Thermal Conductivity	$Wm^{-1}K^{-1}$	0.1451 + 1.9631 x 10^{-4} · **T**, [°C]	235 - 600
Dynamic Viscosity	Pa·s	0.0061091 - 2.2574 x 10^{-5} · **T** + 3.766 x 10^{-8} · $\mathbf{T^2}$ - 2.2887 x 10^{-11} · $\mathbf{T^3}$, [°C]	235 - 600
Surface Tension	$N\ m^{-1}$	0.4594 - 4 x 10^{-5} · (**T** – 518), [K]	235 - 427

Table 2.2 – HITEC© thermal properties implemented in DIAEE version of RELAP5/MOD3.3 code, [38].

Parameter	Unit	Function (T in Celsius)	Range T [°C]
Density	kgm^{-3}	2080 - 0.7324 · **T**	175 – 500
Specific Heat	$Jkg^{-1}K^{-1}$	1560	200 - 500
Thermal Conductivity	$Wm^{-1}K^{-1}$	0.4465 + 0.1788 x 10^{-3} · **T** - 1.1486 x 10^{-6} · $\mathbf{T^2}$	200 - 500

Dynamic Viscosity	Pa·s	$2.1554 \times 10^{-4} \cdot \exp(1006.4131/(\mathbf{T} + 83.7755))$	252 - 500
Surface Tension	N m^{-1}	$0.14298 - 5.56 \times 10^{-5} \cdot \mathbf{T}$	297 - 397

2.2.2 Addition of new heat transfer correlations

For liquid metals, a complete set of heat transfer correlations were implemented in the code subroutine managing the Heat Transfer Coefficient (HTC) evaluation. In particular, the following correlations were introduced:

- For circular tubes or plates: Seban-Shimazaki [40], Cheng-Tak [41], Lubarsky and Kaufman [42];
- For bundles: Ushakov [43], Mikityuk [44], Kazimi-Carelli [45], Graber-Rieger modified by Sha and Launder for large P/D [46];

Such correlations represent the state-of-the-art for liquid metal heat transfer applications. They were adopted to properly assess the PbLi thermal field in the correspondent loop of the ITER WCLL-TBS (see **§** 6). For non-metal fluids, such as HITEC©, Sieder-Tate [47] correlation was also implemented. It was used to properly simulate the molten salt heat transfer coefficient in the heat exchangers thermally coupling the primary and intermediate cooling loops of DEMO WCLL (see **§** 4.1.4).

2.2.3 Addition of helicoidally geometry

For the steam generators coupling the DEMO WCLL intermediate loop to the Power Conversion System (PCS), Helicoidally Coil Steam Generators (HCSG) were selected (see **§** 3.6). In RELAP5/Mod3.3 there were no specific models to assess the thermal transfer in such geometry. For this reason, new correlations were implemented in the code to extend its applicability to HCSG technology. In particular, for the tube bundle outer HTC Zukauskas correlations were introduced, [48]. The latter consider the annuli created between the pipe banks and the eventual variation of tube pitches among the bundle rows. Instead, for the tube bundle inner HTC, it was used Mori-Nakayama correlations, [49].

After these modifications, RELAP5/Mod3.3 was able to properly calculate the heat transfer coefficient in helically coiled tubes, but there was still an issue regarding the dry-out. In this geometry, such phenomenon shows up at higher thermodynamic quality values with respect to straight tube bundle. Normally, the code compares Critical Heat Flux (CHF) to local heat flux to check if thermal crisis occurs in the heated subchannel. CHF correlations present in the code best suit to imposed heat flux systems, such as core subchannels, and serve little purpose in imposed temperature systems, such as steam generators. Indeed, within helically coiled tubes, a dry-out region, rather than a dry-out point, can be identified, delimited by the dry-out points on inner tube wall and outer tube wall. Dry-out shows up first on the inner wall where the liquid film is thinner due to centrifugal force pushing the liquid towards the outer wall. However, the mixing effect due to turbulent flow generally prevails on phases stratification. Therefore, if only the outer wall is heated, dry-out quality can be referred to the latter. In view of the results obtained by Roumy at high pressures, [50], dry-out quality on the outer wall is always greater than 0.94. Hence, for this geometry, it was taken the decision to bypass CHF check originally implemented in

the code and perform a thermodynamic quality check based on the Roumy reference value. Thermal crisis control loop is highlighted in red in Figure 2.1.

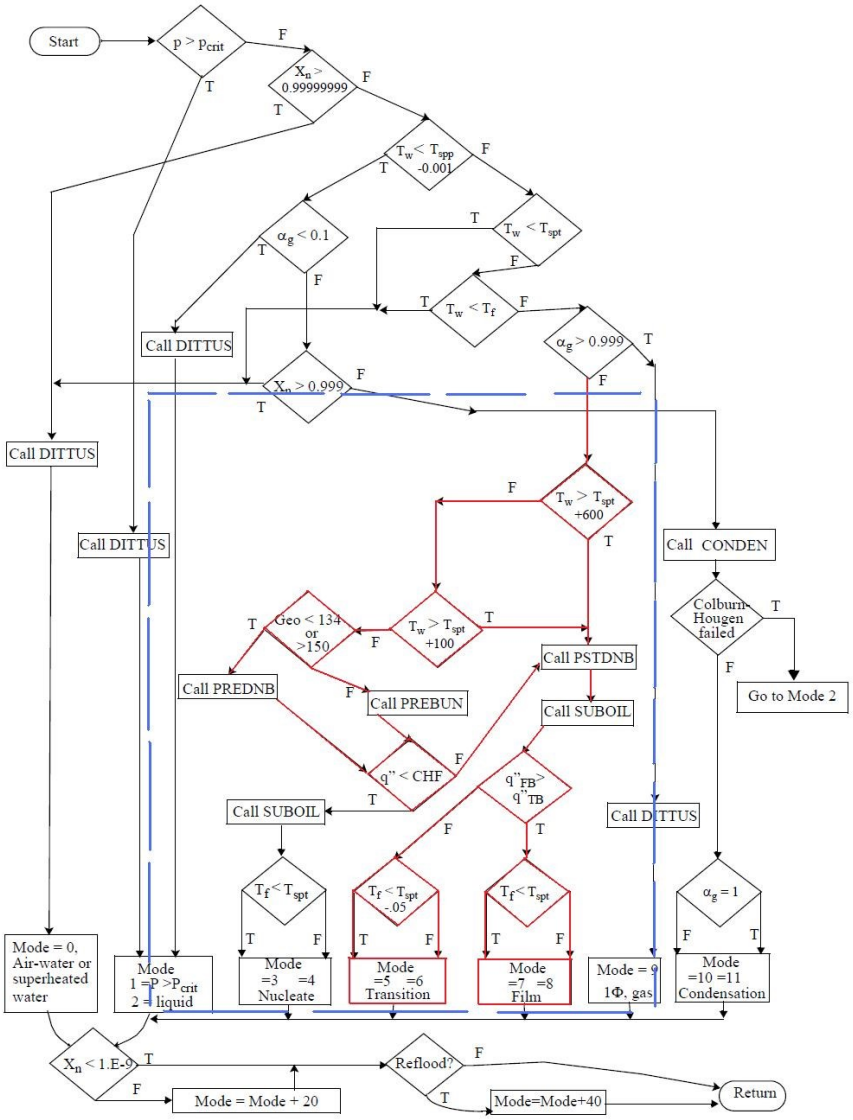

Figure 2.1 – Thermal crisis control loop implemented in RELAP5/MOD3.3 code, [36].

To preliminary assess the effectiveness of this new modelling approach implemented in the code a test case was selected to be investigated. It consisted in ICSP Test SP3, performed at the experimental facility OSU-MASLWR (Oregon State University - Multi Application Small Light Water Reactor), [51]. For a comprehensive description of the facility, as well as of the purpose of the experimental campaign conducted there, refer also to [52][53]. In Figure 2.2 it is shown the overview of the primary cooling system of the OSU-MASLWR facility. The reactor core is simulated with a Fuel Pin Simulator (FPS). This component is located in the bottom region of the Reactor Pressure Vessel (RPV). The HCSG, coupling primary and secondary loops, is composed of vertical helical tubes, and is located in the RPV upper part. Such configuration ensures enough axial distance between the power source and heat sink thermal centers. For this reason, natural circulation is exploited for core cooling in both normal and abnormal conditions. The primary flow passes through the FPS and goes upstream within the Hot Leg (HL) riser arriving to the upper plenum. Then, it flows downstream through the HCSG bundle and the Cold Leg (CL), returning into the lower plenum.

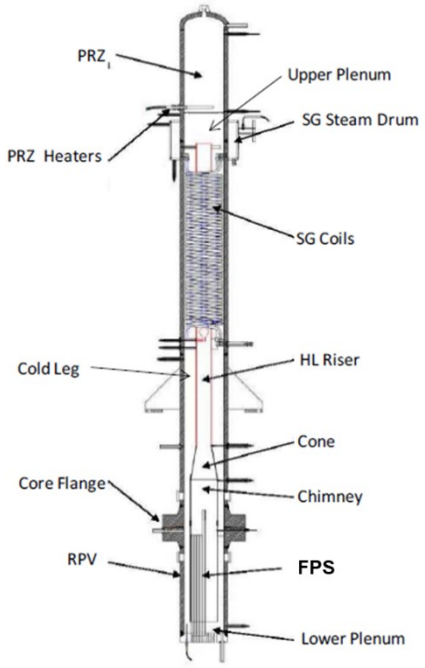

Figure 2.2 – Overview of the primary cooling system of OSU-MASLWR facility.

ICSP Test SP3 was a power manoeuvring test foreseeing seven FPS power steps in the range of 80 – 320 kW. Feedwater at the HCSG secondary side was increased accordingly. The aim of the experiment was to investigate the primary system natural circulation and secondary system superheating for a variety of core power levels and feedwater flow rates. The best Figure Of Merits (FOM) to evaluate the code performances in simulating the heat transfer through the HCSG are the primary temperatures (considered at FPS inlet and outlet, see Figure 2.3a) and the secondary outlet temperature, shown in Figure 2.3b.

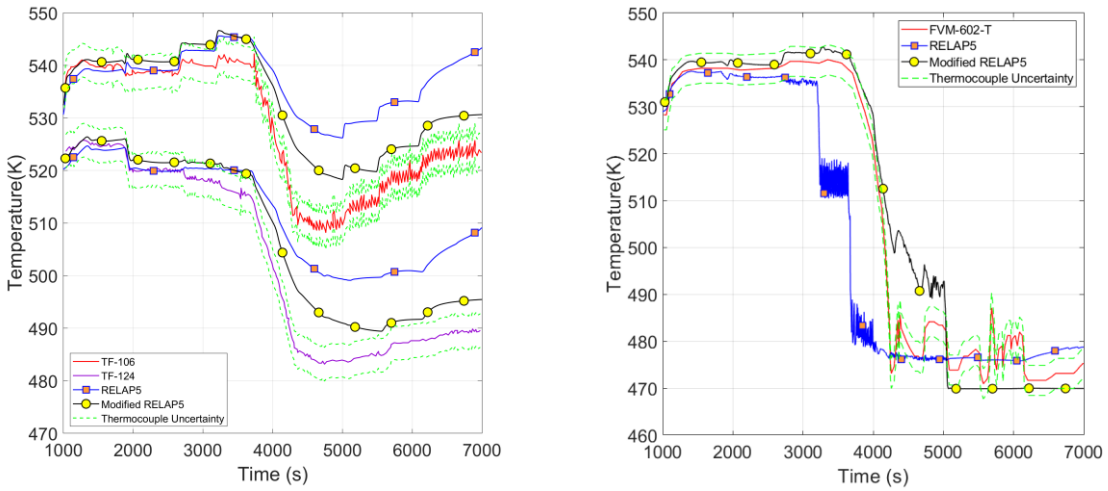

Figure 2.3 – ICSP test SP3, comparison between experimental data and simulation outcomes:(a) FPS inlet/outlet temperatures; (b) HCSG secondary side outlet temperature.

In Figure 2.3 (both a and b), experimental data are represented by a red line and are reported with the correspondent error band, individuated by a pair of dashed green lines. Calculation outcomes of standard (blue line with orange squared markers) and modified (black line with yellow round markers) RELAP5 versions are quite similar for low power values. The effects of the code modifications are more visible at higher power levels when the heat transfer within the HCSG plays a more important role. Indeed, above a certain power threshold, nearly 200 kW (corresponding to 3500 s), the default version shows limited capabilities to reproduce the test. On the contrary, the trends related to the modified version fit quite well the experimental data. In particular, the decrease of the secondary side steam outlet temperature occurring at 4000 s is predicted with enough accuracy (Figure 2.3b). This confirms the effectiveness of the modelling approach implemented in the DIAEE version of the RELAP5/Mod3.3 code. Such results are presented and more widely discussed in [54]. In the future developments of the research activity, the modified version will be tested against experimental data coming from other facilities where HCSG technology is present in order to enhance the code reliability in simulating such components. Once terminated the validation period, the same will be used to perform the full thermal-hydraulic characterization of the HCSG installed in the DEMO WCLL intermediate loop.

3 DEMO WCLL PRE-CONCEPTUAL DESIGN

3.1 DEMO reactor.

According to the EU *Roadmap*, [3][4], ITER must be followed by DEMO reactor as the remaining crucial step towards the exploitation of fusion power. The major requirements for-DEMO power plant are, [55]:

- Produce net electricity for the grid at the level of few hundred MWs;
- Breeding *in-situ* the necessary amount of tritium to close its fuel cycle, i.e. achieving a Tritium Breeding Ratio (TBR) greater than one;
- Demonstrate an adequate level of reactor availability (at least several full power years);
- Minimize the production of radioactive waste, without long-lived radioisotopes (i.e. avoiding the need of a long-term storage);
- Demonstrate a satisfactory readiness of all the technologies needed for the construction of a first-of-a-kind commercial fusion power plant.

At the end of 2020, DEMO just concluded the pre-conceptual design phase. Its current baseline design point foresees the major features reported in Table 3.1, [55][56]. DEMO normal operations are characterized by a pulsed plasma regime, based on eleven pulses per day, [57]. Each pulse is composed by two hours of flat-top at full power, alternating with ten minutes of dwell time. Power is ramp-down and ramp-up in nearly one hundred seconds. During dwell time, only decay heat is still produced in the blanket, corresponding to nearly 2% of the reactor rated power. The CAD model of DEMO tokamak is shown in Figure 3.1, [58].

Table 3.1 – DEMO baseline design parameters, [55][56].

Parameter	**Unit**	**Value**
Aspect ratio	-	3.1
Major/minor radius	m	9.0/2.9
Toroidal field, axis/coil-peak	T	5.9/>12.5
Auxiliary heating power (flat top)	MW	50
Fusion power (flat top)	MW	2000
Electric output	MW	500
DEMO plant lifetime	Full power years	~7-8
Starter/Second Blanket lifetime	dpa	20/50
TBR (required/design target)	-	1.05/1.15
Plasma volume	m^3	~2500

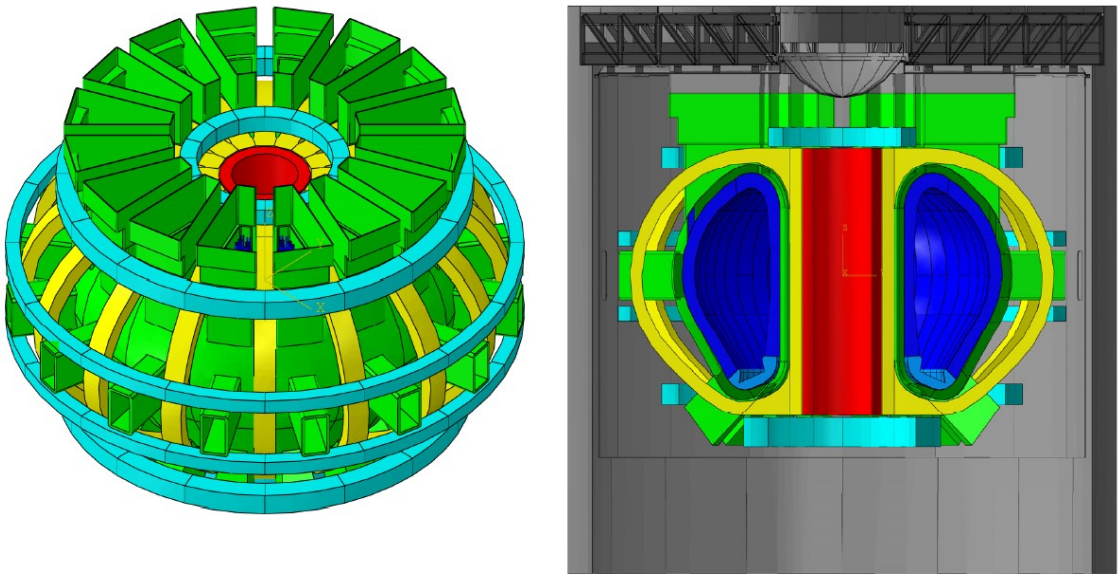

Figure 3.1 – CAD model of DEMO tokamak, [58].

3.2 WCLL Breeding Blanket.

As discussed in **§** 1.3.1, the Breeding Blanket (BB) is one of the key components of the fusion reactor. It will be used to convert into heat the energy generated within the plasma (in the form of fast neutrons, charged particles, heat flux). Moreover, the nuclear reactions between the incoming neutrons and the breeder produce the tritium needed to close the fuel cycle. Lastly, the blanket must shield the vacuum vessel and superconducting coils, avoiding high energy radiations to reach these vital components.

In the framework of the EUROfusion Programme, two breeding blanket concepts were selected for the DEMO R&D strategy: Water-Cooled Lead-Lithium and Helium-Cooled Pebble Bed, [9]. The WCLL is the concept investigated during these three years of research activity. Its reference design foresees, [59][60]:

- The ferritic-martensitic steel (EUROFER-97) as structural material, because of its reduced activation;
- Liquid lead-lithium enriched at 90% in Li^6 as breeder, neutron multiplier and tritium carrier;
- Water at PWR conditions as coolant (295–328 °C and 15.5 MPa).
- An armour, consisting of a thin tungsten layer, is assumed to cover the FW component.

The DEMO blanket design adopted for modelling purposes is the WCLL2018.v0.6, based on Single Module Segment (SMS) approach, [59][60]. The overall blanket component is divided in 16 sectors (22.5°) in toroidal direction. The CAD model of one DEMO sector is shown in Figure 3.2. Each sector consists in three poloidal segments in the Outboard Blanket (OB, green in Figure 3.2) and two poloidal segments in the Inboard Blanket (IB, red in Figure 3.2). They are respectively located radially inwards and outwards with respect to the plasma chamber. Segments host the BB elementary cells. BReeding Cells (BRC) are piled up in the poloidal direction. Their geometry varies inside the segment according to the poloidal position and differs also between IB and OB segments.

The reference breeding cell is the WCLL2018.v0.6 Central OB (COB) equatorial cell, described in detail in [61][62]. The cell dimensions are: 135 mm in poloidal direction, 1000 mm of radial thickness and 1504 mm of toroidal width. The detailed cell layout is shown in Figure 3.3, [61][62]. The FW plasma facing area is protected by a tungsten armour of 2 mm. The FW total thickness is 25 mm. The component is cooled with water flowing in square channels having a 7×7 mm section and equally distributed along the poloidal height.

Radially outwards with respect to FW there is the Breeder Zone (BZ). There, the nuclear interactions between high-energy neutrons coming from the plasma and liquid breeder occur. Neutron kinetic energy is converted into heat. Such thermal power is removed by a system of 22 Radial-Toroidal (RT) C-shaped Double Walled Tubes (DWTs). They have an external diameter of 13.5 mm and a thickness of 1.375 mm. DWTs are displaced in horizontal planes situated at different poloidal elevations and are split in three arrays along the radial direction. Their disposition was optimized during the last years of design activities to match the blanket requirements, [62]. The lead-lithium enters the BRC from the bottom, flows in radial direction, from the Back Plate (BP) to the FW, goes up in poloidal direction and returns radially, from the FW to the BP. PbLi flow path is indicated in Figure 3.4, [63]. A BaFfle Plate (BFP) is foreseen in the cell layout, dividing the BZ in two poloidal zones and ensuring the proper PbLi circulation (Figure 3.4). In addition, five Radial-Poloidal (RP) stiffening plates are present. They channel the total PbLi mass flow in six parallel rectangular paths, see Figure 3.3. Finally, toroidal stiffening plates poloidally separates the BRCs belonging to the same segment (see Figure 3.4).

The outer section of the breeding cell (in radial direction) is devoted to house both PbLi and water manifolds, as shown in Figure 3.3. These components are spinal rectangular channels flowing along the overall poloidal direction. Their inlet/outlet connections are visible in Figure 3.2. The Back Supporting Structure (BSS) is a continuous steel plate in poloidal direction, with a radial thickness of 100 mm which represents the backbone of the blanket segment.

The power balance of WCLL blanket is collected in Table 3.2, [64]. FW is heated up by the incident Heat Flux (HF) and the Neutron Wall Load (NWL), while BZ thermal power is due to neutron-breeder nuclear reactions.

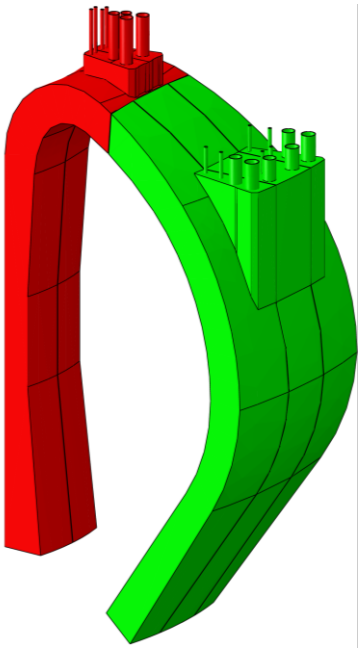

Figure 3.2 – CAD model of one DEMO sector (of sixteen). Green segments belong to outboard blanket, red ones to inboard blanket.

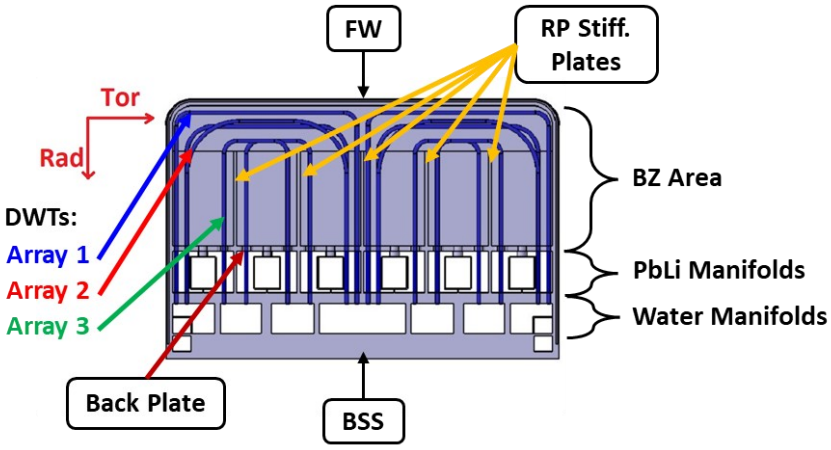

Figure 3.3 – Radial-toroidal section of the WCLL COB equatorial cell, [61][62].

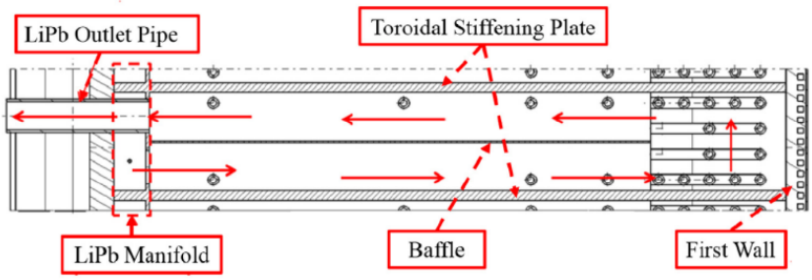

Figure 3.4 – Radial-poloidal section of the WCLL breeding cell with the indication of PbLi flow path, [63].

Table 3.2 – Power balance of WCLL blanket, [64].

Parameter	Unit	Value
Average FW Heat Flux (HF)	MW/m^2	0.22
Total power from FW HF	MW	272.7
Total nuclear heating[1]	MW	1650.3
FW total power	MW	439.8
BZ total power	MW	1483.2
WCLL BB total power	MW	1923.2

[1] Total nuclear heating is the sum of thermal power produced in the BZ due to neutron-breeder reactions and of the Neutron Wall Load insisting on FW surface

3.3 DEMO WCLL BoP.

In DEMO reactor, the Balance of Plant consists of the complex 'chain' of systems used to remove the pulsed thermal power generated by the plasma and deposited in the blanket, the divertor (DIV) and the vacuum vessel and to convert it into electricity to be delivered to the external grid. The batch of primary cooling systems belonging to DEMO BoP constitute the Primary Heat Transfer System (PHTS). In WCLL blanket, first wall and breeder zone are cooled by two independent circuits, namely the FW PHTS and the BZ PHTS. In the same way, divertor plasma facing components and cassette body own separate cooling systems, called DIV-PFU PHTS and DIV-CAS PHTS. Finally, the VV PHTS is deputized to refrigerate the vacuum vessel.

The transfer of plasma power to the electrical grid can be performed by using either direct or indirect coupling design options, [65][66]. Different BoP variants are currently under investigation in the framework of WPBoP research activity. For each variant, the main design constraints are avoiding the plant disconnection from the grid at each dwell phase and limiting the impact of related temperature transients to the structures [57]. The three main concepts are described below.

Direct Coupling Design (DCD) with a small Energy Storage System (ESS): It foresees that, during pulse phase, all the thermal power removed from breeding blanket by correspondent PHTS is driven to PCS by means of Once Through Steam Generators (OTSG). In these components, steam is produced in suitable conditions to feed the turbine. In addition, the heat generated in the vacuum vessel and divertor is used to preheat the PCS feedwater. This is possible thanks to the integration of DIV PHTS and VV PHTS in the train of feedwater heaters. This solution is common to all the BoP options. Hence, WCLL DCD BoP is designed to maximize the production of electrical power during pulse. Instead, during dwell, the system goal is feeding the turbine at about 10% of the rated steam mass flow, in order to keep the plant connected to the grid (i.e., the generator synchronized). A small molten salt ESS is installed in order to compensate for the power deficit, producing the needed steam to feed the turbine during the dwell phase. ESS is provided with electrical heaters to transfer thermal power to the molten salt during pulse, using a small part of the electricity produced by the generator during this phase. The required molten salt (i.e. HITEC) inventory is about 2700 tons, stored in a hot tank of nearly 1500 m^3.

Direct Coupling Design (DCD) with auxiliary boiler: an alternative DCD solution was conceived substituting the small ESS with an auxiliary boiler. This component is always kept in operation, during both pulse and dwell phases. It provides 250 MW of power, ensuring during dwell time a steam flow rate of 10% of the nominal value. The large size of the auxiliary boiler, required to operate the BoP at minimum load during dwell, even if feasible, is what makes this solution less convenient than the precedent one.

Indirect Coupling Design (ICD): in this case, only BZ PHTS delivers thermal power directly to PCS, by means of two OTSGs. Instead, the FW PHTS is connected to an Intermediate Heat Transfer System (IHTS) equipped with a large ESS. The thermal coupling is provided by two water/molten salt Heat EXchangers (HEX). The ESS consists of two tanks filled with HITEC molten salt at different temperatures. During pulse, the ESS accumulates a fraction of the FW thermal power, storing molten salt in the hot tank. Then, during dwell, this energy is transferred to the PCS through four Helicoidally Coil Steam Generators (HCSGs). Such configuration allows to guarantee a continuous and near constant turbine load (i.e., electrical power delivered to the grid) in both pulse and dwell phases. The large size of the ESS tanks (around 11000 m^3 each) is the main drawback of this solution. The PhD research activity discussed in this document dealt with this BoP variant[1]. The CAD model of DEMO WCLL tokamak integrated with ICD BoP is show in Figure 3.5, .

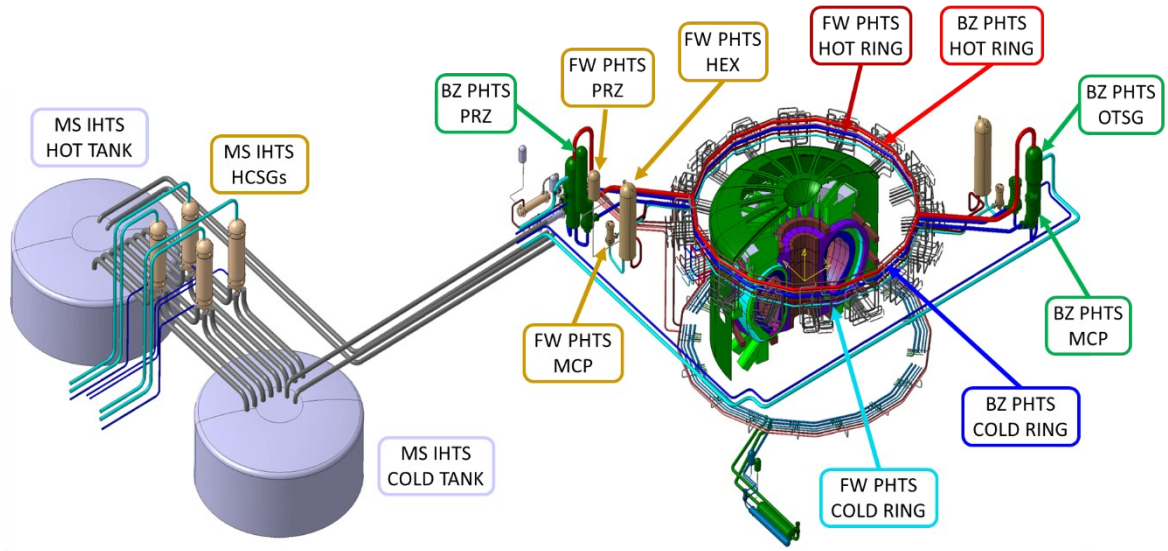

Figure 3.5 – CAD model of DEMO WCLL tokamak integrated with ICD BoP, [63].

[1] When the simulation activity discussed in this PhD thesis started (back in 2017), the Indirect Coupling Option was the only one present. Later, in the last years of Framework Programme 8, the other (direct) solutions were proposed to reduce or eliminate the presence of the large ESS tanks. In addition, the thermal-hydraulic model prepared to perform transient calculations (described in **§** 4.1) is focused on the BB PHTS with the goal of evaluating its performances during operational and accidental scenarios. From the BB PHTS point of view, when passing from ICD to DCD, the only difference lies in the substitution of FW HEXs with FW OTSGs. The transient behavior of such components can be assumed similar to the one of the correspondent steam generators belonging to the BZ PHTS, widely studied and discussed in this manuscript. Hence, for the purpose of the current simulation activity, the BoP option selected has a reduced influence. For this, till the end of FP8 research activities, the ICD solution was maintained to perform the DEMO WCLL transient analysis.

3.4 DEMO WCLL BB PHTS

The PHTS design foresees two loops for each system (FW and BZ), symmetrically disposed along the tokamak circumference (i.e. toroidal direction), [64]. The main PHTS components outside the vacuum vessel are:

- The hot and cold rings, distributing and collecting the PHTS mass flow from/to the loops and the tokamak sectors;
- The sector manifolds, divided in collectors (hot) and distributors (cold), connecting the rings to the tokamak sectors;
- The loop piping, connecting the main loop vessel components;
- The BZ OTSGs and the FW HEXs;
- The Main Coolant Pumps (MCP), providing the primary flow;
- The pressurizer (PRZ) system, one per PHTS, ensuring the pressure control function.

3.4.1 PHTS piping

PHTS piping was sized considering a maximum fluid velocity within the component of 15 m/s. Pipeline routing and length was the result of CAD activities performed during the pre-conceptual design phase. The main pipeline features for FW and BZ PHTS are reported in Table 3.3 and Table 3.4, [67]. What is worth to be emphasized is the function of hot and cold rings. These special components represent the hydraulic interface between the PHTS loops and the in-VV cooling circuits (one per sector). Hot ring collects the hot flow coming from the sectors and distribute it to the loops to be cooled. Vice versa, the cold ring receives the cold water exiting the PHTS heat sink (BZ OTSGs or FW HEXs) and delivers it to the tokamak sectors. In each ring, the loop connections are diametrically opposed and the sector connections are equally distributed along the toroidal coordinate. Thus, they are characterized by four parallel flow paths, shown in Figure 3.6a and Figure 3.6b for hot and cold ring.

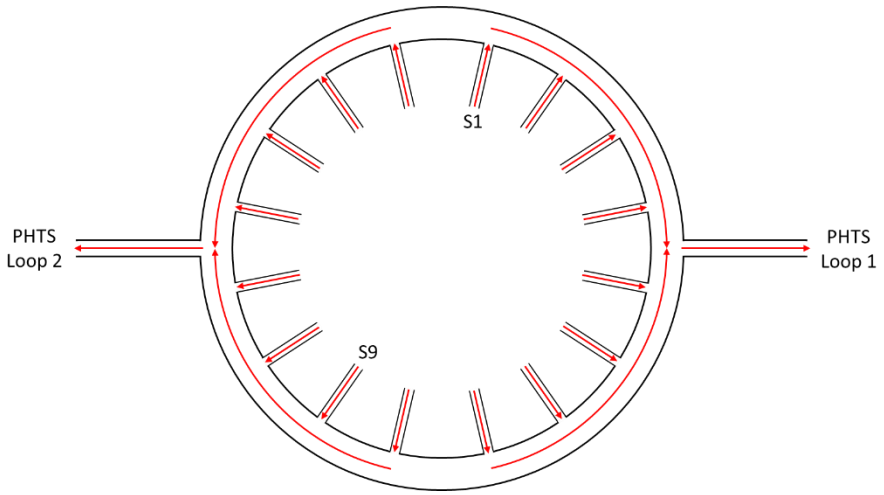

(a)

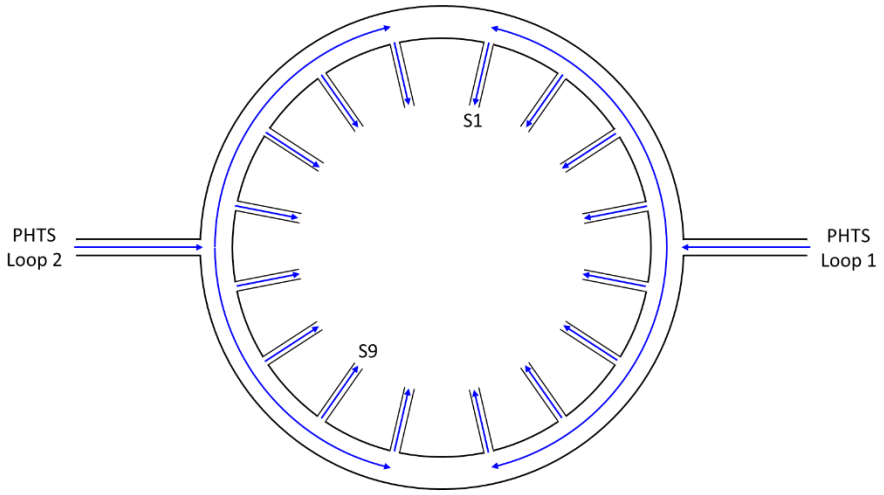

(b)

Figure 3.6 – Water flow paths in PHTS hot ring (a) and cold Ring (b).

Table 3.3 – BZ PHTS pipeline features, [67].

Parameter	**Comp. per PHTS**	**DN (EN 10220, [68])**	**Thickness [mm]**	**Length [m]**
Hot Ring	1	650	50	146.5
Cold Ring	1	650	50	146.5
Hot leg	2	850	70	45.6
Loop seal	2	650	50	5.6
Cold leg	4	650	50	24.3
Surge line	1	150	14.2	12.7

Table 3.4 – FW PHTS pipeline features, [67].

Parameter	**Comp. per PHTS**	**DN (EN 10220, [68])**	**Thickness [m]**	**Length [m]**
Hot Ring	1	350	28	169.2
Cold Ring	1	350	28	169.2
Hot leg	2	500	40	29.3
Loop seal	2	500	40	11
Cold leg	2	500	40	16.5
Surge line	1	150	14.2	23.7

3.4.2 PHTS pump system

BB PHTS pump system was conceived to provide the needed primary flow to cool the two blanket subsystems (FW and BZ). Pressure drop profiles along the overall primary cooling circuits were evaluated by using theoretical correlations and the required pump head assessed, [64]. A total of six pumps are foreseen in the BB PHTS pre-conceptual design. Four MCPs, two per loop, are installed in the cold legs of the BZ PHTS. The lasting pumps belong to the FW PHTS (one per loop). The preliminary value postulated for the component efficiency is of 78%. The design outcomes are reported in Table 3.5, [67]. Proven LWR technology was selected for PHTS application. FW and BZ pumps can be small and medium vertical, single stage, centrifugal pumps already adopted in PWRs, [69].

Table 3.5 – BB PHTS pump system features, [67].

Parameter	Unit	FW PHTS	BZ PHTS
Rated speed	rad/s	124.5	124.5
Rated Density	kg/m^3	736.6	736.6
Rated Mass flow	kg/s	1136.8	1915.6
Rated Volumetric flow	m^3/s	1.54	2.60
Rated Head	MPa	0.94	0.95
Rated Efficiency	-	0.78	0.78
Rated Torque	Nm	13403	25567
Rated motor power	MW	1.60	3.02
Component per PHTS	-	2	4
Total motor power	MW	3.20	12.1

3.4.3 BZ OTSGs

Even if this is the first time such technology was proposed for nuclear fusion applications, OTSGs was used and operated for decades in the field of nuclear fission power plants, in particular in PWR applications, [70]. The OTSG design foresees a straight-tube, straight-shell layout, with flat tube sheets and hemispherical primary heads. An overview of the OTSG design is shown in Figure 3.7. Primary system is bounded by hemispherical heads, tube sheets and tube bundle. Primary coolant enters from the OTSG top and flows downwards, exiting from the component bottom. Secondary side is the steam-producing section. It is bounded by the shell, named vessel, the tube outer surface and the tube sheets. A cylindrical shroud, called riser, surrounds the tube bundle and channels the secondary flow along the thermal height. Subcooled feedwater enters the steam generator laterally, in the lower vessel (downcomer) section. Firstly, it is preheated by aspirating

steam coming from the tube bundle region (recirculated flow). Then, secondary water moves through the annular downcomer. It reaches the vessel bottom in nearly saturated conditions. Later, it rises in the central shroud where it boils to dry steam and then it is superheated. Once reached the top, steam is turned by the tube sheet and directed to the annulus between riser and vessel, in the OTSG upper section. Here, it flows downwards to the two outlet nozzles, connected laterally. Starting from the shroud bottom, as feedwater is converted to superheated steam, three heat transfer regions can be identified: Nucleate Boiling Region (NBR), Film Boiling Region (FBR) and SuperHeat Region (SHR), [70]. The former is where saturated feedwater begins to boil. Tube outer surface remains wetted while small bubbles rapidly form and break away from it. Thanks to the turbulence due to bubble formation, this heat transfer mode ensures a high heat transfer coefficient. For this, most of the primary-to-secondary thermal exchange occurs in the NBR. The nucleate and forced convective boiling continue until enough water is vaporized and the liquid layer is replaced by steam on the surface of the tubes. Therefore, film boiling occurs at high qualities after the dry-out point and fully develops within a very short axial distance. In the film boiling heat transfer, the heat flux is sharply reduced and heat transfer occurs by convection through the steam and evaporation of entrained liquid droplets in the saturated core. At FBR top, only dry steam is present. In the final SHR, thermal power transferred from primary fluid is used to produce superheated steam. Regarding the OTSGs to be installed in BZ PHTS, their design is still at a pre-conceptual stage. Such design was scaled from existent units still operating in nuclear fission power plants. Steam generator rated power was used as scaling factor. OTSG technology was considered to be appropriate to be installed in PHTS circuits since the primary (PHTS itself) and secondary (PCS) sides water thermodynamic conditions are comparable with respect to the ones of a PWR, [64]. Indeed, PHTS water enters the OTSGs (i.e. exits from the BB) at 328 °C and it is cooled down to 295 °C. Primary pressure is 15.5 MPa. On the secondary side, feedwater is admitted at 238 °C and PCS reference pressure is set to 6.41 MPa. The main design data are reported in Table 3.6. The connection between riser and vessel, allowing the recirculation, is located at nearly 60% of the thermal height.

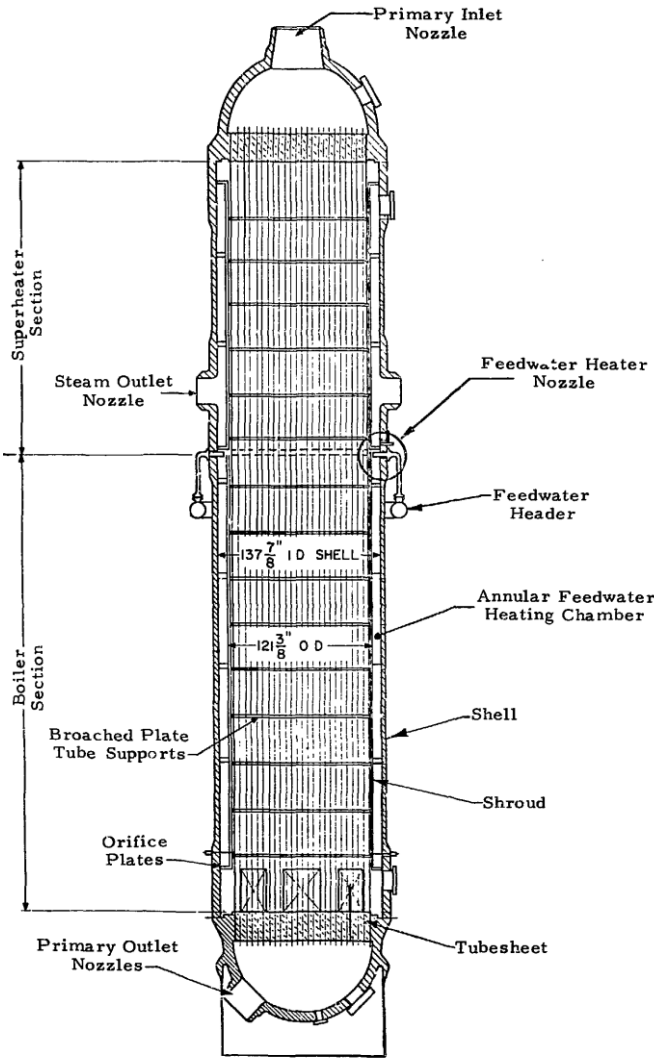

Figure 3.7 – Once-through steam generator layout, [70].

Table 3.6 – BZ OTSGs features, [67].

Parameter	**Unit**	**Value**
Number of units (per PHTS)	-	2
Rated Power (per component)	MW	742
Number of tubes	-	7569
Thermal height	m	12.99
Tube outside diameter	mm	15.88
Tube thickness	mm	0.89

Pitch to diameter ratio	-	1.28
Lattice	-	square
Heat transfer area	m^2	4903
Vessel external diameter	m	2.9
Thermal insulation	mm	100
Design temperature	°C	345
Design pressure	MPa	17.83

3.4.4 FW HEXs

FW HEXs are vertical, U-shaped, pure counter-current, water-molten salt heat exchangers. Their reference layout is shown in Figure 3.8. Primary coolant flows within tubes. PHTS hot and cold legs are connected to the bottom of inlet and outlet plenum. The heat exchanger shell side belongs to the intermediate loop. HITEC enters and exits the component laterally, near to the bottom. By design, the molten salt velocity was kept below 3 m/s to avoid excessive corrosion and erosion phenomena on the steel surfaces. For this reason, an INCONEL alloy was chosen for tube bundle. According to their pre-conceptual design, PHTS water thermal cycle is the same of BZ OTSGs (see previous section). HITEC is admitted at low pressure (still to be defined) and 280 °C and exits at 320°C. Table 3.7 summarizes the main HEX parameters, [67].

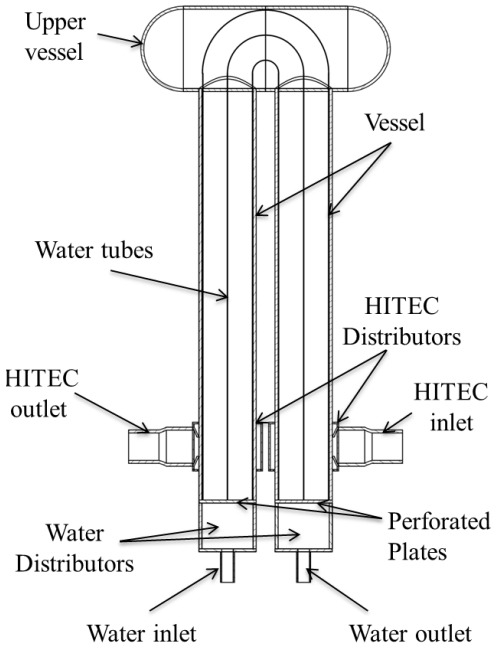

Figure 3.8 – FW heat exchanger layout, [67].

Table 3.7 – FW HEXs features, [67].

Parameter	Unit	Value
Number of units (per PHTS)	-	2
Rated Power (per component)	MW	220
Number of tubes	-	5211
Thermal height	m	28.9
Tube outside diameter	mm	15.88
Tube thickness	mm	0.89
Pitch to diameter ratio	-	1.28
Lattice	-	square
Heat transfer area	m^2	7513
Vessel external diameter	m	1.9
Thermal insulation	mm	100
Design temperature	°C	345
Design pressure	MPa	17.83

3.4.5 PHTS pressure control system

In each PHTS circuit, the pressurizer system guarantees the pressure control function, maintaining the water pressure at the required value independently on the temperature variations of the coolant induced by the pulsed plasma operation and, in general, by other transient conditions. The main component of this system is the steam bubble pressurizer, connected to the loop 1 hot leg by means of a surge line. Since the water thermodynamic conditions are similar, for both BZ and FW PHTS, the pressurizer volume was scaled from PWR design, [69]. The scaling factor adopted was based on the ratios between circuit total inventories and reactor total thermal power. A further safety margin was applied and the resulting component size increased.

The pressurizer is equipped with On/Off and proportional electric heaters and a spray line connected to the loop 1 cold leg and controlled by a valve. These systems are installed to face, respectively, under and overpressure transients occurring during both normal operations and abnormal conditions. The proportional heaters are set to operate in a range of pressure around the PHTS loop reference one. These heater banks are supplied by a varying input current that is a function of the pressure deviation signal. Normally, these components are energized at half current when pressure is at nominal value (null error), are cut off when this parameter reaches the higher setpoint and are at full power with pressure at lower setpoint. Instead, pressurizer

backup heaters are normally de-energized heater banks turning on if pressure drops below the setpoint adopted for this component (lower than the one of the proportional heaters). They are simply on-off type with no variable control. The heaters electrical power was scaled from PWR design, [69], by using a scaling factor based on reactor thermal power and applying a safety margin. The spray valve controller is set to modulate the valve flow starting from a lower setpoint up to a higher one correspondent to the fully open status. Pressurizer sprays operate to prevent lifting of the relief valve. The cold leg water admitted through these components is extremely effective in limiting pressure increases during transient or accident conditions. The correspondent flow capacity was sized by scaling from PWR design, [69].

In case of abnormal transients, if spray nozzles fail in reducing pressure, at the top of pressurizer is also foreseen the presence of a Pilot (Power)-Operated Relief Valve (PORV) and a Safety Relief Valve (SRV). A dedicated line connects these components to the pressure relief tank, allowing the discharge of steam. The PORV is provided for plant operational flexibility and for limiting the number of challenges to the pressurizer SRV. For this reason, the former is provided with a lower setpoint than the latter.

The main design data related to both BZ and FW PHTS pressurizer systems are contained in Table 3.8, [67]. An overview of the pressurizer component and related equipment is shown in Figure 3.9, [69]. The pressure control function setpoints, chosen considering the PWR design [71], are gathered in Table 3.9, [67].

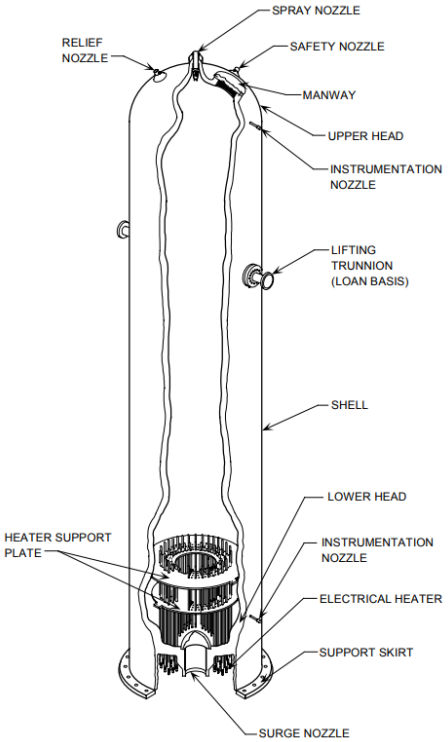

Figure 3.9 – Overview of pressurizer component and related equipment, [69].

Table 3.8 – BB PHTS pressure control system features, [67].

Parameter	Unit	FW PHTS	BZ PHTS
Pressurizer volume	m^3	39.3	101.5
Proportional heater bank power	kW	800	1200
On/Off heater bank power	kW	1600	2400
Spray line flow capacity	kg/s	17.9	36.2
PORV throat section	m^2	1.52 × 10−3	1.84 × 10−3
SRV throat section	m^2	1.52 × 10−3	1.84 × 10−3
PORV/SRV area change rate[1]	s^{-1}	10	10

[1] Valve area change rate is the reciprocal of the valve opening/closing time.

Table 3.9 – BB PHTS pressure control function, [67].

Parameter	Unit	FW PHTS	BZ PHTS
Reference Pressure	bar	155	155
Proportional heater bank lower setpoint	bar	154	154
Proportional heater bank higher setpoint	bar	156	156
Back-Up heater bank on/off setpoint	bar	154	154
Spray Valve start opening setpoint	bar	157	157
Spray valve fully open setpoint	bar	160	160
PORV valve opening setpoint	bar	170	170
PORV valve closing setpoint	bar	165	165
SRV opening setpoint	bar	178	178
SRV closing setpoint	bar	173	173

3.5 Integration of Breeding Blanket with PHTS.

Each WCLL blanket sector is linked to the PHTS through the in-vessel piping system, shown in Figure 3.10, [67]. It consists of Feeding Pipes (FP) and sector manifolds. The former are vertical

pipes connected to the back of the segments and managing the inlet/outlet of FW and BZ primary coolant from blanket. Sector manifolds link the feeding pipes to the PHTS hot and cold rings. These pipelines are routed through the upper port associated to each DEMO vacuum vessel sector and continue also outside VV. Table 3.10 collects the main data related to feeding pipes and sector manifolds.

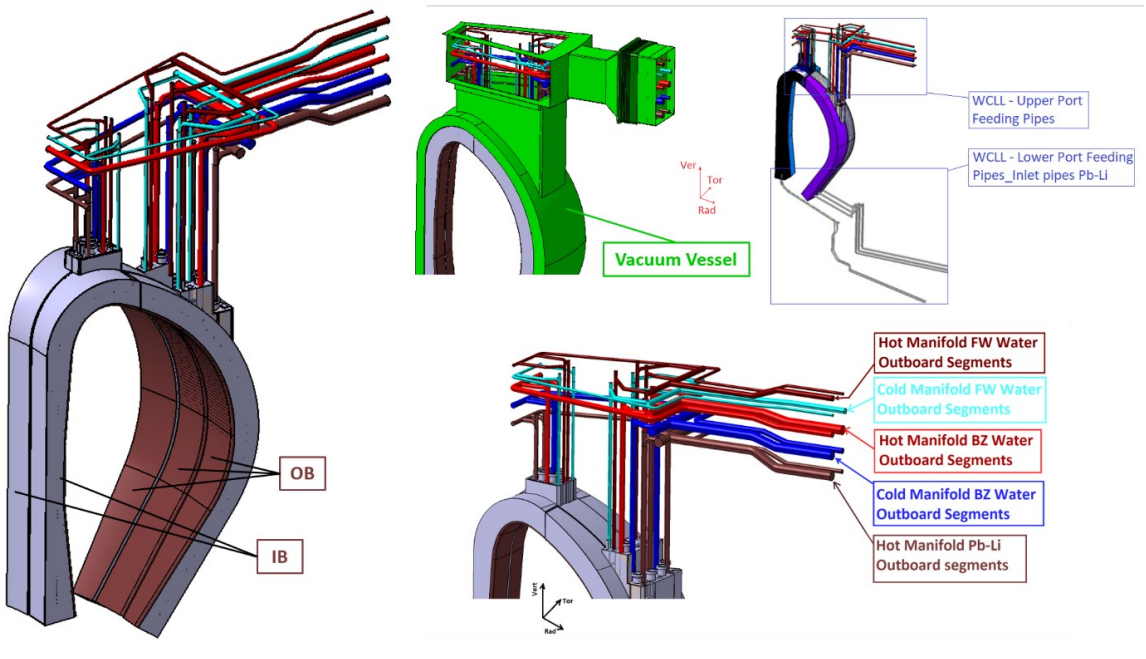

Figure 3.10 – Integration between WCLL blanket and PHTS, [67].

Table 3.10 – BB PHTS integration pipeline features, [67].

Parameter	DN (EN 10220, [68])	Thickness [mm]	Total Length [m]
FW IB inlet distributors	DN-100	8.8	281.2
FW LIB/RIB inlet FPs	DN-100	8.8	186.5
FW LIB/RIB outlet FPs	DN-100	8.8	203.9
FW IB outlet collectors	DN-100	8.8	281.2
BZ IB inlet distributors	DN-200	17.5	280.3
BZ LIB/RIB inlet FPs	DN-150	12.7	128.1
BZ LIB/RIB outlet FPs	DN-150	12.7	149.1
BZ IB outlet collectors	DN-200	17.5	279.9
FW OB inlet distributors	DN-200	17.5	180.8
FW COB inlet FPs	DN-125	11.0	126.4

FW LOB/ROB inlet FPs	DN-125	11.0	293.9
FW COB outlet FPs	DN-125	11.0	133.1
FW LOB/ROB outlet FPs	DN-125	11.0	301.6
FW OB outlet collectors	DN-200	17.5	183.3
BZ OB inlet distributors	DN-350	28.0	170.3
BZ COB inlet FPs	DN-200	17.5	111.5
BZ LOB/ROB inlet FPs	DN-200	17.5	236.1
BZ COB outlet FPs	DN-200	17.5	122.7
BZ LOB/ROB outlet FPs	DN-200	17.5	267.9
BZ OB outlet collectors	DN-350	28.0	176.3
Total			**4094.1**

3.6 Intermediate heat transfer system

The IHTS delivers power from FW PHTS to PCS, [64]. The system function is to flatten the pulsed operating regime of DEMO reactor according to the design requirement of continuous and nearly constant electrical power delivered to the grid. The intermediate coolant is HITEC Molten Salt (MS). IHTS is equipped with an Energy Storage System that accumulates a fraction of the FW thermal power during the plasma pulse and deliver it to the PCS during the dwell time. The power fraction to be accumulated during pulse is calculated to obtain a constant turbine load during the overall operating regime (pulse and dwell). The energy storage is constituted by a system of two tanks filled with molten salt at different temperatures. During pulse, there is a net HITEC flow rate going from the cold tank to the hot one and here accumulated. During dwell, the hot molten salt flows through the Helicoidally Coil Steam Generators and power is delivered to the PCS. The list of the IHTS main components is reported in Table 3.11. All the data related to IHTS vessel components and piping are derived from [64]. The operating parameters of FW HEXs and IHTS HCSGs during both pulse and dwell are collected in Table 3.12 and Table 3.13, [64].

Table 3.11 – DEMO WCLL ICD option: IHTS list of components, [64].

Component	**#**
Cold tank (CT)	1
Pipelines from CT to FW HEXs	2
FW HEXs (shell side)	2
Pipelines from FW HEXs to hot tank	2
Hot Tank (HT)	1

Pipelines from HT to HCSGs	8
HCSGs	4
Pipeline from HCSGs to CT	8

Table 3.12 – FW HEXs operating parameters during pulse and dwell phases, [64].

Parameter	**Unit**	**Pulse**	**Dwell**
FW HEXs operating power	MW	220	0
N° of operating units	-	2	0
PHTS water inlet temperature	°C	295	~310[1]
PHTS water outlet temperature	°C	328	~310[1]
PHTS water mass flow	kg/s	1136.8	1136.8
MS inlet temperature	°C	280	280
MS outlet temperature	°C	320	280
MS mass flow	kg/s	3524	0

[1] See **§** 4.4.1 for further details.

Table 3.13 – HCSGs operating parameters during pulse and dwell phases, [64].

Parameter	**Unit**	**Pulse**	**Dwell**
N° of operating units	-	1	4
HCSGs operating power	MW	266.2 (1) 0 (3)	521.60
MS inlet temperature	°C	320	320
MS outlet temperature	°C	280	280
MS mass flow	kg/s	4266 (1) 0 (3)	8345
PCS water pressure	MPa	6.41	6.41
PCS water inlet temperature	°C	238	238
PCS water outlet temperature	°C	299	299
PCS water mass flow	kg/s	145 (1) 0 (3)	284.2

4 DEMO WCLL BB PHTS TRANSIENT ANALYSIS

4.1 Thermal-hydraulic model

4.1.1 Nodalization techniques

To carry out the simulation activity, a full model of the blanket component and correspondent PHTS circuits was prepared by using RELAP5/Mod3.3 system code, [35]. In particular the modified version developed at DIAEE was used (see **§** 2, [37]). General rules to obtain a good mesh were all followed when realizing the reactor nodalization.

- The node to node ratio is defined as the ratio between the length of two adjacent control volumes. Within the overall mesh, it should be kept as uniform as possible. In this way, nodalization results more homogeneous, reducing the possibility of numerical error occurrence. The chosen reference value was of 1.25.

- The 'Slice nodalization technique' was adopted while realizing the nodalization scheme. A vertical segmentation of the overall system to be modelled, i.e. the DEMO WCLL BB PHTS, was performed on the basis of reference selected quotes. Such quotes were chosen to keep the actual design elevations. The axial mesh related to all the system components (in/out-vessel piping, BZ OTSGs, FW HEXs, pumps, pressurizers) was obtained respecting these reference fixed heights. As a result, the same mesh length (or submultiple) was used for the vertical control volumes belonging to different nodalization regions positioned at the same axial level. This technique improves the capability of the code to reproduce natural circulation. When adopted, fluid properties are evaluated at the same axial elevations for all the nodalization regions, resulting in a proper evaluation of the natural circulation driving force and avoiding an error source on the simulation outcomes, [72].

- The fluid and material inventories were rigorously maintained. In such a way, the system thermal inertia was simulated in the best possible manner, as well as its thermal-hydraulic behavior (i.e. pressure drops, heat transfer, etc.).

In the following sections, the RELAP5 thermal-hydraulic model is described in detail. In particular, **§** 4.1.2 reports the properties used for fluids and materials. For sake of clarity, the tables associated to this section are reported in annex A1. **§** 4.1.3 and 4.1.4 describe the nodalization adopted for blanket component and out-vessel BB PHTS, respectively.

4.1.2 Fluids and materials

4.1.2.1 Fluids

In RELAP5 code, for each system, a fluid type must be specified. Its properties, adopted in all the code packages (pressure drops, heat transfer, etc.) are stored in an external data file, named *tpf + fluid name*, [35]. For example, the one related to water is called *tpfh2o*. To add new working fluids or modify the properties of an existing one such files must be added or updated.

DEMO WCLL primary coolant is water at typical PWR conditions: pressure 15.5 Mpa and temperature at blanket inlet/outlet of 295-328 °C. Water properties adopted for calculations are the ones implemented in the original version of RELAP5/Mod3.3 code, [13].

The molten salt selected for DEMO IHTS application is HITEC. It is a ternary mixture of the nitrate and nitrite salts $NaNO_3$, $NaNO_2$ and KNO_3 with a molar composition of 7:49:44 and a weight composition of 7:40:53, [38]. HITEC molten salt could not be selected as working fluid in RELAP5/Mod3.3. The fluid, as well as its thermal properties, was introduced in the DIAEE version of the code, as stated in **§** 2.2.1. The experimental correlations selected to simulate the molten salt thermal-hydraulic behavior are collected in Table 2.2. An external data file named *tpfhit* was prepared for this purpose.

4.1.2.2 Materials

For solid materials involved in the heat transfer problem, RELAP5 code prompts the user to enter the needed thermal properties. The required input consists of two tables collecting the thermal conductivity and heat capacity trends against temperature, [35]. These properties were used to solve the Fourier's law for heat conduction in solid layers, [75].

The structural material adopted for DEMO WCLL blanket is a Reduced Activation and Ferritic/Martensitic steel developed and produced in Europe, for this reason designated EUROFER-97, [59][60]. The thermal properties used for this study are discussed in [73][74] and gathered in Table A1.2.

In DEMO WCLL blanket, liquid lead-lithium deserves as breeder, neutron multiplier and tritium carrier. In the blanket model adopted for the current simulation activity the PbLi is not simulated as a working fluid but as a solid layer belonging to RELAP5 heat structure components. The reasons behind this modelling choice are discussed in **§** 4.1.3. The material properties, already reported in **§** 2.2.1, were entered in the input deck as illustrated by Table A1.3.

The FW plasma facing area is protected by a tungsten layer of 2 mm thickness (see **§** 3.2). This armour is foreseen to avoid pollution of plasma by carbon resulting from sputtering between the particles escaping the plasma and the blanket structural materials, [59][60]. Thermal properties entered in the model for this material were derived from [75] and collected in Table A1.4.

For the PHTS pipelines the material selected is AISI 316L(N) (ASTM UNS S31653). It is also used for BZ OTSGs and FW HEXs shell and internals, [57]. It was chosen since applicable at the DEMO WCLL PHTS design temperature (345 °C) and due to its high weldability and corrosion resistance. The austenitic steel thermal properties were taken from ASME BPVC Section II, [76]. They were entered as tabulated in Table A1.5.

All the PHTS pipelines and vessel components are provided with thermal insulation to avoid excessive loop heat losses. The insulator thickness varies from component to component according to its reference operating temperature. Design values were obtained from [67]. An example of suitable material for PHTS application is reported in [77]. Its thermal properties, shown by Table A1.6, were preliminary used for calculation purposes.

The BZ OTSGs and FW HEXs tube material selected is INCONEL 690 (ASTM UNS N06690), [67]. This material has more favorable mechanical properties than AISI 316 L(N) allowing to reduce tubes thickness while substantially maintaining the same thermal conductivity. The material properties were derived from ASME code [76] and entered in the model as in Table A1.7.

The PHTS pressurizers (one for each system) are equipped with electrical heaters to compensate negative coolant density fluctuations. Both a proportional bank and an On/Off back-up bank are present (see **§** 3.4.5, [67]). These electrical heaters consist in a bundle of Heating RoDs (HRD)

located nearly at the tank bottom. Watlow® datasheet were preliminary selected as reference for the HRD design parameter, [78]. Within the HRDs, constantan is used as electrical conductor and a ceramic material as insulator. HRDs are also provided with an external layer of ALLOY 800 (ASTM UNS N08811) to increase the corrosion resistance. The constantan and ceramic thermal properties were taken from [78], while for ALLOY 800 ASME code was used [76]. Thermal properties for these materials are contained in Table A1.8, Table A1.9 and Table A1.10. The list of references adopted is collected in Table 4.1.

Table 4.1 - References adopted for material properties.

Material	**References**
EUROFER97	[73][74]
Lead-lithium	[39]
Tungsten	[75]
AISI 316L(N)	[76]
Thermal insulator	[77]
INCONEL 690	[76]
Constantan	[78]
Ceramic	[78]
ALLOY 800	[76]

4.1.3 Blanket

From the hydrodynamic point of view, each blanket sector was simulated by using a dedicated batch of hydraulic components and by separating the hydraulic models of BZ and FW primary circuits. Nevertheless, the two systems are thermally coupled within the breeding cell. For this, RELAP5 heat structure components were used to simulate in detail the heat transfer phenomena taking place inside the BRC. During transient simulations, the BZ and FW thermal coupling has a significant influence on the circuit thermal-hydraulic behavior.

As discussed in **§** 3.2, each DEMO sector is constituted by five poloidal segments (three for OB and two for IB). The BZ and FW cooling circuits here contained were collapsed in some equivalent pipe components, three for each PHTS. The OB and IB segments were grouped as following: LOB/ROB, COB, LIB/RIB. LOB and ROB, as well as LIB and RIB, were lumped since they have similar design (still at a preliminary stage) and the same thermal-hydraulic performances were expected for them.

For both BZ and FW PHTS, each of the three equivalent pipes model the overall water flow path inside the vacuum vessel. The components associated to each segment and considered for simulation purposes are: (1) inlet feeding pipe; (2) inlet spinal water manifold; (3) DWTs or FW channels; (4) outlet spinal water manifold; (5) outlet feeding pipe. The control volumes belonging to these equivalent pipes are characterized by different hydraulic properties (flow area, hydraulic diameter, etc.) in order to properly simulate all the aforementioned components. For the equivalent pipes corresponding to LOB/ROB and LIB/RIB, the control volume flow area and hydraulic diameter, as well as the water mass flow, were evaluated considering the reference data belonging to both segments. In such a way, the pressure drops through these components

were correctly modelled. For the inlet/outlet feeding pipes, as well as the sector collectors and distributors, geometrical properties and routing were derived from CAD model, differentiated for each segment. Pipeline features were maintained in the input deck.

Regarding the breeding cell, the most studied design belongs to the one located at the COB equatorial plane, [59]-[62]. For this reason, its layout was adopted as reference and also used for all the other BRCs poloidally distributed along the overall segment. Concerning the cells constituting ROB, LOB, LIB and RIB segments, the reference COB layout was scaled by using the material inventories derived from the CAD model.

DWTs, providing BZ cooling function, are in parallel within the breeding cell. They are split into three arrays along the radial direction. Each array is characterized by a different C-shape in the radial-toroidal plane, [61][62]. Such complex flow path for BZ coolant was modelled by lumping all the DWTs in parallel and selecting a reference DWT layout. For this purpose, the second array was chosen, that is the mid-one along the radial direction. It was considered sufficiently representative of the average geometrical features of all the DWTs present in the breeding cell.

BZ and FW inlet/outlet water manifolds consist in spinal rectangular channels running along the back of the segment, radially inwards with respect to the back supporting structure (see Figure 3.3). They follow the segment curved profile. For the equivalent pipe components related to IB segments, the manifold length was assumed equals to half the segment length along the external curved profile. Instead, for the pipes related to OB segments, the length adopted was the previous one minus the height difference between the top of the OB segments and the elevation where the OB feeding pipes are connected (see Figure 3.2 and Figure 3.10). This modelling approach allowed to locate, for all the segments, the control volumes representing the DWTs or the FW channels at the tokamak mid-quote. Assuming in first approximation a constant power source term along the poloidal direction, the tokamak mid-quote corresponds also to its thermal center. Hence, in the RELAP5 model, the design height difference between heat source (blanket breeding cells) and heat sink (the BZ OTSGs and the FW HEXs) thermal centers was maintained. This parameter is of primary importance in all the transients concerning natural circulation, such as in LOFA. In a first approximation, COB manifold layout, described in [59], was also used for LOB/ROB and LIB/RIB segments. For any segment, control volume flow area was calculated to maintain the BZ and FW water manifolds inventory. Hydraulic diameter was evaluated based on the actual manifold geometry.

The RELAP5 heat structure components were used in the input deck to accomplish several functions: account for the blanket solid material inventories (tungsten and EUROFER-97); simulate the breeder (simplifying the input); introduce the power source terms (heat flux and nuclear heating); represent the heat transfer phenomena taking place within the breeding cell; model the pipeline thermal insulation (for sector collectors/distributors and inlet/outlet feeding pipes).

The lead-lithium flow path through the blanket was not modelled in this work from a hydrodynamic point of view. This allows to reduce the number of overall control volumes present in the model and the correspondent simulation time. Within the breeding cell, where the thermal exchange between PbLi and DWTs/FW channels is significant, the liquid metal convective heat transfer coefficient was neglected and only the conductive heat transmission was considered, simulating the lead-lithium as a layer of structural material belonging to RELAP5 heat structures. However, the breeder velocity inside the breeding cell is very low (0.01 mm/s, [59]). Hence, preliminarily, the convective contribution to the heat transfer should be negligible.

A dedicated heat structure was used to simulate the FW front surface. A tungsten layer and a EUROFER thickness were modelled. The EUROFER thickness is the actual one present between the

plasma chamber and the FW cooling channels. The heat flux reported in [61] was applied as boundary condition for the plasma-facing surface. An average value was adopted since no poloidal differentiation was considered in the model. The radial segments of the FW component were simulated with a separate heat structure. In this case, only a EUROFER thickness was considered since the tungsten armor is not present. To take into account the heat transfer between FW channels and DWTs, a further heat structure was added. In the radial-toroidal plane, DWTs are divided into three arrays with different layouts. The same DWT reference layout chosen for the hydrodynamic model was used in the thermal problem also. The radial distance between the FW cooling channels and the selected DWT is composed by: a first EUROFER layer, representing the FW thickness between FW cooling channels and FW internal surface; a PbLi layer, corresponding to the radial distance between the FW internal surface and the selected DWT layout; a second EUROFER layer, modelling the DWTs thickness. This heat structure allows to thermally couple the BZ and FW cooling circuits. Heat transfer between DWTs and PbLi inside the breeding cell is not limited to the contribution modelled with this HS component. The other heat transfer phenomena were also simulated by means of another dedicated heat structure. This component is also useful to account for the total breeder inventory within the breeding cell. Finally, two further heat structures were used to model the EUROFER inventory in the water and PbLi manifold region and in the back supporting structure, respectively.

Nuclear heating associated to each heat structure component was computed thanks to the power density radial profiles presented in [62] and by considering the actual material inventory distribution within the breeding cell, (see Figure 3.3). It was introduced in the input deck as an internal power source term, differentiated for each heat structure. For each sector, the batch of heat structures described so far (six) was replicated for LOB/ROB, COB and LIB/RIB (for a total of eighteen).

The pipeline heat losses were modelled considering as external boundary conditions a constant containment temperature (30 °C), and a constant heat transfer coefficient (8 W/m2K). The HTC considered is the sum of the convective and radiative contributions. For lower temperatures (< 50 °C), as in the case of the pipeline insulation external surface, the correlation for radiative HTC can be linearized, and this term can be sum to the convective one. The specific value adopted for the overall HTC derives from engineering judgement and experience.

A schematic view of the blanket nodalization is provided in Figure 4.1. The model shown refers to only one of the sixteen identical toroidal sectors. For further details regarding the blanket nodalizations see annex A2.

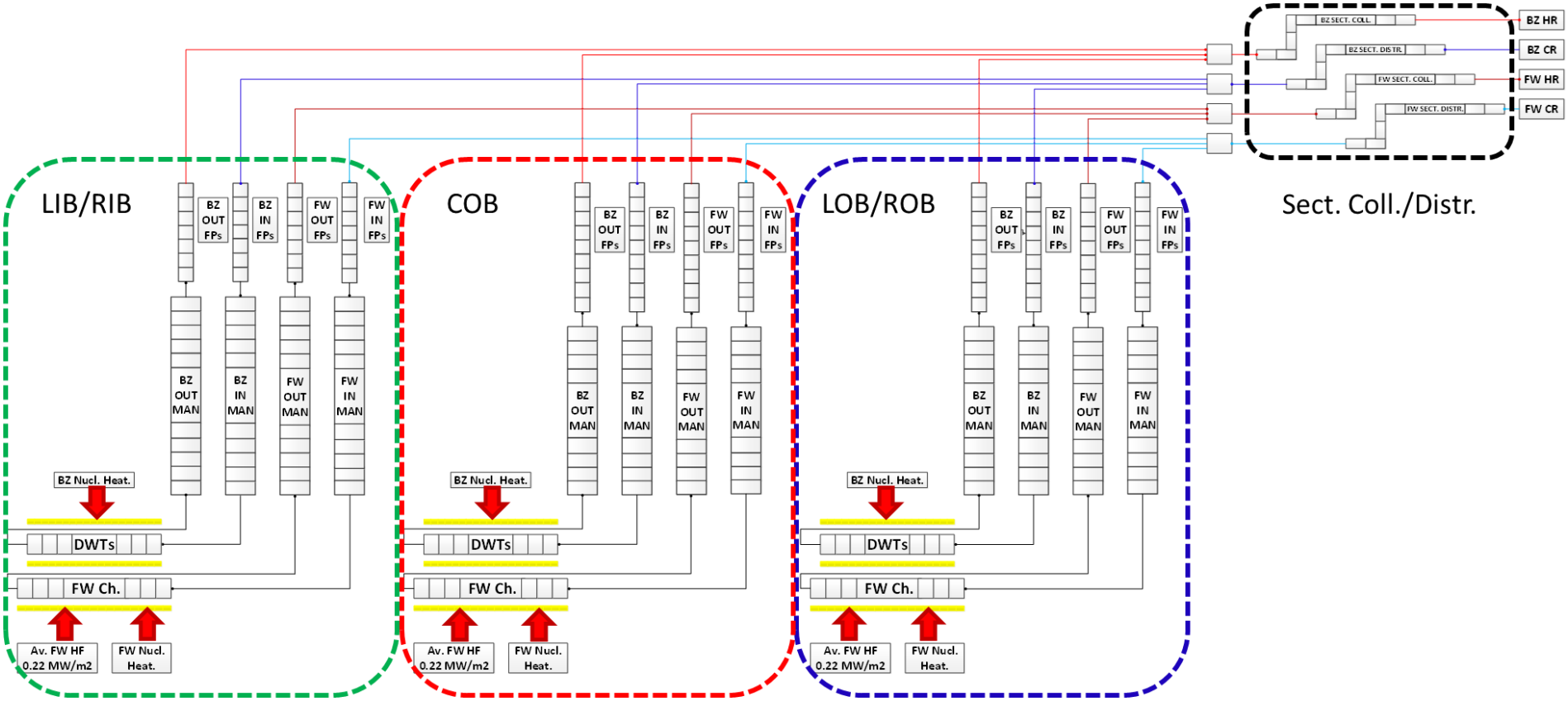

Figure 4.1 – Schematic view of RELAP5 blanket model (sector one of sixteen).

4.1.4 PHTS

Referring to the primary cooling system section outside the vacuum vessel, all main equipment and pipelines were modelled in detail by using one-dimensional components. The schematic view of one (of two) PHTS loop is provided by Figure 4.2 and Figure 4.3, respectively for BZ and FW. The routing of the BB PHTS pipelines was derived from the current CAD model. K-loss coefficients for tees, elbows and area changes were calculated by using formulas in [79]. They were associated to pipe component internal junctions to correctly evaluate the concentrated pressure drops. A pipe component was adopted to simulate each line separately (i.e. hot and cold legs, loop seals). Hot and cold rings have a dedicated model made up of four pipes and two multiple junctions. Each pipe simulates a quarter of the ring (90°). One multiple junction component manages the connections between pipes (to close the ring) and between the rings and the hot/cold legs. The other multiple junction component links the hot/cold rings with the sector collectors/distributors. These connections are equally distributed along the overall ring length to maintain the toroidal symmetry characterizing the DEMO reactor. Pipeline modelling is visible in Figure 4.2 and Figure 4.3. An example of ring nodalization is shown in Figure 4.4. Pipeline thermal insulation was modelled associating a heat structure to each pipe component. The external surface boundary condition adopted for these heat structures was the tokamak building atmosphere, modelled with a constant temperature and heat transfer coefficient. Their values are the same already discussed in **§** 4.1.3.

The BB PHTS pump system consists of six (four for the BZ and two for the FW) centrifugal single stage pumps. They are equally divided in the two loops constituting each PHTS. The MCPs were modelled by using RELAP5 pump components provided with a Proportional-Integral (PI) controller to set the design mass flow value.

The BZ OTSG design foresees PHTS water flowing inside the tube bundle and PCS water flowing in shell side. The same vertical mesh was adopted for the control volumes of all the RELAP5 components simulating the OTSG primary and secondary sides (see Figure 4.2). Primary side was modelled with two branches, representing the inlet and outlet hemispherical heads, and an equivalent pipe simulating the tube bundle. OTSG secondary side was simulated with four pipes, corresponding to lower/upper annular downcomer sections and to lower/upper riser sections. Each OTSG was provided with two steam lines to avoid excessive pipeline pressure drops due to steam velocity. Feedwater line was simulated with a time-dependent volume and a time-dependent junction to set the PCS water inlet thermodynamic conditions, and with a pipe to simulate the pipeline section before the OTSG entrance. Steam lines were modelled up to the Turbine Stop Valves (TSVs) and equipped with steam line Safety Relief Valves (SRVs). PCS SRVs consists in three steps of relief valves provided with increasing setpoint: 90%, 95% and 100% of the PCS system design pressure (115% of the operating pressure reported in [57],[60]). The relief valves related to step one, two and three were sized to discharge 75%, 37.5% and 37.5% of the OTSG steam mass flow, considering chocked flow occurring in the throat section. Hence, the full set of SRVs is able to discharge the overall OTSGs steam mass flow with an additional conservative margin of 50%. Main data related to PCS SRVs are collected in Table 4.2. RELAP5 heat structures were used to simulate the thermal transfer taking place within the steam generators, as well as the component heat losses. Furthermore, they allow to account for the OTSG steel inventory (i.e., thermal inertia).

Table 4.2 - PCS steam line SRV features.

SRV Parameter	Unit	Step 1	Step 2	Step 3
Throat section	m^2	1.80×10^{-2}	9.00×10^{-3}	7.50×10^{-3}
Area change rate[1]	s^{-1}	10	10	10
Opening setpoint	bar	66.4	70.0	73.7
Closing setpoint	bar	64.1	64.1	64.1

[1] Valve area change rate is the reciprocal of the valve opening/closing time.

FW HEXs are pure countercurrent heat exchangers with PHTS water and IHTS molten salt flowing inside tube bundle and shell, respectively. Primary side nodalization is similar to the one of the BZ OTSGs, while secondary side is modelled with an equivalent pipe component (see Figure 4.3). IHTS hot and cold legs were also included in the input deck. Also in this case, heat structures were used to simulate the heat transfer phenomena, the heat losses and the steel inventory related to each heat exchanger. The molten salt heat transfer coefficient was calculated with Sieder-Tate correlation, [47].

The time-dependent junctions located on the BZ OTSGs feedwater lines and FW HEXs IHTS side cold legs were provided with temperature control systems. They are required to obtain the design PHTS water temperature at blanket inlet, [59][60]. The BZ OTSGs and FW HEXs design was performed considering that they must exchange their nominal power when operating at End of Life (EOL) conditions. For this, both tube fouling and tube plugging phenomena were taken into account. At Beginning of Life (BOL) conditions, when no tube plugging and fouling factors are foreseen, the OTSGs and HEXs exchanged power exceeds the nominal value. This causes a significant alteration of the temperature field in the overall PHTS system and, in particular, at blanket inlet. To keep the PHTS parameters at the design values in BOL condition, a control system is required. It was developed to ensure constant water thermodynamic conditions at blanket inlet in any operational condition. PHTS temperature is read at OTSG/HEX outlet and then compared with the temperature target setpoint, [59][60], producing an error. The error signal is scaled by using a PI controller. The controller output range goes from zero to 110% of rated PCS feedwater/IHTS HITEC mass flow at EOL condition. The resulting output is the mass flow imposed by the time-dependent junctions simulating the BZ OTSGs and FW HEXs secondary side inlet. A scheme of the control logic implemented is shown by Figure 4.5.

Each PHTS circuit is equipped with a pressure control system (see Figure 4.2 and Figure 4.3). Its goal is keeping the water pressure at the required value, compensating the variations induced by eventual coolant temperature fluctuations and, in general, by other transient conditions. The main system component is the steam bubble pressurizer, connected to the loop one hot leg thanks to a surge line. They were both simulated with a dedicated pipe component. The associated heat losses were considered by using heat structures. The pressurizer is provided with On/Off and proportional electric heaters and a spray line connected to the loop one cold leg and controlled by a valve. These systems are installed to face, respectively, under and overpressure transients occurring during both normal operations and abnormal conditions. Pressurizer heaters were simulated with heat structures. The spray valve controller is set to modulate the valve flow starting from a lower setpoint up to a higher one correspondent to the fully open status. The surge and spray line routing was derived from CAD model and strictly maintained in the model. At the top of the pressurizer are also present a PORV and a SRV. They discharge steam in a dedicated

line connecting the pressurizer to the pressure relief tank (simulated with a time-dependent volume). The PORV is more used during normal operations while SRV is more safety-oriented. For this reason, the former is provided with a lower setpoint than the latter. PORV and SRV were modelled with RELAP5 valve components.

As stated in § 4.1.1, material inventories were strictly maintained in the input deck. Such modelling approach ensures to properly simulate the system thermal response during transient conditions. For the PHTS components outside vacuum vessel, a summary is provided by Table 4.3 and Table 4.4, respectively for BZ and FW primary circuits.

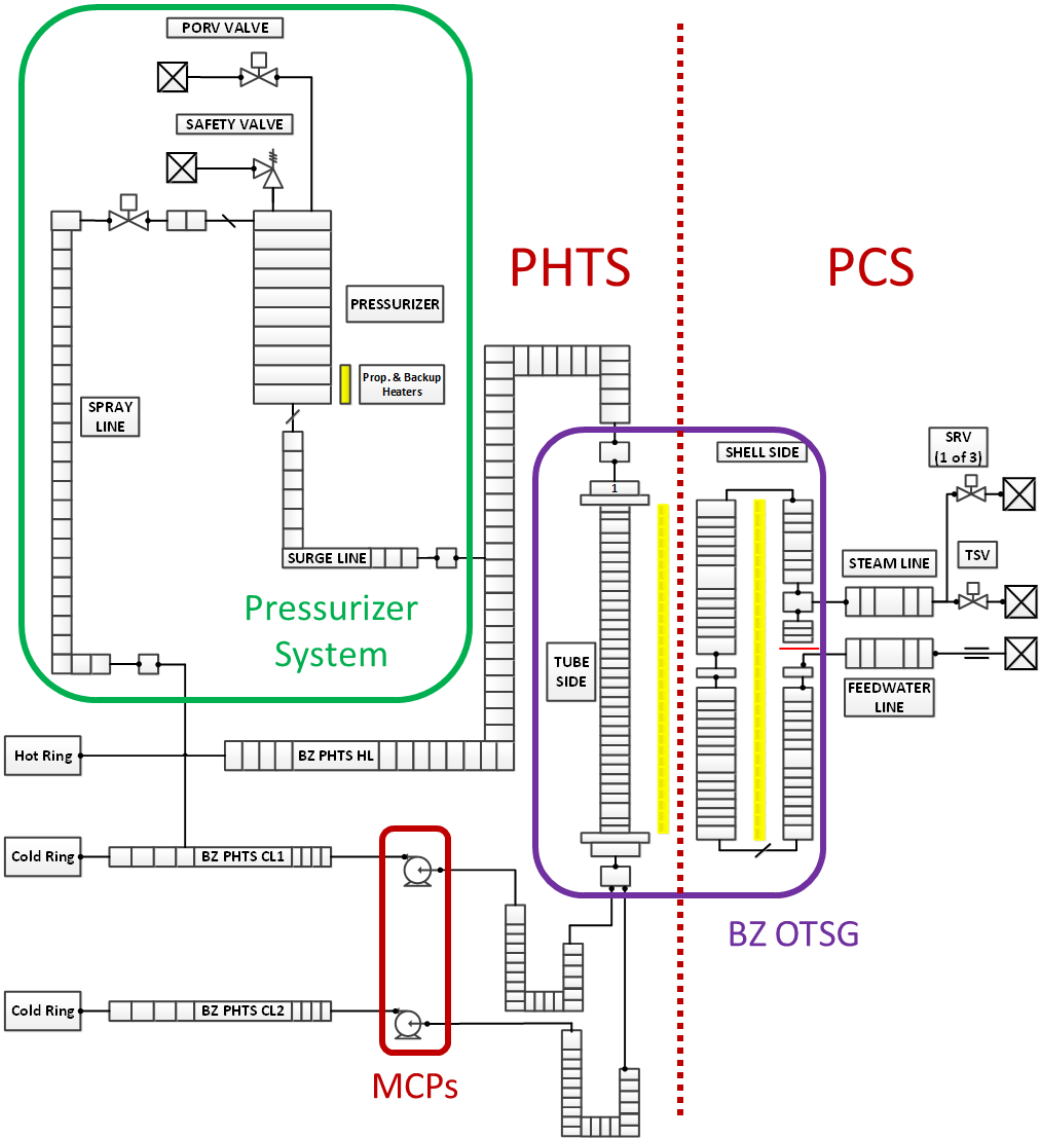

Figure 4.2 – Schematic view of the RELAP5 model related to BZ PHTS loop one.

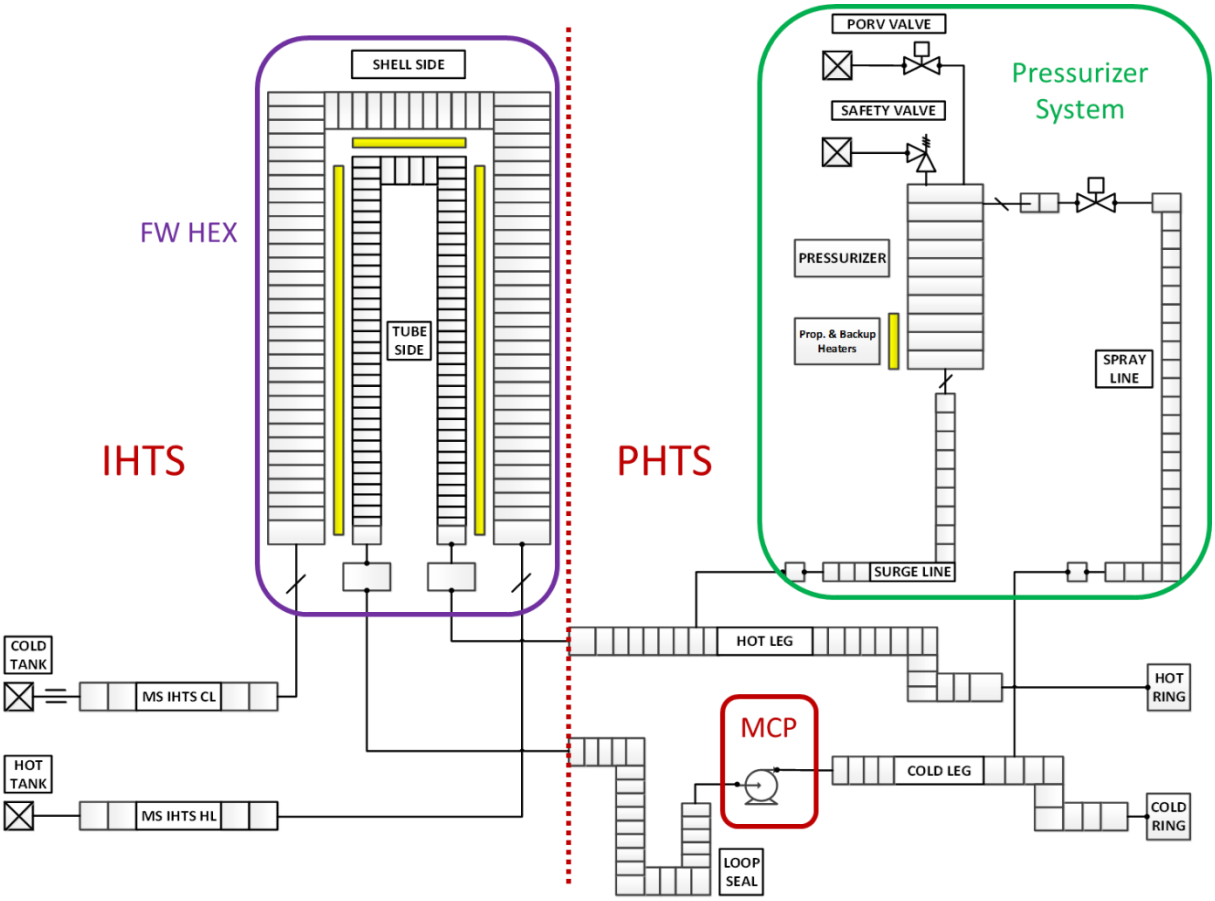

Figure 4.3 – Schematic view of the RELAP5 model related to FW PHTS loop one.

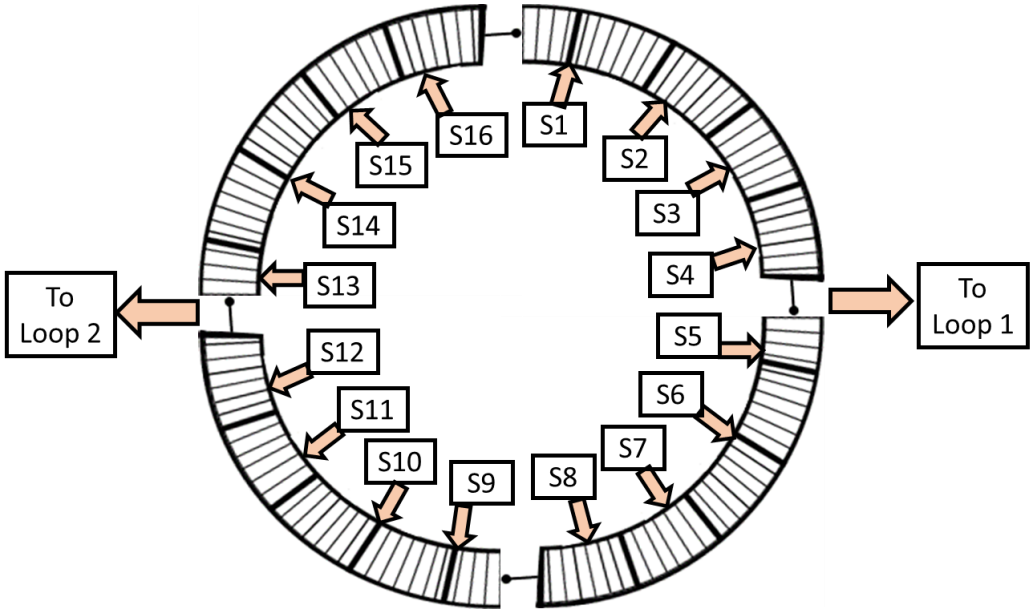

Figure 4.4 – Example of PHTS ring nodalization: FW hot ring.

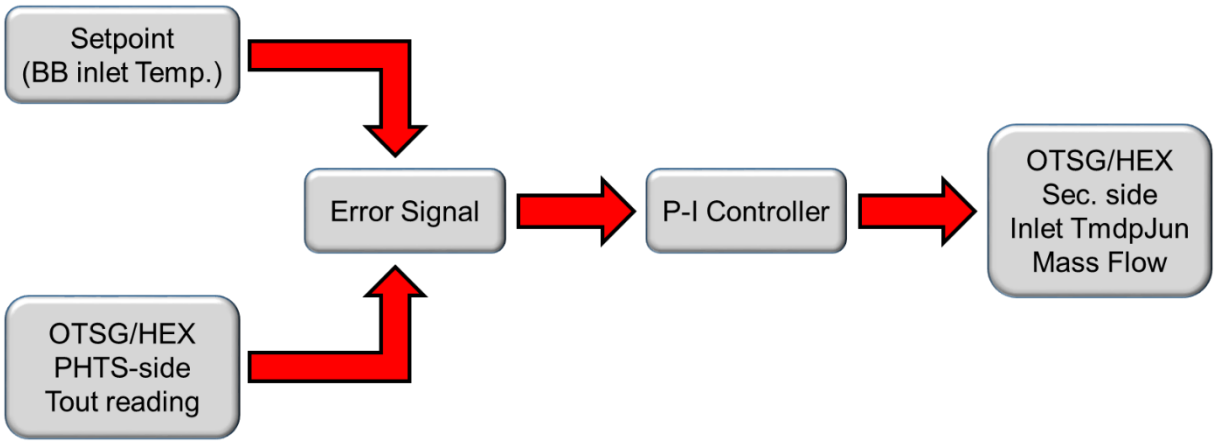

Figure 4.5 – Temperature control system implemented at BZ OTSGs/FW HEXs secondary side inlet.

Table 4.3 – Material inventories for BZ PHTS components outside vacuum vessel.

BZ PHTS Component	**Unit**	**Inventory [m^3]**					
		Water		**Steel**		**Thermal Insulator**	
		RELAP5	**Design**	**RELAP5**	**Design**	**RELAP5**	**Design**
Hot Ring	m^3	36.1	36.1	14.0	14.0	43.1	43.1
Cold Ring	m^3	36.1	36.1	14.0	14.0	35.0	35.0
Hot Legs	m^3	37.6	37.6	15.9	15.9	33.8	33.8
Loop Seals	m^3	5.5	5.5	2.1	2.1	5.3	5.3
Cold Legs	m^3	24.5	24.5	9.5	9.5	23.8	23.8
Surge Line	m^3	0.2	0.2	0.1	0.1	1.1	1.1
BZ OTSGs	m^3	48.8	48.8	88.7	88.7	32.4	32.4
Pressurizer	m^3	101.5	101.5	25.7	25.7	13.3	13.3
Total	**m^3**	**290.3**	**290.3**	**170**	**170**	**187.8**	**187.8**

Table 4.4 – Material inventories for FW PHTS components outside vacuum vessel.

FW PHTS Component	Unit	Inventory [m^3]					
		Water		Steel		Thermal Insulator	
		RELAP5	Design	RELAP5	Design	RELAP5	Design
Hot Ring	m^3	11.9	11.9	4.9	4.9	30.3	30.3
Cold Ring	m^3	11.9	11.9	4.9	4.9	24.2	24.2
Hot Legs	m^3	8.4	8.4	3.5	3.5	13.9	13.9
Loop Seals	m^3	3.2	3.2	1.3	1.3	4.2	4.2
Cold Legs	m^3	4.8	4.8	1.9	1.9	6.3	6.3
Surge Line	m^3	0.4	0.4	0.2	0.2	2.0	2.0
FW HEXs	m^3	54.1	54.1	51.9	51.9	40.1	40.1
Pressurizer	m^3	39.3	39.3	10.2	10.2	7.3	7.3
Total	**m^3**	**134**	**134**	**78.8**	**78.8**	**128.3**	**128.3**

4.2 Transient analysis

The following sections present the main results obtained performing the thermal-hydraulic transient analysis of the BB PHTS cooling circuits. For this purpose, the RELAP5 model discussed so far was used. Firstly, in **§** 4.3, full plasma power condition at Beginning of Life was simulated. The system behavior in this scenario was fully characterized. Simulation outcomes were compared with design values in order to assess the appropriateness of the thermal-hydraulic model prepared.

Then, this steady-state calculation was used as initial condition to simulate some operational and accidental transients. The DEMO reactor normal operations were simulated, including both pulse and dwell phases (**§** 4.4.1). The BB PHTS performances were analyzed. Moreover, in the same section, it is presented a benchmark exercise involving DEMO reactor power fluctuations (**§** 4.4.2). System codes results were compared with the more detailed ones obtained with ANSYS CFX in order to evaluate the effectiveness of the thermal-hydraulic model developed for the blanket component.

Finally, the blanket primary cooling system response during accidental conditions was investigated. The selected transients to be studied belong to the category of "Decrease in reactor coolant system flow rate" (**§** 4.5). This transient analysis was aimed at understanding the thermal-hydraulic response of the blanket component and related primary circuits. In this way, it was possible to evaluate the appropriateness of their pre-conceptual design and the eventual need of mitigation actions to withstand such accidental scenarios.

4.3 Full plasma power state

Full plasma power state at beginning of life condition was simulated. The total blanket thermal power indicated in Table 3.2 was supplied as boundary condition. It was distributed between different source terms: FW heat flux, FW nuclear heating and BZ nuclear heating. The blanket heat structures, discussed in **§** 4.1.3, were used for this purpose.

PCS feedwater thermodynamic conditions at OTSG inlet were imposed as boundary conditions (see **§** 3.4.3). The same was done for HITEC molten salt at HEX secondary side inlet (see **§** 3.4.4). RELAP5 time-dependent volumes were used. Time-dependent junctions simulating PCS feedwater/IHTS HITEC mass flow were provided with temperature control systems, as described in **§** 4.1.4. Finally, FW and BZ primary pumps were equipped with PI controller to match the design mass flow in both PHTS circuits.

Another key issue to cope with while simulating the BB PHTS was evenly distribute the total system mass flow among the sixteen tokamak sectors. Such orificing procedure was needed since the hot and cold rings introduce an asymmetry between different water flow paths. The connections between sector manifolds and rings are equally distributed along the ring circumference (i.e. toroidal coordinate). Instead, the connections between hot/cold legs and rings are diametrically opposed, at the distance of half a ring one to each other. Hence, there are sectors more or less distant from the loop connections. This produces a hydraulic dissymmetry in the different water flow paths and a non-uniform distribution of the total PHTS mass flow among the sixteen sectors. The orificing strategy consisted in the addition of concentrated pressure drops at the inlet of sector distributors, differentiated for each sector. In the RELAP5 model, K-coefficients were used to simulate such minor head losses. The outcomes of the orificing procedure are collected in Table 4.5.

Table 4.5 – Full plasma power state: outcomes of orificing procedure.

	BZ PHTS		FW PHTS	
Sector	**Δp [kPa]**	**Mass flow [kg/s]**	**Δp [kPa]**	**Mass flow [kg/s]**
1	113.4	478.8	63.4	141.8
2	107.1	478.6	57.2	141.9
3	97.5	478.9	52.4	142.1
4	87.6	479.3	52.4	142.6
5	87.6	479.3	52.4	142.6
6	97.5	478.9	52.4	142.1
7	107.0	478.6	57.2	141.9
8	113.3	478.8	63.4	141.8
9	113.3	478.8	63.4	141.8
10	107.1	478.6	57.2	141.9
11	97.6	478.9	52.4	142.1
12	87.7	479.3	52.3	142.6
13	87.6	479.3	52.3	142.6
14	97.5	478.9	52.4	142.1
15	107.0	478.6	57.2	141.9
16	113.2	478.8	63.4	141.8

Table 4.6, Table 4.7, Table 4.8 and Table 4.9 summarize the main simulation outcomes. The parameters indicated in the tables with (BC) are the ones set as boundary conditions. A time step sensitivity was performed, varying this parameter from 1.0×10^{-3} s to 5.0×10^{-3} s. No sensible differences in the results were observed. Results in Table 4.6 to Table 4.9 are for a time step of 5.0×10^{-3} s.

Table 4.6 – Full plasma power state: BZ PHTS and PCS main parameters.

System	**Parameter**	**Unit**	**RELAP5**	**Design**	**Rel. Diff. [%]**
PHTS	Mass flow (per pump)	kg/s	1915.6	1915.6	0.00%

	Hot leg temperature	°C	328.2	328	0.06%
	Cold leg temperature	°C	295	295	0.00%
	Pump head	MPa	0.942	0.953	-1.15%
	Pressurizer pressure	MPa	15.6	15.5	0.65%
PCS	Feedwater mass flow	kg/s	**392.8**	**404**	**-2.77%**
	Feedwater inlet temperature **(BC)**	°C	238	238	0.00%
	Steam outlet temperature	°C	**314.6**	**299**	**5.22%**
Power Balance	Blanket power removed by BZ PHTS	MW	1482.4	1483.2	-0.05%
	OTSG power (per component)	MW	744.5	741.6	0.39%
	Total pumping power	MW	11.9	12.1	-1.65%
	Pressurizer heaters power	MW	1.08E-02	0.0	0.00%
	Total system heat losses	MW	**0.60**	**0.80**	**-25%**

Table 4.7 – Full plasma power state: FW PHTS and IHTS main parameters.

System	Parameter	Unit	RELAP5	Design	Rel. Diff. [%]
PHTS	Mass flow (per pump)	kg/s	1136.8	1136.8	0.00%
	Hot leg temperature	°C	328.1	328	0.03%
	Cold leg temperature	°C	295	295	0.00%
	Pump head	MPa	0.826	0.843	-2.02%
	Pressurizer pressure	MPa	15.6	15.5	0.65%
IHTS	HITEC mass flow	kg/s	**2955.6**	**3524**	**-16.1%**
	HITEC inlet temperature **(BC)**	°C	280	280	0.00%
	HITEC outlet temperature	°C	**327.7**	**320**	**2.41%**
Power Balance	Blanket power removed by FW PHTS	MW	438.3	439.8	-0.34%

	HEX power (per component)	MW	219.8	219.9	0.05%
	Total pumping power	MW	3.05	3.2	-4.69%
	Pressurizer heaters power	MW	4.87E-03	0.0	0.00%
	Total system heat losses	MW	**0.45**	**0.56**	**-19.6%**

Table 4.8 – Full plasma power state: PHTS water characteristics at blanket inlet/outlet.

PHTS	**Segment**	**PHTS water**				
		Mass flow [kg/s]		**Inlet Temp. [°C]**		**Outlet Temp. [°C]**
		RELAP5	**Design**	**RELAP5**	**Design**	**RELAP5**
BZ	**LOB/ROB**	255	127.5 (LOB) 127.5 (ROB)	295	295	327.8
	COB	127.5	127.5	295	295	329.6
	LIB/RIB	96.4	48.2 (LIB) 48.2 (RIB)	295	295	328.6
FW	**LOB/ROB**	71.0	35.5 (LOB) 35.5 (ROB)	295	295	324.4
	COB	35.5	35.5	295	295	327.3
	LIB/RIB	35.6	17.8 (LIB) 17.8 (RIB)	295	295	336.8

Table 4.9 – Full plasma power state: blanket relevant temperatures.

Parameter	**Unit**	**LOB/ROB**	**COB**	**LIB/RIB**
Max. tungsten temperature	°C	376.3	377.5	378.6
Max. EUROFER temperature (first wall)	°C	372.7	373.9	375.1
Max PbLi temperature	°C	379.2	378.1	350.2
Max. EUROFER temperature (manifold region)	°C	328	329.9	328.9
Max. EUROFER temperature (back supporting structure)	°C	328	329.9	328.9

In BOL condition, the OTSG heat exchange capacity increases due to the absence of tube plugging and fouling (see discussion in **§** 4.1.4). This produces a reduction in the required PCS feedwater

mass flow (-2.77%) and a higher steam outlet temperature (+5.22%, Table 4.6). The same occurs in the FW HEXs, where the secondary HITEC flow lowers (-16.1%) and the outlet temperature correspondingly rises (+2.41%, Table 4.7).

For both FW and BZ PHTS, the control systems implemented in the input deck are able to provide water at the blanket inlet with the required temperature and mass flow, see Table 4.8. However, setting the design values for the water inlet TH conditions produces water outlet temperatures different for the various segments. The discrepancy is less significant in the BZ system but quite important in the FW one (above all for IB segments). Simulation outcomes underline the need, during the conceptual design phase, of a revision of the mass flow distribution between OB and IB segments in order to obtain a uniform outlet temperature for all the segments. For what concerns lead-lithium and the other blanket materials, simulated in the input deck by means of RELAP5 heat structures, their most relevant temperatures are reported in Table 4.9.

Pressure control system set the reference PHTS pressure in the pressurizer component. Hence, during normal operations, the pressure at blanket inlet is: 159.2 bar for the BZ and 158.7 bar for the FW. These values derive from the pressure balance in the PHTS circuits, considering the pressure drops along the overall loop (see Figure 4.6 and Figure 4.7). Indeed, in the current PHTS design, pressurizers are far away from the blanket inlet and there are significant pressure drops between these components. In the conceptual design phase these pressure values will be checked to evaluate their consistency with the blanket design. If they were to be considered unappropriated, the pressurizer position in the PHTS circuit, as well as the pressure control function implemented, must be revised in order to match the pressure requirement.

It is also important to underline that, for both BZ and FW PHTS, the system heat losses calculated by the code are lower than the design values (see Table 4.6 and Table 4.7). This is due to the fact that in the theoretical calculations, for conservative reasons, the insulator thermal conductivity was assessed at the pipeline operating temperature, as stated in [67]. This is the maximum temperature along the pipeline radial profile. As a consequence, also the insulator thermal conductivity was overestimated with respect to its actual value. Instead, RELAP5 code is able to perform a more detailed calculation and to refine the system heat losses evaluation.

The RELAP5 model developed was tested also from the hydraulic point of view in order to demonstrate its capability in properly predict the PHTS system pressure drops. The theoretical pressure profiles were computed following the indications in [64][67]. Figure 4.6 and Figure 4.7 show the comparison between RELAP5 and theoretical pressure drops profiles for BZ and FW systems.

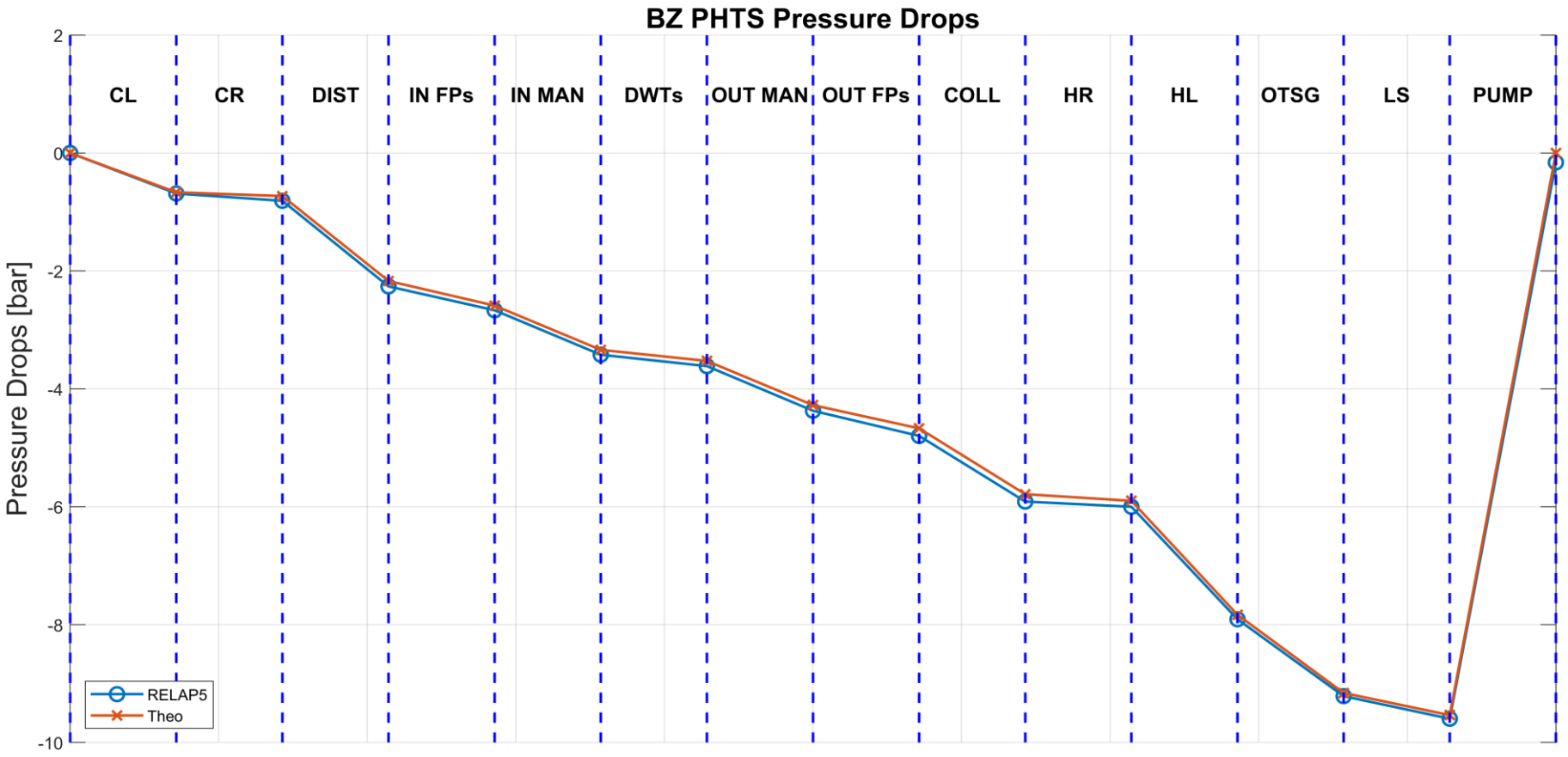

Figure 4.6 – BZ PHTS pressure drops profile: comparison between RELAP5 results and theoretical calculations.

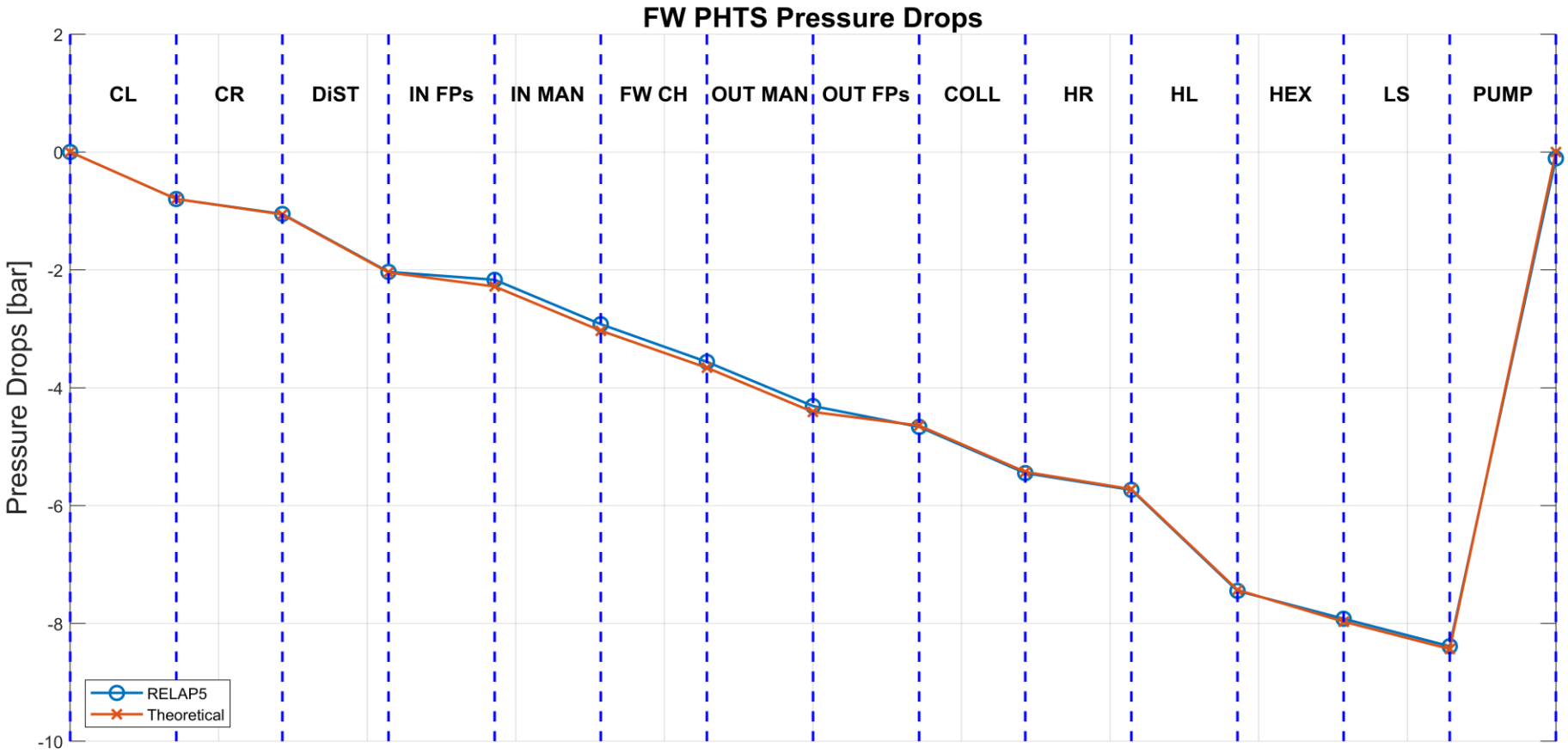

Figure 4.7 – FW PHTS pressure drops profile: comparison between RELAP5 results and theoretical calculations.

4.4 DEMO reactor operative scenarios

4.4.1 Normal operations

DEMO reactor normal operations are characterized by a pulsed plasma regime, based on eleven pulses per day with a burn time (power pulse) of two hours and a dwell time of 10 minutes, [57].

The plasma power ramp-down and ramp-up curves are still under study. The reference ones adopted for the current calculations were derived from [80]. Plasma power curves were implemented in the model by means of general table components (relative power vs time). They are collected in Table 4.10, Table 4.12 and Table 4.12. For what concerns the ramp-up, two power trends are available in [80]. The former (named RU1) is characterized by a smoother transition, while in the latter (called RU2) the plasma power experiences a peak (115% of rated power) before converging to the nominal value. Analyses were performed with both curves, with small differences detected in the simulation outcomes. In addition, since RELAP5 general table components allow the user to input up to a maximum of 99 points, the fluctuations around the nominal value characterizing the final part of the power trends were flattened. During dwell time, after the end of power ramp-down, only decay heat is left. Its time trend was derived from [80] and it was added at the end of ramp-down curve (see Table 4.10). For sake of clarity, ramp-down and ramp-up curves are shown in Figure 4.8. The grey background on the left end of the figure stands for flat-top phase for the ramp-down curve and for the dwell time for the ramp-up trends.

Table 4.10 – Plasma ramp-down curve: tabulation of relative power values vs time, [80].

Time from Plasma Shutdown [s]	Rel. Power[1] [–]	Time from Plasma Shutdown [s]	Rel. Power [–]
0	1.000	26	0.382
2	0.943	28	0.348
4	0.887	30	0.315
6	0.832	32	0.284
8	0.779	34	0.256
10	0.728	36	0.229
12	0.678	38	0.205
14	0.631	40	0.182
16	0.584	42[2]	0.162
18	0.540	44	0.019
20	0.498	45	0.017
22	0.457	1 h	0.009
24	0.419	1 day	0.002

[1] Relative values refer to nominal power in full plasma power state.

[2] This is the end of the ramp-down curve. Next value belongs to decay heat trend.

Table 4.11 – Plasma ramp-up curve RU1: tabulation of relative power values vs time, [80].

Time from End of Dwell Time [s]	Rel. Power[1] [–]	Time from End of Dwell Time [s]	Rel. Power [–]	Time from End of Dwell Time [s]	Rel. Power [–]
0	0.009	28	0.739	56	0.853
2	0.009	30	0.707	58	0.884
4	0.009	32	0.693	60	0.909
6	0.018	34	0.679	62	0.946
8	0.035	36	0.667	64	0.972
10	0.059	38	0.656	66	0.969
12	0.094	40	0.649	68	0.960
14	0.139	42	0.625	70	0.976
16	0.200	44	0.640	72	0.991
18	0.276	46	0.655	74	0.994
20	0.435	48	0.692	76	0.992
22	0.589	50	0.733	78	1.000
24	0.692	52	0.777	80	1.000
26	0.743	54	0.808	150	1.000

[1] Relative values refer to nominal power in full plasma power state.

Table 4.12 – Plasma ramp-up curve RU2: tabulation of relative power values vs time, [80].

Time from End of Dwell Time [s]	Rel. Power[1] [–]	Time from End of Dwell Time [s]	Rel. Power [–]	Time from End of Dwell Time [s]	Rel. Power [–]
0	0.009	14	0.725	36	0.879
1	0.009	15	0.881	38	0.881
2	0.009	16	0.996	40	0.875
3	0.011	17	1.075	42	0.879
4	0.022	18	1.127	44	0.891
5	0.037	19	1.148	46	0.901
6	0.057	20	1.141	48	0.920
7	0.083	22	1.066	50	0.946
8	0.116	24	1.015	52	0.958
9	0.158	26	0.968	54	0.978
10	0.211	28	0.937	56	1.000

11	0.292	30	0.896	58	1.000
12	0.409	32	0.880	60	1.000
13	0.557	34	0.875	150	1.000

[1] Relative values refer to nominal power in full plasma power state.

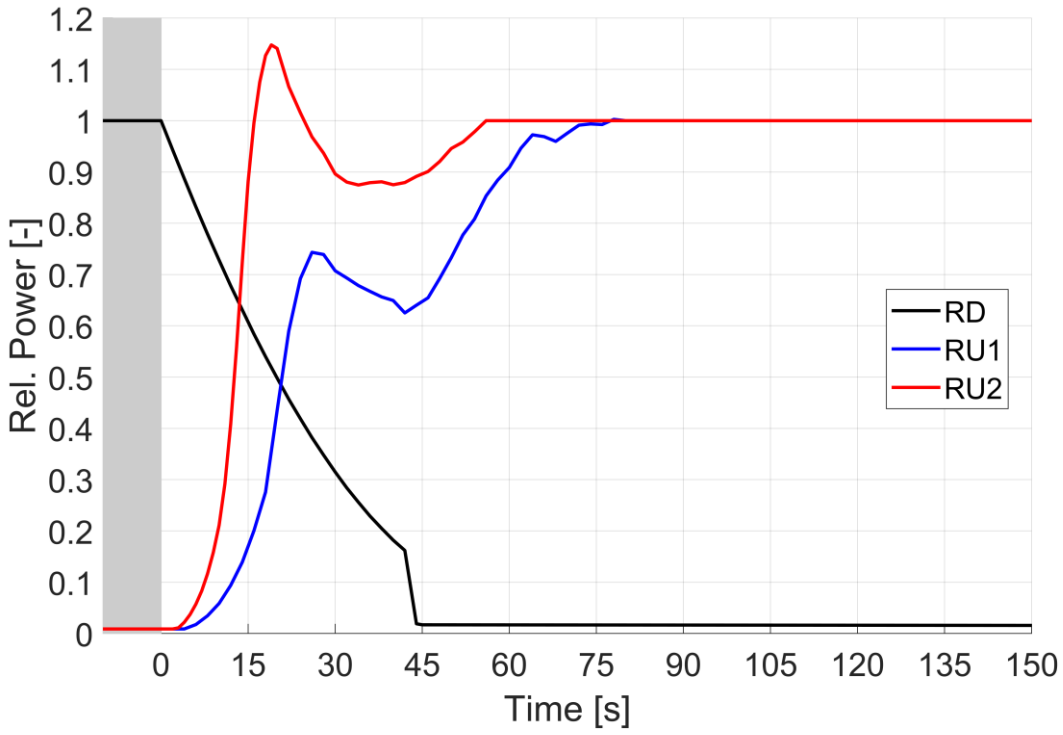

Figure 4.8 – Plasma ramp-down (RD) and ramp-up (RU1, RU2) curves: relative power vs time, [80].

Transient calculations were carried out involving the overall normal operations, including pulse-dwell and dwell-pulse transitions. As for DEMO requirement, the BZ and FW primary pumps are kept running at nominal velocity for the whole simulation. For this, the PI controllers acting on these components are disabled. At their place, the rotational velocity at full plasma power state is imposed as constant boundary condition. Furthermore, during dwell time, PHTS circuits must be operated at the system average temperature (nearly 310 °C). No control strategies related to BZ OTSGs and FW HEXs are available. Thus, the PI controllers regulating the BZ OTSG feedwater and the FW HEX molten salt mass flows are deleted and these parameters are imposed as boundary conditions. As a preliminary tentative, their trends are supposed to be proportional to the plasma power ramp-down and ramp-up curves.

The ramp-down starts after 100 s of full plasma power state. In the figures of this section, such initial steady-state condition is highlighted with a grey background. Moreover, timeline was reset to have the plasma ramp-down starting at 0 s Transient calculation was run for 4000 s, for an overall simulation time of 4100 s. Figure 4.9 reports the simulation outcomes related to the main PHTS thermal-hydraulic parameters.

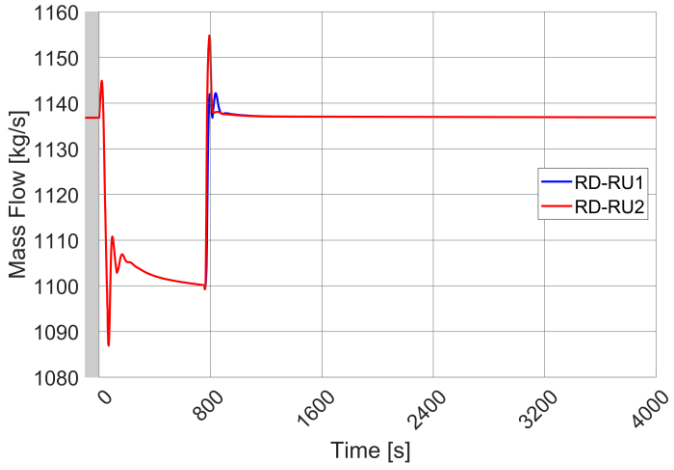
Mass Flow [kg/s]
Time [s]
RD-RU1
RD-RU2

(a)

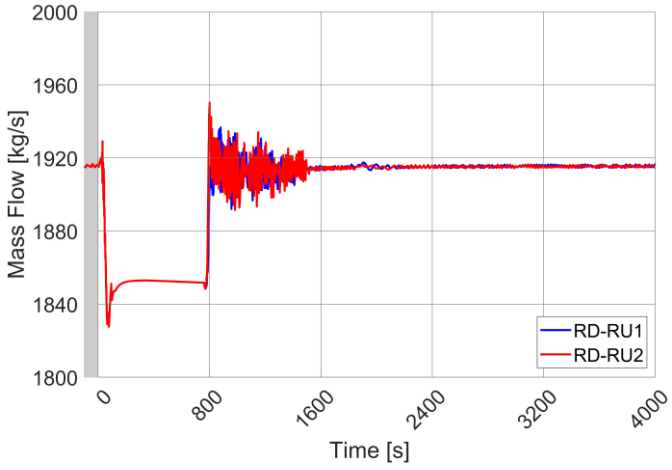
Mass Flow [kg/s]
Time [s]
RD-RU1
RD-RU2

(b)

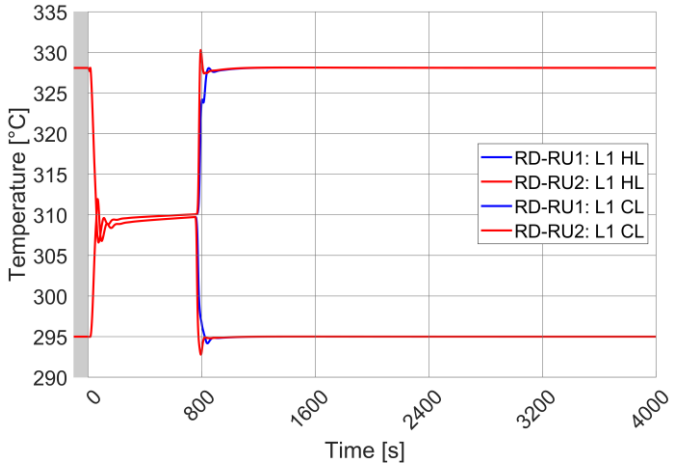
Temperature [°C]
Time [s]
RD-RU1: L1 HL
RD-RU2: L1 HL
RD-RU1: L1 CL
RD-RU2: L1 CL

(c)

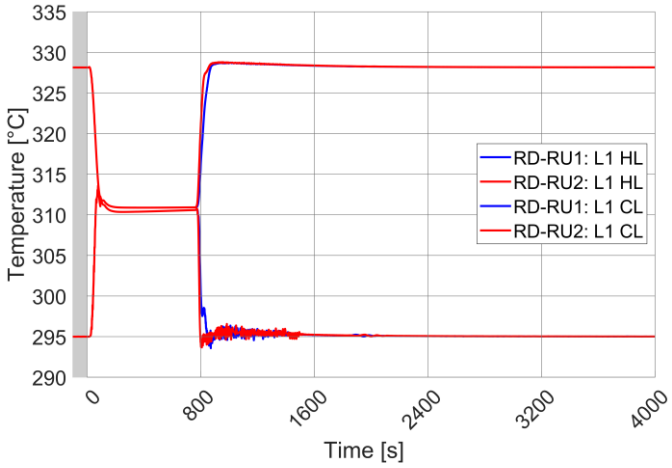
Temperature [°C]
Time [s]
RD-RU1: L1 HL
RD-RU2: L1 HL
RD-RU1: L1 CL
RD-RU2: L1 CL

(d)

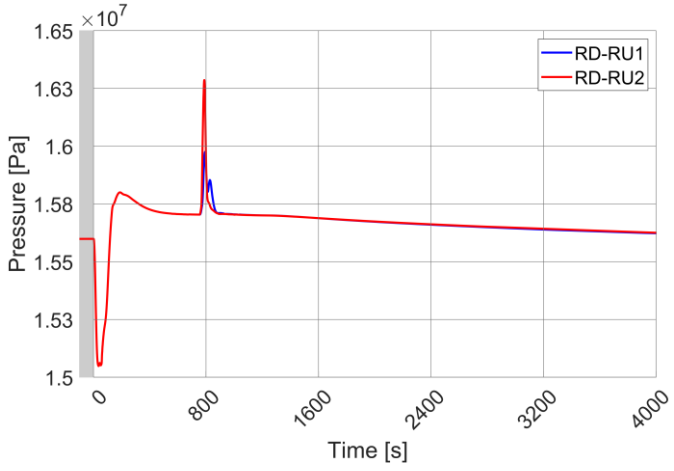
×10^7
Pressure [Pa]
Time [s]
RD-RU1
RD-RU2

(e)

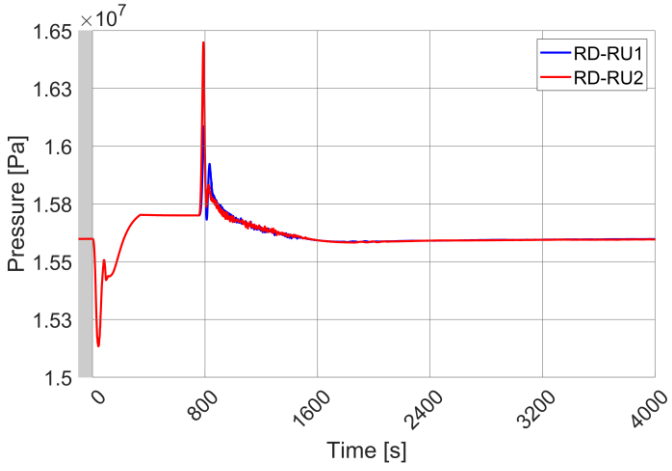
×10^7
Pressure [Pa]
Time [s]
RD-RU1
RD-RU2

(f)

Figure 4.9 – DEMO normal operations, comparison between transients involving RD-RU1 and RD-RU2 plasma power curves: primary pump flow for FW **(a)** and BZ **(b)** systems; temperatures in primary loop 1 (L1) hot leg (HL) and cold leg (CL) for FW **(c)** and BZ **(d)** systems; pressurizer pressure for FW **(e)** and BZ **(f)** systems.

The trends imposed to the BZ OTSGs feedwater and FW HEXs molten salt mass flows prove to be effective in keeping the PHTS average temperature during dwell at the required value (310 °C, see Figure 4.9c for FW and Figure 4.9d for BZ). This is the main goal of the simulations performed. However, such management strategy shall be refined in the future developments of the research activity. The most visible issue to be addressed is the presence of oscillations in the BZ system (see Figure 4.9b, d and f). They last for hundreds of seconds, from the end of the ramp-up curve onwards. Calculations reported in Figure 4.9 were carried out with a time step of 5.0×10^{-3} s. They were repeated varying this parameter from 1.0×10^{-3} s to 1.0×10^{-2} s and the oscillations increased in both directions. Their origin lays in the BZ OTSGs. The blanket component, with its high thermal inertia has the effect of smoothing such fluctuations. This is clearly visible in Figure 4.9d, looking at the different time trends of the cold and hot leg temperatures. The latter, located downwards the blanket, does not experience the oscillations of the former, placed directly at the exit of the steam generators. The oscillations could be generated by multiple factors:

- Modelling choices, such as mesh length chosen for the OTSGs CVs.
- Design operational point chosen for this component. Thermal-hydraulic instabilities could be associated to this set of operational parameters.
- Type of steam generator.

A wider computational activity aimed at investigating in detail the BZ OTSG operational field is out of the scope for the current calculations. However, a sensitivity on the BZ OTSG model will be performed in the future to assess if the nature of the oscillations is purely numerical. In addition, an extended experimental campaign is planned for the next years to address this aspect, [81].

FW system is not affected by fluctuations and better highlights the difference between RU1 and RU2 curves. In the first case, the power ramp-up is smoother and also the hot leg temperature (blue line in Figure 4.9c) rises regularly from the system average value to the nominal one. RU2 presents a peak nearly at the end of the ramp-up phase. This spike is visible in the hot leg temperature (red line in Figure 4.9c) even if significantly reduced by the thermal inertia of the FW system inside the blanket. The maximum temperature experienced is 330 °C, only 2° above the nominal value. The same power spike is not present in the BZ hot leg temperature (red line in Figure 4.9d) due to the far higher inertia of the BZ system inside blanket. In conclusion, as expected, the difference between RU1 and RU2 in terms of blanket outlet temperature is quite negligible.

The temperature peaks match the pressure increases in Figure 4.9e and Figure 4.9f. In both systems, the pressurizer sprays are sufficient to withstand the pressure excursion without challenging the PORV.

Finally, the PHTS primary pumps are kept running at nominal velocity during the overall simulation, i.e. volumetric flows are constant. The correspondent mass flows experience only a slight decrease during dwell time (Figure 4.9a and Figure 4.9b), due to the water density decrease (i.e. temperature increase) within the component.

4.4.2 Power fluctuations

Within the framework of WPBoP and WPBB pre-conceptual design phase research activities, ANSYS CFX and RELAP5 codes were used in the evaluation of the thermal-hydraulic performances for different purposes, based on the specific characteristics of each numerical tool. The former was used to study in detail and optimize the design of the COB equatorial cell. DEMO normal operations were simulated, including both pulse and dwell phases. Latest studies and results in this field are reported in [59][60][61][62]. Instead, RELAP5 allows the transient analysis of blanket component and related PHTS at a system level. Both normal operations and accidental conditions were investigated, as discussed in this PhD thesis. As already stated in **§** 4.1.3, breeding blanket was modelled by means of equivalent components characterized by lumped parameters. The effectiveness of this approach can be checked by comparing system code results with the most refined ones obtained with ANSYS CFX simulations. Furthermore, performing transient analyses with the finite volume model allows to more precisely evaluate the capability of the reference COB equatorial model to provide adequate structures cooling and suitable water conditions for energy production, while the boundary conditions are time-dependent. For this, a benchmark exercise was performed, involving the models described in **§** 4.1 and in [61][62]. Plasma power fluctuations transient was selected as reference scenario to be simulated with both methodologies. Two different analyses were considered. The first deals with three identical subsequent positive power spikes, while the second foresees a train of positive-negative-positive power peaks. These power oscillations are represented by symmetrical Gaussian curves, characterized by a period of 30 s. In the first case, named low power fluctuations, overpower peaks represent an increase of 2.81% with respect to the rated value. In the second case, called high power fluctuations, overpower/underpower spikes correspond to +10%/-7.5% of the nominal power. Referring to high power fluctuations, Figure 4.10 shows the outcomes of CFX and system codes. BZ and FW PHTS water temperatures at blanket inlet and outlet are the selected parameters for comparison. The transient calculation starts from the steady-state condition of flat top at full power (pulse). In Figure 4.10, it represents the first 10 s of simulation. After, the three power fluctuations are respectively centered at 25 s, 55 s and 85 s. The total simulation time is equal to 125 s to evaluate the maximum temperature reached after the last positive spike.

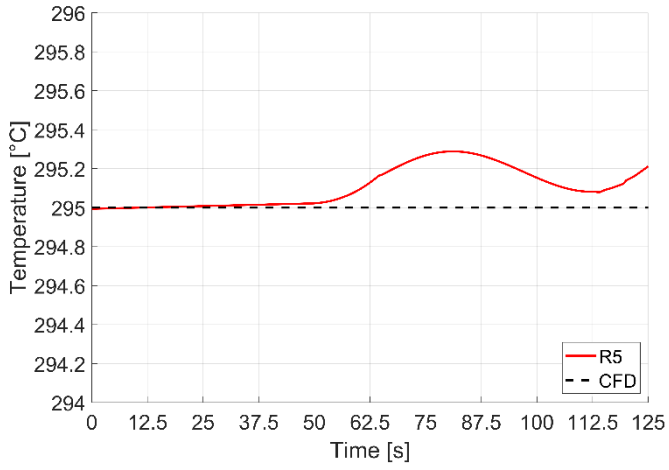

(a)

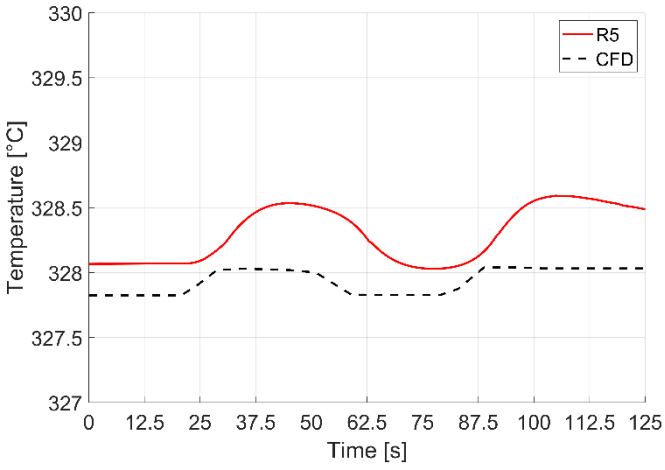

(b)

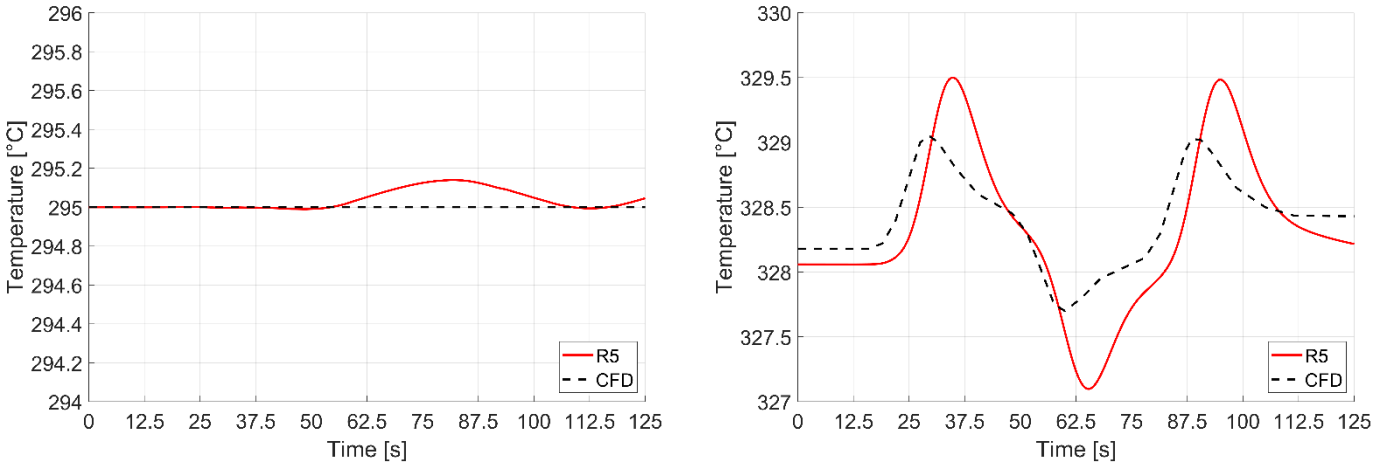

Figure 4.10 – High power fluctuations transient, comparison between ANSYS CFX and RELAP5 codes: BZ PHTS water temperatures at blanket inlet **(a)** and outlet **(b)**; FW PHTS water temperatures at blanket inlet **(c)** and outlet **(d)**.

Regarding the BZ outlet (Figure 4.10b), CFX temperature trend shows fluctuations caused by the power peaks. Such alterations are few seconds delayed with respect to power spike occurrences. Moreover, significant plateaus can be observed due to the large thermal inertia of lead-lithium. For this, the maximum reached temperature is significantly smoothed (only +0.2 °C with respect to the rated value). A slight build-up effect can be highlighted at the end of transient, mainly due to the system inertia and the unbalance between positive and negative fluctuations. Concerning the FW outlet (Figure 4.10d), oscillations in the CFX trend are higher than the ones referred to BZ. FW channels are very near to the plasma facing surface. Hence, FW cooling water is strongly influenced by the power spikes, almost recreating the Gaussian trend. Temperature excursions (+0.8/-0.4 °C with respect to rated value) are more significant compared to the ones in Figure 4.10b, since the FW EUROFER thermal inertia is lower than the one offered by PbLi. Even in this case, outlet temperature spikes are delayed of few seconds with respect to power peaks and a slight build-up effect can be observed at the end of transient. Comparing CFX and system code results in Figure 4.10b and Figure 4.10d, several aspects can be underlined. Firstly, the initial steady-state temperatures for both BZ and FW are slightly different. RELAP5 model, being a system code based on lumped parameters, once given in input the design power source terms and obtained the right water inlet conditions (temperature and mass flow) provides the design blanket outlet temperatures for both circuits (with a neglecting deviation, lower than 0.1 °C in both cases). Instead, the 3D simulations performed with ANSYS CFX are able to predict more accurately the thermal coupling between these two systems and the deriving water outlet temperatures. To reduce this discrepancy, control systems associated to water inlet conditions in RELAP5 model must be tuned taking into account CFX calculation outcomes. Secondly, oscillations related to system code results in Figure 4.10b and Figure 4.10d are higher than the correspondent ones associated to 3D simulations. This means that RELAP5 underestimates the FW EUROFER and PbLi thermal inertia. Also, this parameter must be slightly refined in the system code model to enhance the code simulation capability with respect to breeding blanket. It must be underlined that, referring to the third positive spike in Figure 4.10b and Figure 4.10d, discrepancies between RELAP5 and CFX trends are also influenced by different conditions at blanket inlet, as shown in Figure 4.10a and Figure 4.10c for BZ and FW, respectively. System code is able to consider the

feedback coming from the PHTS steam generators/heat exchangers. Blanket Inlet temperatures experience an increase whose delay depends on the time needed to flow through the entire PHTS circuit. Thus, a possibility to obtain the best results is to externally couple system code and 3D calculations. This is an iterative process where CFX provides more accurate parameters to refine the RELAP5 model and this one is used to update the inlet conditions for finite volume model computation. Such procedure will be furtherly investigated in the future developments of simulation activity related to WPBB and WPBoP. However, Results in Figure 4.10a to Figure 4.10d show a general good agreement and confirm the effectiveness of the lumped parameters approach adopted in the RELAP5 model with respect to the inlet/outlet parameters analyzed.

4.5 'Decrease in reactor coolant system flow rate' accident category

Different faults that could result in a decrease of the BB PHTS primary flow were postulated and investigated. These events are discussed in this section. Simulations were performed with the goal of the design improvement. The selected accidental scenarios were:

- Partial loss of forced primary coolant flow, **§** 4.5.2;
- Complete loss of forced primary coolant flow, **§** 4.5.2;
- Primary pump shaft seizure (or locked rotor), **§** 4.5.3;
- Inadvertent operation of a loop isolation valve, **§** 4.5.4.

Firstly, the most limiting of the above primary flow decrease event was chosen. It consists in the complete loss of forced circulation in both FW and BZ PHTS. In this 'worst case' scenario, **§** 4.5.1, even if very unlikely, a sensitivity was performed on the flywheel to be added to the PHTS main coolant pumps in order to keep the system temperatures at acceptable values.

4.5.1 'Worst case scenario': sensitivity on the PHTS primary pumps flywheel

The full plasma power state was conservatively chosen as initial condition for the accidental analysis since it comports the highest thermal loads for the PHTS cooling systems. The LOFA Postulated Initiating Event (PIE) is the complete loss of flow in both the BZ and FW PHTS. In the transient simulations, PIE occurs after 20 s of plasma power flat-top. In the figures of this section timeline was reset to have PIE at 0 s and the previous steady-state phase was highlighted with a grey background. A time step sensitivity was performed varying this parameter from 1.0×10^{-3} s to 5.0×10^{-3} s. No sensible differences in the simulation results were observed. Time trends reported in the following figures are for a time step of 5.0×10^{-3} s.

A preliminary actuation logic was proposed and implemented for some reactor components. It foresees: **i)** Plasma Termination (PT) is triggered by a low flow signal on primary pumps; **ii)** IHTS mass flow ramp-down follows the plasma shutdown with a delay of 10 s; **iii)** Turbine Trip (TT) is actuated by a low signal on the OTSG steam outlet temperature; **iv)** turbine trip is followed by PCS feedwater ramp-down and TSVs closure; **v)** PHTS pressurizer heaters are cut off on a low-level signal in the component or following the turbine trip; **vi)** pressurizer sprays are disabled after the primary pump trip. The ramp-down curve used to simulate plasma shutdown was derived from [80]. With the adoption of this curve, a potential plasma disruption is avoided. It is tabulated in Table 4.10 and shown in Figure 4.8. The relative trend should be applied to both nuclear heating and incident heat flux. It lasts 42 s, after which only decay heat is left (nearly 2% of the reactor rated power, [57]).The PCS TSVs are supposed to close in 0.5 s. In this transient simulation, the PI controller related to PHTS primary pumps is disabled. For these components, the rotational velocity at plasma power flat-top is imposed as a constant boundary condition until the PIE occurs (first 20 seconds of the simulation). Later, the component coast-down is ruled by the torque-inertia equation. The temperature control systems related to PCS feedwater and IHTS mass flow are also removed. At the transient beginning, these secondary flows are imposed as constant boundary conditions adopting the values obtained for them at plasma power flat-top. Once triggered by the correspondent signal, the secondary pump coast-down was very preliminary simulated with a linear trend that goes from the nominal value to zero in 10 s.

A sensitivity was carried out to assess the impact on the main PHTS parameters of adding a flywheel to the BZ and FW primary pumps. Several values were selected for the component

moment of inertia. They are reported in Table 4.13. For what concerns case 1, only motor and impeller contributions were considered and the value indicated in Table 4.13 was calculated by using formulas in [82]. From case 2 to case 5, an increasing flywheel was added. Results shown in the following are also presented in [83].

Table 4.13 – Selected values for PHTS primary pumps moment of inertia (flywheel sensitivity).

System	Unit	Case 1	Case 2	Case 3	Case 4	Case 5
BZ	$kg \cdot m^2$	558	1000	2000	3000	4000
FW	$kg \cdot m^2$	222	524	1048	1573	2097

After PIE, PHTS primary flow starts to decrease in FW and BZ systems. The focus on the primary pump coast-down is reported in Figure 4.11a and Figure 4.11b. The addition of an increasing flywheel slows down the mass flow drop in the PHTS circuits. This effect is sensible in the first 100 s of transient when the forced circulation is prevalent. Later, only natural circulation is left, and the mass flow trend is the same for all the calculations.

The delay in the mass flow decrease also postpones the triggering of plasma shutdown, actuated by a low flow signal. Different times are reported in Table 4.14. This impacts on the BZ and FW PHTS temperature peaks at blanket outlet, shown in Figure 4.11c and Figure 4.11d. These spikes, occurring at transient beginning, are due to the relative balance between decreasing trends belonging to plasma power and primary flow. Even though plasma shutdown is called very close to PIE (i.e. primary pump trip), plasma heating decreases slower than the pump flow and the PHTS temperatures at blanket outlet experience a peak. The flywheel addition to primary pumps, slowing down their deceleration, smoothes these spikes, avoiding excessive temperatures within the blanket component. PHTS peak temperatures for different cases are collected in Table 4.14.

After 10 s from plasma shutdown, IHTS mass flow starts to decrease and the FW HEXs lose their cooling function. Without the power source and the heat sink, the FW system tends to the average temperature (Figure 4.11d). Increasing the primary pump flywheel speeds up this temperature transient, even producing a temporary temperature inversion for the highest value of the parameter (case 5 in Figure 4.11d). Indeed, according to FW PHTS thermal balance, at reduced power (HEXs nearly disabled), higher mass flow rates (i.e. increasing flywheel) correspond to lower temperature differences between hot and cold branches.

The time when turbine trip occurs is shown in Table 4.14 for each transient simulation. In the time window between PIE and turbine trip, BZ OTSGs are able to remove power from the primary circuit. Even after this event, a residual cooling capability is periodically offered by the steam generators in correspondence with the steam line SRVs openings. As a consequence of this lasting cooling function, the blanket inlet (i.e. OTSG outlet) temperature initially decreases and only in the mid-term tends to the average one (Figure 4.11c). The flywheel addition smooths the temperature drop and accelerates the reaching of the average system temperature, as for the FW PHTS. For the BZ system, a temporary temperature inversion is experienced for all the flywheel values. In the long term, when natural circulation establishes, this phenomenon disappears for both FW and BZ systems (see **§** 4.5.2.1 and 4.5.2.2).

Finally, Figure 4.11e and Figure 4.11f report the BB PHTS pressure trends. In BZ PHTS (Figure 4.11e) the flywheel influence is notable. Starting from case 4, its addiction avoids the opening of pressurizer PORV. In FW PHTS (Figure 4.11f) the effect of flywheel on the system pressure is not

so linear. This is due to the fact that the secondary system is lost short after the transient beginning, as discussed above. The plasma power removed from blanket by the primary coolant is 'trapped' in the primary system, provoking the pressure rise. The latter parameter increases with the delay of plasma shutdown (proportional to MCP flywheel) but decreases with the temperature smoothing (due to higher primary flow rate induced by the flywheel addition). Hence, PORV opens only in the extreme cases, 1 and 5, while in the central ones the two effects tend to counterbalance. The timing of the first PORV opening in both systems, if any, is reported in Table 4.14 for the different cases.

Considering all the BZ and FW PHTS parameters, case 4 was selected as the best one. In the following analyses, FW and BZ primary pumps were provided with the flywheel values associated to this case.

Table 4.14 – Complete LOFA in FW and BZ PHTS: early transient summary table.

#	Unit	Case 1	Case 2	Case 3	Case 4 (best)	Case 5
PT triggering time	s	0.5	0.5	1	**1.5**	2.5
TT triggering time	s	35.5	38.5	45	**52**	56
BZ PHTS peak temp. at blanket outlet	°C	348	346	342	**339**	337
FW PHTS peak temp. at blanket outlet	°C	351	342	335	**332**	330
BZ pressurizer PORV first opening time	s	225	242	291	-	-
FW pressurizer PORV first opening time	s	35.5	-	-	-	45.5

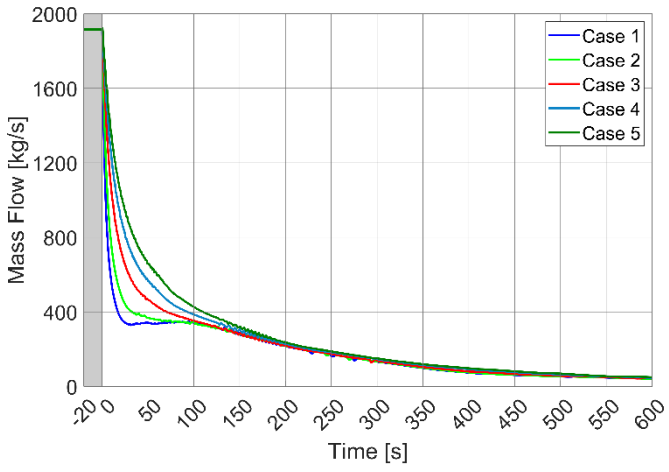

(a)

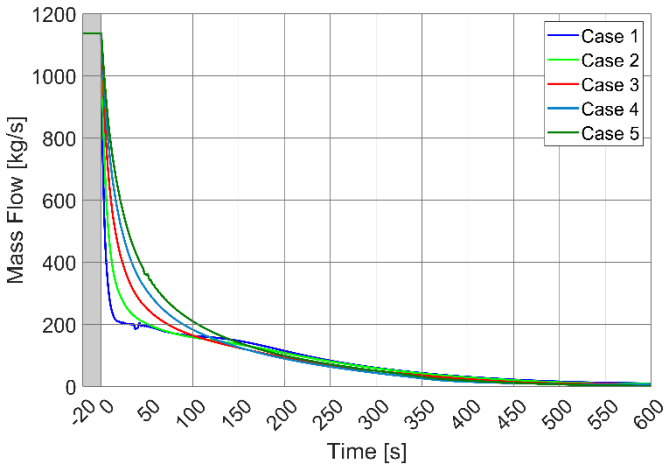

(b)

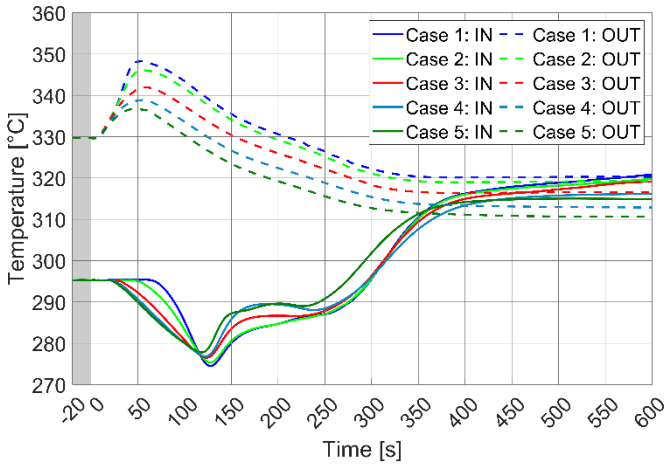

(c)

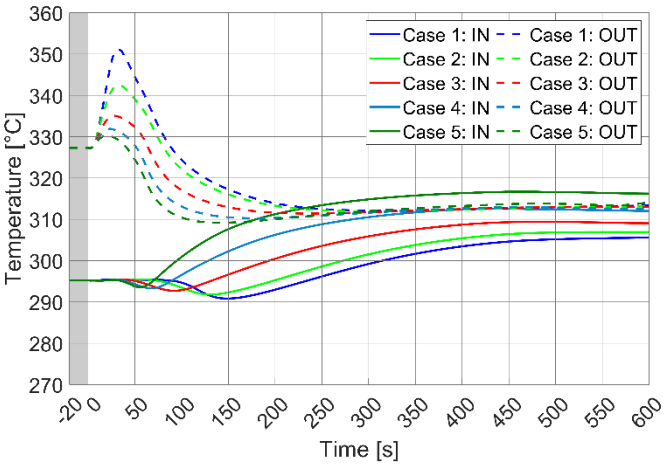

(d)

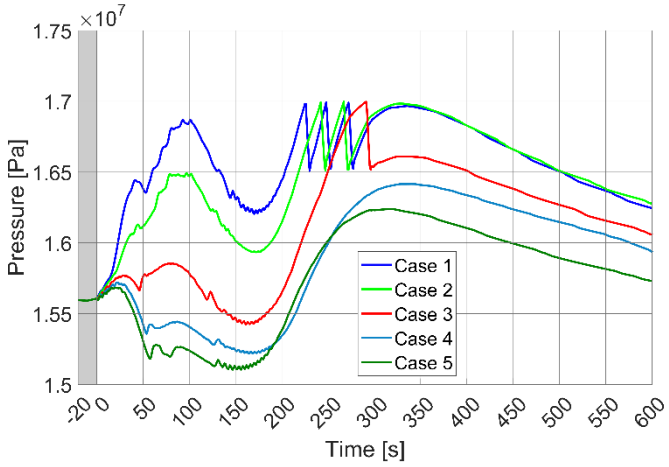

(e)

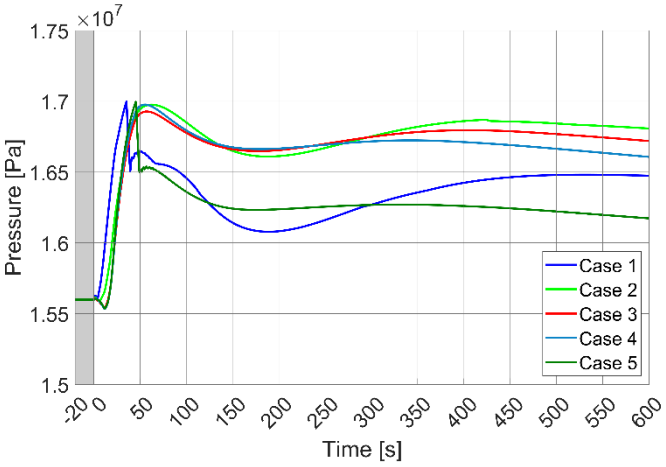

(f)

Figure 4.11 – Complete LOFA in both BZ and FW PHTS (early time), sensitivity on primary pump flywheel: **(a)** BZ primary pumps mass flow (one of four); **(b)** FW primary pumps mass flow (one of two); **(c)** BZ PHTS temperatures at blanket inlet/outlet (sector one of sixteen); **(d)** FW PHTS temperatures at blanket inlet/outlet (sector one of sixteen); **(e)** BZ system pressure in pressurizer component; **(f)** FW system pressure in pressurizer component.

4.5.2 Partial and complete LOFA scenarios

The selected PIEs analyzed in this section are partial and complete loss of flow accidents, when interesting either BZ or FW PHTS primary pumps. Simulations were replicated also considering the influence of Loss of Off-Site Power (LOSP), occurring in combination with the initiating event. The matrix of the transient calculations performed is presented in Table 4.15.

Table 4.15 – Matrix of transient calculations related to partial and complete LOFA.

Case ID	PIE	System involved with PIE	Loss of off-site power [Yes/No]
LF1	Partial LOFA	FW PHTS	no
LF2	Complete LOFA	FW PHTS	no
LF3	Partial LOFA	BZ PHTS	no
LF4	Complete LOFA	BZ PHTS	no
LF5	Partial LOFA	FW PHTS	yes
LF6	Complete LOFA	FW PHTS	yes
LF7	Partial LOFA	BZ PHTS	yes
LF8	Complete LOFA	BZ PHTS	yes

Primary pumps coast-down is ruled by the torque-inertia equation reported below.

$$T_{em}\,(\omega)\;-\;T_{hyd}\,(\omega)\;-\;T_{fr}\,(\omega)\;=\;I\cdot d\omega/dt \tag{4.1}$$

In the previous equation, $T_{em}\,(\omega)$ is the motor electromagnetic torque, that during coast-down is zero, $T_{hyd}\,(\omega)$ is the hydraulic torque due to system pressure drops, $T_{fr}\,(\omega)$ is the pump frictional torque due to losses inside the component, ω is the rotational velocity and I is the pump moment of inertia. Its values were derived by the sensitivity analysis performed on the 'worst case' scenario described in the previous section. In particular, 3000 kg·m^2 and 1573 kg·m^2 were adopted for BZ and FW primary pumps, respectively.

An actuation logic, involving some components of the DEMO reactor, was proposed and preliminary investigated. It was inspired by the one used for Generation III + nuclear power plants. The following features were implemented:

- Plasma termination is actuated by one of the following signals: **(i)** low flow on PHTS primary pumps (<80% of rated value, see Table 3.5); **(ii)** high pressure on PHTS pressurizers (>167 bar); **(iii)** high temperature at BZ/FW outlet feeding pipes (2 °C below the saturation temperature at the PHTS reference pressure).
- Turbine Trip is triggered by one of the following signals: **(i)** plasma termination; **(ii)** low steam flow (<85% of rated value, see Table 4.6) or **(iii)** low steam temperature (2 °C above the saturation temperature at the PCS reference pressure) at OTSG secondary side outlet.
- Turbine trip is followed by: **(i)** PCS feedwater ramp down; **(ii)** TSVs closure.

- PHTS pressurizer heaters are cut off: **(i)** on low-level signal in the correspondent component or **(ii)** following the turbine trip.
- Spray line flow is interrupted only when all the primary pumps belonging to a PHTS are off. The hypothesis is that redundant spray lines are connected to both PHTS loops.

The margin adopted for the temperature signals was selected to account for the typical uncertainty related to a thermocouple reading. For what concerns the PHTS primary pumps, different management strategies were considered whether or not the loss of off-site power is assumed. If not, for a BZ or FW primary pump, correspondent trip can occur following: **(i)** initiating event or **(ii)** a high-temperature signal at component inlet (5 °C below the saturation temperature at the PHTS reference pressure). The margin was chosen to avoid pump cavitation in any transient scenario. If loss of off-site power is assumed, turbine trip was added to the previous switch off conditions. Indeed, when external power fails in combination with PIE, the turbine is the only element ensuring the AC power needed for the MCPs operation. The PI controller associated to BZ and FW primary pumps and used in the plasma power flat-top calculation is disabled. The rotational velocity is imposed as a constant boundary condition until the pump trip is not triggered. From this moment, the component coast-down is ruled by the torque-inertia equation reported above.

Also, the management strategy for molten salt IHTS mass flow was differentiated according to the presence or not of off-site power. If available, HITEC® mass flow is ramp-down 10 s after the initiating event. Conservatively, it is assumed that PIE occurs at the end of plasma pulse when the ESS cold tank is nearly empty. For this, the HITEC® mass flow must be stopped shortly after the Start of Transient (SOT). If off-site power is lost, turbine trip is added as a ramp-down condition. In fact, in this scenario, the turbine is the only element ensuring the AC power needed for the molten salt pumps operation.

The temperature control systems adopted for the plasma power flat-top scenario and related to PCS feedwater and IHTS mass flow are disabled. These parameters are imposed by means of time-dependent junctions and respond to the actuation logics described above. As a preliminary tentative, their ramp-down is simulated with a linear trend going from nominal value to zero in 10 s. Steam line TSVs are supposed to close in 0.5 s. The curve adopted for plasma ramp-down is the one discussed in the previous section and tabulated/shown in Table 4.10/Figure 4.8, [80].

The initiating event occurs after 100 s of plasma power flat-top, indicated with grey background in the figures of this section. Timeline was reset in the plots to have PIE at 0 s. Transient calculation was run for 9000 s (2.5 hr), for an overall simulation time of 9100 s. Different time steps were adopted in the calculation. In the first part of the transient, when thermal excursions are expected to be more significant, a lower time step was used (5.0×10^{-3} s). In the final part, this parameter was increased (1.0×10^{-2} s) to speed up the simulation. Following results are also discussed in [84].

4.5.2.1 LOFA involving FW PHTS

FW system transient evolution

After PIE, FW PHTS primary flow starts to decrease. In cases LF1 and LF5, initiating event involves only loop 1 pump (partial LOFA), instead, in sequences LF2 and LF6, both loop pumps are stopped (complete LOFA). Low flow is detected shortly after the SOT and plasma termination is triggered. Consequently, also turbine trip is actuated. In LF5 scenario, where loss of off-site power is

assumed, this causes the stop of the FW pump not interested from PIE. For this reason, in transients LF2, LF5 and LF6, the coast-down of both loop pumps is nearly contemporaneous and these cases have a quite similar accidental evolution. Case LF1 differs from the others since loop 2 pump continues to provide primary flow up to nearly the End of Transient (EOT). A summary of the transient calculations characterized by PIE involving FW pumps is offered by Table 4.16.

Table 4.16 – Summary table for LOFA transients involving FW PHTS.

Event/Parameter	**Unit**	**LF1**	**LF2**	**LF5**	**LF6**
PIE (LOFA)	-	Partial (FW)	Complete (FW)	Partial (FW)	Complete (FW)
Loss of off-site power	yes/no	no	no	yes	yes
PT signal occurrence	s	1.5	1.5	1.5	1.5
TT signal occurrence	s	1.5	1.5	1.5	1.5
TSVs start to close	s	1.5	1.5	1.5	1.5
Start of PCS feedwater ramp-down	s	1.5	1.5	1.5	1.5
Start of IHTS mass flow ramp-down	s	10	10	1.5	1.5
Time of FW PHTS water temperature peak	s	15	24	23	23
FW PHTS water temperature peak [1]	°C	329	332	332	332
Time of BZ PHTS water temperature peak	s	-	-	60	60
BZ PHTS water temperature peak [1]	°C	-	-	339	339
FW MCP Trip occurrence (pump not interested by PIE)	s	7696	-	1.5	-
BZ MCPs Trip occurrence	s	7112	7084	1.5	1.5
Time to evacuate BZ OTSGs secondary side inventory	s	500	500	2200	2200
Water mass discharged from BZ OTSGs sec. side	kg	13,281 (per OTSG)	14,718 (per OTSG)	12,795 (per OTSG)	15,465 (per OTSG)
FW PORV first opening time (Long Term)	s	7344	1284	2200	1988
Total FW PHTS water mass discharged at EOT	kg	1301	2094	1398	1352

BZ PORV first opening time (Long Term)	s	6776	6736	4512	4192
Total BZ PHTS water mass discharged at EOT	kg	6724	5831	5482	4417

[1] For all the sixteen sectors, both the BZ and FW PHTS water temperatures were detected at the outlet of COB segment. For each PHTS, peak temperature reported in the table is the maximum among all the temperature readings.

Case LF1

As already stated, loop 2 pump continues to provide primary flow. The transient results dissymmetrical with respect to the toroidal dimension. The sixteen sectors experience different flows (Figure 4.12a), with higher values in the ones nearest to the active pump. Consequently, also the PHTS temperatures at blanket inlet/outlet are differentiated. Figure 4.12b reports the values referred to all sixteen sectors. COB segment was chosen as reference to plot simulation results. Forced flow due to loop 2 pump significantly smooths the temperature peak at blanket outlet. The maximum increase (associated to the sectors nearest to the failed pump) is of only one degree (Table 4.16) with respect to rated value. The temperature excursion is quite negligible.

Another interesting effect is the flow inversion in loop 1 (negative mass flow in Figure 4.12c). The pressure drops related to the blanket component are so high that a part of the flow provided by loop 2 pump goes through loop 1 in reverse direction instead of flowing in the blanket sectors. The reverse flow also causes a temperature inversion in the correspondent loop (Figure 4.12d). After the trip of loop 2 pump (see Figure 4.12c and Table 4.16), forced circulation is lost and the establishment of natural circulation restores the original temperature field in loop 1 (Figure 4.12d). In loop 2, the forced circulation provokes a quick convergence of the system temperatures. Later, they start to positively drift. This occurs since blanket decay heat (2% of rated reactor power) overwhelms the system heat losses. The temperature slope is of nearly 12 °C/hr (25 °C in 7500 s). In the case of forced circulation (LF1), the curve slope is higher than the one associated to sequences dominated by natural circulation (LF2, LF5 and LF6, Figure 4.14c). This can be justified considering that the PHTS coolant is also heated by pumping power. Such contribute (few MWs as reported in Table 4.7) is of the same order of magnitude of the decay heat. Once loop 2 pump is stopped, when forced circulation is lost and natural circulation establishes, if simulation time were increased, the temperature slope for LF1 scenario would become the same as other transients.

For what concerns the FW PHTS pressure, the presence of forced circulation (even if reduced with respect to rated value) avoids the challenging of pressurizer PORV at SOT (Figure 4.13a). In the mid-long term, since loop 2 pump is active also pressurizer sprays are still available. The system pressure is kept constant for a long time interval (Figure 4.13b). During it, with the increase of the system temperature, spray intervention in reducing pressure becomes less and less effective. In fact, from time to time, they introduce in the pressurizer control volume water at higher enthalpy. The level in the component increases almost linearly, as shown in Figure 4.13c. At a certain point, sprays are unable to perform the pressure control function and the system pressure start to rise triggering the PORV (Figure 4.13b, for the timing see Table 4.16). The valve opens when the pressurizer is nearly solid (Figure 4.13c). From this moment, pressure in the PHTS follows a sawtooth trend due to the PORV periodical openings. This is the way used by FW system to

dissipate the decay heat produced in the blanket. The total water mass discharged from FW PHTS at EOT is reported in Table 4.16.

The trend of the maximum EUROFER temperature in the FW component is shown by Figure 4.13d. After plasma shutdown, the material temperature drops driven by PHTS water temperatures. Instead, in the mid-long term, FW component is heated up by the decay heat and experiences the same temperature slope of PHTS water.

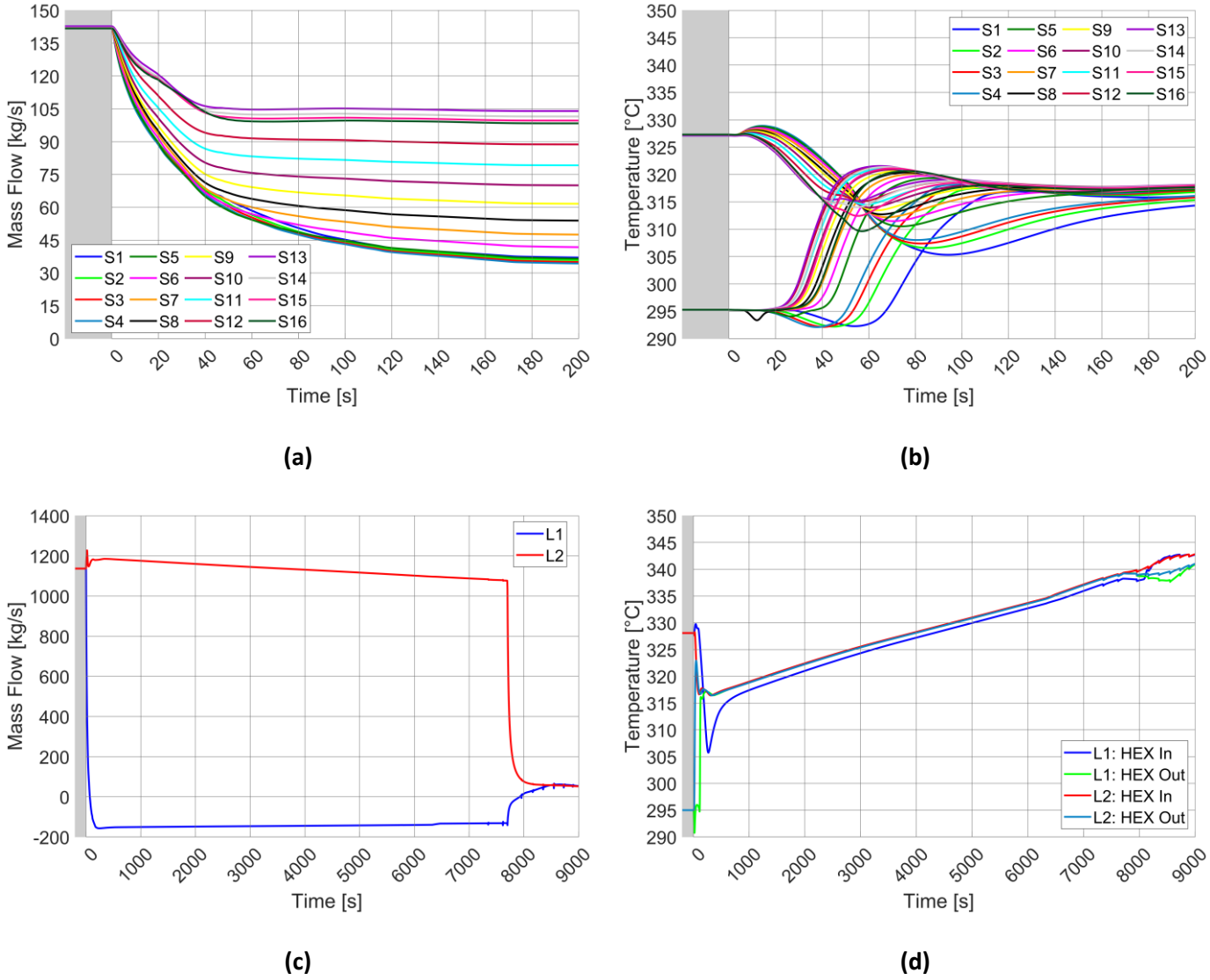

Figure 4.12 – Partial LOFA on FW PHTS without loss of off-site power (LF1 transient): **(a)** Mass flow in FW sectors (early time); **(b)** FW PHTS water temperatures at BB inlet & outlet (all sectors, early time, COB segment); **(c)** Mass flow elaborated by FW PHTS MCPs (full range); **(d)** FW PHTS water temperatures at Heat EXchangers (HEXs) inlet & outlet (full range).

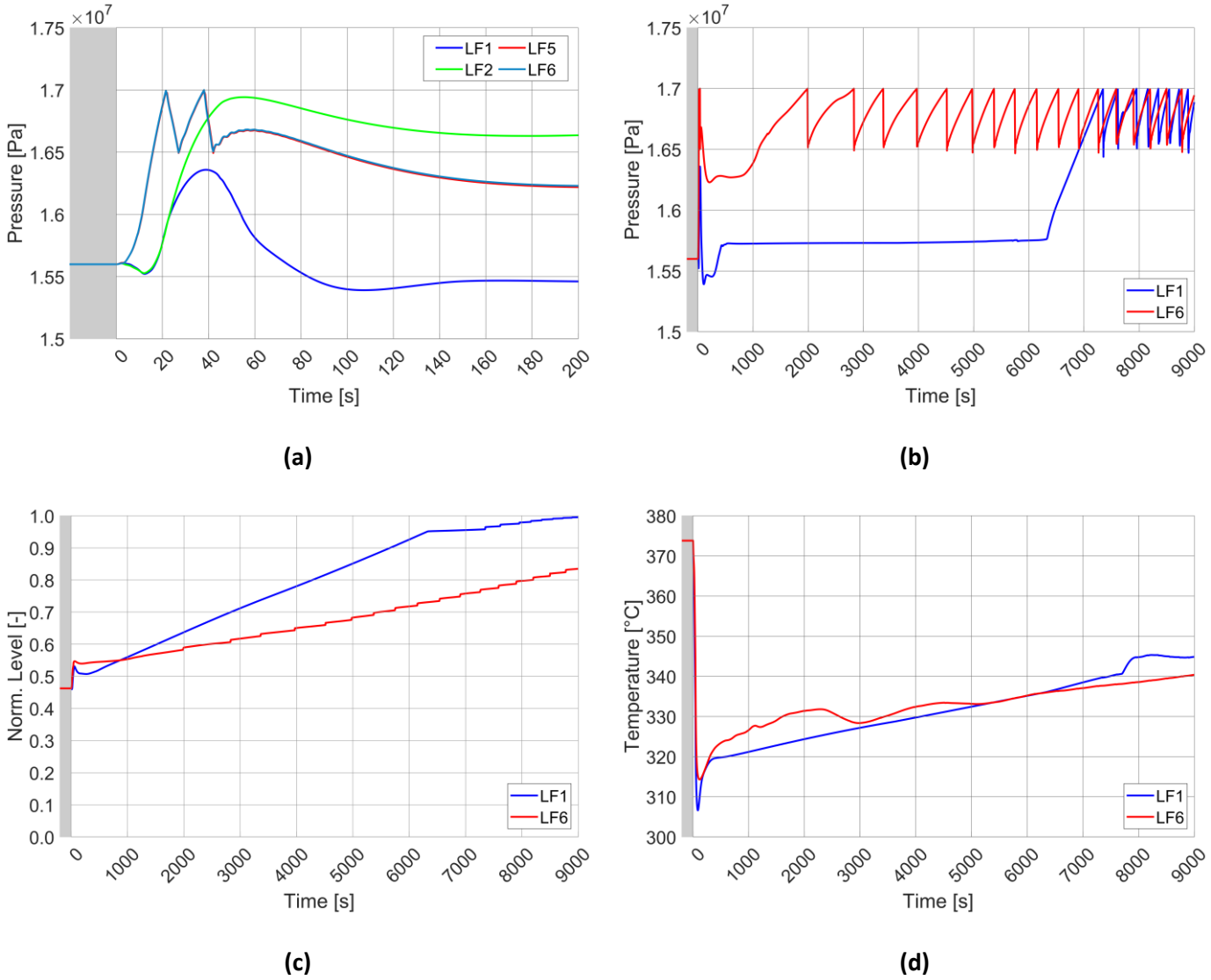

Figure 4.13 – Comparison between LF1 and LF6 transients: **(a)** Pressure in FW PHTS (early time); **(b)** Pressure in FW PHTS (full range); **(c)** Collapsed level in FW pressurizer (normalized, full range); **(d)** Maximum EUROFER temperature in FW component (full range).

Cases LF2, LF5 and LF6

The FW PHTS mass flows through blanket sectors follow the pump coast-down. It is shown for LF6 sequence in Figure 4.14b. For all the considered accidental scenarios, as already discussed before, the coast-down of both primary pumps is nearly contemporaneous. Hence, these transients result symmetrical with respect to the toroidal dimension. This is clearly visible in Figure 4.14a reporting the FW PHTS temperatures at blanket inlet/outlet (COB segment). Values are plotted for all the sixteen sectors, with a single color for each case considered. Outlet temperatures experience a slight increase due to the short time window between the occurrence of initiating event (i.e., start of pump/pumps coast-down) and the plasma termination. After that, since pump coast-down advances more slowly than plasma shutdown, outlet temperatures decrease. Peak temperature is the same for all the sectors and for all the cases (Table 4.16). In LF5 and LF6 scenarios, where loss

of off-site power is assumed, IHTS mass flow is ramp-down following the turbine trip, while in LF2 sequence it is available for the first 10 s of the transient. As a result, in this latter case, blanket inlet temperatures initially decrease (blue trends in Figure 4.14a) and restart to increase only after the mass flow ramp down. Instead, in LF5 and LF6 transients, they start immediately to increase, since secondary flow is lost shortly after the SOT (red and green lines in Figure 4.14a). However, apart from this initial difference, the inlet temperatures have a quite similar trend for all the cases.

The loss of the heat sink also produces a sudden increase in the FW PHTS pressure, as shown by Figure 4.13a. For LF5 and LF6 sequences, the pressure rise is managed by the pressurizer PORV. Instead, in LF1 and LF2 scenarios, the availability of the IHTS mass flow avoids the opening of this component. In the long term, referring to FW PHTS parameter trends, no sensible differences are detected between cases LF2, LF5, LF6. For this reason, only results associated to LF6 sequence were plotted in the figures reported in this section.

During FW pump coast-down system reaches a quite uniform temperature (Figure 4.14c). It takes a long time interval before the natural circulation establishes in the system. During it, FW temperatures also experience an inversion. Once the natural circulation is completely established, FW temperatures start to positively drift due to the residual decay heat produced in the blanket. The system heat losses are not able to counterbalance this source term. The PHTS temperatures rise of 10 °C in the last 4000 s of simulation with a slope of nearly 9 °C/hr. As discussed before, this parameter is lower than the one observed for case LF1.

During accidental evolution, pressure in FW PHTS system increases (Figure 4.13b). Pressurizer sprays are disabled since all the system pumps are off. Pressure rise continues up to the PORV opening setpoint. With respect to LF1 sequence, the timing of this event is significantly anticipated (Table 4.16). Later, the system pressure begins to cycle accordingly with the valve component multiple openings. Discharging mass through the PORV is the way adopted by the FW system to dissipate the decay heat produced in the blanket. The total amount of water evacuated from FW PHTS at EOT is reported in Table 4.16. The level in the pressurizer is shown in Figure 4.13c, normalized with respect to the total height of the component. Pressure rise produces a continuous mass insurge (i.e., level increase) in the tank. A step up in the water level is experienced any time PORV opens to discharge mass. At EOT the component is nearly solid.

Finally, Figure 4.13d reports the trend of the maximum EUROFER temperature in the FW component. The peak present in the PHTS water BB outlet temperatures (Figure 4.14a) is not visible in the material temperature trend. The FW thermal inertia, even if low, completely smooths this temperature excursion. In the long term, the trend follows that of the PHTS water.

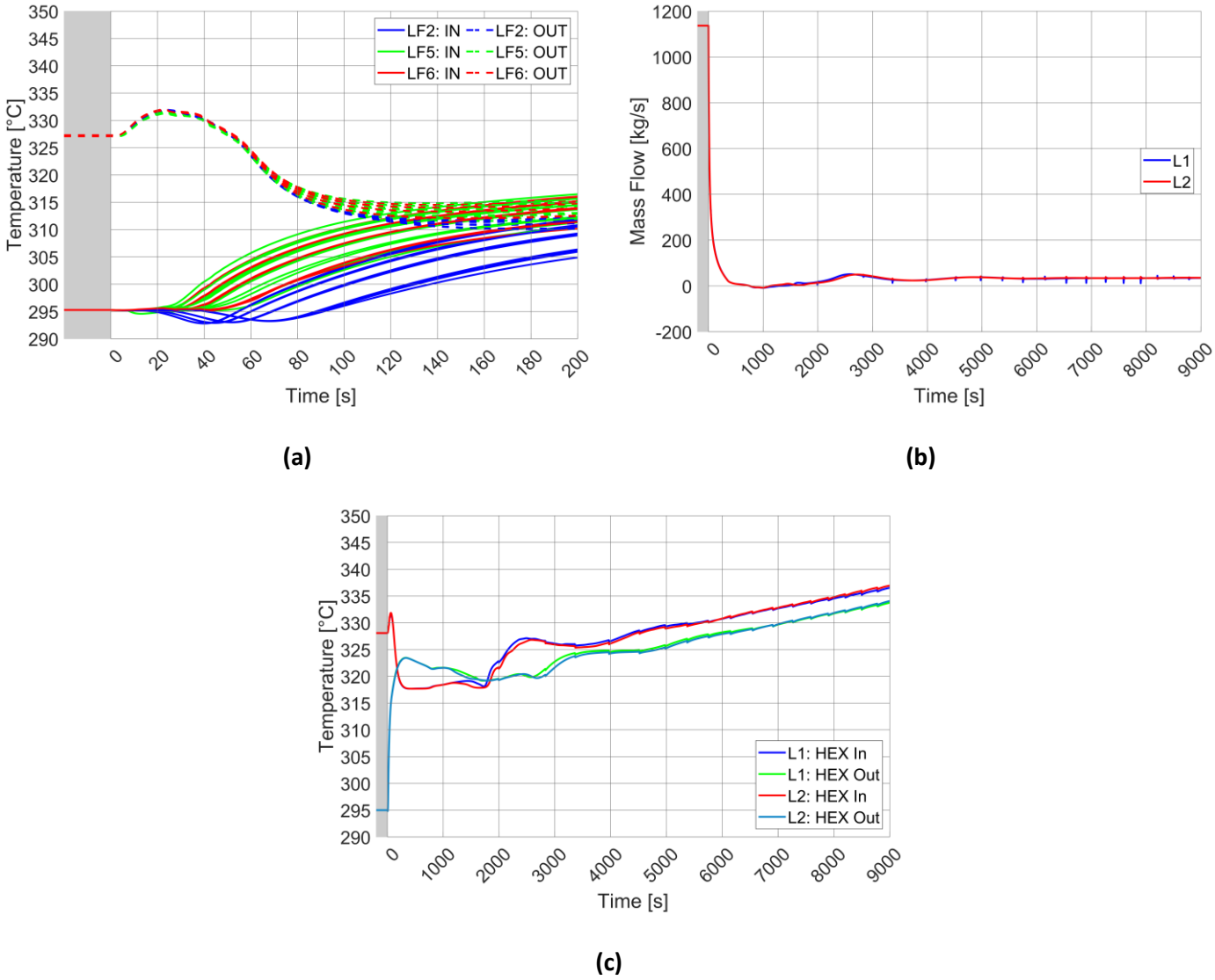

Figure 4.14 – Parameter trends in FW PHTS for LOFA transients characterized by natural circulation (LF2, LF5, LF6): **(a)** FW PHTS water temperatures at BB inlet & outlet (all sectors, early time, COB segment); **(b)** Mass flow elaborated by FW PHTS MCPs (full range, only LF6); **(c)** FW PHTS water temperatures at HEXs inlet & outlet (full range, only LF6).

BZ system transient evolution

The BZ PHTS performances are strongly influenced by the presence of off-site power. If available, as in sequences LF1 and LF2, system pumps continue to provide primary flow (see Figure 4.15d that is referred to loop 1 pump 1). Among the interested cases, LF1 was selected to represent the scenarios characterized by the presence of off-site power and only its parameters are plotted in the following figures. Initially, a continuous slight decrease can be detected in the flow trend. It is due to the rise of system average temperature. This causes the decrease of water density in the pump component and also an increase of the loop pressure drops. These two combined effects produce the reduction of the mass flow elaborated by BZ pumps. When the temperature at the component inlet reaches the setpoint, pump trip occurs and forced circulation is lost (for the

timing see Table 4.16). If loss of off-site power is assumed, as in scenarios LF5 and LF6, BZ pumps are stopped following the occurrence of turbine trip and forced circulation is lost shortly after the SOT (Figure 4.15d). Natural circulation establishes in the BZ system. LF6 was selected as reference case to plot simulation results related to the absence of off-site power. The presence or not of the forced circulation (i.e. off-site power) is the main element affecting the BZ PHTS behavior during such transients.

Forced Circulation (LF1 and LF2 Cases)

When plasma shutdown and turbine trip are triggered, BZ system loses the power source (plasma pulse) and the heat sink (PCS feedwater) at the same time, while maintaining primary flow at nearly nominal value. This combination of factors produces the convergence of the system hot and cold temperatures to a common value (Figure 4.15a). No temperature peak is detected at blanket outlet in any sector. Figure 4.15a is related to COB segment, but this is still valid for LOB/ROB and LIB/RIB.

The plasma shutdown takes more time (42 s, Table 4.10) with respect to PCS feedwater ramp-down (10 s) and, above all, TSVs closure (0.5 s). This leads to a power unbalance and a consequent pressure spike in both BZ PHTS and PCS. In BZ PHTS, Figure 4.15b, the power surplus is dissipated by multiple openings of the pressurizer PORV. In the same way, the PCS pressure transient is managed by the steam line SRVs (Figure 4.15c). All three steps of this valve system are forced to intervene to limit the pressure increase. The maximum value experienced is slightly above the PCS design pressure. This demonstrates the appropriateness of the current valve design.

In the mid-term, BZ system is cooled down by the OTSGs (Figure 4.15e, related to BZ loop 1). Their residual cooling capability is due to the flow circulating in the steam generators any time the SRVs open to reduce the PCS pressure. This cooling system is available until a significant water inventory is present in the OTSGs secondary side. As shown by Figure 4.15f (loop 1 OTSG), the water level in the steam generator riser drops to zero at SOT in correspondence with the power surplus due to plasma shutdown. After that, water level is still present only in the lower downcomer. This is the water inventory available in the mid-term at the OTSGs secondary side. Any time SRVs open to reduce PCS pressure, level decreases. Once the lower downcomer has been completely evacuated, (for the timing and the total amount of mass discharged see Table 4.16), the dominant effect on the BZ temperatures is the presence of the decay heat. System heat losses are unable to dissipate such thermal power. Temperatures start to positively drift (Figure 4.15e) with a slope of nearly 12 °C/hr (22 °C in 6500 s, from 500 s to 7000 s). Even for the BZ system, the curve slope related to the forced circulation (LF1 and LF2 sequences) is higher than the one associated to cases dominated by natural circulation (LF5 and LF6). The difference is due to the pumping power, acting as an additional source term of the same order of magnitude of the decay heat. After BZ pump trip, whose timing is reported in Table 4.16, when forced circulation is lost and natural circulation establishes, if simulation time were increased, the same temperature slope would be observed for all the cases.

The BZ pressure goes down during the cooling transient provided by the OTSGs in the mid-term (Figure 4.15g). Its value drops even below the nominal one. This is possible because the pressurizer heaters are offline due to turbine trip. After the complete blow-down of OTSGs secondary side inventory, the system pressure rise following the temperature trend. This increase is limited by the pressurizer sprays that are still active since their operation depends on the BZ pumps. With the increase of the system temperature, they introduce in the pressurizer control volume water at higher enthalpy, reducing the effectiveness of their pressure control action. The

pressurizer level also increases almost linearly during this time interval. It is reported in Figure 4.15h normalized with respect to the component height. When the pressurizer is nearly solid, sprays are unable to perform the pressure control function and the system pressure restart to rise, triggering the PORV. The timing of this event is in Table 4.16. From this moment, PHTS pressure starts to cycle. In this way, PORV component dissipates the decay heat produced in the blanket. The total PHTS mass discharged at EOT is shown in Table 4.16.

Natural Circulation (LF5 and LF6 Cases)

In these cases, with plasma termination and turbine trip, also the BZ pumps trip is triggered. The BZ system loses at the same time: the power source (plasma shutdown), the heat sink (turbine trip) and the primary flow (pumps trip). The PHTS water temperature trends at blanket inlet/outlet (Figure 4.15a, COB segment) result from the relative balance between these decreasing parameters. Initially, the plasma power is dominant and a temperature spike can be detected at the blanket outlet. The peak value is reported in Table 4.16. Then, the primary pump coast-down, which lasts more than the plasma shutdown curve, becomes prevalent and the system temperatures converge.

The initial power surplus produces a pressure spike in both BZ PHTS and PCS. In the former, Figure 4.15b, it is managed by the pressurizer PORV, while in the latter, Figure 4.15c, the pressure transient is limited by the steam line SRVs. All three steps are necessary to limit the pressure rise. The observed maximum value is slightly above the PCS design pressure, proving the effectiveness of the SRVs design even in these scenarios.

In the mid-term, BZ system is cooled down by the OTSGs, as shown in Figure 4.15e regarding loop 1. As already discussed, their residual cooling capability is available until a significant water inventory is present at OTSGs secondary side. The presence of natural circulation (with respect to forced circulation) increments the time needed to the SRVs to evacuate the OTSGs secondary side inventory (see different timing collected in Table 4.16 and trends reported in Figure 4.15f). The lower primary flow in the steam generator (with respect to the one ensured by forced circulation) decreases the overall heat transfer coefficient and, consequently, the thermal power removed by PCS. This slows down the pressure rise in the secondary system and increases the time interval between two subsequent SRVs openings. With natural circulation, the OTSGs cooling capability lasts more than cases dominated by forced circulation.

Terminated the water inventory in the OTSGs secondary side lower downcomer, the dominant effect on the BZ temperatures is the presence of the decay heat. They start to drift positively. The temperature slope is lower than the one due to forced circulation because of the absence of pumping power. Temperatures rise of 10 °C in the last 4000 s of simulation (nearly 9 °C/hr).

During the cooling transient provided by the steam generators, system pressure decreases unlimited by pressurizer heaters (Figure 4.15g). They are disabled from the occurrence of turbine trip. Later, once evacuated the OTSGs secondary side inventory (the total mass discharged is provided by Table 4.16), the system pressure starts to rise. Pressurizer sprays are off since no pumps are available in the circuit. The PORV opening setpoint is reached quite faster (compare timing gathered in Table 4.16). From this moment, PHTS pressure follows the sawtooth trend already discussed. The trend of water level in the pressurizer (Figure 4.15h) is similar to the one reported in Figure 4.13c for LF6 sequence. The parameter evolution and the phenomenology occurring in the component are the same. At the end of the transient, the tank is nearly solid. The total BZ PHTS water mass discharged by PORV at EOT is indicated in Table 4.16.

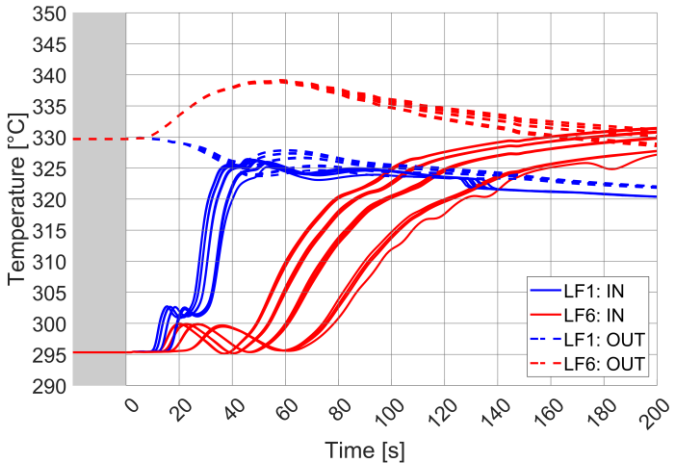
Temperature [°C]
Time [s]
LF1: IN
LF6: IN
LF1: OUT
LF6: OUT

(a)

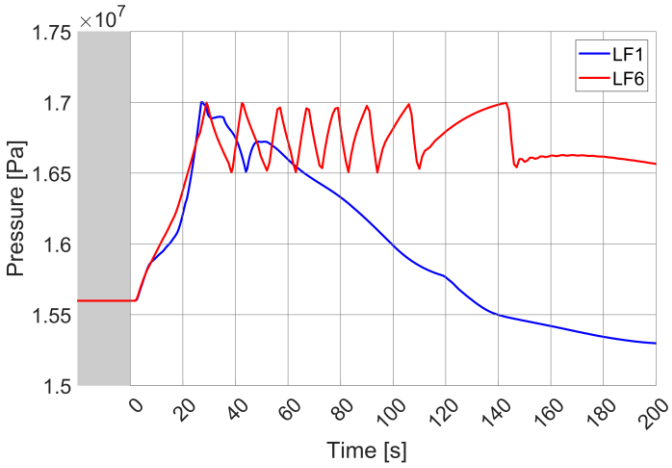
×10^7
Pressure [Pa]
Time [s]
LF1
LF6

(b)

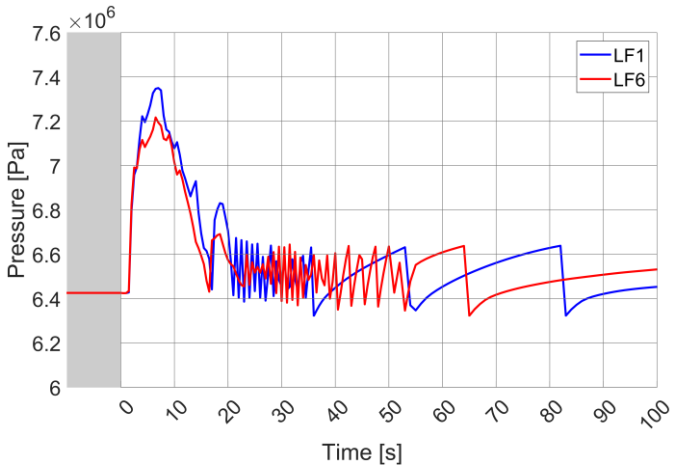
×10^6
Pressure [Pa]
Time [s]
LF1
LF6

(c)

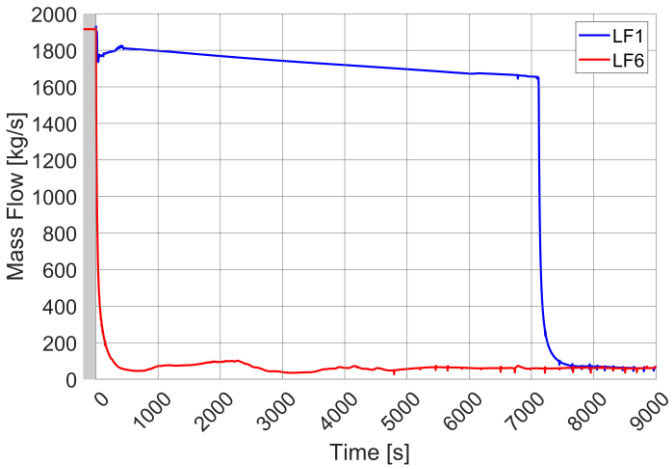
Mass Flow [kg/s]
Time [s]
LF1
LF6

(d)

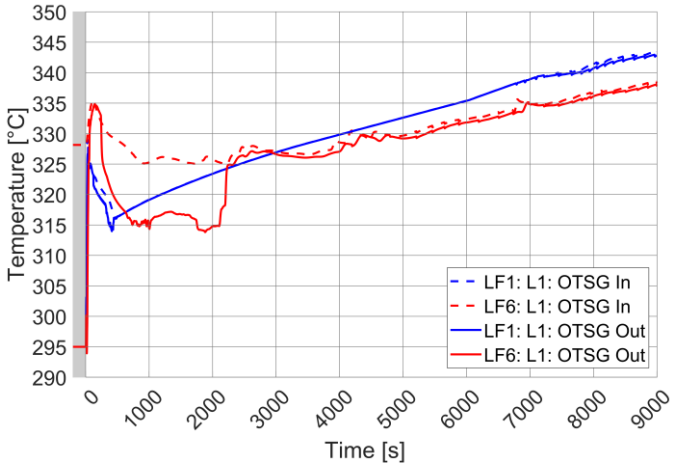
Temperature [°C]
Time [s]
LF1: L1: OTSG In
LF6: L1: OTSG In
LF1: L1: OTSG Out
LF6: L1: OTSG Out

(e)

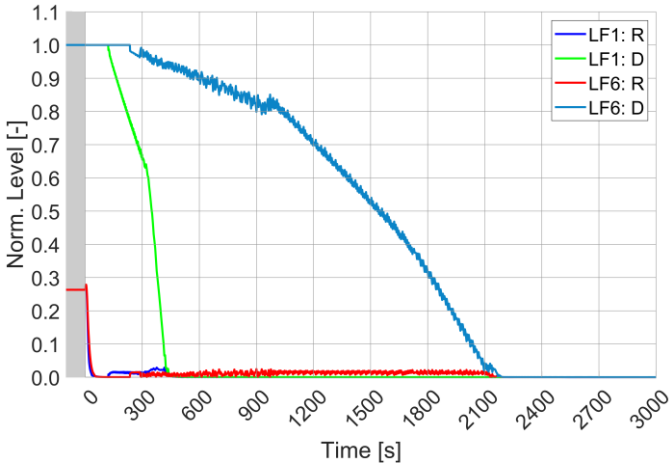
Norm. Level [-]
Time [s]
LF1: R
LF1: D
LF6: R
LF6: D

(f)

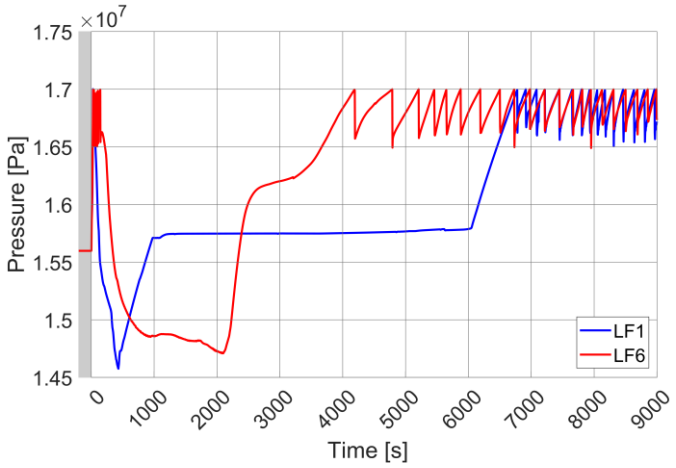

(g)

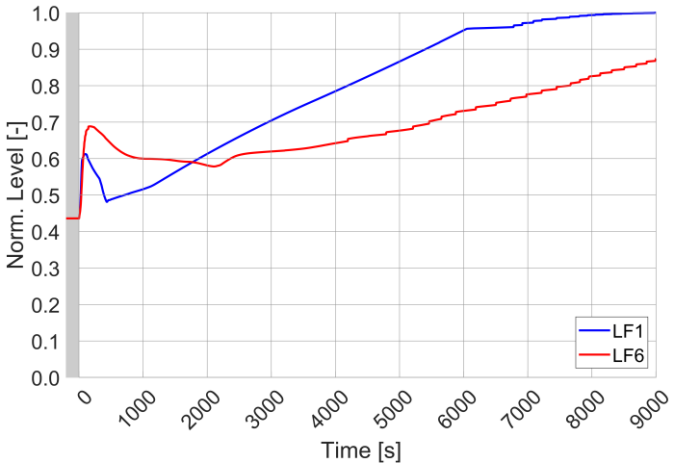

(h)

Figure 4.15 – Comparison between LF1 and LF6 transients: **(a)** BZ PHTS water temperatures at BB inlet & outlet (all sectors, early time, COB segment); **(b)** Pressure in BZ PHTS (early time); **(c)** PCS pressure at OTSGs secondary side outlet (early time); **(d)** Mass flow elaborated by BZ loop 1 MCP 1 (full range); **(e)** BZ PHTS water temperatures at OTSG inlet & out-let (loop 1, full range); **(f)** Collapsed level in loop 1 OTSG secondary side riser (R) and lower downcomer (D) (normalized, full range); **(g)** Pressure in BZ PHTS (full range); **(h)** Collapsed level in BZ pressurizer (normalized, full range).

4.5.2.2 LOFA involving BZ PHTS

BZ system transient evolution

Once PIE occurs, the primary flow elaborated by interested pump/pumps starts to decrease. In LF3 and LF7 transients, only loop 1 pump 1 is stopped (partial LOFA), while, in LF4 and LF8 sequences, all system pumps are involved in the accident (complete LO-FA). Low flow takes few seconds to be detected, actuating the plasma shutdown. Consequently, also turbine trip is triggered. In case LF7, where a loss of off-site power is assumed, turbine trip causes the stop of all the system pumps not interested from initiating event. For this reason, in LF4, LF7 and LF8 scenarios, the coast-down of all the BZ pumps is nearly contemporaneous and these cases have a similar accidental evolution. The only different sequence is LF3, where loop 1 pump 2 and loop 2 pumps continue to provide primary coolant flow. They are stopped on high-temperature signal at nearly EOT. Summarizing, for what concerns BZ PHTS, the selected cases can be grouped in the same way already seen for FW PHTS in **§** 4.5.2.1. Main events and parameters related to the LOFA transient simulations involving BZ pumps are collected in Table 4.17.

Table 4.17 – Summary table for LOFA transients involving BZ PHTS.

Event/Parameter	**Unit**	**LF3**	**LF4**	**LF7**	**LF8**
PIE (LOFA)	-	Partial (BZ)	Complete (BZ)	Partial (BZ)	Complete (BZ)
Loss of off-site power	yes/no	no	no	yes	yes

PT signal occurrence	s	2.5	2.5	2.5	2.5
TT signal occurrence	s	2.5	2.5	2.5	2.5
TSVs start to close	s	2.5	2.5	2.5	2.5
Start of PCS feedwater ramp-down	s	2.5	2.5	2.5	2.5
Start of IHTS mass flow ramp-down	s	10	10	2.5	2.5
Time of FW PHTS water temperature peak	s	-	-	24	23
FW PHTS water temperature peak [1]	°C	-	-	331	331
Time of BZ PHTS water temperature peak	s	30	58	59	59
BZ PHTS water temperature peak [1]	°C	333	340	340	340
FW MCPs Trip occurrence	s	7496	8440	2.5	2.5
BZ MCPs trip occurrence (pumps not interested by PIE)	s	7260	-	2.5	-
Time to evacuate BZ OTSGs secondary side inventory	s	600 (L1) 460 (L2)	2150	2150	2150
Water mass discharged from BZ OTSGs secondary side	kg	15,017 (L1) 17220 (L2)	15,037 (per OTSG)	14,871 (per OTSG)	12,885 (per OTSG)
FW PORV first opening time (Long Term)	s	7332	8576	2248	2284
Total FW PHTS water mass discharged at EOT	kg	1034	247	1444	1356
BZ PORV first opening time (Long Term)	s	6952	4412	4164	4168
Total BZ PHTS water mass discharged at EOT	kg	6113	4592	4541	5025

[1] For all the sixteen sectors, both the BZ and FW PHTS water temperatures were detected at the outlet of COB segment. For each PHTS, peak temperature reported in the table is the maximum among all the temperature readings.

Case LF3

In this case, the loop 1 pump 2 and the loop 2 pumps are still active after the turbine trip (off-site power is available). The loop 1 pump 2 increases the mass flow provided (Figure 4.16c). From the point of view of this component, loop 1 branch hosting the failed pump becomes an alternative flow path. The pressure drops related to this path is less than the ones associated to a blanket sector, even with the failed pump acting as a minor head loss. Thus, for loop 1 pump 2 the curve of the hydraulic resistance decreases and, being a constant rotational velocity imposed as a boundary condition for the component, the result is an increase of the mass flow provided and a drop of the pump head. Instead, the operation of loop 2 pumps is only slightly altered with respect to the nominal state. The transient is dissymmetrical with respect to the toroidal dimension. The sixteen sectors experience different flows (Figure 4.16a) and, consequently, inlet/outlet COB temperatures (Figure 4.16b). Higher mass flows (i.e., lower outlet temperatures) correspond to the sectors located diametrically opposite with respect to the failed pump (four of sixteen). However, the forced flow availability significantly smooths the temperature peaks at COB outlet (only few degrees above the nominal value).

As observed in FW system for case LF1, a flow inversion can be detected in the BZ system branch where the failed pump is located (blue line in Figure 4.16c). The pressure drops related to the blanket component are so high that a part of the flow provided by loop 1 pump 2 is recirculated through this alternative flow path. Differently from LF1 sequence, the reverse flow does not cause a temperature inversion in loop 1, see blue (hot temperature) and green (cold temperature) lines in Figure 4.16d. In fact, each loop pump is hosted in a branch going from the OTSG outlet plenum to the cold ring. Even if there is a reverse flow in one of these branches, the primary flow through the hot leg and the steam generator is ensured in the right direction by the operation of the pump still active. The effect of the failed pump is visible in Figure 4.16d. The reduced flow in loop 1 with respect to loop 2, slows down the cooling transient provided by the OTSGs in the mid-term. Loop 2 steam generator runs out its cooling capability one hundred seconds earlier than the correspondent in loop 1 (see Table 4.17 for timing and water mass discharged). From this moment, no sensible differences are detectable between the TH performances of the two loops.

BZ temperatures positively drift since blanket decay heat overwhelms the system heat losses. The temperature slope is of nearly 11 °C/hr (25 °C in 8000 s). This is the same value obtained for BZ system in LF1 and LF2 scenarios, when LOFA transients involve FW PHTS and off-site power is available to ensure the BZ pumps operation. Forced circulation confirms to produce a higher curve slope than the one associated to natural circulation (see Figure 4.17b related to case LF8). As already discussed, the PHTS coolant additional heating is caused by pumping power. Pump trip occurs due to a high-temperature signal at the component inlet (the correspondent timing is reported in Table 4.17). Later, forced circulation is lost and natural circulation establishes (Figure 4.16c). The temperature slope starts to decrease accordingly (Figure 4.16d).

The plot of BZ pressure trend is not included in the following since it is the same of LF1 and LF2 transients (see Figure 4.15g). The presence of pressurizer sprays, ensured by the BZ pumps still active, allows to control the system pressure for nearly two hours. Then, the decay heat is evacuated by discharging PHTS water through the PORV. The relevant parameters are contained in Table 4.17.

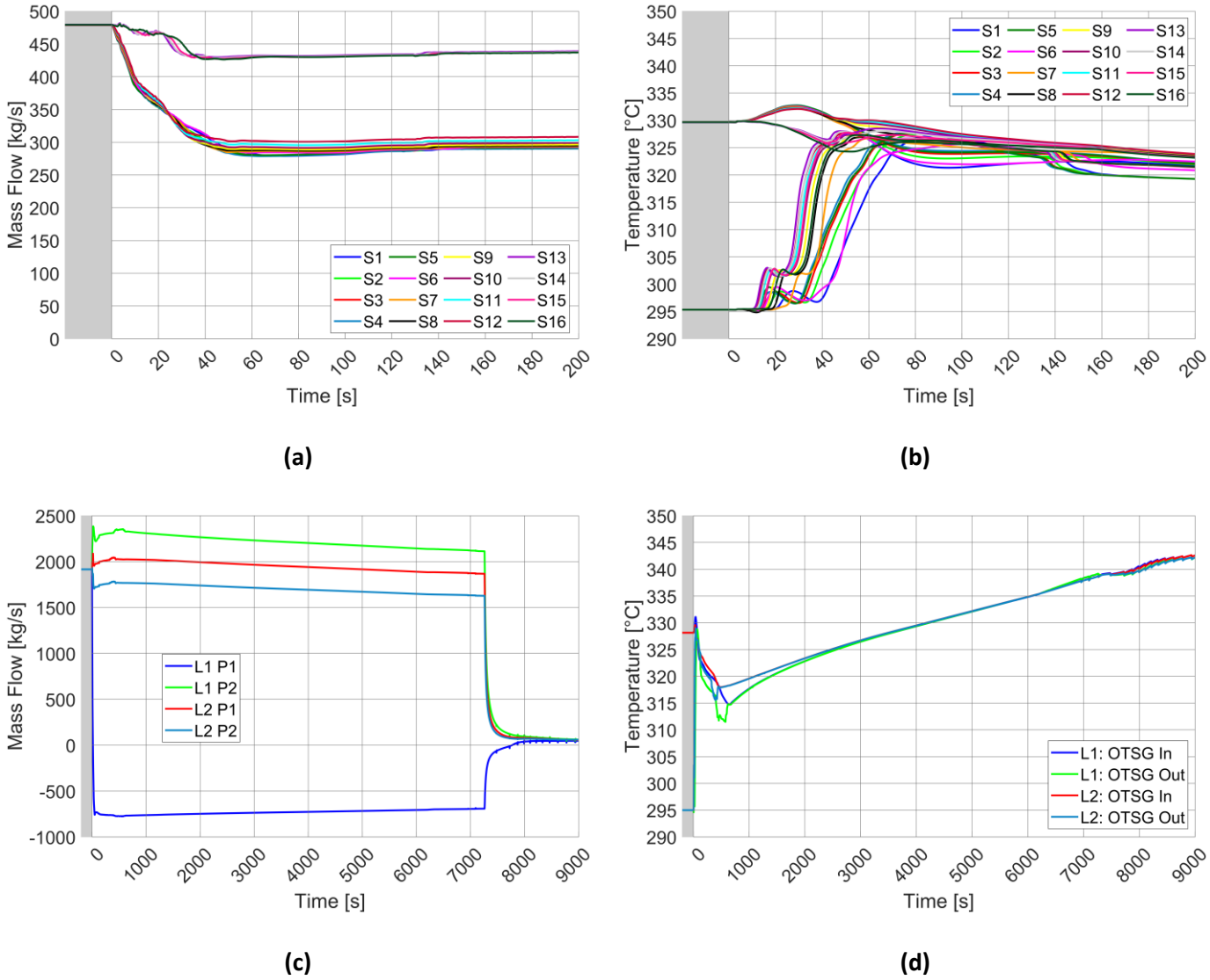

Figure 4.16 – Partial LOFA on BZ PHTS without loss of off-site power (LF3 transient): **(a)** Mass flow in BZ sectors (early time); **(b)** BZ PHTS water temperatures at BB inlet & outlet (all sectors, early time, COB segment); **(c)** Mass flow elaborated by BZ PHTS MCPs (full range); **(d)** BZ PHTS water temperatures at OTSGs inlet & outlet (full range).

Cases LF4, LF7 and LF8

The considered cases have an accidental evolution very similar to the one described in **§** 4.5.2.1 for LF5 and LF6 sequences. In these scenarios, trip occurs for all the BZ pumps after few seconds from the SOT (see Table 4.16 and Table 4.17), albeit for different reasons. The resulting transients are quite symmetrical with respect to the toroidal dimension. PHTS temperatures at blanket inlet/outlet are the same for all the sectors. They are reported in Figure 4.17a for LF4, LF7 and LF8 scenarios. Among the different cases, no sensible differences are detectable in the temperature peak at COB outlet. The maximum values, indicated in Table 4.17, are close to the ones observed for LF5 and LF6 transients (Table 4.16). Also the BZ system long-term behavior is nearly the same. As an example, the PHTS water temperatures at OTSGs inlet/outlet are plotted for case LF8 in

Figure 4.17b. The trend is very similar to the analogous contained in Figure 4.15e for LF6 sequence. After pump coast-down, natural circulation establishes in the system, influencing the BZ thermal-hydraulic performances. A detailed description of the transient evolution is provided in **§** 4.5.2.1, in the paragraph referring to BZ PHTS. A quantitative comparison between all the interested cases can be performed looking at the main timing and TH parameters related to the BZ system contained in Table 4.16 and Table 4.17.

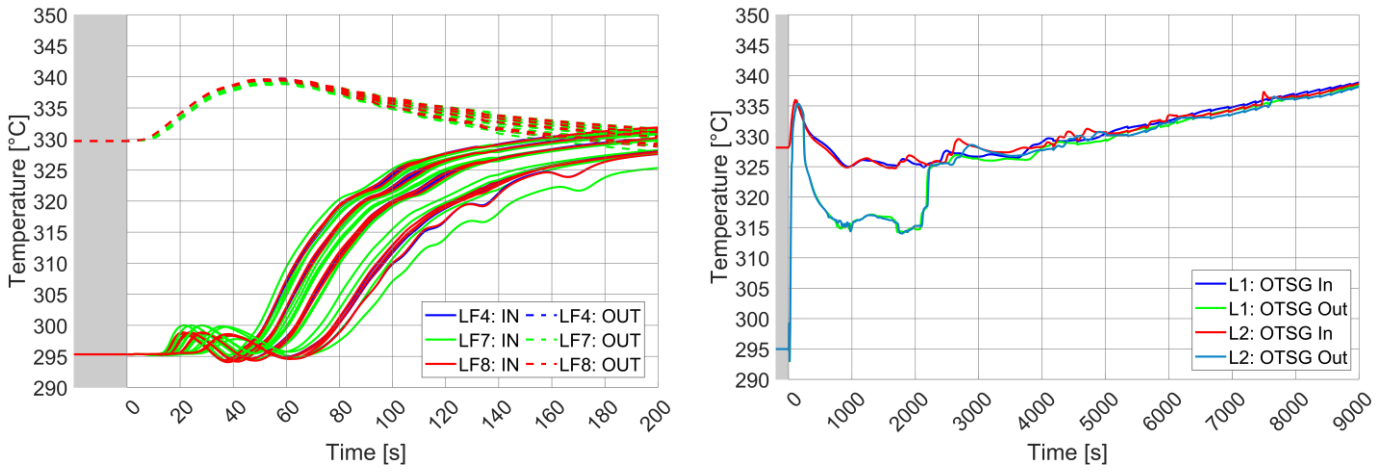

(a) **(b)**

Figure 4.17 – Parameter trends in BZ PHTS for LOFA transients characterized by natural circulation (LF4, LF7, LF8): **(a)** BZ PHTS water temperatures at BB inlet & outlet (all sectors, early time, COB segment); **(b)** BZ PHTS water temperatures at OTSGs inlet & outlet (full range, only LF8).

FW system transient evolution

Considerations related to FW system are of the same kind of the ones done in **§** 4.5.2.1 about BZ PHTS. FW pumps are not interested from PIE and the system performances are strongly influenced by the presence of off-site power. If available, as in LF3 and LF4 scenarios, FW pumps continue to provide primary flow. The slight parameter decrease is due to the increase of the system average temperature. (Figure 4.18c). Pump trip occurs after more than two hours from the initiating event (Table 4.17). It is triggered by a high-temperature signal at the component inlet. The simulation is characterized by the presence of the forced circulation. Instead, if the loss of off-site power is assumed, as in cases LF7 and LF8, FW pump are stopped following the turbine trip and forced circulation is lost few seconds after SOT (Figure 4.18c). Natural circulation establishes in the FW system, influencing its TH behavior during the overall simulation.

Forced Circulation (LF3 and LF4 Cases)

Due to the presence of forced circulation, FW temperatures converge very quickly to an average value (Figure 4.18d). Transient is symmetrical with respect to toroidal dimension and, for all the blanket sectors, no temperature peak is present at blanket outlet (Figure 4.18a). HITEC® secondary flow is available for the first 10 s after initiating event. This element, combined with the

suitability of forced circulation in the primary system, avoids the opening of the pressurizer PORV in the early time (Figure 4.18b).

In the long term, FW HEXs are not able to provide any cooling capability and system heat losses do not counterbalance the blanket decay heat. An additional source term is represented by the pumping power. FW temperatures start to drift positively (Figure 4.18d). The associated temperature slope is of nearly 11 °C/hr (20 °C in 7000 s). The EUROFER maximum temperature in the FW component follows the same time trend of the PHTS water (Figure 4.18e). Once pump trip is triggered, the forced circulation is lost and the natural circulation establishes. The temperature slope decreases to the value related to simulations characterized by natural circulation (LF7 and LF8 scenarios).

Pressure transient for the considered cases (Figure 4.18f) is similar to the one described for LF1 sequence (see **§** 4.5.2.1 and Figure 4.13b). After the heat sink loss, FW pressure is limited by pressurizer sprays. When sprays become unable to perform their control function (due to system temperature increase), the management of system pressure switches to PORV component (timing of this event is reported in Table 4.17, as well as the total mass discharged from the valve at EOT). The plot of pressurizer level related to cases LF3 and LF4 is not included in the following since very similar to the one reported in Figure 4.13c for LF1 transient.

Natural Circulation (LF7 and LF8 Cases)

For the considered cases, plasma shutdown, turbine trip, FW pump trip and IHTS mass flow ramp-down occur at the same time. The PHTS water temperatures at COB inlet/outlet are collected, for all the sectors, in Figure 4.18a. Their trends result from the relative balance between plasma power, primary flow and secondary flow, all decreasing parameters but with different time slope. COB outlet temperatures experience a slight increase since initially the plasma power is prevalent. Then, since the pump coast-down (Figure 4.18c) takes more time than the plasma shutdown (see Table 4.10) the outlet temperatures start to decrease. Peak value is the same for all the sectors and for all the cases, as reported in Table 4.17.

Due to the unavailability of forced circulation in both primary and secondary systems, the initial power surplus produces a sudden increase in the FW PHTS pressure, Figure 4.18b. Pressurizer PORV intervenes to manage this pressure transient.

During the FW pump coast-down, system reaches a quite uniform temperature (Figure 4.18d). Later, while natural circulation establishes, system temperatures experience an inversion. In the long term, the original temperature field is restored and FW temperatures positively drift. The temperature slope is lower (nearly 9 °C/hr) than the one observed for cases LF3 and LF4, since the additional source term due to pumping power is missing.

After FW pump trip, pressurizer sprays are disabled. System pressure increase can be only limited by the PORV intervention (Figure 4.18f). The valve opening occurs quite earlier with respect to LF3 and LF4 sequences (compare different timing reported in Table 4.17). From this moment, the system pressure begins to cycle accordingly with the valve component multiple interventions. The PHTS mass discharged at the EOT is indicated in Table 4.17.

Figure 4.18e reports the trend of the maximum EUROFER temperature in the FW component. The peak related to PHTS water present at blanket outlet (Figure 4.18a) here is not visible. Temperature excursion is smoothed by the FW thermal inertia, even if low. After plasma termination, material temperature drops driven by PHTS water temperature. Instead, in the long

term, FW component is heated up by the decay heat. The temperature slope is the same of the PHTS water trend.

Summarizing, the considered cases have accidental evolutions very similar to the one described in **§** 4.5.2.1 for LF2, LF5 and LF6 transients. The common factor to all these scenarios is the occurrence of FW pump trip after few seconds from the SOT (see Table 4.16 and Table 4.17), albeit for different reasons. Hence, the forced circulation is immediately lost and the natural circulation influences the system TH performances during the overall simulation. A qualitative comparison between the interested cases can be performed by looking at the parameter trends collected in Figure 4.13 and Figure 4.14 (where LF6 sequence was used as reference) and Figure 4.18 (using LF8 as selected scenario). For the same purpose, but from a quantitative point of view, parameters and timing contained in Table 4.16 and Table 4.17 can be used.

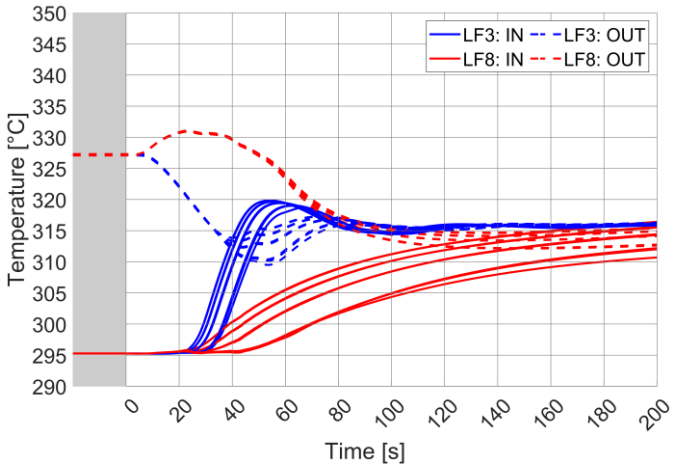

(a)

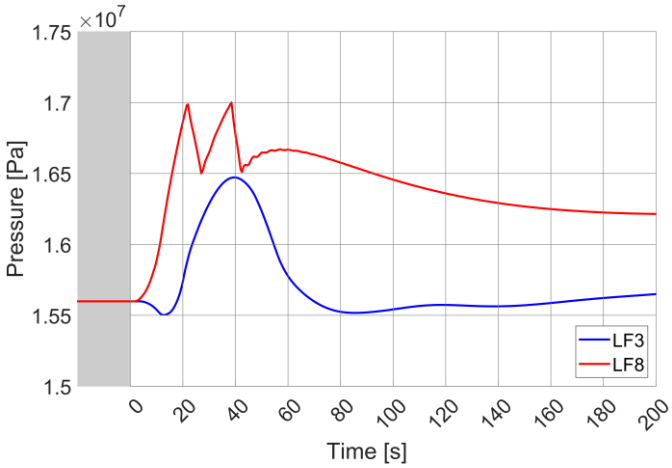

(b)

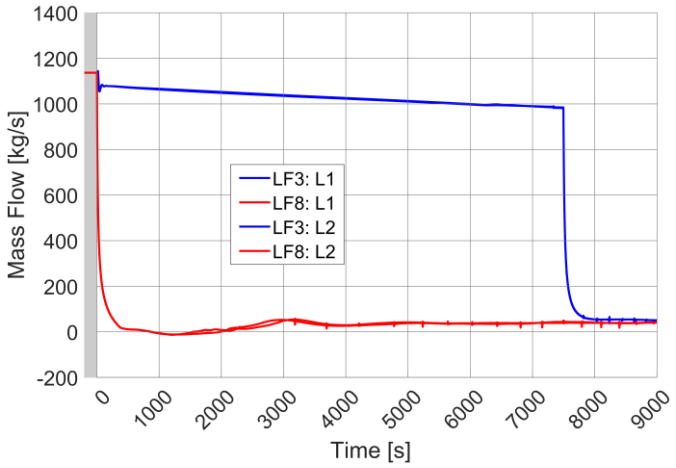

(c)

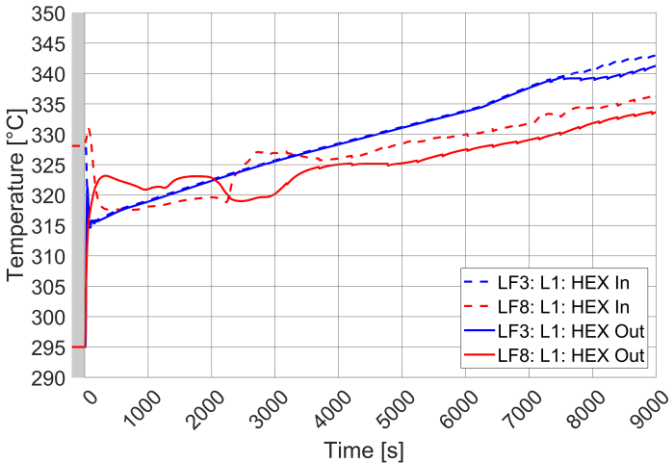

(d)

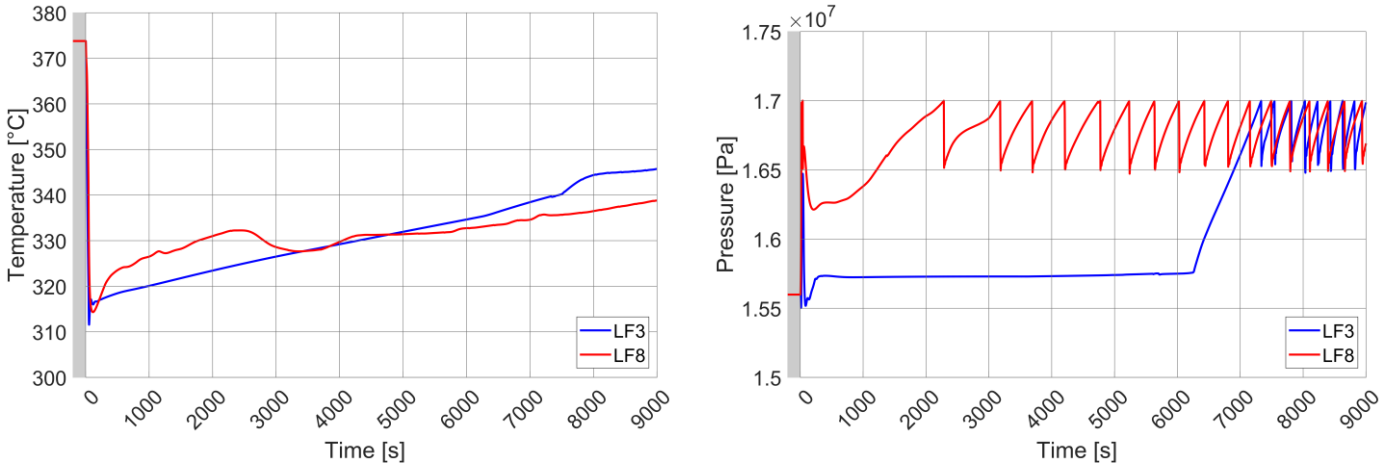

(e) **(f)**

Figure 4.18 – Comparison between LF3 and LF8 transients: **(a)** FW PHTS water temperatures at BB inlet & outlet (all sectors, early time, COB segment); **(b)** Pressure in FW PHTS (early time); **(c)** Mass flow elaborated by FW MCPs (full range); **(d)** FW PHTS water temperatures at HEX inlet & outlet (loop 1, full range); **(e)** Maximum EUROFER temperature in FW component (full range); **(f)** Pressure in FW PHTS (full range).

4.5.2.3 Discussion

Results presented in the previous section highlight how the type of circulation (natural or forced) characterizing each cooling system is the main element influencing the correspondent TH performances. According to the considered case, BZ and FW systems can have the same kind of circulation or not. However, as a general rule, for the suitability of the forced circulation in a primary cooling circuit is mandatory the presence of the off-site power. If its loss is assumed in combination with the initiating event, at the occurrence of turbine trip forced circulation is lost in both systems, if not already missing in one of them according to the specific PIE considered. In fact, the turbine generator set is the only element ensuring the AC power needed for the pump operation and it is disconnected after the turbine trip. If forced circulation is available, the following TH behavior can be observed in BZ and FW systems.

- Few seconds after the SOT, the temperature spikes at blanket outlet characterizing the trend of both BZ and FW PHTS water are significantly smoothed.
- In FW system, the availability of forced circulation in both primary and secondary (only for the first 10 s) circuits limits the pressure increase and avoids the intervention of the pressurizer PORV in the short term.
- The OTSGs cooling capability lasts less. The presence of forced circulation in the primary cooling system enhances the steam generator heat transfer coefficient, increasing the thermal power transferred to the PCS. This reduces the time between two subsequent steam line SRVs openings and speeds up the evacuation of the water mass present in the OTSGs secondary side. Once terminated, the steam generators are no more able to provide any cooling function to the BZ PHTS.
- For more or less two hours from PIE occurrence, the system pressure is controlled by the pressurizer sprays. The first PORV intervention in the long term is significantly delayed.

- The temperature slope characterizing both BZ and FW systems (thermally coupled) is higher since pumping power is added to the power balance. This is valid until the pump trip is triggered in each system.

Summarizing, forced circulation improves the BZ and FW TH performances in the short term, smoothing the temperature spikes, but reduces the ones in the mid-long term. In fact, it shortens the cooling interval provided to the BZ PHTS by the steam generators and increases the temperature slope experienced by BZ and FW systems, reducing the reactor grace time. The best management strategy for PHTS pumps is to use, at the SOT, the forced circulation they provide, in order to avoid excessive temperatures in the blanket, and then stop them, to increase the reactor grace time. To prove the effectiveness of this control logic, case LF3 was run again adding a new trip signal to PHTS primary pumps. The level in the BZ OTSGs lower downcomer is monitored and when it reaches the 1% of the rated value in full plasma power state, both BZ and FW pumps are stopped. LF3 (partial LOFA in BZ PHTS without loss of off-site power) was selected as reference case since it is one of the two (together with LF1) where forced circulation is available for both primary cooling systems, even if reduced in the one involved in the PIE. The PHTS water temperatures at loop 1 OTSG/HEX inlet/outlet are reported in Figure 4.19. As shown, this new pump management strategy combines the benefits of forced circulation in the short term and of natural circulation in the long term.

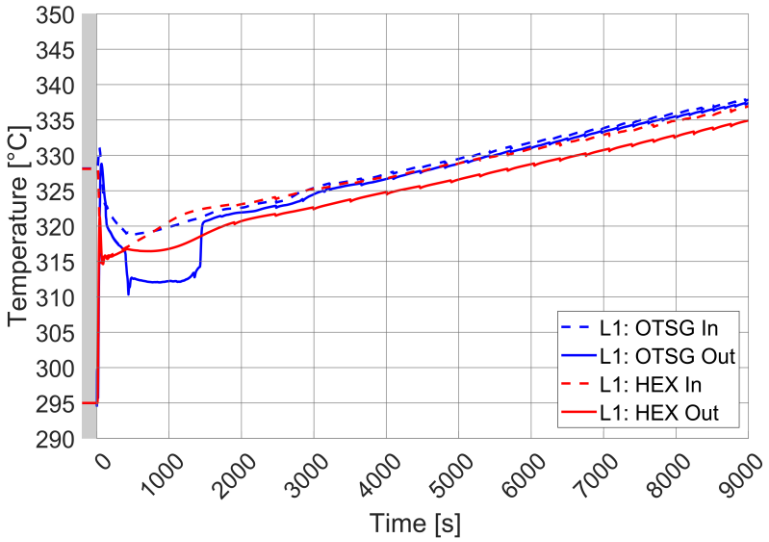

Figure 4.19 – Partial LOFA on BZ PHTS without loss of off-site power, new blanket primary pumps management strategy: BZ PHTS water temperatures at loop 1 OTSG inlet & outlet and FW PHTS water temperatures at loop 1 HEX inlet & outlet (full range).

In all the transient simulations, included the one discussed in this section, BZ and FW systems experience a positive temperature drift in the mid-long term. It is due to the unbalance between decay heat produced in the blanket and system heat losses, with the former overwhelming the latter. The temperature slope is higher if the forced circulation is still active. In these cases, it must be added another source term to the power balance, represented by the pumping power. In the calculations performed, no Decay Heat Removal (DHR) system was implemented in the input deck and the power surplus is managed by the pressurizer PORV. Power in excess produces a pressure increase and when this parameter reaches the PORV opening setpoint, PHTS water mass is discharged with its associated enthalpy content. This is the way adopted by BZ and FW system to dissipate the power surplus. However, a DHR system is foreseen for DEMO reactor in accidental conditions, as discussed in [58].

4.5.2.4 Conclusions

Simulation outcomes highlight the appropriateness of the current PHTS design with respect to the accidental scenarios analyzed. Blanket temperatures do not experience excessive excursions during the plasma shutdown. Pressure transients in BZ PHTS, FW PHTS and PCS are effectively managed by the related relief systems. The results underline a strong dependence of the PHTS TH performances on the type of circulation characterizing each primary cooling circuit. The forced circulation is of great importance in the management of the initial power transient, while the natural circulation is advisable in the long term to increase the reactor grace time. On the basis of the calculation outcomes, a revised BB PHTS primary pump management strategy was defined for the cases where the off-site power is available. It combines the short term benefits of forced circulation and the long term advantages of natural circulation. In the long term, BZ and FW systems are heated up by the blanket decay heat, overwhelming the system heat losses. In the current simulations, the power surplus is dissipated by the pressurizer PORV that opens and discharges PHTS water mass and related enthalpy. In the future developments of the activity, the DHR system foreseen for DEMO reactor will be implemented in the input deck to evaluate the effectiveness of its mitigation action.

4.5.3 Locked Rotor/Shaft Seizure

Another initiating event belonging to the category 'Decrease in reactor coolant system flow rate' selected to be investigated was the Locked Rotor/Shaft Seizure (LR/SS). Such transient was studied when involving either a BZ or a FW primary pump. The influence on the accidental evolution of the loss of off-site power was also evaluated, for a total of four different cases considered.

PIE was simulated by decreasing the rotational velocity of the failed pump from rated value to zero in 1 s. The management strategy described in **§** 4.5.2 for some reactor components was adopted also in these transient calculations.

The PI controllers used in the plasma power flat-top calculation to set the primary flow and the required temperature at blanket inlet were disabled. Pump rotational velocity was imposed as a constant boundary condition until the occurrence of the pump trip. After that, the component coast-down is ruled by the torque-inertia equation (see equation 4.1). For FW and BZ primary pumps the moment of inertia values selected in **§** 4.5.1 were adopted. PCS feedwater and IHTS HITEC© flow at OTSGs/HEXs secondary side inlet were provided as boundary conditions by using time-dependent junctions. Such components respond to the actuation logics described in **§** 4.5.2.

The plasma ramp-down curve was the same of the previous transient simulations, see Table 4.10/Figure 4.8. Calculations were run assuming initiating event occurring after 100 s of plasma power flat-top. Such initial phase is represented in the figures of this section with a grey background. Timeline was reset in the plots to have PIE at 0 s. Transient calculations lasted 9000 s (2.5 hr), for an overall simulation time of 9100 s. Different time steps were used. Initially, when the transient dynamic is expected to be faster, a lower time step was used (5.0×10^{-3} s). In the final part, this parameter was increased (1.0×10^{-2} s) to speed up the simulations.

For each transient calculation analyzed in this section, there is an analogous one in **§** 4.5.2 related to partial LOFA. The only difference between these two scenarios is that LR/SS causes failed pump velocity to drop to zero nearly instantaneously, while, in the partial LOFA, failed pump decelerates following the torque/inertia equation. Hence, in the first case, the loss of primary flow is quite faster and the resulting temperature transient for both blanket component and PHTS circuits is more severe. For this reason, analysis of the results in the following section was focused on the early time (200 s) after the SOT. In the long term, both initiating events have similar accidental evolution and BB PHTS behavior. The related discussion is available in **§** 4.5.2. Results explained in the following are also analyzed in [85].

4.5.3.1 LR/SS involving FW PHTS primary pump without LOSP

The PIE involves FW PHTS loop 1 primary pump. The presence of off-site power is postulated. As previously stated, failed pump rotational velocity drops to zero in one second. Control system immediately (<0.5 s) detects the flow decrease (see Figure 4.20a) and actuates the plasma shutdown. As a consequence, also turbine trip is triggered, followed by PCS feedwater coast-down and TSV closure.

Since off-site power is available, loop 2 pump continues to operate at nearly nominal conditions (see Figure 4.20a). Its primary flow is unevenly distributed between the sixteen sectors, according to their position. The sector interested by the maximum flow rate is the 13th since it is the nearest to loop 2 (i.e. the operative pump, see Figure 4.4). On the contrary, sector 4, the nearest to the failed pump, is the one experiencing the minimum cooling flow and the most severe

temperature transient. Mass flow trends plotted in Figure 4.20b for sectors 4 and 13 envelop the ones related to all the other sectors (not reported). The same rationale is used for the FW PHTS water temperatures at blanket inlet and outlet. Only the ones of sector 4 (worst case) and sector 13 (best case) are plotted in Figure 4.20c. The maximum water temperature registered at blanket outlet is of 347 °C and it occurs 20 s after the SOT. In a short time interval (few seconds) around this event, the steam quality in the final section of FW channels reaches nearly the 10% (Figure 4.20d). However, the associated Departure from Nucleate Boiling Ratio (DNBR) calculated by the code is >> 1. No thermal crisis is thus expected in the cooling channels. Nevertheless, it must be noted that the blanket model prepared for the current simulation activity is not able to investigate the local behavior of FW component since no poloidal differentiation is performed. In addition, the heat flux used as boundary condition is the average one related to the overall reactor. Although, this parameter varies significantly along the tokamak poloidal dimension, arriving at values far higher than the mean. In conclusion, the DNBR computed by the code is only an average parameter evaluated for the overall FW component. For this reason, more detailed analyses are needed in the future to evaluate the DNBR at different poloidal locations inside the blanket.

Material temperatures in the FW component are reported in Figure 4.20e, for both tungsten (W) and EUROFER (EU). Sector 4 is chosen as worst case and COB is used as reference segment. The effect of the water temperature spike is not visible in the figure and this is due to the FW thermal inertia that, even if low, is enough to absorb the thermal fluctuation. What is experienced by FW materials is the temperature decrease caused by the plasma termination. Water temperature increase also produces also a pressure peak in the FW system (Figure 4.20f). Although, the pressure transient is quite reduced and it is managed by the pressurizer sprays, avoiding PORV intervention. FW sprays are still operative since loop 2 pump is on and provides forced circulation.

One last phenomenon to be discussed is the flow inversion in loop 1, highlighted by the negative values shown in Figure 4.20a. It is produced by the significant pressure drops associated to the blanket component, see Figure 4.7. For this, part of the flow provided by loop 2 pump goes through loop 1 in the reverse direction instead of flowing in the BB sectors. The reverse flow causes a temperature inversion in the correspondent loop.

Regarding the BZ PHTS, since LOSP is not assumed, all the primary circuit pumps keep on running at nominal velocity, ensuring nearly the rated primary flow. After plasma termination, the water temperatures at blanket inlet/outlet converge to a common value since no power source is left. As an example, Figure 4.20g collects the ones related to sector 1. The pressure spikes reported in Figure 4.20f and Figure 4.20h for the PHTS and PCS are due to the management strategy adopted for the secondary system. In fact, plasma termination and turbine trip occur simultaneously. Plasma power decreases with an exponential trend lasting nearly 40 s (before dropping to decay heat). Instead, feedwater is linearly reduced to zero in 10 s and, above all, TSVs close in 0.5 s. This misalignment between the power source and the heat sink cooling capability causes a power surplus that is dissipated by the correspondent PHTS and PCS pressure control systems. In particular, all three steps of SRVs intervene at the secondary side, while BZ pressurizer sprays and PORV manage the pressure transient in the primary circuit. In both systems, pressure does not exceed the design value, demonstrating the appropriateness of the PHTS and PCS pressure control function.

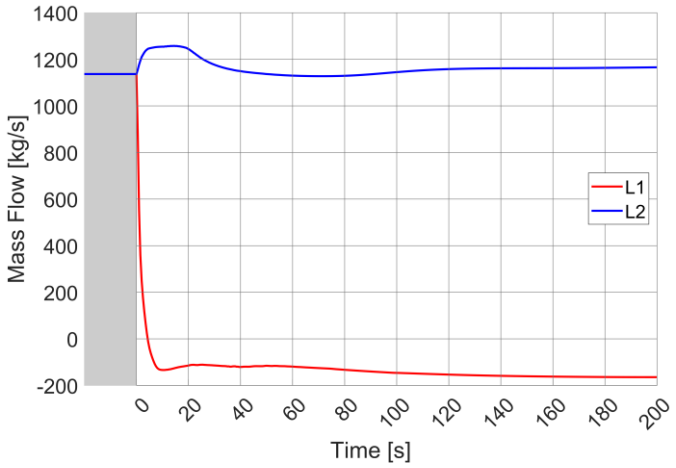
Mass Flow [kg/s]
Time [s]
L1
L2

(a)

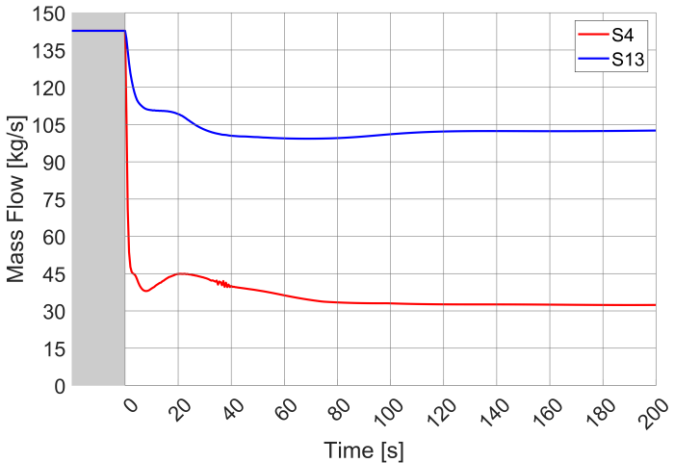
Mass Flow [kg/s]
Time [s]
S4
S13

(b)

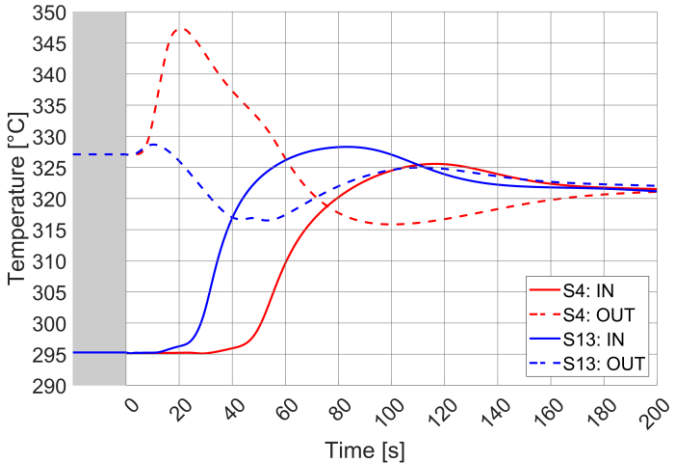
Temperature [°C]
Time [s]
S4: IN
S4: OUT
S13: IN
S13: OUT

(c)

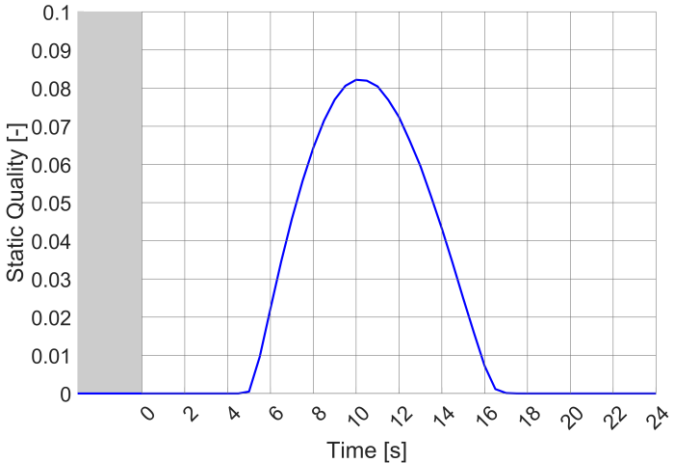
Static Quality [-]
Time [s]

(d)

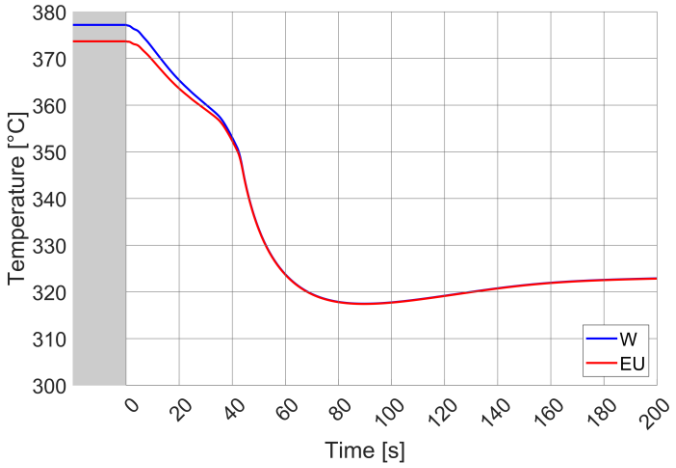
Temperature [°C]
Time [s]
W
EU

(e)

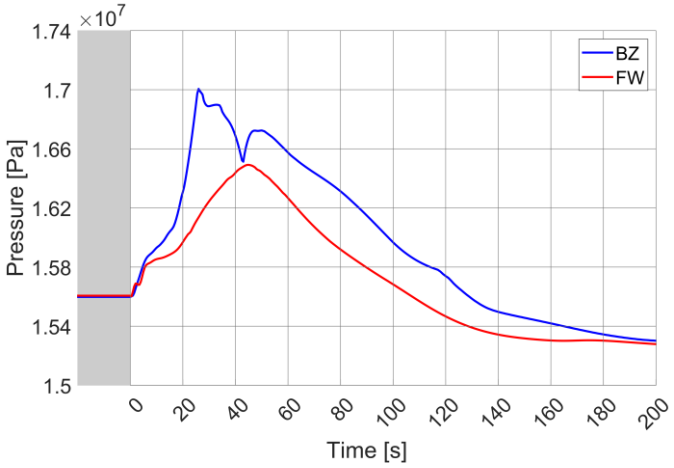
Pressure [Pa]
Time [s]
BZ
FW

(f)

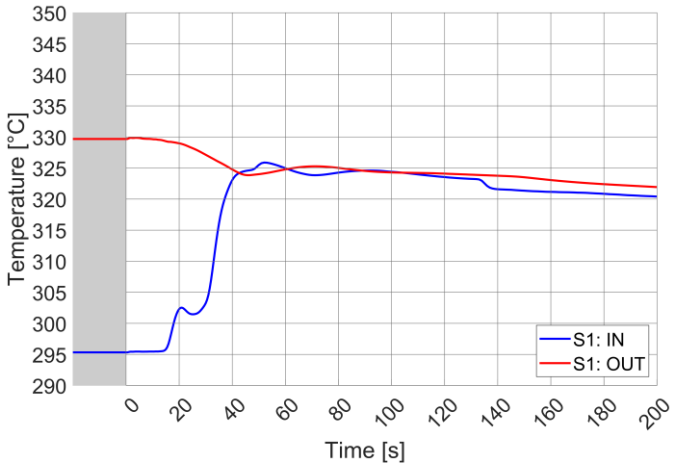

(g)

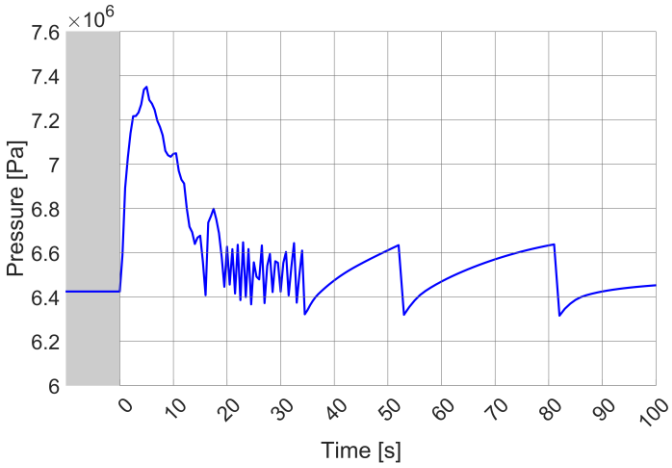

(h)

Figure 4.20 – LR/SS involving FW PHTS loop 1 pump without LOSP: FW primary pumps mass flow **(a)**; FW sectors mass flow, sector 4 and 13 **(b)**; FW PHTS water temperatures at BB inlet/outlet, sector 4 and 13 **(c)**; Steam quality at FW channels exit, sector 4 **(d)**;Tungsten (W) and EUROFER (EU) temperatures related to FW component in sector 4 COB segment **(e)**; FW and BZ PHTS pressures **(f)**; BZ PHTS water temperatures at BB inlet/outlet, sector 1 **(g)**; PCS pressure **(h)**.

4.5.3.2 LR/SS involving BZ PHTS primary pump without LOSP

LR/SS accident affects one of the pumps of BZ PHTS loop 1. As for the previous scenario, the component low flow is immediately (<0.5 s) detected by the control system, triggering plasma termination and turbine trip.

As shown in Figure 4.21a, the BZ pumps not interested from PIE are still working thanks to the availability of off-site power. While loop 2 pumps keep operating at nearly nominal conditions, the active component of loop 1 increases the provided mass flow. From its point of view, two alternative flow paths are now available: the blanket sectors and the loop 1 branch where failed component is situated. The pressure drops associated to the second path are significantly lower, even with the crashed pump acting as a minor head loss. For this reason, the curve of hydraulic resistance associated to loop 1 active pump decreases, while the rotational velocity is maintained constant being imposed as a boundary condition. As a consequence, the pump surges the provided mass flow and decreases the head. The reverse flow in the branch hosting the failed component (negative values of red line in Figure 4.21a) does not cause temperature inversion in the correspondent loop. Looking at Figure 4.2, it is possible to note that each BZ OTSG is connected to the cold ring by means of two pipelines, each one equipped with a primary pump. If one of them crashes, as in this transient, the other ensures the flow through the loop in the right direction. Instead, in FW system, since only a primary pump is foreseen for each loop, both flow and temperature inversions occur, in case of component failure.

The total BZ flow is distributed among the sixteen sectors according to their relative position with respect to the failed pump. For this reason, even in this case, sector 4 represents the worst case and sector 13 the best one, enveloping all the others. Mass flows and water temperatures at blanket inlet and outlet are plotted for the sectors of interest in Figure 4.21b and Figure 4.21c, respectively. The maximum water temperature detected at blanket outlet is 335.5 °C (at 25 s after

SOT). It is well below the saturation temperature at the nominal system pressure (15.5 MPa), thus no thermal crisis is expected within DWTs. The lower peak with respect to FW system is due to the large thermal inertia offered by PbLi flowing in the breeder zone.

The phenomenology behind the occurrence of the pressure spikes shown in Figure 4.21d and Figure 4.21e, respectively referred to PHTS and PCS, has been already discussed in the previous section. Another aspect is worth to be pointed out. As visible, the amplitude of the pressure peak in PCS system is reduced with respect to the analogous in Figure 4.20h. At the same time, more PHTS PORV interventions (represented by the number of teeth in the sawtooth trend) are needed to manage the pressure transient in the primary system (compare Figure 4.21d with Figure 4.20f). Both these effects are caused by the reduction of primary flow in the BZ circuit due to the PIE. The lower primary flow produces a decrease of the overall heat transfer coefficient in the BZ OTSGs, i.e. of the thermal power transferred to the secondary side. This increments the power load that must be managed by the primary pressure control system and, correspondently, diminishes the one deputized to PCS SRVs.

Regarding the FW PHTS, the current accidental scenario is of no particular concern. Off-site power ensures the operation of primary pumps. After plasma termination, the lack of a source term, together with the presence of rated primary flow, leads water temperatures to converge to a common value, as reported in Figure 4.21f. Sector 1 is used as reference. HITEC secondary flow is available at the transient beginning, guaranteeing enough cooling capability to remove the thermal power related to the plasma shutdown. Pressure transient is similar to the one in Figure 4.20f.

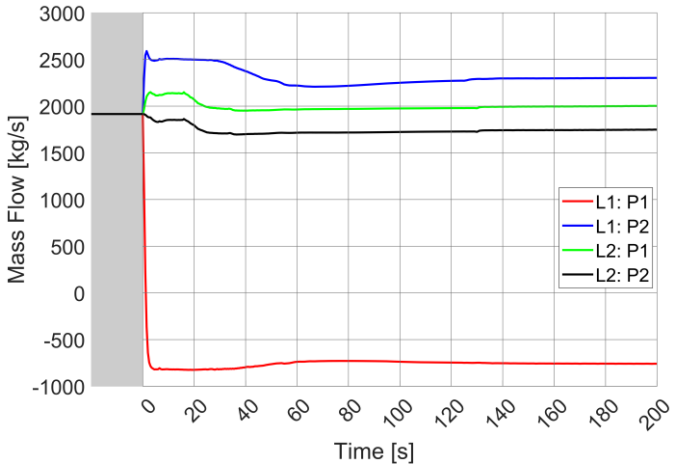

(a)

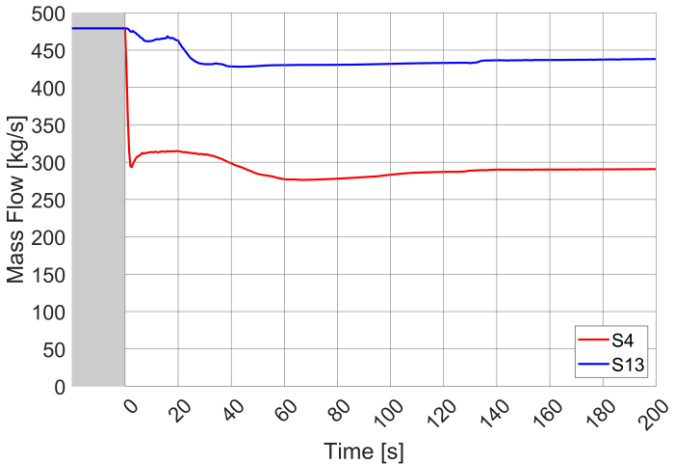

(b)

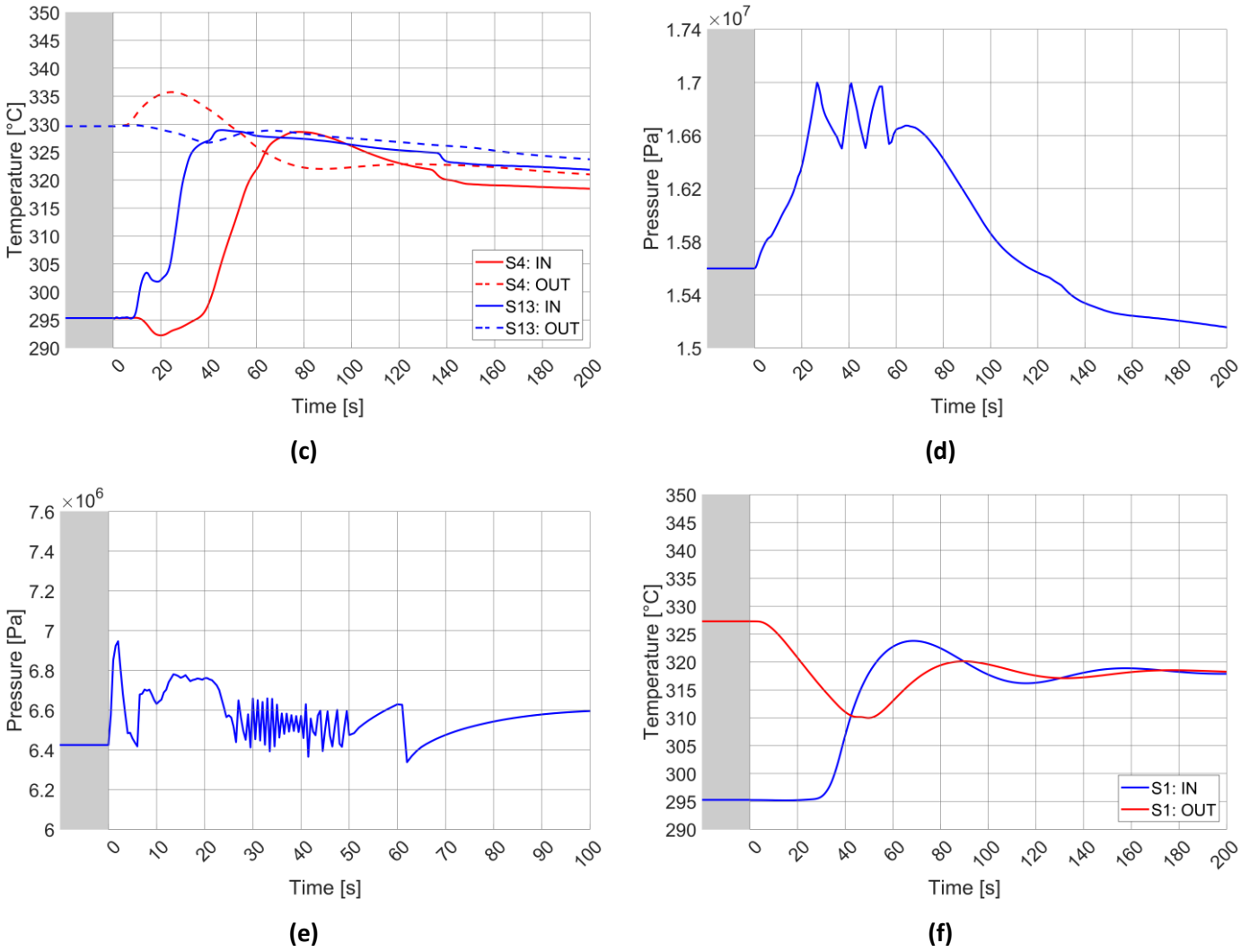

Figure 4.21 – LR/SS involving BZ PHTS loop 1 pump without LOSP: BZ primary pumps mass flow **(a)**; BZ sectors mass flow, sector 4 and 13 **(b)**; BZ PHTS water temperatures at BB inlet/outlet, sector 4 and 13 **(c)**; BZ PHTS pressure **(d)**; PCS pressure **(e)**; BZ PHTS water temperatures at BB inlet/outlet, sector 1 **(f)**.

4.5.3.3 Influence of Loss Off-Site Power

When LR/SS occurs, either involving a FW or a BZ pump, plasma termination and turbine trip are always triggered in less than one second from the SOT. In fact, flow associated to failed component rapidly drops and it is immediately detected by the control system. If LOSP is assumed occurring in combination with the initiating event, steam turbine is the only lasting component that can provide the AC power needed for primary pumps operation. This means that, when turbine trip is called, all BZ and FW pumps (except the one interested from the initiating event) are cut off and start decelerating according to the torque/inertia equation (see equation 4.1). In conclusion, when LR/SS and LOSP are considered together, in less than one second, even if for different reasons, all the primary pumps are off. This is visible in Figure 4.22a and Figure 4.22f, respectively referred to FW and BZ primary pumps. Whether or not PIE is located in a specific circuit (FW or BZ) mainly affects the flow symmetry in the related system (see blue lines in Figure 4.22a and red lines in Figure 4.22f). Such dissymmetry results in an uneven flow distribution between tokamak sectors (see Figure 4.22b and Figure 4.22g), with a more severe temperature

transient for the ones nearest to the failed component (Figure 4.22c and Figure 4.22h). Also in this case, only parameters referred to sector 4 (worst case) and sector 13 (best case) are plotted. The behavior of the other sectors is enveloped. Dissymmetrical effects are more pronounced at the transient beginning due to the different decreasing trend associated to crashed component (sharp drop to zero in one second) with respect to the other system pumps (exponential trend due to torque/inertia equation). Also their stopping times are different, but the influence of this parameter is negligible since less than one second occurs between initiating event and turbine trip. In the long term, after all system pumps have stopped and natural circulation has established in both BZ and FW PHTS, flow in the two loops and sixteen sectors returns quite symmetrical. Only a small deviation can be detected, mainly influencing the loop flows, caused by the crashed pump acting as minor head loss due to the locked rotor or shaft seizure. Although, it is quite negligible. This aspect of BB PHTS long term behavior is well evidenced in **§** 4.5.2.1 and 4.5.2.2.

In the early time after SOT, because of the combination of initiating event and off-site power unavailability, both BZ and FW PHTS lose nearly simultaneously: the power source (plasma termination is triggered), the heat sink (PCS Feedwater and IHTS flow are ramp down) and the primary flow (primary pumps are crashed or stopped). The water temperatures at blanket inlet and outlet reported in Figure 4.22c and Figure 4.22h (respectively for FW and BZ sector 4, worst case) result from the relative balance between these decreasing parameters. Initially, the plasma power is prevalent, producing a temperature peak at blanket outlet. The effect of the LOSP assumption on the maximum water temperature is clear. Producing the loss of forced circulation in the primary cooling circuits, it causes the rise of this parameter. This can be detected in both systems and in both accidental scenarios, i.e. LR/SS involving either BZ or FW PHTS. The presence of the initiating event in a specific circuit furtherly increases water temperatures in the correspondent system, due to the sharp flow reduction caused by the failed pump. For BZ PHTS, water temperature at sector 4 outlet reaches a maximum of 339 °C (50 s after SOT) in case of crashed pump belonging to FW system, and of 344 °C (55 s after SOT) if failed pump is located in BZ circuit. Such temperatures are below the saturation temperature referred to PHTS nominal pressure. Hence, no thermal crisis is expected in the DWTs. Regarding FW system, maximum water temperature at sector 4 outlet is equals to 331 °C and 351 °C (both nearly at 20 s after SOT), respectively for LR/SS involving BZ or FW system. In this latter case, the steam quality in the final section of the FW channels reaches nearly the 10%. Trend is similar to the one reported in Figure 4.20d. LOSP assumption does not significantly affect this parameter (i.e. the transient dynamic in the first seconds after SOT). Moreover, also in this scenario, the DNBR computed by RELAP5 is always >> 1 and thus thermal crisis is expected to not occur in the cooling channels. The considerations made on this parameter in **§** 4.5.3.1 are still valid. After the spike, system temperatures converge to a common value (see Figure 4.22c and Figure 4.22h) since the primary pump coast-down lasts more than the plasma shutdown.

The initial power surplus is managed by the primary and secondary pressure control systems, as reported in Figure 4.22e, Figure 4.22i and Figure 4.22j, respectively related to FW PHTS, BZ PHTS and PCS pressures. As discussed in **§** 4.5.3.2, the loss of primary forced circulation strongly reduces the overall HTC (i.e. heat transfer to secondary side) within BZ OTSGs and FW HEXs. As a consequence, the majority of the thermal power in excess must be dissipated by the pressurizer PORV, increasing the number of component openings (compare Figure 4.22e with Figure 4.20f and Figure 4.22i with Figure 4.21d). It is important to underline that the stop of all the system pumps also disables the pressurizer sprays. Hence, in these accidental transients, the pressurizer PORV become the first line of intervention against the over pressurization.

Finally, for what concerns material temperatures (W and EU) related to FW component, they are reported in Figure 4.22d. What is worth to be emphasized is that FW thermal inertia is able to

absorb the water temperature spike also in these cases. The prevalent effect is still the plasma shutdown causing the decreasing temperature trends reported in the figure.

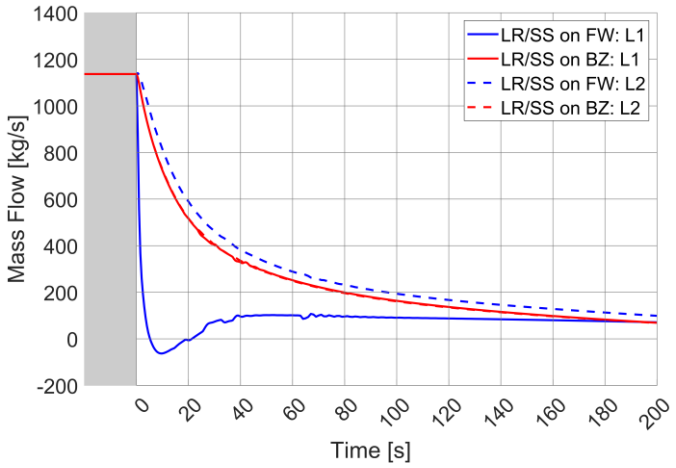

(a)

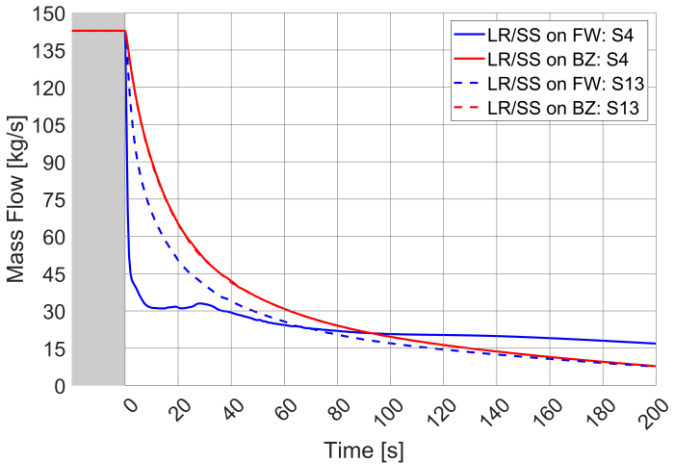

(b)

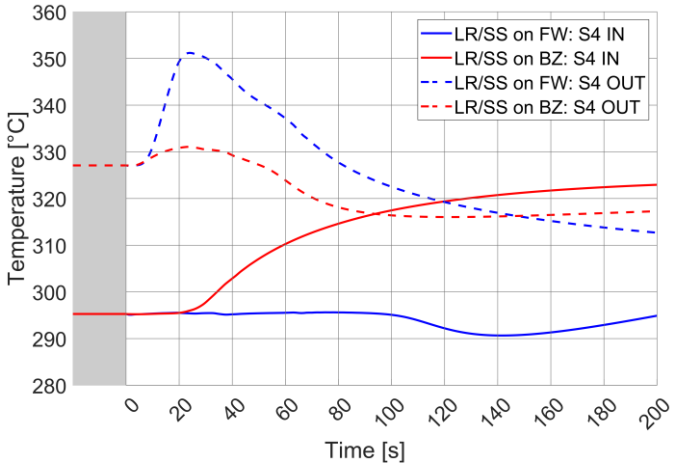

(c)

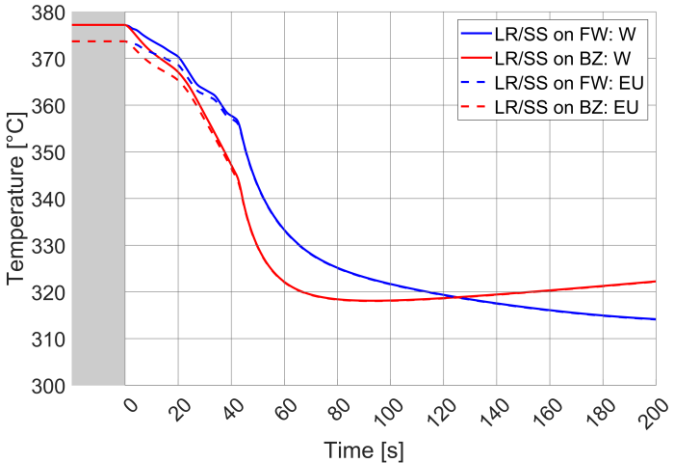

(d)

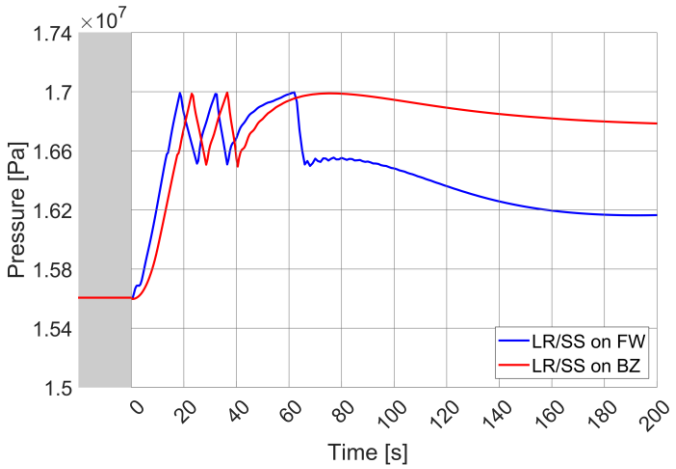

(e)

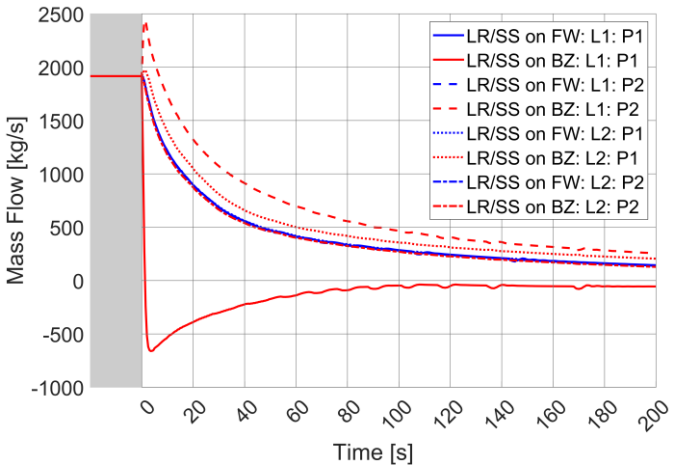

(f)

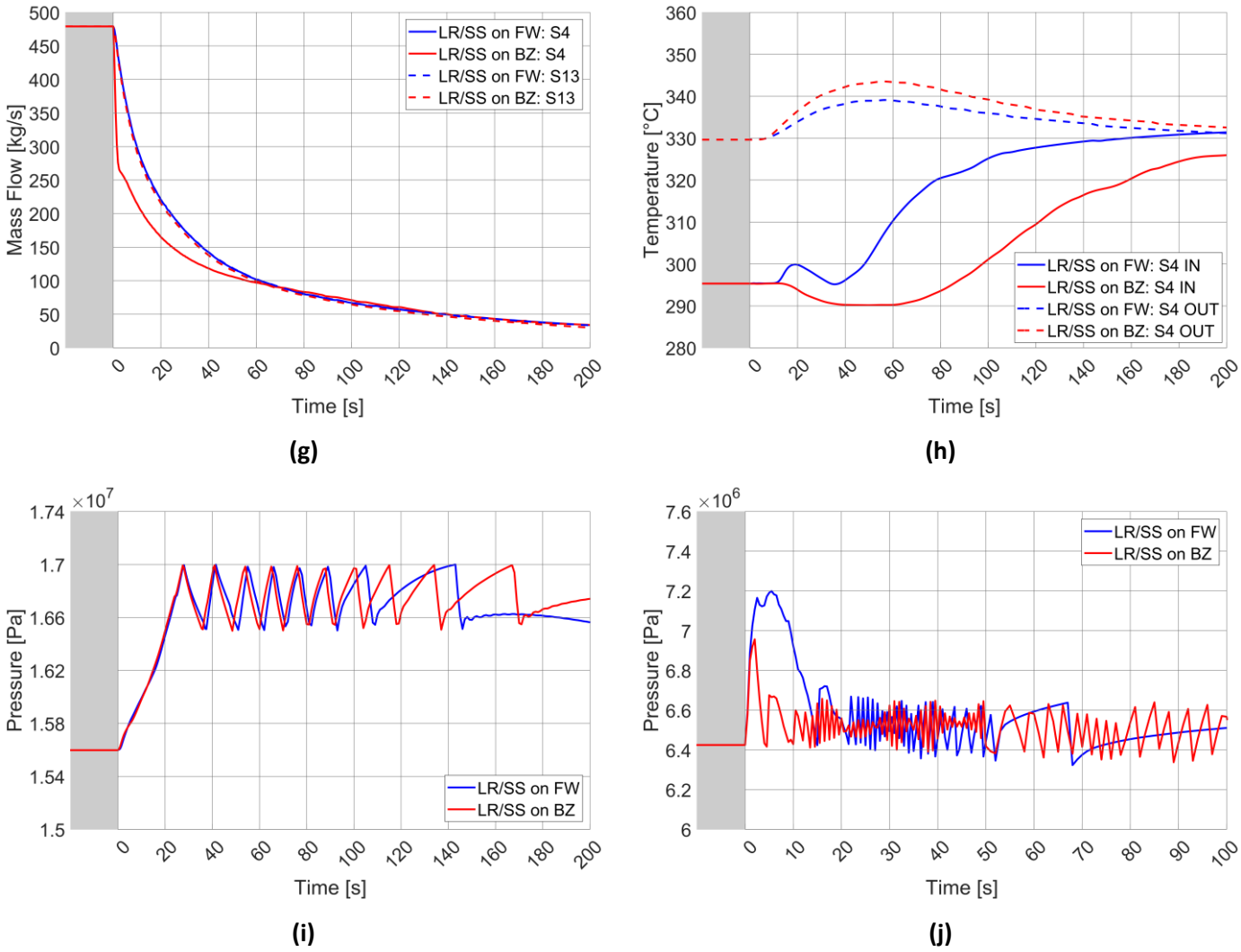

Figure 4.22 – Influence of LOSP on LR/SS accident: FW primary pumps mass flow **(a)**; FW sectors 4 and 13 mass flow **(b)**; FW PHTS water temperatures at BB inlet/outlet, sector 4 **(c)**; Tungsten (W) and EUROFER (EU) temperatures related to FW component in sector 4 COB segment **(d)**; FW PHTS pressure **(e)**; BZ primary pumps mass flow **(f)**; BZ sectors 4 and 13 mass flow **(g)**; BZ PHTS water temperatures at BB inlet/outlet, sector 4 **(h)**; BZ PHTS pressure **(i)**; PCS pressure **(j)**.

4.5.3.4 Conclusions

Locked rotor/shaft seizure was investigated when involving either a BZ or a FW pump. The influence of the loss of off-site power on the accidental evolution was also studied. The main blanket and PHTS parameters were assessed, such as mass flows, temperatures and pressures. The simulation outcomes proved the appropriateness of the current blanket and PHTS design in withstanding such accidental conditions. In all the transients analyzed, the occurrence of thermal crisis was not detected in both FW channels and DWTs. However, since no poloidal discretization was performed in the model developed for the current simulation activity, more detailed analyses in this field are recommended in the future development of the design activities. Finally, the implemented primary and secondary pressure control functions demonstrated to be able to manage the transients of this parameter in the correspondent systems in an effective way.

4.5.4 Inadvertent operation of a loop isolation valve

The primary coolant inventory in PHTS circuits is quite significant, see Table A2.14 for the section inside vacuum vessel and Table 4.3 and Table 4.4 for the one outside. In case of ex-vessel LOCA, this amount of water is discharged in the Tokamak Cooling Room (TCR). Moreover, if an in-vessel LOCA occurs, FW PHTS water inventory is spilled onto the vacuum chamber. In both cases, as widely discussed in [16][17], to reduce the PHTS water mass discharged, isolation valves could be installed in the primary cooling systems. Transient analyses were performed in the framework of Work Package Safety and Environment (WPSAE) activities, [16][17], placing the isolation valves at the inlet/outlet of DEMO sector segments. In this way, the number of these components is very high, generating some concerns about the reliability of the entire DEMO reactor. It is also possible to locate the isolation valves at the inlet/outlet of PHTS loops, significantly reducing their numbers. The transient analysis presented in this section deals with accidental sequences involving the inadvertent operation of one of these loop isolation valves.

Initiating event consists in the sudden closure of the isolation valve related to BZ or FW loop 1 hot leg. For the FW PHTS, there is no difference in choosing either the isolation valve on the hot leg or the one on the cold leg. In both cases, the sudden closure provokes the loss of a cooling loop. For the BZ PHTS, the inadvertent operation of a cold leg isolation valve causes only the loss of the related pump ad not of the entire loop. For conservative reason, the accidental sequence selected to be investigated is the one referred to the closure of the isolation valve on the hot leg. The isolation valve is supposed to close in 0.5 s. The influence of the loss of off-site power, occurring in combination with the initiating event, was also evaluated for these accidental sequences. Thus, four different simulations were run and their outcomes compared.

The actuation logic discussed in **§** 4.5.2 was used again in these transient scenarios. The only differences are related to the signals adopted for plasma termination and primary pump trip. First, it is important to recall that, for the latter components, the rotational velocity is imposed as a constant boundary condition until the correspondent trip is not triggered. From this moment, the pump coast-down is ruled by the torque-inertia equation (see equation 4.1). When occurs the isolation valve closure, the pump/pumps belonging to the failed loop experience a decreasing suction pressure and an increment of the static head. Being the rotational velocity constant (i.e. imposed pump characteristic curve), this results in an increase of the pump head and a drop in the mass flow elaborated by the component/components. Thus, to detect in an effective way the initiating event, a high-pump head signal was added among the others triggering the plasma shutdown. The same signal was also implemented between the ones actuating the pump trip.

The PI controllers used in the plasma power flat-top calculation to set the required temperature at blanket inlet are disabled. PCS feedwater and IHTS mass flows are imposed as boundary conditions by means of time dependent junction components. Their actuation logic is the same described in **§** 4.5.2. The plasma ramp-down curve is the one already considered for previous calculations (Table 4.10/Figure 4.8).

The initiating event occurs after 100 s of full plasma power state (grey background in the figures). Timeline was reset in the plots to have PIE at 0 s. Transient simulations were run for 9000 s (2.5 hours), for an overall problem time of 9100 s. Different time steps were adopted. At the transient beginning, when thermal excursions are expected to be more significant, a lower time step was used (5.0×10^{-3} s). In the final part, this parameter was increased to speed up the calculations (1.0×10^{-2} s).

4.5.4.1 Accidental sequences not involving loss of off-site power

First, consider the inadvertent operation of the isolation valve installed on the FW loop 1 hot leg. The primary flow in the failed loop immediately drops to zero. The head provided by the correspondent pump starts to increase (as explained in the previous section). In less than one second, it reaches the maximum value triggering the pump trip and the plasma termination. As a consequence, also the turbine trip is called. Due to the availability of off-site power, loop 2 primary pump keeps operating at nearly nominal conditions. Its flow is distributed among the tokamak sectors according to their relative position with respect to the active component. The nearest/farthest sectors are the thirteenth and the fourth, respectively (see Figure 4.4). The mass flows associated to these sectors, enveloping the ones related to all the others, are shown in Figure 4.23a. While plasma is shutdown, to lower flows correspond higher temperatures at blanket outlet (see Figure 4.23b). Note that in sector 13, the temperature rise is quite negligible. The maximum temperature, related to sector 4, is reached at 17 s and approaches the 350 °C. The void fraction in the outlet section of the corresponding FW channels is reported in Figure 4.23c. At the transient beginning, when the temperature peak occurs, such parameter rises up to 20%. However, DNBR calculated by the code is >> 1. No thermal crisis is thus expected in the cooling channels. After this initial spike, no further vapor production is detected at the FW channels outlet for the rest of the transient. It is important to note that the delay of the temperature peak in Figure 4.23b with respect to the void fraction one in Figure 4.23c is due to the water crossing time in the FW outlet spinal manifold (few seconds). The water temperature transient also produces a little increment of the FW structural materials (tungsten and EUROFER, Figure 4.23d). Even if the component thermal inertia is low, it is enough to significantly smooth the temperature excursion. Indeed, the peak experienced is of almost + 7 °C with respect to rated value (Table 4.9). In the long term, when only decay heat is present and FW HEXs do not provide any cooling function, FW PHTS converges to a common temperature and this parameter starts to positively drift. The slope is determined by the power unbalance between decay heat and heat losses. The system behavior is the same described for the other accidental sequences investigated in the previous sections and characterized by forced circulation (see **§** 4.5.2).

For what concerns the BZ PHTS, its performances are identical to the ones plotted for LF1 case in Figure 4.15. In less than one second, the system loses the power source and the heat sink. Although, the plasma power goes down slower than the PCS feedwater. This produces a power unbalance managed by the PHTS and PCS pressure control systems. Once evacuated the energy associated to the plasma shutdown, BZ system converges to a common temperature positively drifting because of the prevalence of the blanket decay heat on the circuit heat losses.

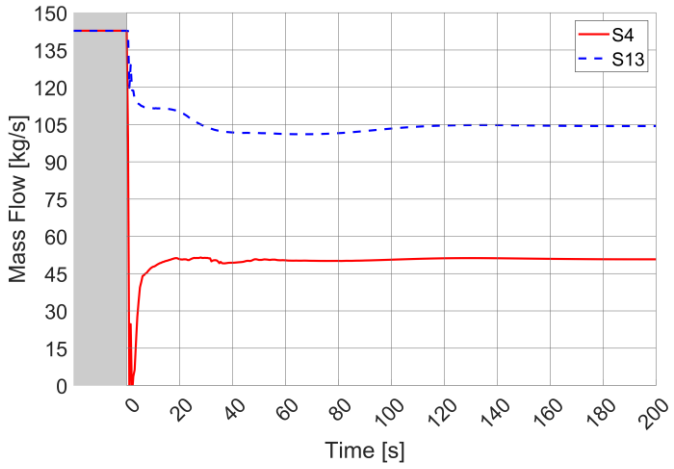

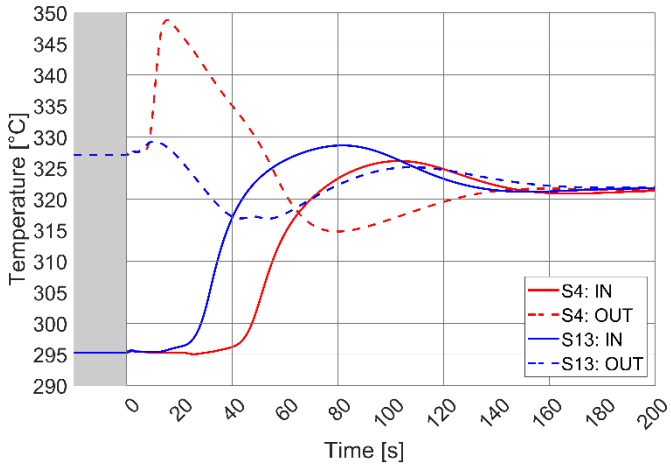

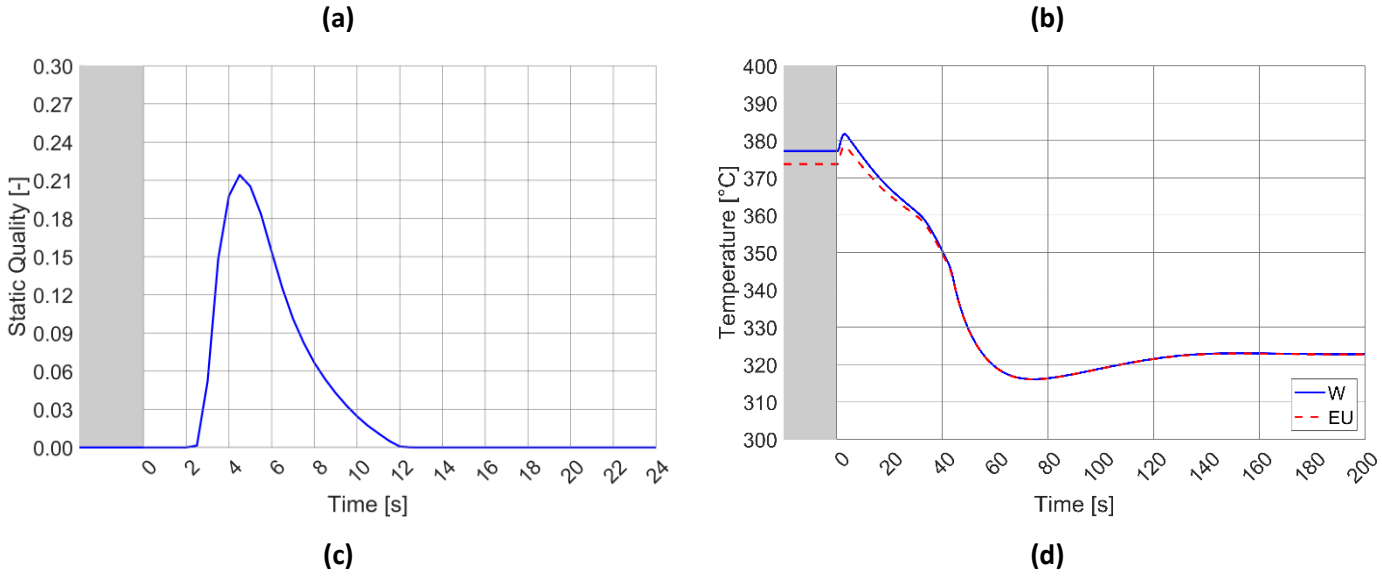

Figure 4.23 – Inadvertent operation of the isolation valve installed on the FW loop 1 hot leg: FW sectors mass flow, sector 4 and 13 **(a)**; FW PHTS water temperatures at BB inlet/outlet, sector 4 and 13 **(b)**; Steam quality at FW channels exit, sector 4 **(c)**;Tungsten (W) and EUROFER (EU) temperatures related to FW component in sector 4 COB segment **(d)**.

When the inadvertent operation of the loop isolation valve is considered in the BZ PHTS, the behavior described above for FW and BZ systems are mirrored. After the initiating event, thanks to the availability of off-site power, the latter is characterized by only half the nominal primary flow. It is distributed in the tokamak sector according to their relative position with respect to failed loop (assumed to be loop 1). Figure 4.24a reports the trends for sectors 4 and 13, the worst/best case respectively. During plasma shutdown, BZ sectors have the same performances of FW ones in the previous accidental sequence. Sector 13 experiences a negligible flow reduction and temperature excursion. The maximum temperature at blanket outlet (345 °C) is registered for sector 4 at nearly 50 s. The PHTS and PCS pressure control systems manage the initial power unbalance. After, BZ system transient evolution is the same described in **§** 4.5.2 for the cases characterized by forced circulation. The only difference is the suitability of only one OTSG in the mid-term (the one belonging to the failed loop does not provide any cooling function).

Regarding the FW system, the accidental sequence is exactly the same described for LF3 and LF4 in **§** 4.5.2 (see Figure 4.18).

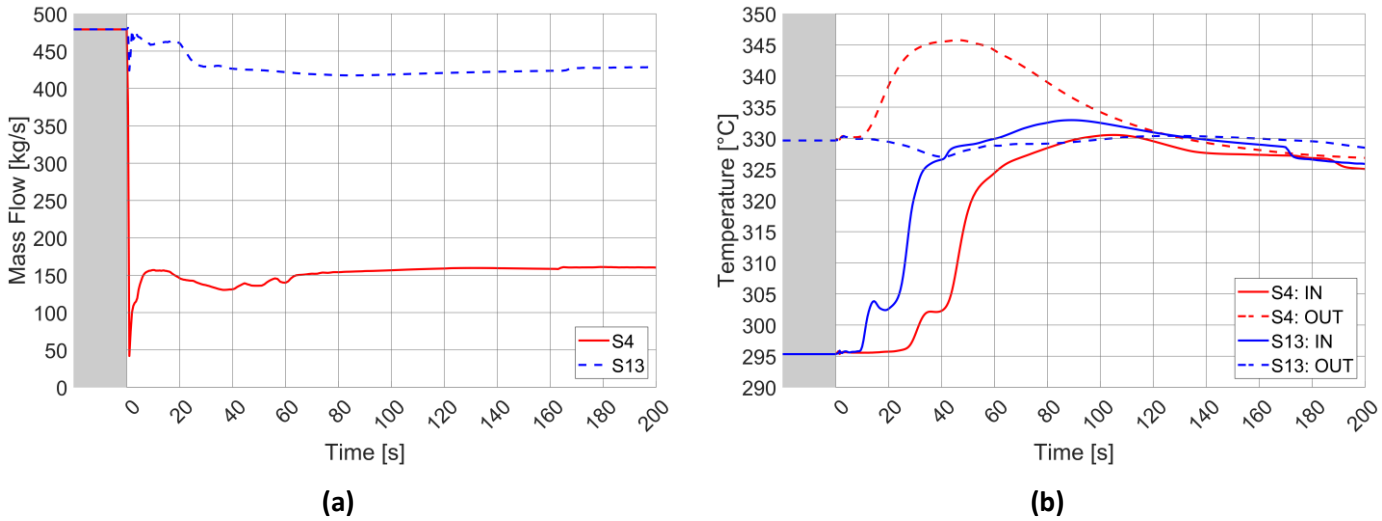

Figure 4.24 – Inadvertent operation of the isolation valve installed on the BZ loop 1 hot leg: BZ sectors mass flow, sector 4 and 13 **(a)**; BZ PHTS water temperatures at BB inlet/outlet, sector 4 and 13 **(b)**.

4.5.4.2 Accidental sequences involving loss of off-site power

The calculations discussed in the previous section were repeated assuming the loss of off-site power occurring in combination with the initiating event. In these new accidental sequences, once the high-pump head signal is detected in the components belonging to the failed loop, the overall primary flow starts to decrease (instead of only one half). In fact, the activation signal triggers both the pump trip (in the failed loop) and the plasma termination. The latter is followed by turbine trip. This provokes the unavailability of on-site power that, combined with the postulated loss of off-site power, leads to the cut-off of the pump/pumps installed on the active loop. This is clearly visible in Figure 4.25a and c, referred to FW and BZ sectors respectively. As before, sectors 4 and 13 were selected to be plotted since their flow trends envelope the others. When the initiating event involves a circuit (either FW or BZ), its influence is observed in the fast flow drop experienced by sectors located near the failed loop. As an example, see blue solid line in Figure 4.25a (FW sector 4) and red solid line in Figure 4.25c (BZ sector 4). Later, the coast-down of pump/pumps belonging to the active loop allows to restore a minimum flow rate in such sectors. As already stated, during plasma shutdown, low flows are associated to higher temperatures at blanket outlet. The combined effect of loss of off-site power and initiating event on this parameter is quite significant. To allow a quantitative assessment, water temperatures at blanket inlet/outlet are collected for sector 4 (worst case) in Figure 4.25b (FW PHTS) and Figure 4.25d (BZ PHTS). When PIE involves FW system, water temperature rises up to 354.5 °C (21 s, Figure 4.25b). Void fraction at the outlet of the corresponding FW channels arrives to 30 %, following the temperature spike. However, even in this case, DNBR calculated by the code is >> 1 and no thermal crisis is thus expected in the components. When the initiating event is related to BZ system, the maximum is equals to 352 °C (67 s, Figure 4.25d).

In the long term, natural circulation establishes in FW and BZ systems in both accidental scenarios. Its influence on the PHTS thermal-hydraulic performances is widely discussed in **§** 4.5.2.

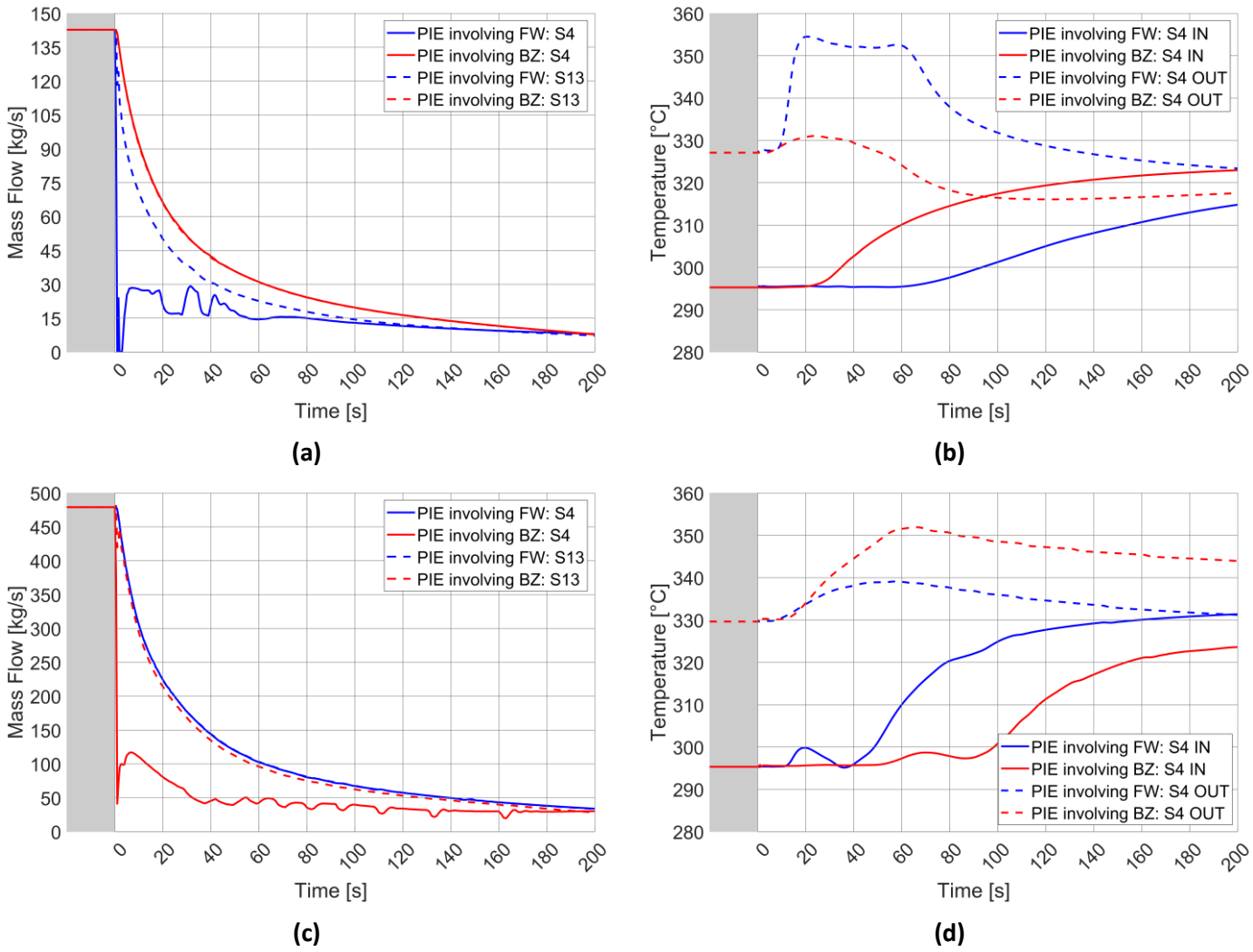

Figure 4.25 – Influence of loss of off-site power on the inadvertent operation of loop isolation valve transients: FW sectors 4 and 13 mass flow **(a)**; FW PHTS water temperatures at BB inlet/outlet, sector 4 **(b)**; BZ sectors 4 and 13 mass flow **(c)**; BZ PHTS water temperatures at BB inlet/outlet, sector 4 **(d)**.

4.5.4.3 Conclusions

It is important to note that this initiating event leads to the worst possible scenarios investigated in the category of 'Decrease in reactor coolant system flow rate'. When LOSP is postulated, the system flow available to cope with the plasma power is the minimum among all the transients analyzed in **§** 4.5. Indeed, a loop is interrupted (the associated flow is zero) and the pump/pumps belonging to the other are cut-off at the transient beginning (due to the unavailability of off-site power). The correspondent blanket outlet temperatures are the maximum experienced by BZ and FW systems among all the cases considered (compare the peaks in the figures of **§** 4.5). Void fraction spikes are detected at the outlet section of the FW channels belonging to the most stressed blanket sectors (e.g. sector 4). However, thermal crisis is not expected in these components. The initial power unbalance is effectively managed by the pressure control systems whose BZ and FW PHTS, as well as PCS, are provided. In the long term, the only issue to be addressed in the removal of the blanket decay heat. In conclusion, the PHTS layout proves to be appropriated to withstand all the design basis accidents investigated in the selected category.

5 ITER WCLL TEST BLANKET SYSTEM CONCEPTUAL DESIGN

5.1 Framework

A breeding blanket ensuring the tritium self-sufficiency is a mandatory component for DEMO reactor. The component direct testing in ITER facility is not possible, since the reactor will be operated at different conditions with respect to the ones expected for DEMO, [31]. In particular, lower neutron wall load and neutron fluence are foreseen, as well as a relatively short pulse phase (hundreds of seconds) compared to the one assumed for DEMO (two hours, see **§** 3.1). Nevertheless, several studies showed that significant feedbacks can be obtained by testing in ITER some mock-ups, called Test Blanket Modules, provided with the same structural and breeding materials supposed to be used in DEMO blanket, [86]. Clearly, these TBMs must be designed by using proper engineering scaling, [87]. Experimental data coming from these tests can be effectively used to validate reference neutron, thermal mechanics and thermal-hydraulic codes, and their possible coupling, [31]. For this reason, during the third ITER council (2008), it was established the so-called ITER Test Blanket Module program, [30]. According to [31], the major testing objectives are: **(i)** demonstrate the breeding blankets structural integrity under combined and relevant thermal, mechanical and electromagnetic loads; **(ii)** validate the theoretical predictions on tritium breeding; **(iii)** perform the tritium recovery and evaluate the process efficiency and the radioisotope inventories in the different blanket materials; **(iv)** assess the temperature field within strongly heterogeneous breeding blanket concepts; **(v)** study the integral performances of blanket components.

Initially the test of six mock-ups was planned. The chosen options were discussed in [31]. In 2018, the R&D strategy was strongly revised and the number of tested modules lowered to four. Also the selected blanket concepts were changed, with the insertion of WCLL option next to the previously chosen HCPB, HCCR and WCCB. The new R&D strategy is widely presented in [32]. From 2018, an intense research activity was conducted within the EUROfusion Work Package WPPMI in order to perform the pre-conceptual and conceptual design phases of ITER WCLL Test Blanket System. The overall work (i.e. TBS) was divided in 'Part A', related to TBM set and 'Part B', referring to its related ancillary systems. For the latter, R&D effort was led by ENEA and involved many European research institutions and universities, including DIAEE of Sapienza University of Rome. The entire work was supervised also by Fusion for Energy, that is the European Union organization managing Europe's contribution to ITER reactor, [33]. By the fall of 2020, both design phases were concluded and the system successfully underwent its Conceptual Design Review. Among the TBM ancillary systems, the most relevant is the Water Cooling System, acting as primary cooling circuit of the TBM module. The design and thermal-hydraulic characterization of this circuit was up to DIAEE. The work done within this framework will be presented in the following sections.

5.2 WCLL-TBS allocation in the tokamak building

Each test blanket system is functionally independent from the others, [32]. Within the ITER tokamak building, two equatorial ports, namely the #16 and the #18, are reserved to host the four TBMs (one for each pair, see Figure 5.1). Test blanket modules are installed within the vacuum vessel and backboned by a shield. The ensemble of TBM and shield is the so-called TBM set, shown in Figure 5.2, and it is contained inside the Port Plug (visible in Figure 5.4). Each pair of

TBM sets share the same Port Plug and Port Cell (PC) areas. In particular, WCLL-TBM is located in Port Cell #16, near to HCPB concept (Figure 5.4). The TBM is fed thanks to pipelines running through the Pipe Forest (PF). All the fluids (coolant and eventually breeder) needed to operate the TBM are provided by these lines. The TBM ancillary system components are situated partially in a self-sustained steel structure called Ancillary Equipment Unit (AEU, see Figure 5.4) and partially in other rooms of the tokamak building (see Figure 5.1). The AEU is protected from the radiation damage by a bioshield, located radially outwards with respect to the pipe forest (Figure 5.4). Referring to the WCLL-TBS, the main ancillary systems are:

- Water Cooling System, whose thermal-hydraulic parameters were chosen in accordance with the DEMO WCLL requirements for power extraction (see **§** 5.4).
- Coolant Purification System (CPS), for the purification of the primary water coolant.
- Lead-lithium loop, ensuring the tritium breeding through liquid metal circulation within the TBM breeder units.
- Tritium Extraction System (TES), connected to the lead-lithium loop, consisting in a helium circuit for the tritium extraction from the PbLi flow.
- Tritium Accountancy System (TAS), whose function is the measurement of the tritium concentration in the PbLi flow.
- Neutron Activation System (NAS), whose function is the monitoring of the local neutron flux and fluence inside the TBM set.

Most of the TBS equipment is placed in the level one Port Cell #16 and in the level four TCWS Vault. Both locations are connected by means of Connection Pipes (CPs) installed within a Vertical Shaft (VS). Instead, TES is entirely located in a dedicated building. The different locations hosting the WCLL-TBS are shown in Figure 5.1 and Figure 5.4. Further details are given in [89][90].

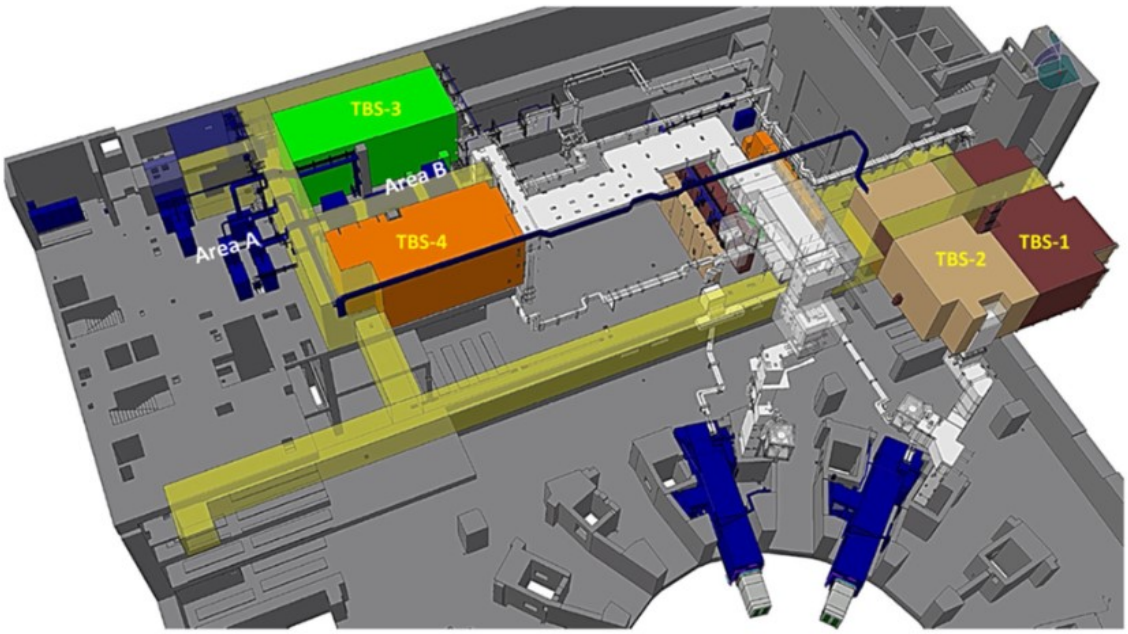

Figure 5.1 – Space reserved to Test Blanket Systems within the ITER tokamak building, [32].

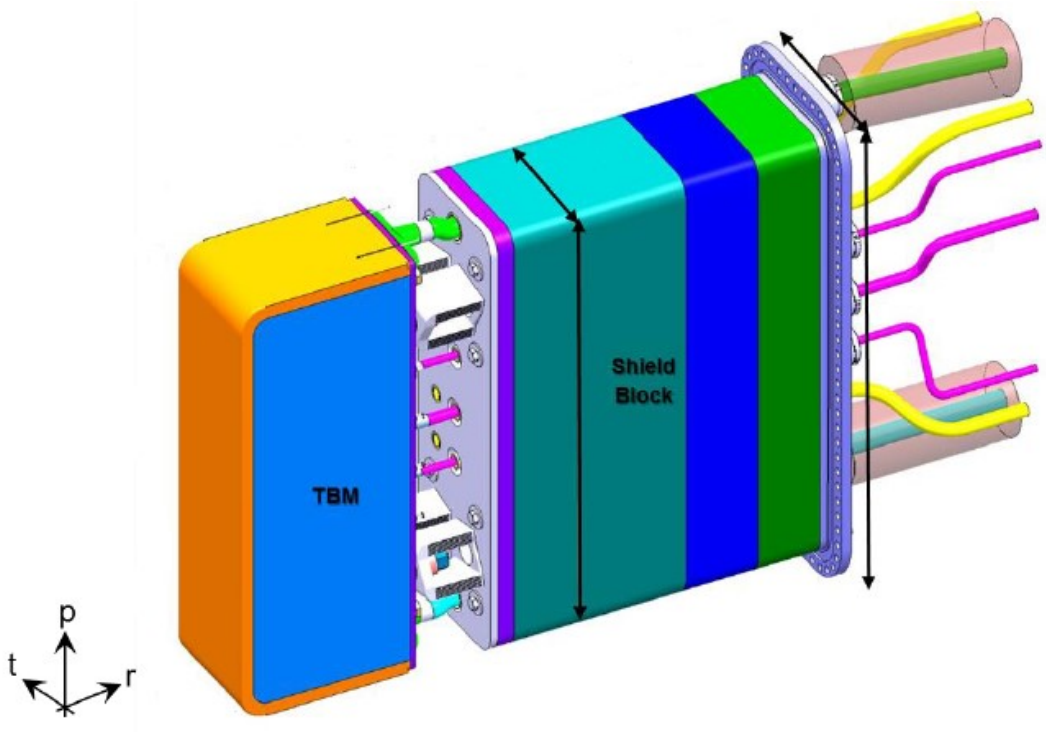

Figure 5.2 – Isometric view of the TBM set (test blanket module and related shield block), [88].

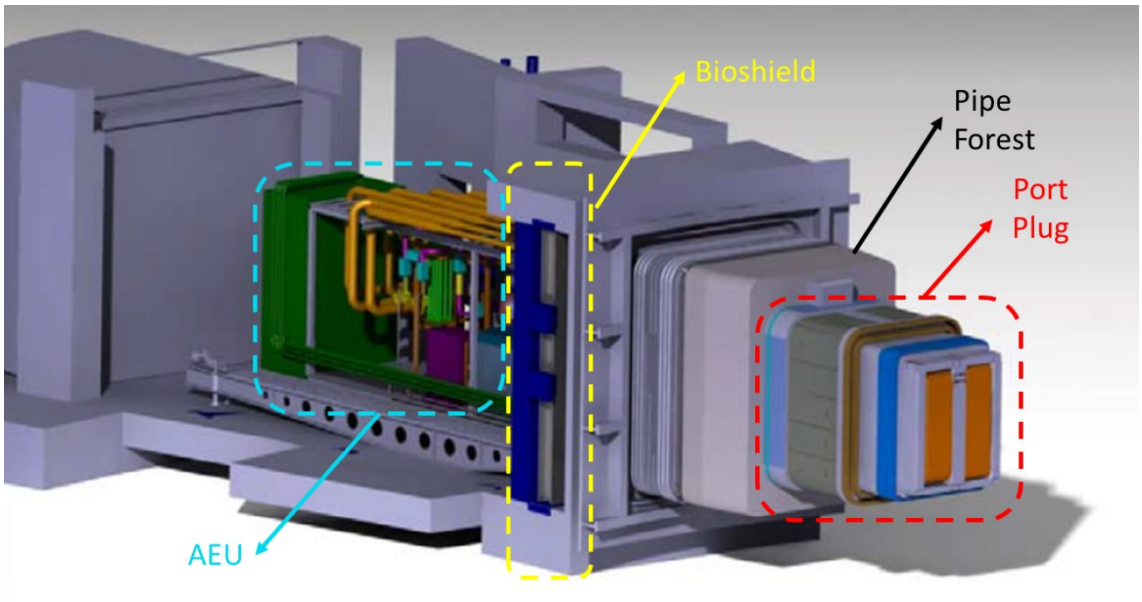

Figure 5.3 – Overview of Port Cell #16, hosting the WCLL-TBM, [32].

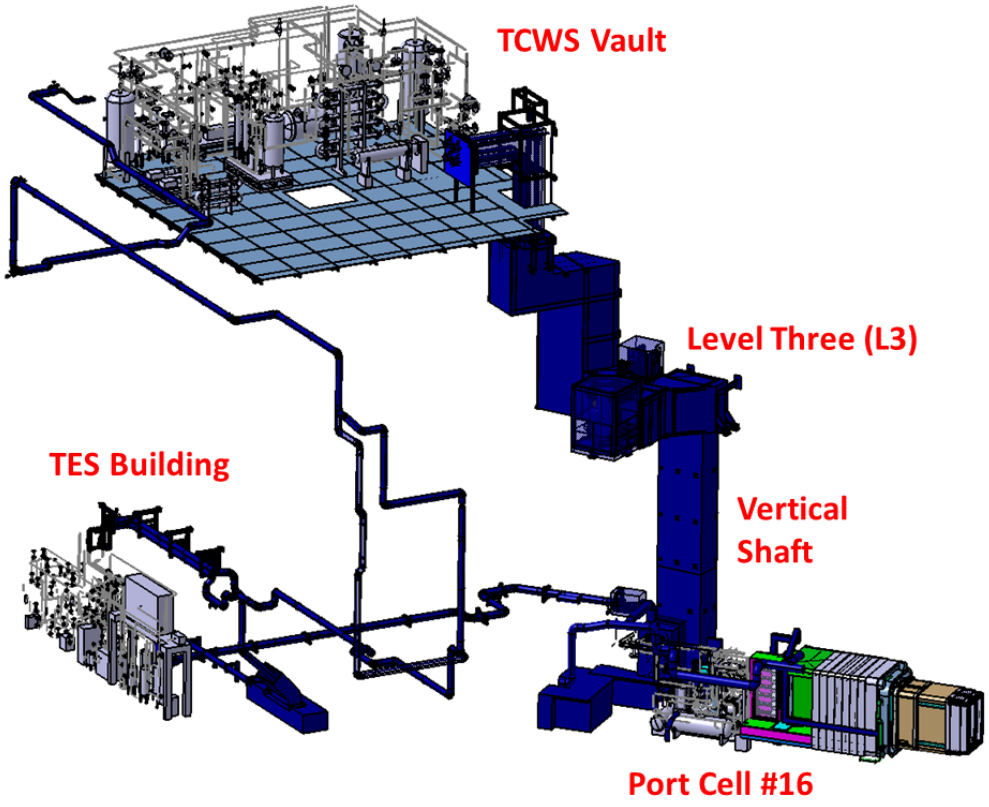

Figure 5.4 – Tokamak building areas where WCLL-TBS is located, [90].

5.3 WCLL-TBM layout

The TBM component was designed by a multi-disciplinary team coordinated by the French Commissariat à l'énergie atomique et aux énergies alternatives (CEA). Its layout is finely described in [88]. Since the component was included in the thermal-hydraulic model of the overall TBS, its main layout features are recalled in the following.

The WCLL test blanket module was developed for ITER application with the main goal of manufacturing a DEMO blanket mock-up. For this, the concept relies on reduced-activation ferritic/martensitic steel EUROFER as structural material, the eutectic Pb-15.7Li, enriched at 90% in ^{6}Li, as tritium breeder and neutron multiplier and water as coolant. The latter is operated at typical PWR conditions with inlet/outlet temperatures of 295/328 °C at a pressure of 15.5 MPa.

The TBM dimensions are 685 mm × 462 mm × 1670 mm (radial x toroidal x poloidal). Its exploded view is provided by Figure 5.5. The box is externally enclosed by a big U-shaped plate directly facing the plasma, named First Wall (yellow in Figure 5.5), and two lateral closure plates, named Side Caps (SC, light blue in Figure 5.5). FW is actively cooled by 32 "vertical" (i.e. radial-poloidal oriented) one pass channels in counter current one other two. A zoom of the component is offered by Figure 5.6. Internally, the box is constituted by a set of eight stiffening plates (seven horizontals plus one vertical, green in Figure 5.5). This structural grid divides the overall breeder zone in an array of sixteen Breeding Units (BUs). During operation, each BU is filled with slowly flowing liquid breeder. The heat removal is ensured by four parallel U-shaped DWTs (blue and light blue in Figure 5.5). For DEMO relevancy, the DWTs layout (i.e. OD and thickness) is identical to the one presented in **§** 3.2. A total of 60 DWTs are present in the TBM box since the two top

and the two bottom BUs are refrigerated by only three DWTs each. A baffle plate is foreseen in the unit layout, dividing the BZ in two poloidal zones and ensuring the proper PbLi circulation (radial-poloidal-radial, see Figure 5.7a and b). The breeding unit is backboned by a plate provided with windows to allow the inlet/outlet of the liquid breeder. They are clearly visible in Figure 5.7a.

The TBM box is closed by four successive poloidal-toroidal plates, named back plates. The enclosures among two successive back plates act as manifolds for the water flow distribution and breeder routing. Back plates and fluid manifolds are shown in Figure 5.7b. For what concerns water coolant, FW and BZ inlet/outlet pipes are placed in the middle of TBM box back, distributing/collecting water from the dedicated manifolds. They are indicated in Figure 5.5. While for the inlet, FW and BZ have independent headers, the outer one is in common, see Figure 5.7b. Referring to PbLi, its inlet/outlet manifolds are hosted in the same enclosure (between breeding unit back plate and BP1, see Figure 5.7b). This space is divided in four toroidal sections by means of three vertical stiffening plates, as shown in Figure 5.7a. PbLi flows upwards in any section, entering/exiting the breeding units through the suitable windows. The breeder inlet/outlet pipes are located at the bottom/top of the TBM box back, respectively. They are reported in Figure 5.5. Other holes present in the back plates belong to NAS and TAS.

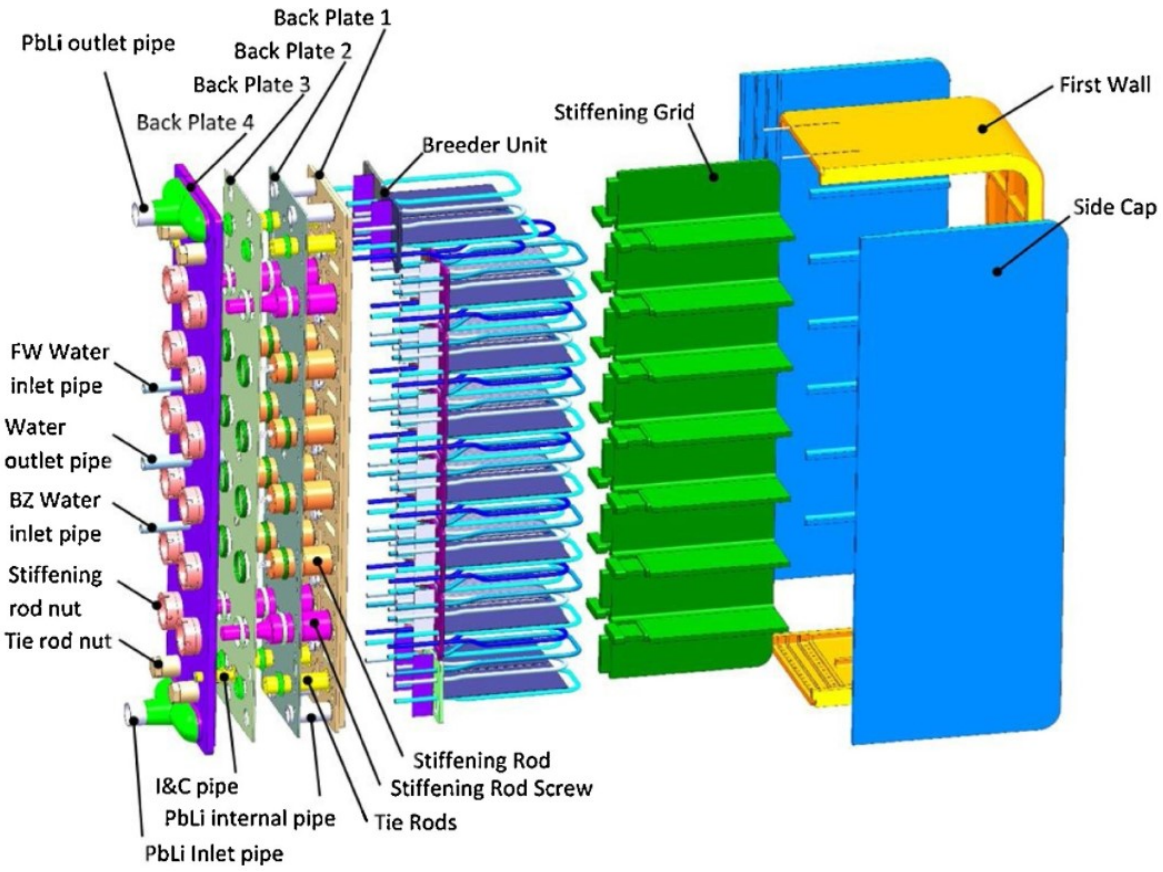

Figure 5.5 – Exploded view of WCLL-TBM box, [88].

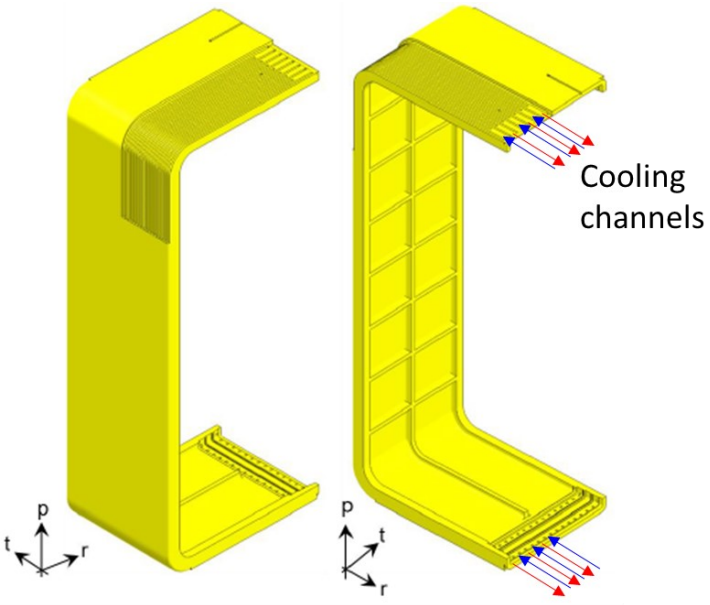

Figure 5.6 – Zoom of the first wall component and its radial-poloidal cooling channels, [88].

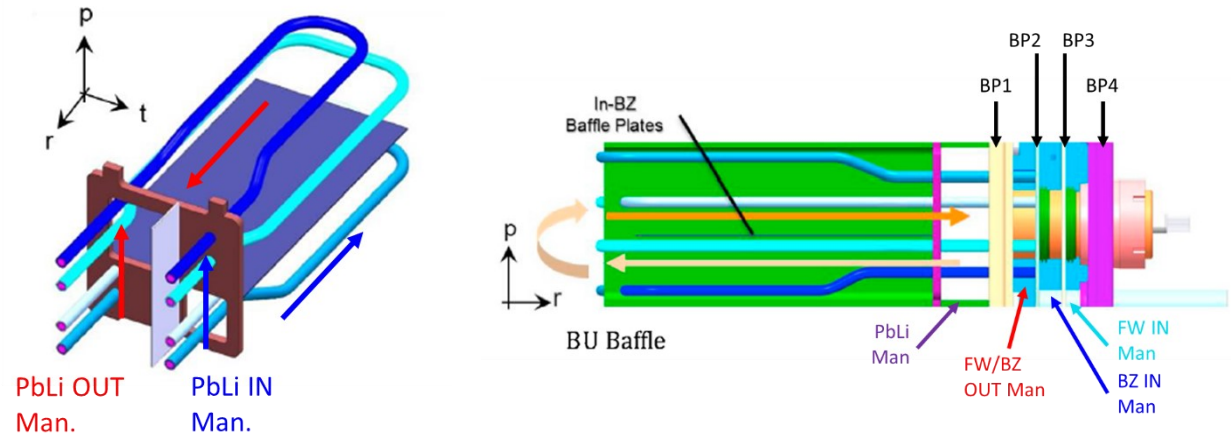

(a) **(b)**

Figure 5.7 – WCLL-TBM breeding unit: isometric view **(a)** and radial-poloidal view **(b)**. PbLi flow path, inlet/outlet manifolds for coolant and breeder and back plates are also indicated, [88].

5.4 WCLL-TBM Water Cooling System

5.4.1 Rationale

The pre-conceptual and conceptual design of this ancillary system was performed at DIAEE of Sapienza University of Rome in collaboration with ENEA, and it was part of the research activity object of this PhD thesis, [89][90]. The Water Cooling System was designed to implement the following main functions: **i)** provide suitable operating parameters to the water flow cooling the TBM in any operational state; **ii)** transfer thermal power from WCLL-TBM to CCWS; **iii)** provide confinement for water and radioactive products; **iv)** ensure the implementation of the WCLL-TBS safety functions. As already stated in **§** 5.1, the relevancy of ITER WCLL-TBM for DEMO blanket is

one of the main objectives of this testing program, [31][32][91]. For this, at the TBM interface sections, it must be ensured the same thermodynamic conditions of DEMO WCLL blanket. In particular, inlet and outlet temperatures of 295 and 328 °C and average pressure of 15.5 MPa.

DEMO blanket foresees two sub-systems, i.e., the First Wall and the Breeder Zone. Each one is cooled by an independent Primary Heat Transfer System, see **§** 3.4. Instead, the reduced thermal power produced in the TBM set (near 700 kW) with respect to DEMO BB (1923 MW, see Table 3.2), allows to use a single water-cooling system for both the FW and the BZ. The WCS primary flow was computed considering the power input term and the required water thermodynamic conditions at TBM inlet/outlet.

The ultimate heat sink for the WCLL-TBM WCS is the ITER Component Cooling Water System (CCWS). With the aim to include an additional barrier between the contaminated primary water and the CCWS coolant, the WCLL-WCS was split in a Primary Loop (PL) and a Secondary Loop (SL). The former contains contaminated water flowing within the TBM-set, while the latter avoids CCWS contamination with primary coolant. In such a way, the CCWS radioactive inventory is kept below the limit in any operative and accidental scenario (note that CCWS is a non-nuclear system). To simplify the WCLL-WCS management, liquid only condition was selected for the SL coolant instead of the two-phase fluid, as in DEMO PCS. It is worth to emphasize that electricity generation is not a purpose of ITER and, thus, steam production is not required.

CCWS provides low pressure water (around 0.8 MPa) at 31 °C. Moreover, a further design constraint regards the CCWS water temperature increase, which must be limited to 10 °C. Hence, there is a considerable difference between the average TBM temperature and the average CCWS temperature. To avoid an excessive temperature excursion, and thus thermal stresses, between the two sides of a single Heat eXchanger (HX), an economizer was installed in the middle of the WCS PL. This leads to the typical “eight” shape configuration for the primary cooling circuit. Therefore, a total of three HXs were considered for the whole WCS, namely:

- HX-0001: the economizer;
- HX-0002: the intermediate heat exchanger between PL and SL;
- HX-0003: the heat exchanger between WCS SL and CCWS.

The TBM is located on the high temperature side of the WCS PL and the water pumps on the low temperature branch, downward the HX-0002. Most of the WCS equipment is installed in the level four TCWS Vault. The rest of the components, including the TBM, is placed in the level one Port Cell #16. Both locations are connected by means of connection pipes hosted in a vertical shaft. The different locations containing a part of the WCLL-TBM WCS are shown in Figure 5.4. The detail of the WCS equipment allocation in TCWS Vault and AEU is offered by Figure 5.8 and Figure 5.9, respectively.

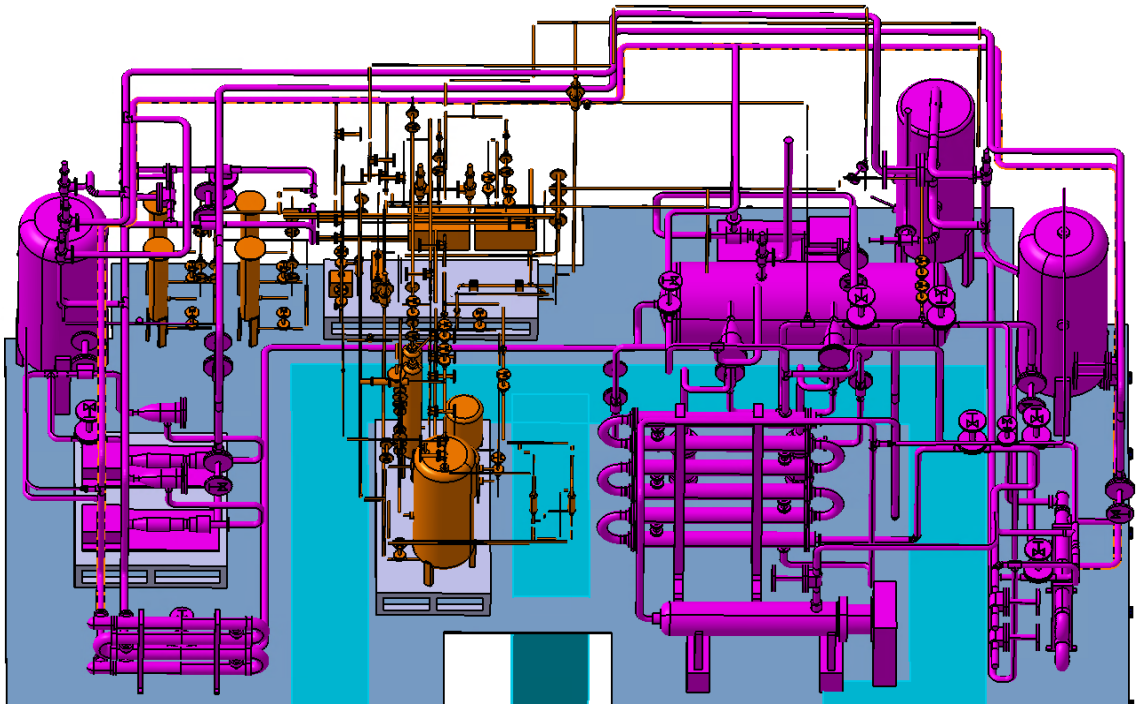

Figure 5.8 – WCS equipment arrangement (pink) in TCWS Vault. Orange components belong to CPS, [89].

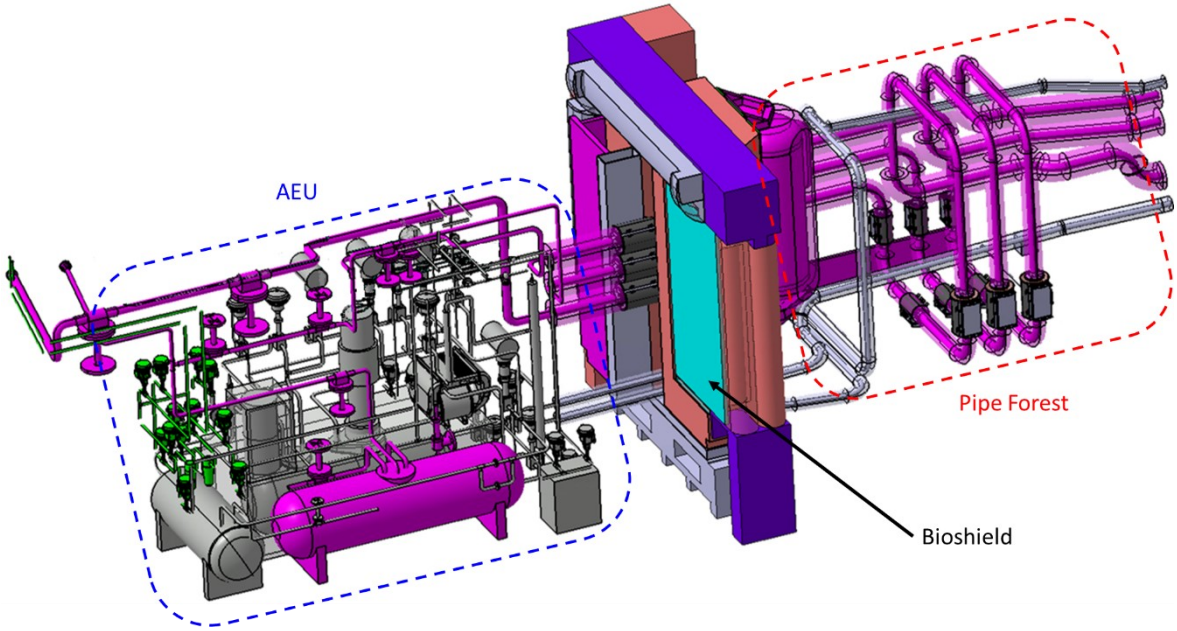

Figure 5.9 – WCS equipment arrangement (pink) in AEU (Port Cell #16). Grey/green components belong to PbLi loop/TES, respectively [89].

5.4.2 Process flow diagram

5.4.2.1 Primary loop

A schematic view of the overall WCS is contained in Figure 5.10, showing all the essential components for the system operation. The rated TBM inlet flow is used to cool down both the FW and the BZ. A calibrated orifice (gross regulation) and a control valve (fine adjustments) are respectively located at the BZ and FW inlet lines to regulate the desired cooling flow rate through the two TBM areas. The regulation system ensures the proper refrigeration of all the TBM internal components.

The economizer limits below 100 °C the average temperature difference between the WCS PL cold branch and the CCWS. This temperature difference was adopted as preliminary sizing criterion for the other two HXs (HX-0002 & HX-0003) as it affects their size and technical feasibility. The economizing function is performed by a hairpin heat exchanger (HX-0001 in Figure 5.10). This technology is already used in PWR nuclear power plants for small heat exchangers, as the ones installed in the Chemical Volume Control System (CVCS). HX-0001 preheats the water directed to the TBM with the hot one coming from the same component. The heat exchanger was sized to provide water to the TBM at the required thermodynamic conditions.

For the intermediate heat exchanger (HX-0002 in Figure 5.10) hairpin technology was also selected. This HX thermally couples WCS primary and secondary loops. The average temperature difference between the WCS PL cold branch and CCWS, mentioned above, was nearly equally distributed between the HX-0002 and the HX-0003. On the secondary side, the HX is equipped with a bypass line and a control valve (VC-0010 in Figure 5.10). This system allows to regulate the HX-0002 feedwater flow rate.

To increase the PL reliability and availability, the current design foresees two identical canned centrifugal water pumps, installed in parallel on the loop cold branch. During WCS Normal Operation State (NOS) only one of the two pumps is on; the other one remains in stand-by to be used as backup. The two circulators were designed to provide independently the rated mass flow needed to cool the TBM. In Figure 5.10 the pump system is equivalently illustrated by a single pump component.

The Normal Operation State is characterized by a pulsed plasma regime with a burn phase followed by a dwell time. An electric heater (HT-0001 in Figure 5.10) is installed in the WCS PL in order to supply the deficiency of TBM thermal power during the dwell time, maintaining a constant temperature at the TBM inlet. During other WCS states, when no plasma pulses are foreseen, the electrical heater keeps the system temperature field as much as possible unmodified with respect to the one during NOS. The series of economizer and electrical heater is provided with a bypass line for temperature regulation at the TBM inlet. Bypass flow is set by means of two control valves: the former (VC-0001 in Figure 5.10), installed in the cold leg, downstream the electrical heater; the latter (VC-0006 in Figure 5.10), placed on the bypass line. This double-control valve system allows to regulate the bypass mass flow from zero up to the WCS primary loop rated flow.

The pressurizer (PRZ in Figure 5.10) system guarantees the pressure control function. It maintains WCS pressure at the required value independently on the temperature variations induced by the pulsed plasma operation or by other transient conditions. As a system operating at high pressure, the WCS PL must be equipped with a protection against low and over-pressure transients. The steam bubble pressurizer is connected to the PL hot leg by means of a surge line. The pressurizer is equipped with electric heaters and a spray line. The latter is connected to the PL cold leg. Spray flow rate is set by means of a control valve. These systems are installed to cope with under

pressure (heaters) and overpressure (sprays) transients occurring during normal operating conditions and to limit pressure changes during transient conditions. In case of overpressure transients, if spray nozzles fail in reducing pressure, the PRZ is equipped with a Pilot Operated Relief Valve (PORV in Figure 5.10) and a Safety Relief Valve (SRV in Figure 5.10). They are both related to a relief line that connects the pressurizer to a Pressure Relief Tank (PRT in Figure 5.10), allowing the steam discharge. The PRT is a volume partially filled of water with a cover gas. The component is equipped with a pressure suppression system (spargers) and a rupture disk as a pressure release device.

A delay and a decay tank are installed at TBM outlet to reduce the $^{16}N/^{17}N$ content inside the WCS water.

5.4.2.2 Secondary loop

The WCS secondary loop is foreseen to hydraulically disconnect WCS PL and CCWS. It avoids the CCWS water contamination, especially in case of heat exchanger tube rupture. The secondary loop is completely located in the TCWS Vault.

The hot water exiting the HX-0002 is led to the heat sink (HX-0003 in Figure 5.10), where it is cooled. Hairpin technology was also selected for the HX-0003. Thermal-hydraulic performances of the CCWS represent sizing constraints for the heat sink design. The heat sink is also equipped with a bypass line and a control valve (VC-0009 in Figure 5.10), to regulate feedwater flow rate.

The SL pump system design follows the one adopted for the primary loop. Two canned centrifugal water pumps are installed in parallel. Each one is sized to provide the SL rated flow independently.

The pressure control function is deputized to the pressurizer system. The main component is the steam bubble pressurizer, connected to the SL hot leg by means of a surge line. The tank (PRZ in Figure 5.10) is provided with the same equipment described for the analogous component in the primary loop: electric heaters, spray line, PORV and SRV. The relief line of these two valves is connected to the WCS PRT.

The CCWS pipeline section placed between the heat sink isolation valves (VG-0016 and VG-0018 in Figure 5.10) is protected against overpressure transients by a safety relief device (SRV in Figure 5.10). It connects this subsystem to the WCS PRT.

The CAD model of WCS equipment installed in TCWS Vault is shown in Figure 5.11, with the indication of all the main components of primary and secondary loops.

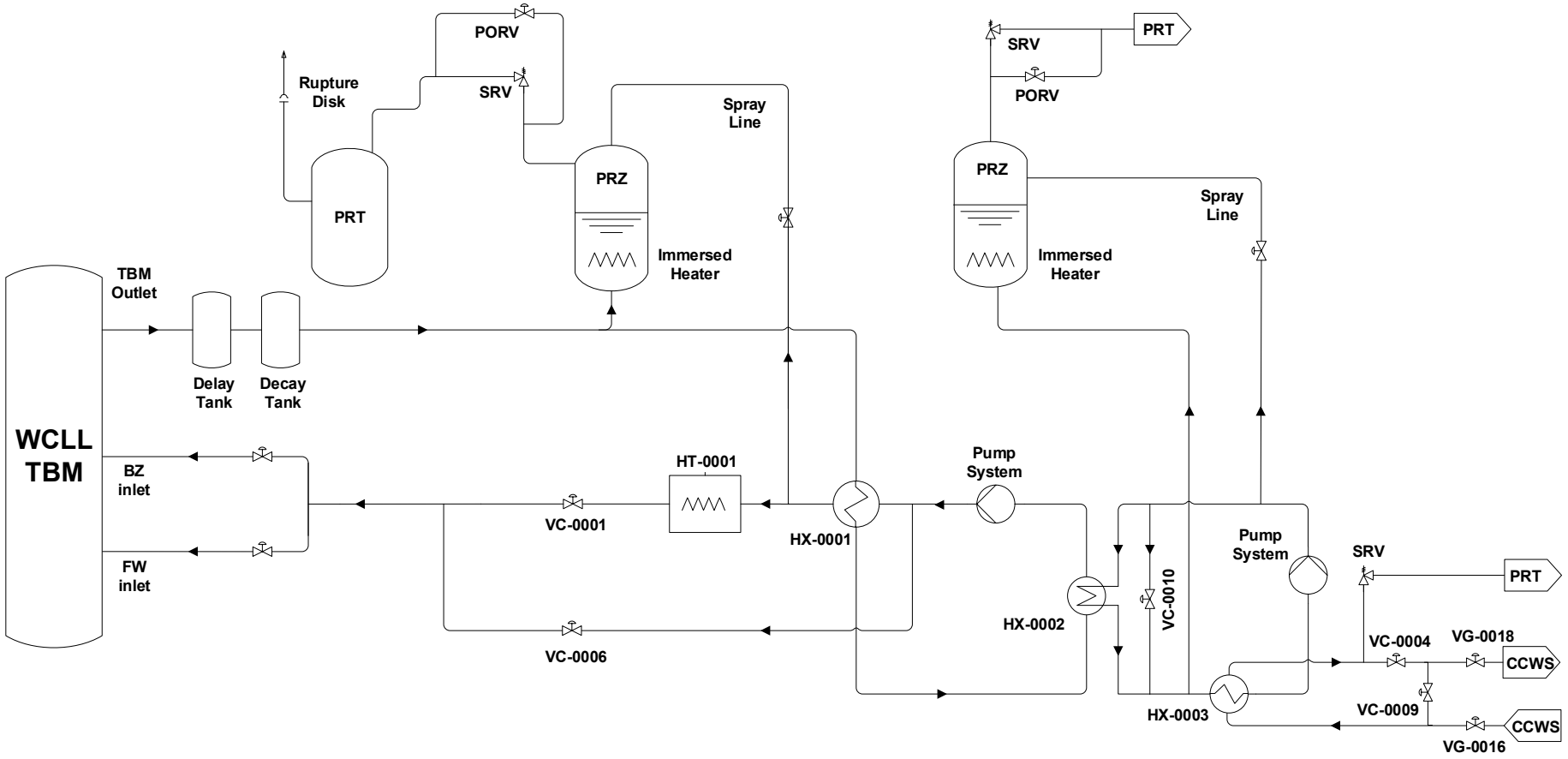

Figure 5.10 – Schematic view of WCLL-WCS circuit, [90].

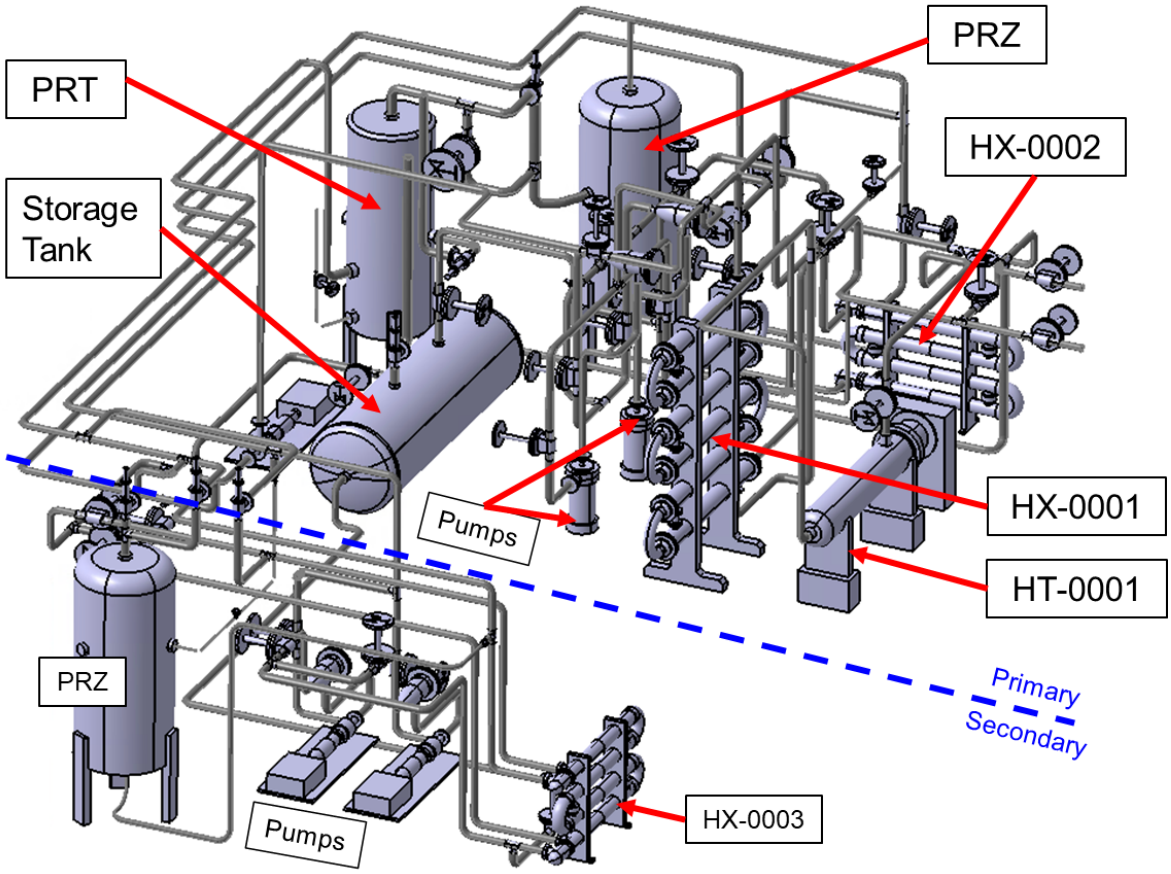

Figure 5.11 –WCS equipment installed in TCWS Vault, with the indication of the main components of primary and secondary loops, [89][90].

5.4.3 Materials

The structural material used for the manufacturing of the WCS components (pressure vessels) and seamless piping is austenitic steel. Since there will be a certain amount of tritium that will permeate inside the WCS system, any material that could be a hydrogen getter shall be avoided. To respect this requirement, the austenitic steel AISI 316L is recommended as WCS reference material. Moreover, it is easy to weld and, as a stainless steel, it does not require a post-weld treatment (compared with equivalent ferritic steels that can be used at the same pressure and temperature). In addition, the material is widely used in the nuclear industry, which means that the technologies for manufacturing pressure vessels from this material are well established and documented. Thermal properties adopted for the austenitic steel in the WCS design were derived from ASME BPVC Section II, [76].

For the thermal insulation of vessels, piping and components, preformed microporous insulation shells (filament reinforced pyrogenic silica) was selected, [92]. The insulation thickness was sized with the requirement to keep external surface temperature below 50 °C for safety purposes. The estimated overall heat losses are below 1% of the TBM rated power.

5.4.4 Heat exchangers

The hairpin design was selected for all the WCS heat exchangers. The main advantage of this technology is the possibility to achieve high efficiency while having a very compact design with respect to a traditional Shell and Tubes. The hairpin is a proven technology for PWR reactors. It is already used for small single-phase heat exchangers connected to the primary circuit, for example in the CVCS circuit of French European Pressurized Reactor (EPR).

The heat exchanger layout consists in multiple straight horizontal fluid passages vertically arranged and linked by 180° curves. From the fluid-dynamic point of view, the hairpin heat exchanger is a pure counter-current device with hot fluid flowing inside the tube bundle and cold fluid within the shell. Heat transfer occurs only through the horizontal straight passages.

Tube sheets are foreseen at the beginning and at the end of each straight passage. Fluid exiting from the tube bundle is collected within the 180° curves and enters the following straight passage. Within the shell side, water flows from a straight passage to the next one through the inlet/outlet nozzles located slightly before the flanged connections. For constructive reasons, it is always recommended to use an even number of straight fluid passages. An example of the hairpin technology is presented in Figure 5.12, which shows the technical drawing of the HX-0002.

For the HX-0001 and the HX-0002, INCONEL was selected as tube material. It allows to reduce tube thickness maintaining nearly the same wall conductivity of the austenitic steel. The AISI 316L was used for the HX-0003 tubes. For what concerns the shell, austenitic steel was adopted for all the heat exchangers. Tube and shell steel thicknesses were preliminarily evaluated with ASME Sect. III NC [93].

The heat exchangers design was performed considering the operation at End of Life conditions. Hence, fouling resistances were added to both internal and external tube surfaces and a 10% of tube plugging was taken into account in the calculation of the overall heat transfer surface. The reference internal and external fouling factors were conservatively taken from PWR design (typical commercial values), [94][95], without considering the reduced ITER operational life.

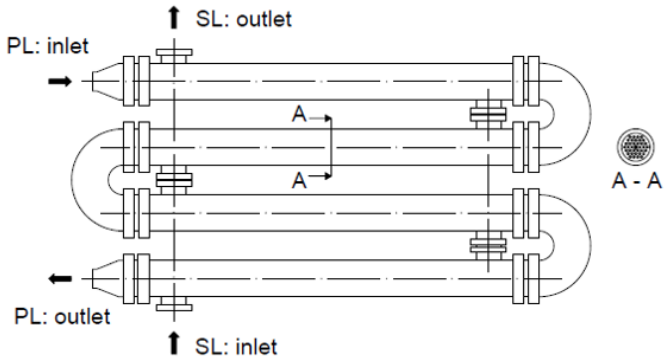

Figure 5.12 –Technical drawing of HX-0002, [90].

5.4.5 Piping and pumps

The WCS piping diameter was sized to avoid excessive pressure drops in primary and secondary loops. Pipeline thickness was preliminarily evaluated following ASME Sect. III NC [93], while the component OD was selected from ASME B36.10M values [96].

For HX-0002 and HX-0003, the heat exchanger design pressure was considered up to the secondary side isolation valves. In this way, at least for a certain period, these sections of the secondary loop and CCWS can be operated with the valves closed. This conservative approach was not assumed for the rest of the correspondent systems.

Concerning the PC#16, due to the severe space constraints in this area, the main sizing criteria for all the components was the space allocation reduction. This was also the key design requirement for the pipelines going from the vertical shaft outlet to the TBM inlet. The pipeline size should be reduced as much as possible taking into account the compatibility of the increasing pressure drops with the maximum pumping capacity of the WCS PL. A sensitivity analysis was carried out to optimize this parameter.

This sizing reduction could not be applied to the pipelines going from TBM outlet to vertical shaft inlet. In fact, in this WCS section, it is required to maintain enough residence time to reduce the N^{16} content in the contaminated water. The pipeline size reduction decreases the residence time in a way that might not be compensated by the delay/decay tanks.

Concerning the pumping system, the selected technology for both WCS PL and SL was the canned centrifugal pump. They were sized calculating the overall loop pressure drops and the required pumping power.

5.4.6 Pressure control system

Primary loop

WCS primary loop hot branch operates at thermodynamic conditions within the typical range of a PWR. For this reason, the pressure control system foreseen in PWR design was adopted [97]. The main component of the system is the steam bubble pressurizer. As for PWR experience, the component volume was sized to accomplish the loop volume variations occurring during the maximum in-surge and out-surge transient conditions. The complete loss of heat source (plasma burn) and the complete loss of heat sink were selected as sizing criteria, respectively related to the out-surge and in-surge transients. The minimum pressurizer ID was calculated to avoid two-phase flow in the PORV valve throat section in case of water discharge during overpressure transients. The thickness was preliminarily evaluated with ASME Sect. III NC [93]. The pressure control function for WCS primary loop was developed according to the PWR experience, as recommended in [97].

The pressurizer is equipped with proportional electric heaters and a spray system. The proportional heaters are set to operate in a range of pressure around the WCS PL reference one. A varying input current, as a function of the pressure deviation signal, is supplied to the heater bank. Normally these heaters are energized at half current when pressure is at setpoint (no pressure error). The variable heaters will be de-energized at the higher pressure setpoint and fully energized at the lower pressure setpoint. The spray line valve is regulated to modulate flow rate starting from a lower pressure setpoint up to a higher one correspondent to fully open valve. The operating range of this device is contained between the WCS PL reference pressure and the PORV valve opening setpoint. The spray system operates to prevent the opening of the pressurizer PORV and SRV. PORV and SRV actuation is required during overpressure transients in case spray nozzles fail in reducing pressure. PORV opening setpoint is lower than the SRV one to limit the number of challenges to the SRV. PORV and SRV area change rate and throat section were scaled from PWR design [97], based on the loop inventory and a safety margin.

In case of overpressure transient steam is discharged from the pressurizer to the PRT. The pressure suppression system of the PRT is based on immersed spargers that help in liquefy the steam coming from the pressurizer. The PRT is also provided with a rupture disk. The volume of this component was scaled from PWR design [97]. The scaling factor was based on the loop inventory and a safety margin. The component sizing was verified by proving its condensing capability in case of mass discharge from primary loop for a complete pulse phase (worst possible scenario).

Secondary loop

The secondary loop pressurizer system was designed following the main outlines discussed for the WCS PL. The main difference was the procedure for sizing the steam bubble pressurizer. The method described for the analogous component of the WCS primary loop was not applicable in this case. Operative conditions of the WCS secondary loop are different from the PWR ones. The strategy adopted was to scale the SL pressurizer from the PL one. The scaling factor was evaluated from the ratio between loop inventories. In addition, a safety margin was applied. The pressurizer equipment was sized by performing numerical simulations concerning operational transients involving the WCS secondary loop. The discharge volume for the SL pressurizer is the WCS pressure relief tank.

5.4.7 Temperature control system

The solution adopted for the electrical heater was a vessel equipped with heating elements immersed in water. The construction is like the one of a Shell and Tubes heat exchanger with the tubes replaced by hairpin heating Rods. The component length is mainly given by the length of the HRDs and the size of the head holding the electric contacts. The sizing power of such heat exchanger is discussed in **§** 6.4. The HRDs selected for the WCS electric heater design were taken from [78]. Austenitic steel was adopted as shell material. Since the component layout is similar to a Shell and Tubes heat exchanger, the Kern methodology was employed to assess thermal-hydraulic performances, such as pressure drops and heat transfer coefficient, [98].

A control system was preliminary implemented in WCS in order to provide the TBM with water at constant temperature over the pulsed regime. This parameter can deviate from the reference value mainly for two reasons. The first one is related to the design approach. Heat exchangers were designed to match nominal power in EOL operation. Hence, under Beginning of Life conditions, the components result oversized, modifying the WCS temperature field. In order to meet required TBM inlet conditions in both EOL and BOL, the mass flow rate across the shell side of the heat exchangers must be regulated. The modulation is obtained with the bypass lines and the control valves (long-term regulation). The second deviation derives from the pulsed operation, leading to fluctuations of the water temperature at TBM inlet. In this case, the regulation is in charge of the electrical heater and it is obtained by tuning the electric power supplied (short-term regulation).

The regulation of the heat exchanger performances is linked to the temperature reading at the tube side (hot fluid) outlet. When the measured temperature decreases below the reference setpoint (i.e., the exchanged power is too high), the bypass valve starts to open, and part of the shell side (cold fluid) flow rate is redirected towards the bypass line. Therefore, heat exchange decreases and temperature at tube side outlet returns to match the reference setpoint. The economizer control system intervenes, under BOL, to compensate the component higher performances and, during NOS, to absorb the TBM outlet temperature fluctuations due to pulsed

regime. Instead, the HX-0002 and heat sink control systems intervene only under BOL to modulate the performances of the correspondent heat exchangers. In fact, during NOS, the temperature fluctuations disappear downward the economizer, as widely discussed in **§** 6.4.

The regulation of the power supplied by the electric heater is based on the acquisition of the TBM inlet temperature. If, for any reason, it drops below the setpoint (295 °C), the electrical heater comes into operation, supplying the deficit and restoring the required inlet temperature. A proportional-integral control system continuously regulates the HT-0001 power.

5.5 WCLL-TBM PbLi loop

The design of this ancillary system was not part of the research activity directly performed by DIAEE (i.e. object of this PhD thesis), [89]. Nevertheless, PbLi loop is thermally coupled with WCS within the TBM box, see **§** 5.3. Thus, it provides fundamental feedbacks influencing the behavior of the water cooling circuit during transient conditions. For this, it was included in the thermal-hydraulic model of the overall TBS and its principal features are recalled in the following.

The main functions to be fulfilled by the PbLi loop are: **i)** provide and maintain PbLi at operating conditions suitable for the WCLL-TBM correct operation; **ii)** ensure the liquid metal circulation in the WCLL-TBM; **iii)** remove impurities from the eutectic alloy; **iv)** remove tritium from TBM and promote external tritium extraction; **v)** provide confinement of PbLi and radioactive products; **vi)** contribute in ensuring safety provisions implementation for WCLL-TBS. Moreover, due to the considerable production of activated elements (both PbLi impurities and corrosion products) and tritium inside the eutectic alloy during its flow through the WCLL-TBM and the rest of the loop, all the main components of the circuit was classified as nuclear pressurized equipment.

The PbLi loop is entirely located in Port Cell #16. The system consists in a closed circuit where forced circulation of the lead-lithium eutectic alloy is ensured in order to allow its chemical make-up, its mass inventory control as well as the tritium extraction, [89]. The main loop components are:

- The Tritium Extraction Unit (TEU);
- The heater (HT-0001);
- The cooler (HX-0001);
- The air-cooled Cold TRap (CTR);
- The storage/recirculation tank;
- The circulation pump;
- The relief tank.

Their arrangement in Port Cell #16 is shown in Figure 5.13, [89]. During Normal Operation State, the PbLi alloy returns from the TBM with a nominal mass flow of 0.65 kg/s. The lead-lithium flow is heated up to 450°C within the electric heater HT-0001. This is the minimum required temperature to enter the tritium extraction unit. TEU main function is extracting tritium from the liquid metal, transforming it by the solubilized state into a suitable gas phase. Once exited the TEU, PbLi stream is cooled down to 300 °C in the cooler HX-0001. Cooling function is provided by a double cooling system. Secondary coolant is air circulating in a closed circuit. At its time, it is refrigerated by water belonging to CCWS, acting as ultimate heat sink.

Then, the primary flow is split into two branches. A first portion, around 0.1 kg/s, enters the cold trap for alloy purification, while the remaining part is directly driven to the storage/recirculation tank. In the cold trap a further PbLi cooling is foreseen, up to a minimum temperature of 260 ˚C. For this purpose, a small air flow taken from the Port Cell #16 is supposed to be used. Two regulation valves control the liquid metal flow directed to the cold trap for purification. They can also be used to complete by-pass the component.

In the storage/recirculation tank, PbLi is kept at a constant temperature of 295-300 °C. From such component, the liquid breeder is pumped by means of the circulation pump and sent again to the WCLL-TBM inlet. During normal operations, storage/recirculation tank will make use of Helium as cover gas. The presence of an inert Helium atmosphere will avoid the oxidation process of lithium in the eutectic alloy. Helium atmosphere will be maintained at 1.1 bar (overpressure of 0.1 bar with respect to ambient air pressure in PC#16).

Finally, a relief tank is installed in the PbLi loop. In case an In-Box LOCA would take place inside the WCLL-TBM, its function is to limit the loop over-pressurization. It is connected to the circuit by means of two rupture disks located on the line linking the TBM outlet to the rest of the circuit.

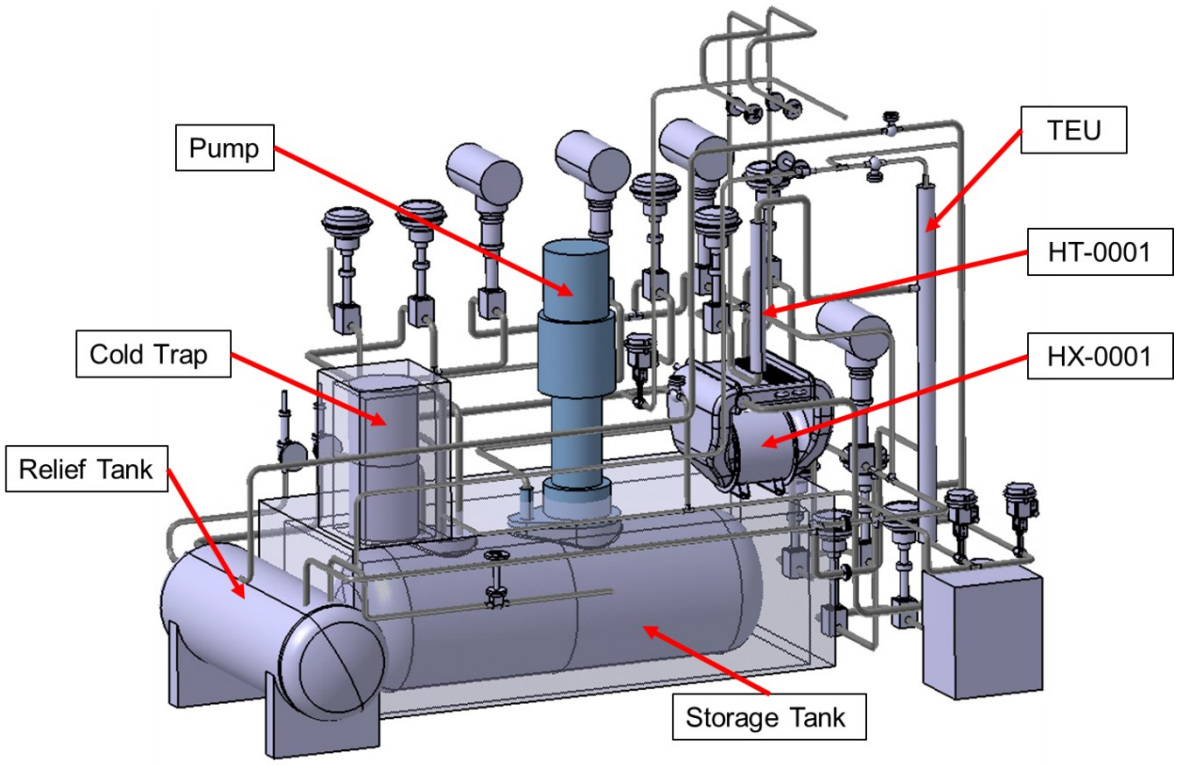

Figure 5.13 –PbLi loop equipment installed in Port Cell #16, with indication of the main components, [89].

6 ITER WCLL-TBM WCS TRANSIENT ANALYSIS

The computational activity discussed in this section consists in a preliminary thermal-hydraulic analysis of the ITER WCLL-TBM WCS. Since this circuit is directly connected to PbLi loop within the TBM, also these two systems were included in the overall TBS model. The main goal of this study was fully characterize the WCS TH performances during operative scenarios and selected abnormal conditions. The expected outcomes of the analysis were the following:

- Pressure and temperature fields.
- Overall pressure drops in NOS and related pump design.
- Margin from PbLi freezing temperature in selected critical points (inside TBM, cold trap outlet, etc.).
- Thermal balance.
- Capability of the WCS design to overcome selected abnormal conditions.

The calculations were carried out with the modified version of the RELAP5/Mod3.3 system code developed at DIAEE and discussed in **§** 2. Among the new features implemented, the ones relevant for the current simulation activity are: PbLi working fluid thermophysical properties in according with [39]; Seban-Shimazaki [40] correlation to properly evaluate the liquid metal heat transfer coefficient within circular tubes or plates.

6.1 Thermal-hydraulic model

The whole thermal-hydraulic model, prepared at DIAEE, is presented in Figure 6.1 and Figure 6.2. General rules to obtain a good mesh were all followed when realizing the system nodalization. In particular, the main features of the input deck are the following:

- Geometrical data for all the pipelines and equipment components keep the reference design;
- Actual elevations were maintained for any component;
- The ratio between the length of two adjacent control volumes was kept below 1.25;
- Fluid and material inventories were maintained for all the systems modelled.

Figure 6.1 shows the modelling of WCS, CCWS and PbLi loop. For space limitations, the figure does not represent actual elevations of the model, as well as of the design. It aims to provide a schematic view of the nodalization, presenting the qualitative elevation differences of the main components and their connections. The relevant components are depicted in grey for the WCS primary system, in light blue for the WCS secondary loop, in green for the CCWS and in orange for the PbLi. They are identified by the name and the component number (following the “#”). The pipelines, simulated with several pipe components, are represented with black lines, identifying some relevant connections, such as valves, pumps, and time-dependent junctions (black arrows). Time-dependent volumes are used to set inlet and outlet boundary conditions for specific components. They are represented with a peculiar symbol (a circle inside a square).

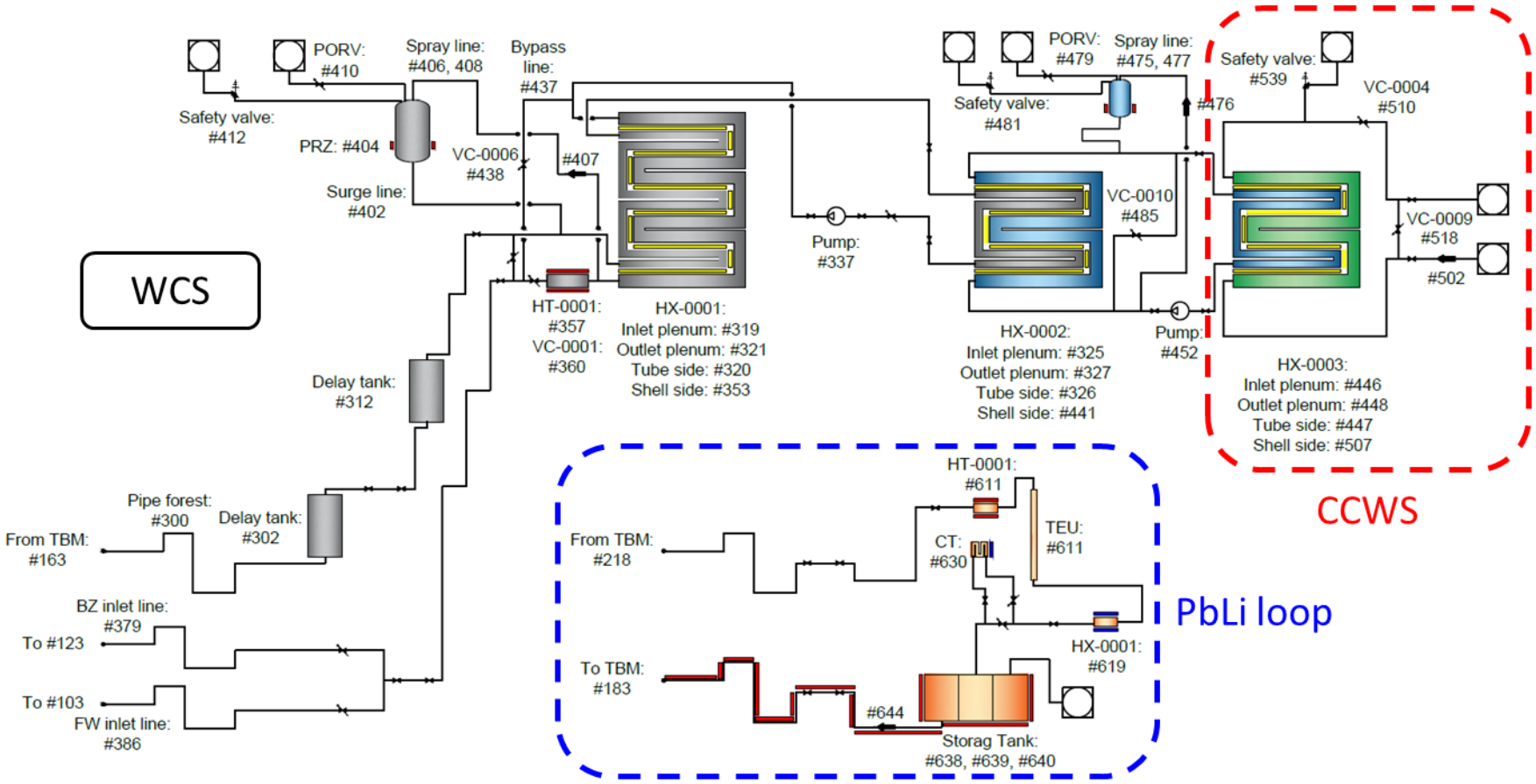

Figure 6.1 – Nodalization scheme of ITER WCLL-TBS: detail of the WCS, PbLi loop and CCWS section in TCWS Vault.

6.1.1 Water Cooling System

Hot water exits TBM and flows through the pipe forest (component #300 in Figure 6.1), placed in Port Cell #16 (see left corner at the bottom of Figure 6.1). It connects TBM outlet with the first delay tank (#302), located just within the Pipe Forest. Exiting the tank, the pipeline installed within the vertical shaft leads hot water first to the second delay tank (#312, at level three of tokamak building) and then to the TCWS Vault. The pipelines were modelled with several pipe components, keeping design features. Each delay tank was simulated with a vertical pipe component, maintaining the nominal inventory and internal diameter (i.e. water residence time).

Within the TCWS Vault, water is headed to the hairpin economizer (HX-0001). Hot water flows across the tubes, pre-heating the water flowing through the shell side. Inlet and outlet plena were modelled with two branch components, maintaining the nominal inventory. The whole tube bundle was collapsed in a single equivalent pipe component. From the hydraulic point of view, this pipe is characterized by the overall flow area but from the length and the hydraulic diameter of a single tube. This modelling approach allows to keep the actual inventory and the hydraulic features of the bundle. The flow area is affected by the operative conditions. As discussed in **§** 5.4.4, the heat exchangers were designed under EOL condition. The goal of the thermal-hydraulic analysis is to verify the WCS performances in both EOL and BOL. From the hydraulic point of view, the main difference is related to the total flow area of the tube bundle. Due to the postulated plugging, under EOL operation the flow area must be reduced of a 10%. The heat exchanger shell side was modelled with a pipe component. It is characterized by the nominal length and the total free flow area. The latter was calculated as the difference between the inner area of the shell and the area occupied by the tubes. Such flow area is not affected by the operative conditions since the effect of the postulated fouling is negligible in terms of flow area blockage. Several heat structures simulate the heat exchange between the two sides. They were used to properly couple the control volumes belonging to primary and secondary sides in order to correctly simulate the pure counter-current configuration belonging to the hairpin technology. In Figure 6.1, the yellow stick between hydrodynamic components represents passive (i.e. no internal power generation) heat structures for the thermal exchange. The heat transfer surface kept the nominal value. Even this parameter is affected by operating conditions. Under EOL it must be lowered of 10% due to the postulated plugging. Referring to tube fouling, the correspondent factors were calculated on the basis of reference data and applied to both sides (internal and external), increasing the thermal resistance. The overall modelling approach so far described for HX-0001 was also applied to the other WCS heat exchangers, since they are all based on the hairpin technology.

Downward the HX-0002, only one of the two primary coolant pumps was modelled. It was simulated with a RELAP5 pump component (#337). Its rated parameters (i.e. head, torque, rotational velocity, etc.) were derived from pump design data. The component was provided with a PI controller, acting on the rotational velocity and setting the nominal mass flow in WCS circuit. The same modelling approach was adopted for the pump system of the secondary loop.

The electric heater was simulated with a pipe component. The goal of the modelling approach was to keep the heat transfer capability (i.e., the HTC) and, at the same time, maintain the component water inventory. Since the component layout resembles the one of a Shell and Tubes, the pipe equivalent flow area was calculated according to the Kern methodology [98]. The hydraulic length was evaluated to maintain the heater actual inventory. This modelling approach results in a longer component. From a hydrodynamic point of view, this discrepancy has no impact on the overall loop pressure drops. Indeed, the heater length is negligible compared to the overall length of the primary cooling system. Regarding the heat transfer surface, its nominal value was maintained by applying specific geometrical factors to the heat structures simulating

the power supplied by heating rods. These active heat structures are represented by a red stick in Figure 6.1. The supplied power is provided by a control variable. The temperature of the control volume at the outlet of the TCWS Vault is compared with the reference setpoint (295°C). An enthalpy error signal is produced, and it is multiplied by the cold leg mass flow rate (acquired just before the control volume). A value of power unbalance is produced and scaled adopting a PI controller, where a minimum value equal to zero is imposed. The resulting signal is divided among the heat structures simulating the heating rods.

Exiting the electric heater, the cooling water descends the vertical shaft reaching the Port Cell #16. The TBM is fed by means of two conduits which provide water to the FW and the BZ systems.

The pressurizer allows to keep the required primary pressure. The component was modelled with a vertical pipe component, composed of seven control volumes. The first and the last CVs simulate the heads of the tank. The overall water inventory was kept by calibrating the flow area of these two CVs. The overall height of the component was also respected. The pressurizer electrical heater was simulated with an active heat structure connected to the second CV from the bottom. Thermal power supplied to the water is obtained from a general table and it is a function of the pressure deviation signal (computed by a control variable). The pressurizer is coupled to the primary loop by using a surge line (#402), connected to the hot leg, and a spray line (#406 and #408), connected to the cold line. The flow rate through the spray line is regulated by a time-dependent junction (#407), tuning the injected value depending on the pressure deviation signal. A trip disables the time-dependent junction in case of accidental scenario (for example loss of flow accident). In case of abnormal operation, if spray nozzles are supposed to fail or are disabled, pressurizer discharges steam firstly through the PORV (#410), and then through the SRV (#412). The two valves were modelled with motor valve components connected to two time-dependent volumes that reproduce the pressure relief tank environment. Opening and closure of these components are regulated by control trips, calibrated with design setpoints. The pressurizer modelling approach was replicated also for the pressure control system of secondary loop.

As presented in **§** 5.4.7, the performances of WCS heat exchangers are regulated by means of bypass lines. The HX-0001/HT-0001 bypass line was modelled with a pipe component (#437) connecting upward the HX-0001 and downward the HT-0001. The pipeline is equipped with a control valve, simulated with a servo valve component (#438). Openings and closures are regulated by a control variable. The temperature reading at the tube-side outlet is compared with the setpoint. An error signal is produced and scaled using a PI controller which operates in the range 0-1. The resulting signal is imposed as valve position for the component #438. This control logic was also adopted for HX-0002 and HX-0003. Concerning the HX-0003, the signal from the PI controller is assumed as valve position for component #518, while valve #510 operates oppositely than #518.

As far as the CCWS connections are concerned, only the circuit section within the TCWS Vault was considered. Inlet temperature and outlet pressure of the coolant are set by two time-dependent volumes. A time-dependent junction imposes the feedwater mass flow rate. The loop is equipped with a safety valve, modelled with a motor valve component (#539). Valve actuation is regulated by a control trip, calibrated on the basis of the design setpoints. When the safety valve opens, the coolant is discharged into the PRT, reproduced with a time-dependent volume.

The heat losses towards the environment were simulated for all the components belonging to the WCS. For the structural material and the thermal insulator, the same thermal properties adopted in DEMO WCLL transient analysis were used. They are discussed in **§** 4.1.2, while their tabular

functions are reported in annex A1. Steel and insulator thicknesses for pipelines and loop equipment were imposed according to design data. On the external surface, HTC and environment air temperature were imposed as boundary conditions (see **§** 4.1.3).

The overall pressure drops of the loops were computed by the code. The geometry and the number of bends were entered in the input deck according to the design. Calibrated K-loss coefficients were introduced to simulate local pressure drops such as abrupt area changes, bends, filters, valves and grids. K-coefficients were calculated by using formulas derived from [79].

6.1.2 PbLi Loop

Although the PbLi loop is not directly involved in the WCS design, it can affect its operations, since the WCS must ensure that metal freezing is avoided in all operational states. For this reason, a detailed thermal-hydraulic model of this system was developed and coupled to the WCS. The nodalization scheme consists of the pipelines, represented by black lines in Figure 6.1, and of the main equipment, depicted in orange.

Exiting the TBM, PbLi flows through the pipe forest, which leads the liquid metal from the port interspace to the ancillary equipment unit area, where all the system is installed. The PbLi enters the electrical heater (#611), which is in charge of increasing the liquid metal temperature to the operational value required from the tritium extraction unit. No information was provided regarding the heater geometry. For the scope of this activity, it was preliminarily considered as a portion of the pipeline, where PbLi is warmed up by heating cables. Active heat structures supply power to the liquid metal. The thermal power is evaluated at each time step with a control variable, following the same control logic adopted for the WCS HT-0001. This approach allows to absorb temperature oscillations due to reactor pulsed operation and to provide PbLi with a constant temperature at TEU inlet.

The tritium extraction unit was preliminary modelled with a descending vertical pipe, keeping actual inventory and elevation change (#611). Downward, the water-air heat exchanger cools-down the PbLi up to the storage tank operating temperature. According to the design, the cooler was simulated with a pipe component. Active heat structures remove the needed power (see blue rectangle in Figure 6.1). The thermal power is regulated with a PI controller. After that, part of the flow rate is directly driven towards the storage tank. The rest of the flow is directed to the cold trap, which has in charge the PbLi purification. During NOS, a fraction of the total PbLi flow rate is continuously headed to the CT for alloy purification. To fulfil this scope, the component is cooled by an air flow, furtherly reducing the PbLi temperature. The unit was modelled with a pipe (#630), following the characteristic geometry of the component. The liquid metal inventory was maintained. The PbLi cooling was simulated by removing a constant thermal power with an active heat structure.

The storage tank was modelled with three vertical parallel pipes (#638, #639 and #640), connected with multiple cross junctions. This modelling approach allows to reproduce buoyancy within the large volume. The cover gas pressure is set with a time-dependent volume connected to the upper part of the pool. A time-dependent junction (#644) reproduces the pump. It fixes the overall mass flow rate through the PbLi loop.

Several heat structures reproduce the heat losses related to each component of the liquid metal loop. For the external conditions, the same boundaries used for the WCS were applied. The heat losses are a crucial aspect for the PbLi loop, especially downwards the CT, since metal freezing

must be avoided and PbLi must be provided at TBM inlet with the required thermodynamic conditions. For this purpose, active heat structures compensate the heat losses that occur through the walls of the storage tank and of the pipelines connecting the tank and the TBM inlet. The necessary thermal power is managed by using a PI controller.

6.1.3 Test Blanket Module

Figure 6.2 shows the TBM nodalization scheme. The figure does not respect the 3D allocation of different elements within the box. It is intended only as a schematic view of the hydraulic components used to simulate the water and PbLi flow paths inside the test blanket module. The reference geometry for such device was derived from [88]. As stated in **§** 5.3, on the back of the breeder zone, four back plates define four manifolds:

- FW inlet manifold: responsible for the water distribution among the FW channels;
- BZ inlet manifold: responsible for the water distribution among the DWTs;
- Water outlet manifold: responsible for water collection from DWTs and FW channels;
- PbLi manifold: responsible for the inlet/outlet of PbLi within the breeder units.

The three manifolds belonging to the water system were modelled with three vertical pipes (one per each manifold), composed of 16 CVs. Reminding that each breeding unit is divided in two by a baffle plate (see Figure 5.7a/b), each control volume was associated to the upper or lower section of a breeding unit. In addition, as vertical length of the manifold CVs, half of the BU poloidal height was assumed. The inventory of each manifold was kept by properly calculating the flow area. Calibrated K-loss coefficients were applied to pipe internal junctions. They simulate the abrupt area changes experienced by water when flowing upwards or downwards within the manifold (the inlet/outlet pipes are located at mid-height of the TBM box back). Such concentrated pressure drops are due to the obstacles present in the water vertical flow path within the manifold, such as TAS and NAS instrumentation, inlet/outlet PbLi pipes and DWTs (in the FW and BZ common outlet header), see Figure 5.7a/b.

The 32 FW channels were collapsed in two equivalent pipes (#107 and #110): one for the descending and one for the ascending channels. In this way, their peculiar counter-current configuration was kept (Figure 5.6). The ascending pipe is connected to the bottom CV of the FW inlet manifold (#105) and to the top CV of the BZ/FW common outlet header (#161), vice versa the descending one. An overall number of 168 heat structures simulates the heat exchange within the FW. In particular:

- 32 HSs for the surface directly facing the plasma. The heat flux from the plasma and the power deposited in the EUROFER thickness were imposed as boundary conditions. In addition, thermal conduction in the poloidal direction was taken into account using several control variables. They evaluate the heat transfer between adjacent portions of the FW on the basis of their structural temperatures.
- 16 HSs for the radial segments of the FW component. The power deposited in the structure was imposed as an internal power source.
- 24 HSs for the EUROFER ribs between FW channels. Internal power source was set as boundary condition. These heat structures were used to properly couple the control

volumes belonging to ascending and descending pipes in order to correctly simulate the counter-current configuration belonging to FW channels.

- 96 HSs for the heat exchange between FW channels and PbLi within the breeding units. These components allow to thermally couple WCS and PbLi loop. Furthermore, the power internally generated in the structures was simulated and imposed as boundary condition.

DWTs were collapsed in 16 equivalent horizontal pipes (#127 to #142), connected at each level of the BZ inlet (#125) and outlet (#161, in common with the FW) manifolds. The modelling approach adopted for water manifolds (see above) allows to keep the DWTs design elevations. The pipe flow area was computed according to the number of DWTs associated to each pipe (remind that top/bottom BUs are refrigerated by three DWTs instead of four). The length of pipe CVs, as well as the K-loss coefficients related to the internal junctions, were used to correctly simulate the different DWT layouts, in terms of overall length and number/type of curves (see Figure 5.7a/b). Up to four different layouts are present in the overall DWTs batch. An overall number of 288 heat structures simulates the heat exchange between DWTs and PbLi within the breeder zone. These components, together with the previous ones related to FW channels, accomplishes the thermal coupling between WCS and PbLi loop. A RELAP5 multiple junction component manages the connections between water manifolds and DWTs. According to design indication in [88], a calibration procedure was performed in order to uniform the temperature at their outlet. For this purpose, calibrated K-loss coefficients were entered in the input deck for the junctions representing the DTWs inlet.

According to reference layout, PbLi manifold is divided in four toroidal sections by means of three vertical stiffening plates running along the overall poloidal height. Exiting the inlet pipe, that is a unique component located at the bottom of the module, the total liquid metal flow is split in two parallel flow paths. The first interests the breeding units on the left, while the second the ones on the right. Eutectic alloy flows upwards in any section, entering/exiting the breeding units through the suitable windows. The parallel flow paths are reunited in the outlet pipe, leading the PbLi outside the test blanket module. Each manifold section was simulated with a vertical pipe component (#187 & #204 for inlet and #197 & #214 for outlet). They are characterized by 16 CVs. The same vertical length used for water manifold CVs was assumed. Thus, ‘slice nodalization technique’ was adopted when realizing the TBM mesh. The breeding units were modelled with 16 pipe components (one per BU, #189 to #196 for the left ones and #206 to #213 for the right ones). An overall number of 208 heat structures reproduces the power generation within the breeder zone. The overall liquid metal inventory within the TBM box was kept by properly computing the flow areas associated to manifold section and BUs pipe components. As for DWTs, a RELAP5 multiple junction component manages the connections between PbLi manifold sections and breeding units. Calibrated K-loss coefficients were entered for the junctions representing the BUs inlet in order to evenly distribute the overall PbLi flow, according to [88].

Finally, the heat exchange through the back plates was simulated with an overall number of 136 HSs.

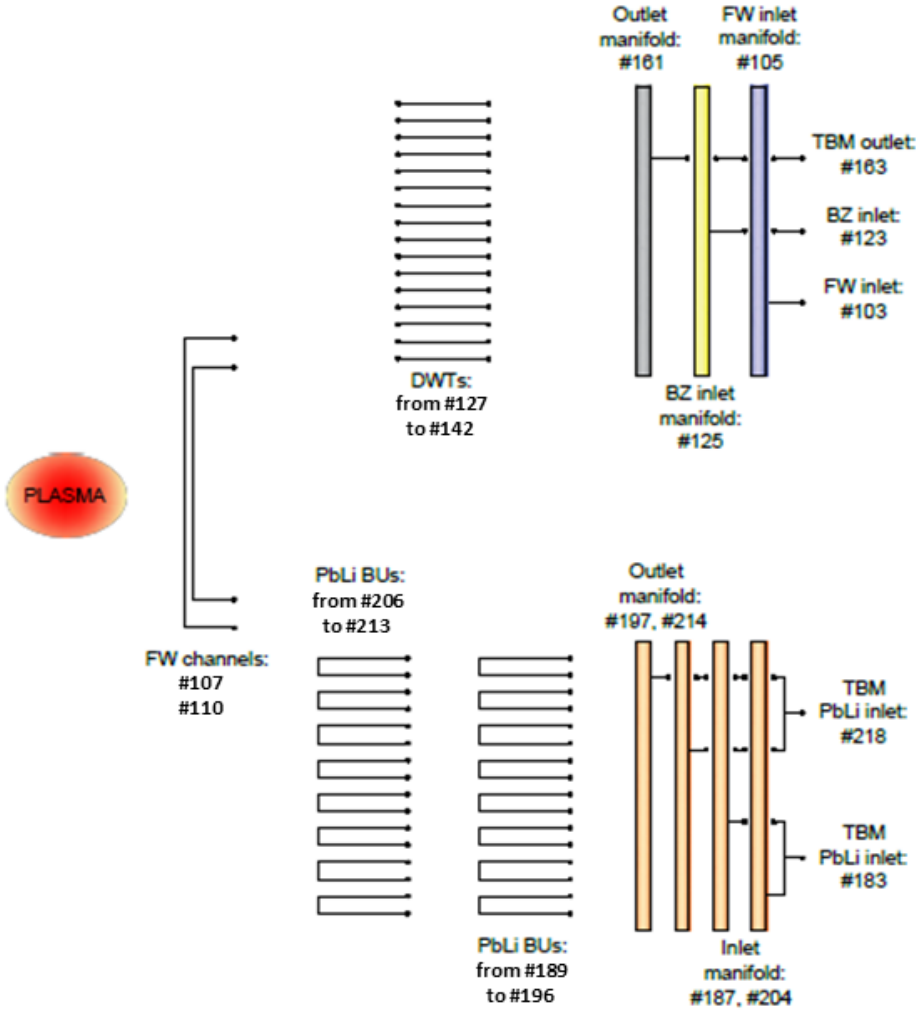

Figure 6.2 – Nodalization scheme of ITER WCLL-TBM.

6.2 Transient analysis

The following sections discuss the main outcomes obtained performing the thermal-hydraulic transient analysis of the ITER WCLL-TBM WCS. To fulfil this scope, the RELAP5 model discussed so far was used. Firstly, full plasma power state was simulated at both BOL and EOL conditions and the differences in the WCS thermal-hydraulic performances were highlighted (**§** 6.3). Such calculations were also needed to test and evaluate the appropriateness of the thermal-hydraulic model prepared.

Then, these steady-state calculations were used as initial condition to simulate operative scenarios and abnormal conditions. The Normal Operation State was the first to be analyzed. Even in this case, simulations were carried out in both BOL and EOL conditions to assess the change in WCS thermal-hydraulic performances with the system aging (§ 6.4).

Finally, the Water Cooling System response during abnormal conditions was studied (§ 6.5). The selected transients to be simulated were:

- LOFA occurring in the WCS secondary loop (**§** 6.5.1);
- LOHS, i.e. loss of flow in the CCWS (**§** 6.5.2).

The goal of this transient analysis was supporting the WCS design. The system capabilities under degraded conditions were investigated and it was verified if the standard control strategies without any external action are capable to maintain the TBM cooling function for an entire ITER pulse. This last condition allows to avoid the triggering of the Fast Plasma Shutdown System, demonstrating that a minor accident in the WCS does not interfere with the ITER global operation.

6.3 Full plasma power state

The steady state calculations were performed to assess the thermal-hydraulic model, reproducing the full plasma power state. Simulations involved both the BOL and EOL operations. An overall thermal power of 723.16 kW was supplied as constant boundary condition by the active heat structures composing the TBM model (see **§** 6.1.3). The power source is distributed among the different terms indicated in Table 6.1. The power distribution is derived from [99].

Table 6.1 – Full plasma power state: source terms, [99].

Parameter	Unit	Value
Total plasma power	kW	723.16
First wall Heat Flux	kW	231.46
Total Nuclear Heating:	kW	491.70
- PbLi	kW	272.0
- EUROFER	kW	202.4
- Water	kW	17.3

The flow rates characterizing the CCWS and the PbLi loop were imposed as boundary conditions with two time-dependent junctions. Referring to CCWS, water inlet temperature and outlet pressure were set by two time-dependent volumes. Instead, the coolant flows through the WCS primary and secondary loops were calculated by the code by using the correspondent pump components (see **§** 6.1.1). The flow rates were derived from the balance between available pump head and the overall loop pressure drops. Table 6.2 and Table 6.3 summarize the most relevant outcomes of the steady state calculations, comparing BOL and EOL results with the nominal values. Parameters indicated with "**(BC)**" were set as boundary conditions. The simulations were repeated assuming four values for the time step (5.0×10^{-3} s, 3.0×10^{-3} s, 2.0×10^{-3} s and 1.0×10^{-3} s). The time step sensitivity highlighted the independence of the calculation outcomes from this parameter.

Table 6.2 – Full plasma power state: simulation results related to WCS and CCWS.

System	Parameter	Unit	Nominal value	BOL	EOL
WCS Primary Loop	System mass flow	kg/s	3.74	3.74	3.74
	HX-0001 mass flow (shell-side)	kg/s	--	3.45	3.74
	TBM outlet temperature	°C	328	327.7	327.7
	HX-0001 outlet temperature (tube-side)	°C	157	156.6	157.8
	HX-0002 outlet temperature (tube-side)	°C	111.4	111.4	111.3
	HT-0001 inlet temperature	°C	--	307.3	293.7
	TBM inlet temperature	°C	295	294.9	294.9
	Pump head	MPa	--	0.773	0.786
	Pressurizer pressure	MPa	15.5	15.5	15.5
WCS Secondary Loop	System mass flow	kg/s	4.3	4.3	4.3
	HX-0002 mass flow (shell-side)	kg/s	4.3	2.7	4.1
	HX-0002 outlet temperature (shell-side)	°C	--	127.9	107.6
	HX-0003 inlet temperature (tube-side)	°C	104.9	104.9	105.2
	HX-0003 outlet temperature (tube-side)	°C	64.9	64.8	64.3
	Pump head	MPa	--	0.116	0.139
	Pressurizer pressure	MPa	2.00	2.05	2.05
CCWS section within TCWS	System mass flow **(BC)**	kg/s	17.3	17.3	17.3

	HX-0003 mass flow (shell-side)	kg/s	--	5.41	15.12
	Inlet temperature **(BC)**	°C	31	31	31
	HX-0003 outlet temperature (shell-side)	°C	--	63.1	42.7
	Outlet temperature	°C	41	41.0	41.2
WCS Power Balance	TBM power to WCS	kW	723.16	718.48	718.51
	HX-0001 power	kW	3112.5	3104.1	3084.7
	HX-0002 power	kW	722.8	723.35	736.09
	HX-0003 power	kW	722.8	724.89	738.23
	HT-0001 power	kW	--	11.96	24.58
	PL pumping power	kW	--	4.01	4.04
	SL pumping power	kW	--	3.3	3.99
	PL pressurizer heaters power	kW	--	1.13	1.17
	SL pressurizer heaters power	kW	--	0.27	0.27
	PL total heat losses	kW	--	11.89	11.70
	SL total heat losses	kW	--	1.75	1.73

Table 6.3 – Full plasma power state: simulation results related to PbLi loop.

System	**Parameter**	**Unit**	**Nominal value**	**BOL**	**EOL**
PbLi Loop TH parameters	System mass flow **(BC)**	kg/s	0.65	0.65	0.65
	TBM outlet temperature	°C	--	330.9	330.9
	HT-0001 outlet temperature	°C	450	449.8	449.8
	HX-0001 outlet temperature	°C	300	300.2	300.2
	Cold Trap outlet temperature	°C	260	259.2	259.2
	TBM inlet temperature	°C	295	295	295
	Pump head	Pa	--	0.115	0.115

PbLi loop Power Balance	TBM power to PbLi	kW	--	4.42	4.42
	HX-0001 power	kW	--	17.99	17.99
	Power removed in cold trap **(BC)**	kW	0.76	0.608	0.608
	HT-0001 power	kW	--	15.48	15.48
	Heating cables: storage tank	kW	--	1.23	1.23
	Heating cables: TBM inlet line	kW	--	0.81	0.81
	Total heat losses	kW	--	3.26	3.26

During full plasma power state, the main requirement related to WCS/PbLi loop operation is to provide water coolant/liquid metal at TBM inlet with the nominal values of mass flow, pressure and temperature. They are all specified in the eponymous column (the fourth) of Table 6.2 and Table 6.3. The most important simulation outcome (see columns five and six of the above tables) is that control systems corresponding to WCS and PbLi loop are able to ensure the required values in both the operational conditions (BOL and EOL).

Referring to WCS primary loop, a difference between the two operative conditions is the coolant flow rate through the HX-0001 shell side. The control system acting on the servo valve component #438 (Figure 6.1, VC-0006 in Figure 5.10) works to match the reference value of the tube side outlet temperature, reported in the fourth column of Table 6.2. For this reason, under BOL operation, when the heat exchanger performances are oversized, part of the primary flow bypasses the HX-0001 shell. Instead, at EOL, the heat exchanger works under reference conditions and the nominal primary flow feeds the component shell. The different flow rates lead to the discrepancy observed in the HT-0001 inlet temperature. Since HX-0001 power is nearly the same in both conditions, lower flow rate (BOL) determines higher temperature at the HX-0001 shell outlet. This also justifies the difference in the power supplied by HT-0001 (lower at BOL). What is worth to be emphasized is that HX-0001 preheats cold coolant directed to the TBM using hot water coming from the TBM itself. Thus, this heat exchanger does not contribute to the power balance of the WCS primary loop. Indeed, its power is transferred from a branch to another, within the circuit itself. Such parameter is reported in Table 6.2 under the headline of 'WCS Power Balance' only for sake of completeness.

Control systems act in a similar way also to regulate the operation of HX-0002 and HX-0003. In these cases, the controlled components are the servo valves #485 and #518 (Figure 6.1, VC-0010 and VC-0009 in Figure 5.10), respectively. The control system responsible for WCS secondary loop must set the required temperature at HX-0002 tube side outlet. Such parameter, belonging to the primary loop, is collected in Table 6.2. At BOL, due to the HX-0002 oversized heat exchange capabilities, part of the secondary flow bypasses the component shell, ensuring the required heat removal. Regarding the CCWS, the cooling water is provided with imposed thermodynamic conditions (see Table 6.2). Moreover, the requirement is to keep the return temperature under 41 °C. In order to respect this upper limit, the control system regulates the water flow through the HX-0003 shell, tuning in this way the power removal. A large discrepancy between BOL and EOL operations is observed in Table 6.2, in terms of water flow and outlet temperature at shell outlet.

The WCS primary pump component sets the required mass flow in both scenarios. As expected, under EOL operation, the overall circuit pressure drops (i.e. pump head) are slightly higher. This is mainly due to: **i)** the postulated tube plugging acting on the heat exchangers (HX-0001 and HX-0002) during EOL; **ii)** the reduced mass flow (i.e. lower fluid velocity) in the branch hosting the HX-0001 shell and the HT-0001 during BOL. The above considerations are still valid for WCS secondary loop. Nominal flow is ensured in both conditions. Although, in this case, due to the reduced length of the secondary circuit, the aforementioned discrepancies (clearly declined within the SL, i.e. HX-0003 tube plugging and HX-0002 reduced shell flow) produce a higher relative difference between BOL and EOL pressure drops (i.e. pump head). Finally, concerning the WCS heat losses, no differences can be detected among the operative scenarios investigated. Thermal insulation ensures a maximum temperature on the outer surface of all the system pipelines and equipment below the reference value of 50 °C.

As far as the PbLi loop is concerned, the temperatures in the main relevant sections are verified in both the operative conditions. It must be noted that PbLi loop modelling does not change from BOL to EOL. Thus, differences among these scenarios were not expected. The overall power supplied to the eutectic alloy, indicated in Table 6.3, is provided by HT-0001 and the heating cables whose storage tank and TBM inlet section pipeline are equipped. The first contribution allows to increase the liquid metal temperature to the value needed for TEU operations (450 °C), and the second one ensures the required TBM inlet temperature (295 °C). The circuit pressure drops (i.e. pump head) were computed also including the magnetohydrodynamic (MHD) contribution within the TBM and pipe forest area, derived from [100]. Also for PbLi loop, design thermal insulation guarantees the pipeline and equipment outer surface temperature below the limit (50 °C).

Evaluate the TBM thermal-hydraulic performances was out of the scope of the research activity carried out by DIAEE. Nevertheless, TBM box contains part of the WCS circuit and constitutes the system source term. In addition, thermal coupling between WCS and PbLi loop occurs inside the module. For this, it is mandatory that the heat transfer phenomena taking place within the component are properly simulated by the thermal-hydraulic model prepared for it. This also enhances the reliability of the feedback given by TBM to WCS circuit during transient calculations. To calibrate the TBM thermal-hydraulic model, the results obtained by CEA using Finite Element Method (FEM) analysis were used, [88]. The available data were adapted to the coarser mesh characterizing the water and PbLi fluid domains in the system code nodalization. The RELAP5 results, discussed in the following, are in good accordance with the ones in [88]. What is worth to be emphasized is that TBM thermal-hydraulic performances do not change from BOL to EOL, since, thanks to the control systems associated to WCS and PbLi loop, water coolant and liquid metal are provided at the module inlet with constant thermodynamic conditions and flow rate.

The DWTs and FW channels temperature profiles along the correspondent thermal length (normalized) are reported in Figure 6.3a and b, respectively. To properly distribute the overall WCS mass flow, the calibration procedure was articulated in two steps. Firstly, the design flow rate values addressed to breeder zone and first wall sub-systems were match by correctly regulating the calibrated orifice and the control valve whose their inlet lines are provided (see **§** 5.4.2.1). Secondly, each contribution was evenly distributed between the equivalent pipe components simulating the DWTs or the FW channels. This uniform distribution was chosen according to design indication in [88]. Indeed, it produces satisfactory preliminary results. In particular, regarding the DWTs, quite similar temperature profiles are obtained in all the equivalent pipe components. A slight deviation can be observed for pipe #1 and #16, representing the lower part of bottom BUs and the top part of top BUs. This can be justified considering that in these two locations only one DWT, instead of two, is present and, thus, it is heated more than the

others. No differences are detectable among the two pipe components simulating the ascending and descending FW channels.

Referring to liquid metal fluid domain, a further orificing procedure was needed. It was aimed at uniformly distribute the overall mass flow among the sixteen pipe components modelling the PbLi parallel flow paths within the breeding units. Even in this case, such distribution was adopted to be aligned with information provided by [88]. It proves to be quite effective, as shown in Figure 6.3c. The thermal length (normalized) considered in the plot follows the radial-poloidal-radial breeder flow path inside the breeding unit. The relative extent of each of the three segments is also indicated in the figure. PbLi temperature profiles are quite similar for all the breeding units, except for #1, #8, #9, and #16, located at the bottom and top of the TBM box. Note that BU numeration goes from #1 to #8 for the left side cells and from #9 to #16 for the right side ones. The interested breeding units experience higher temperatures since provided only with three DWTs instead of four. The maximum PbLi temperatures correspond to the poloidal segment, that is right in front of the FW. Indeed, this is the radially innermost region of the breeder flow path, thus the one where the power generation is maximum. The heat here produced is removed not only by the DWTs but also from the FW channels. Along the poloidal segments, both in inlet and in outlet, the breeder temperature decrease thanks to the effective cooling provided by DWTs. The PbLi temperatures calculated by the system code within the manifolds and the breeding units are also collected in Figure 6.4a and b, where are plotted by using a temperature contour. Even if a coarser mesh was adopted, RELAP5 is able to roughly reproduce a breeder temperature field in good accordance with the one presented in [88].

Finally, the maximum EUROFER temperatures computed by the code for the most relevant TBM components are reported in Table 6.4. The limit of 550 °C is respected, [101]. However, the system code does not have the resolution to investigate hot spots eventually occurring within the breeding unit, above all in the poloidal region just in front of the FW. It must be noted that a detailed analysis of this kind is out of the scope of the research activity presented in this thesis. What can be seen from Table 6.4 is that EUROFER temperatures approach the limit for the components completely immersed in the liquid metal and not cooled from water. Indeed, the maximum temperature for the stiffening plates is far above the one of the DWTs, proving the effectiveness of the water cooling. Baffle plate experiences temperatures well below the ones of the horizontal and stiffening plates since this component is not present in the poloidal region, where the maximum power generation occurs. What is also worth to be noticed is that FW component is characterized by higher temperatures in the back part, the one in contact with the breeding unit, rather than in the front layer, interested by the incident heat flux. This demonstrates the importance of the FW channels in the cooling of the poloidal region, together with the DWTs.

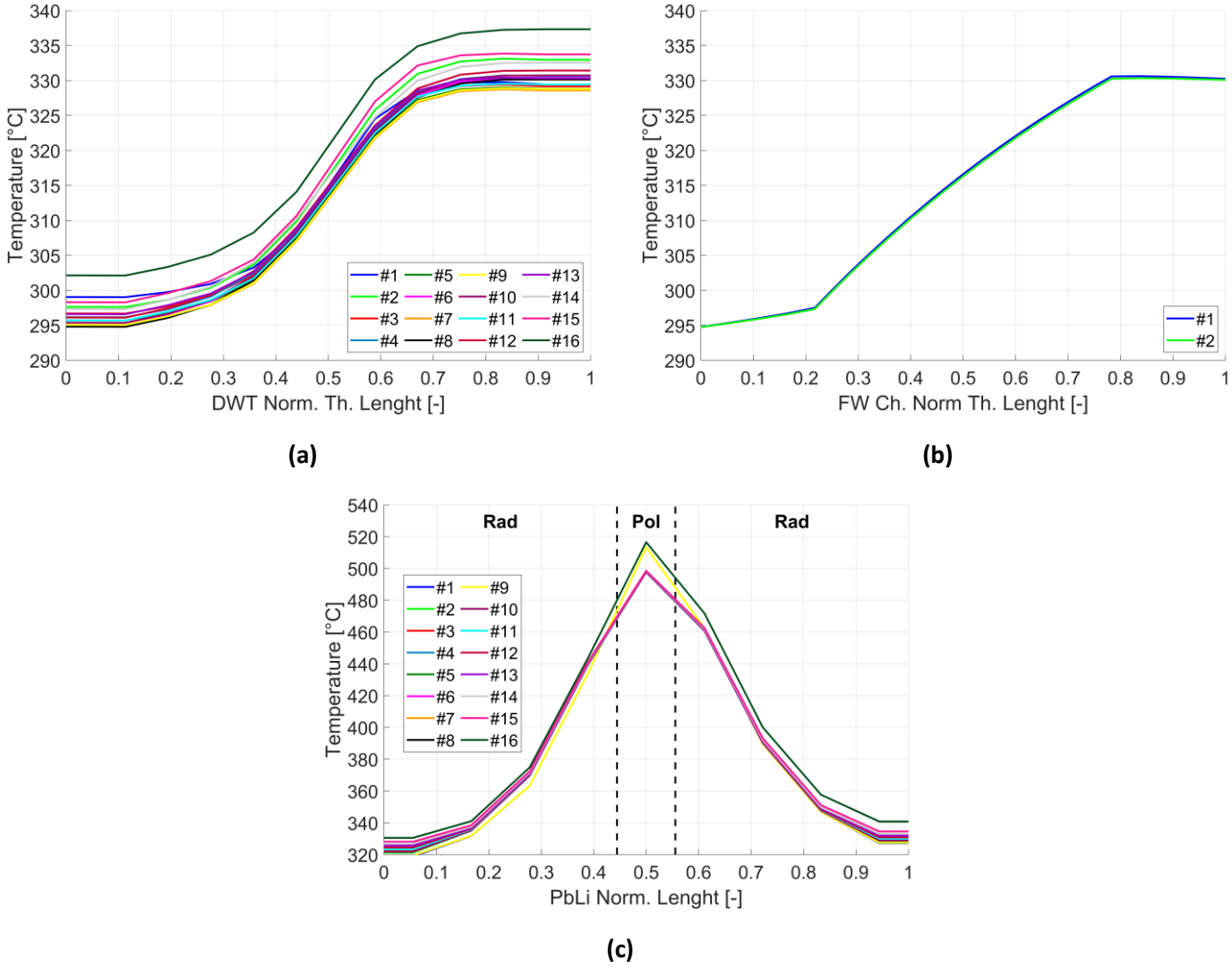

Figure 6.3 – Full plasma power state, insight into TBM box: **(a)** temperature profile along DWTs thermal length; **(b)** temperature profile along FW channels thermal length; **(c)** temperature profile along PbLi flow path within breeding units.

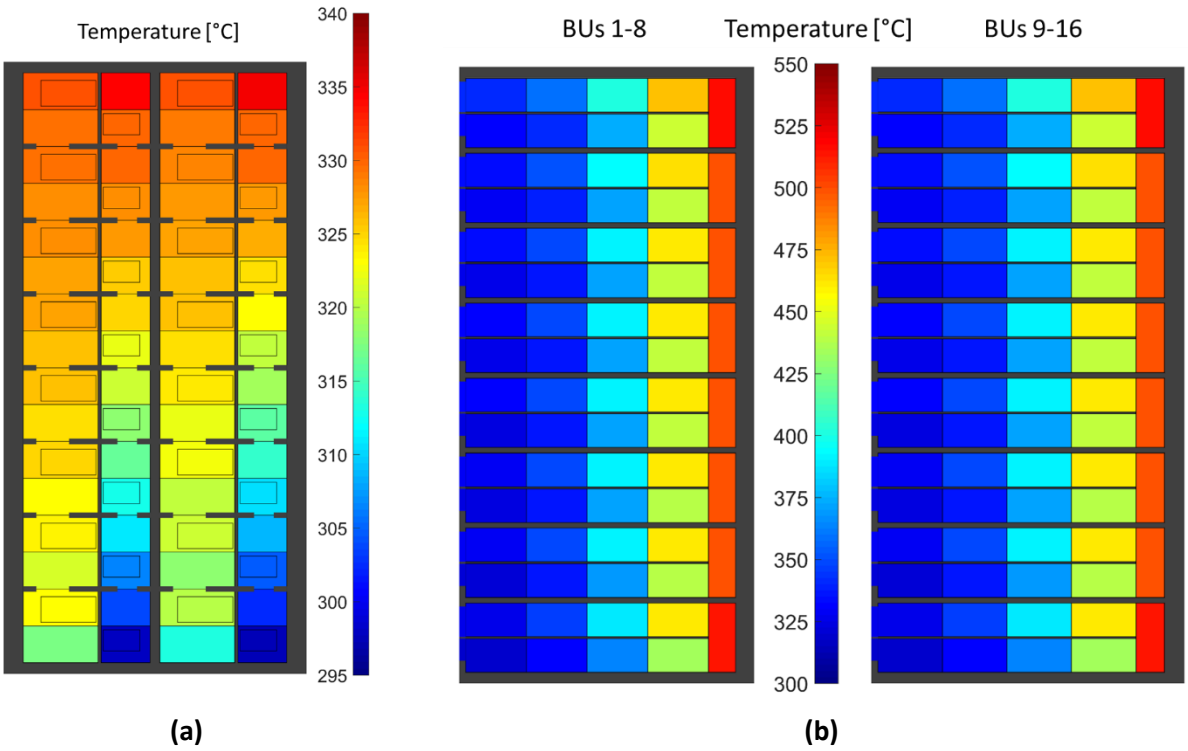

Figure 6.4 – Full plasma power state, insight into TBM: PbLi temperatures in manifolds **(a)** and breeding units **(b)**.

Table 6.4 – Full plasma power state: maximum EUROFER temperatures in some relevant TBM components.

Parameter	**Unit**	**Value**	**Parameter**	**Unit**	**Value**
FW front layer (plasma chamber side)	°C	377.9	DWTs	°C	376.8
FW back layer (breeding unit side)	°C	423.9	BUs back plate	°C	337.4
Side caps	°C	401.7	Back Plate 1	°C	333.4
Vertical Stiffening Plates	°C	516.5	Back Plate 2	°C	319.1
Horizontal Stiffening Plates	°C	514.5	Back Plate 3	°C	298.5
Baffle Plate	°C	456.1	Back Plate 4	°C	294.8

6.4 Normal Operation State

This transient analysis was performed with the aim of studying the TBS behavior during the Normal Operation State. In addition, the WCS and PbLi loop control systems were tested to demonstrate their effectiveness in ensuring stable operations against the pulsed regime characterizing the NOS. Preliminary investigations on this key issue were performed also during the pre-conceptual design phase. Results are examined in annex A3 and in [102]. Simulation outcomes represented important lessons learned for the subsequent (conceptual) design phase. In this framework, new calculations were carried out. They are discussed in this section. Full power steady state results at BOL and EOL, described in **§** 6.3, were used as initial conditions for the transient simulations. The plots reported in the following show the figures of merit selected to analyze the NOS, comparing thermal-hydraulic parameters at BOL and EOL conditions.

A pulsed plasma regime is foreseen during the Normal Operation State, [103]. Full plasma power is reached in 60 s. Flat-top condition is kept for 450 s. After that, power is ramped down in 200 s. Dwell time between two consecutive plasma pulses lasts 1090 s. The power source terms characterizing the WCLL-TBM during pulse phase are reported in Table 6.1. During dwell time, only decay heat is still produced in the module. Neutronic calculations providing its exact relative extent with respect to the rated power are currently not available. For this, the value characterizing the DEMO WCLL blanket was preliminary assumed (2%, see **§** 3.1). In the following plots, pulse phase is characterized by white background while dwell time by grey background.

Transient analysis starts with the flat-top at full power, assuming the steady state initial conditions summarized in Table 6.2 and Table 6.3. Simulations were carried out for 14000 s, corresponding to eight complete cycles of pulsed regime. WCS primary and secondary pumps were kept running at nominal velocity over the whole simulation, maintaining almost constant the correspondent loop mass flow. Such boundary condition was adopted in WCS circuits since relevant for DEMO normal operations, as stated in **§** 4.4.1. Regarding the CCWS, inlet conditions (i.e. temperature and feedwater flow rate) and outlet pressure were kept constant.

Figure 6.5a shows WCS water temperatures at the TBM inlet and outlet sections. The requirements related to the TBM inlet conditions are verified in both operational conditions (BOL and EOL). In particular, inlet temperature is kept by the control system within an acceptable range of +/-3 °C around the reference value (295 °C), while the mass flow in ensured by the primary pump. At the TBM outlet, temperature ranges between a minimum of 295 °C and a maximum of 328.6 °C, following the trend of the plasma power (i.e. the power supplied by the TBM to the WCS, see Figure 6.5b).

The most relevant thermal powers exchanged in the WCS are shown in Figure 6.5b. Comparing BOL and EOL conditions, it reports the trends of the TBM power delivered to the coolant, the HX-0002 heat removal and the HT-0001 supplied power. No sensible differences can be detected between the two operative scenarios. The TBM power delivered to the WCS coolant spans from a minimum of 8.46 kW (dwell time) to a maximum of 680 kW (end of pulse). What is worth to be emphasized is that such parameter does not have the trapezoidal shape expected for it. Power supplied to water coolant is affected by the TBM thermal inertia, even if reduced (see also the comment to Figure 6.8 and Figure 6.9). At the beginning of dwell time, within the TBM, a power surplus (with respect to decay heat contribution) is provided to WCS water by EUROFER and PbLi cooling. The power decreasing trend lasts more than the nominal 60 s (plasma ramp-down, see above). However, the cooling transient is quite fast due to the low box thermal inertia. Later, up to the end of dwell time, water, PbLi and EUROFER inside the module are nearly isothermal and water removes the residual decay heat. During power ramp-up and subsequent flat-top, water

coolant experiences a power deficit, if compared with TBM rated power reported in Table 6.1. The missing power is absorbed by the heating of EUROFER structures and liquid breeder inside the module. What is demonstrated by Figure 6.5a (outlet temperature) and Figure 6.5b (TBM power delivered to WCS) is that flat-top is too short to allow the TBM to reach steady-state condition. This is also true for the WCS section directly interfaced with the module outlet, thus up to the HX-0001 tube side inlet.

Although, Figure 6.5c shows that the control system associated to HX-0001 is able to reduce the oscillations observed at the TBM outlet. The shell mass flow rate is regulated in order to flatten the temperature at tube side outlet. Figure 6.5d compares the shell side mass flow rate calculated under BOL and EOL operations. During BOL, the component oversized heat exchange capabilities lead to a reduction of the needed shell flow rate (with respect to EOL, as already discussed in **§** 6.3). A further diminution occurs during dwell time due to the decrease of thermal power delivered by TBM. The fluctuations of the mass flow are needed to compensate the oscillations of the TBM outlet temperature. The HX-0001 heat exchange is presented in Figure 6.5e. As expected, the difference between BOL and EOL is around null and power follows the pulsed trend of the mass flow across the shell side. The result is an almost constant temperature at the outlet of the tubes, even if residual small ripples are still observed (Figure 6.5c). What is interesting to be noted is that the oscillations in the HX-0001 parameters are delayed with respect to the ones on the TBM outlet temperature. Such effect is due to the presence of the delay and decay tanks, the former located directly in the pipe forest and the latter at level three of the tokamak building (see **§** 5.4.2.1). To reduce the $^{16}N/^{17}N$ content, they significantly slow down the water flow outcoming the TBM, producing the time shift visible between peaks in Figure 6.5a/b and Figure 6.5d/e.

The small lasting oscillations present in the HX-0001 tube side outlet temperature are suppressed by the HX-0002 control system. The correspondent secondary side mass flow is slightly regulated. The little fluctuations detectable in Figure 6.5f allow to obtain a steady temperature at the tube side outlet (Figure 6.5c). The mass flow difference between BOL and EOL is due to the component performances in such operative conditions, as already commented in **§** 6.3. Due to the combined effects of HX-0001 and HX-0002 control systems, HX-0002 operates at constant power during the whole NOS. Indeed, focusing on the tube-side, inlet temperature is imposed (it coincides with the HX-0001 outlet temperature, unless the negligible heat losses) and outlet conditions are regulated to the design temperature (111.4 °C). In addition, mass flow is set by the primary pump. Moreover, all these parameters do not vary from BOL to EOL. Thus, the power removed by HX-0002 (720 kW) is independent from the operative condition. The result is the nearly flat trends collected in Figure 6.5b.

The HT-0001 is deputized to compensate the power unbalance in WCS system. The power supplied by the electric heater is regulated by the control logic presented in **§** 6.1.1. Since the trends of TBM power input and HX-0002 power output do not change from BOL to EOL (dominant terms of the WCS power balance), also the power provided by HT-0001 follows the same curve in both conditions (Figure 6.5b). Such trend is reverted and delayed with respect to the TBM term, spanning from 79.6 kW to 699 kW. The time shift is due to water crossing time in WCS primary loop, principally due to the presence of the delay and decay tanks. Finally, heater inlet/outlet temperatures are reported in Figure 6.5g. Cold water is drawn by the primary pump and flows towards the HX-0001 shell side. Only part of the total flow rate feeds the HX-0001 (see Figure 6.5d). At the shell side outlet (heater inlet), temperature changes in the range of 281.5 – 304.7 °C for BOL and 270.7 – 291 °C for EOL. Discrepancy between the two conditions is justified by the difference in terms of water flow rate, and the oscillating trend follows the fluctuations of the HX-0001 heat exchange. HT-0001 supplies power to the coolant, increasing its temperature (maximum value of 322.6 °C at BOL and 310 °C at EOL). Hot water is mixed with the cold one,

coming from the bypass line, resulting in the almost constant temperature at TBM inlet shown in Figure 6.5a.

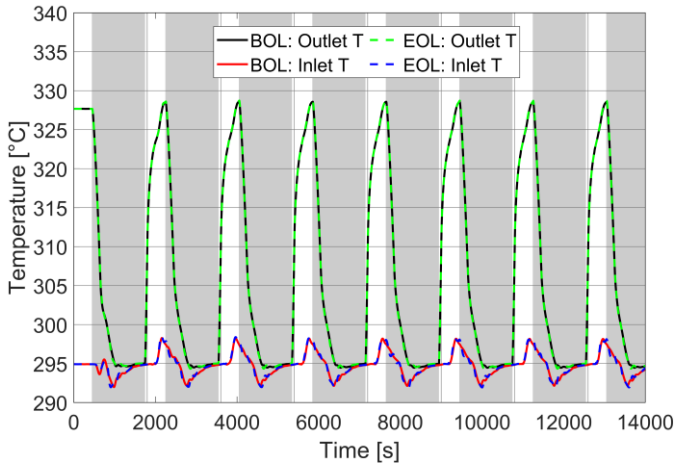

(a)

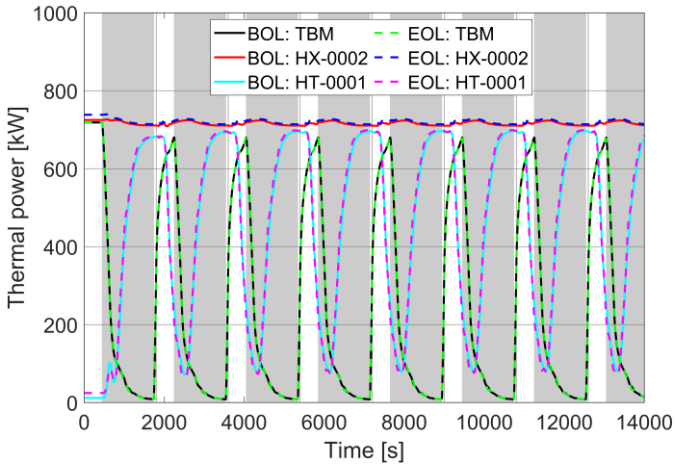

(b)

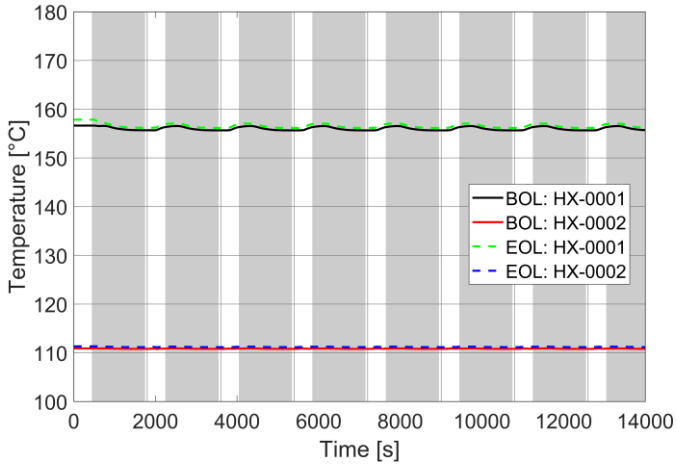

(c)

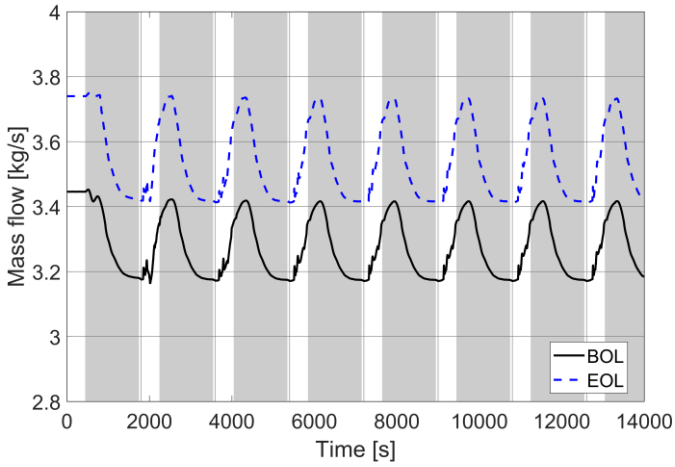

(d)

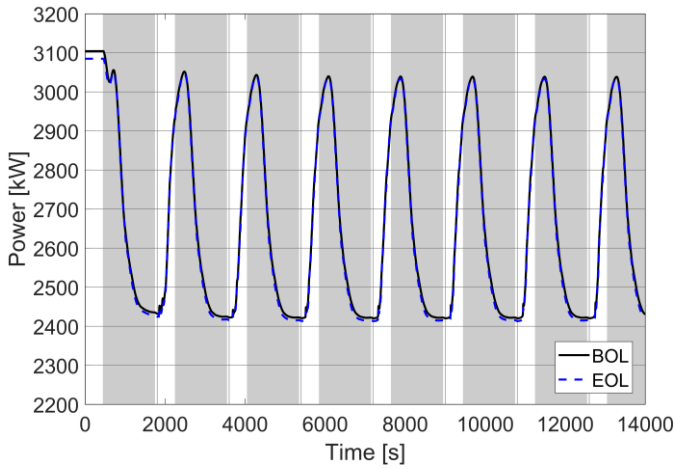

(e)

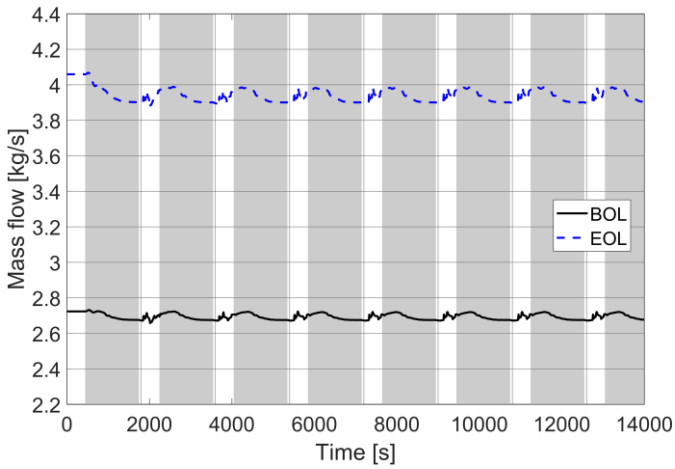

(f)

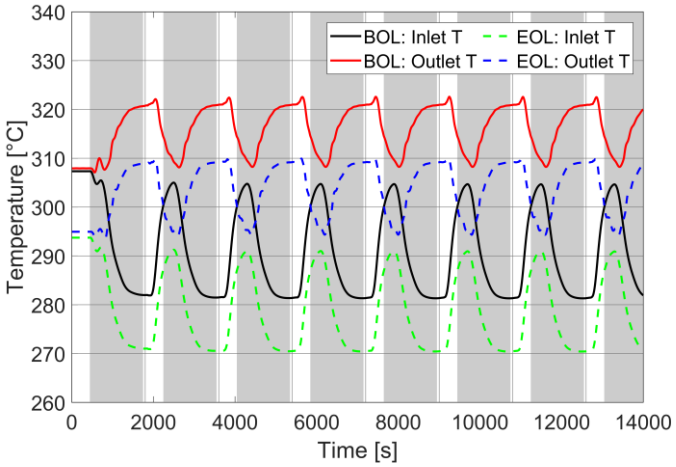

(g)

Figure 6.5 – Normal Operation State, comparison between BOL and EOL conditions: **(a)** WCS temperatures at TBM inlet and outlet; **(b)** WCS primary loop relevant power terms; **(c)** HX-0001 and HX-0002 tube side outlet temperatures; **(d)** HX-0001 shell side mass flow rate; **(e)** HX-0001 power; **(f)** HX-0002 secondary flow rate; **(g)** HT-0001 temperatures.

Figure 6.6a shows the most relevant temperatures of the secondary loop. Thanks to the WCS control systems, the secondary circuit works in a quasi-steady state condition. The reference temperatures are kept almost constant over the whole Normal Operation State. The main difference between BOL and EOL is the HX-0002 shell outlet temperature. Being the power removed from primary side imposed (see paragraph above), this parameter is influenced by the flow rate across the shell heat exchanger. In particular, a lower mass flow rate (BOL) results in a higher outlet temperature (around 128 °C). Downwards the heat exchanger, the hot flow rate is mixed with the cold water, coming from the bypass line, resulting in the reference HX-0003 inlet temperature (105 °C). Under EOL operation, almost the whole flow rate feeds the heat exchanger and the HX-0002 outlet temperature is close to the HX-0003 inlet conditions.

Figure 6.6b reports the CCWS most relevant temperatures. The system operation is quasi-steady state as for the WCS secondary loop. In this case, inlet temperature is fixed as boundary condition. The discrepancy between BOL and EOL observed at the HX-0003 outlet depends on the feeding flow rate (i.e. the heat exchanger performances). At BOL, a lower mass flow (with respect to the rated value) is requested to remove design power. For this, the shell outlet temperature (62.9 °C) exceeds the one required for the CCWS water return (41 °C). However, downwards the HX-0003, hot water is mixed with the cold bypass flow rate obtaining the design return temperature. At EOL, the heat exchanger works at design conditions and also the feeding flow rate and the shell outlet temperature approach the reference values.

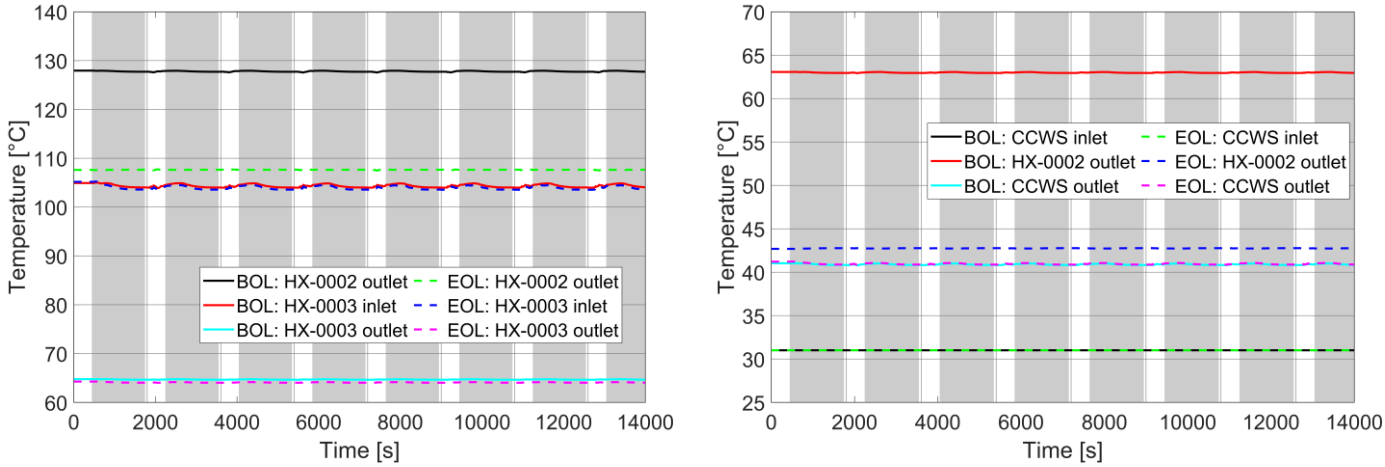

(a) **(b)**

Figure 6.6 – Normal Operation State, comparison between BOL and EOL conditions: **(a)** WCS secondary loop relevant temperatures; **(b)** CCWS relevant temperatures.

Concerning the PbLi loop, Figure 6.7a shows the most relevant temperatures. As expected, no differences are observed between BOL and EOL, since the modelling of the PbLi loop is the same for the two operational states.

TBM inlet conditions match the requirements for the overall Normal Operation State. The mass flow rate is imposed by the time dependent junction to the reference value of 0.65 kg/s. The TBM inlet temperature (295 °C) is ensured by the action of the control system that regulates the power supplied by the heating cables whose storage tank and TBM inlet pipeline are provided. Such power compensates the heat losses.

The temperature at TBM outlet swings in the range of 296 – 322 °C, following the qualitative trend of the power supplied by the TBM to the liquid metal (see Figure 6.7b). Exiting the TBM, the PbLi flows towards the electrical heater, which has the purpose to increase the temperature to the TEU operative value (450 °C). In addition, the HT-0001 absorbs the fluctuations observed at the TBM outlet, providing an almost constant temperature at the TEU inlet. The minimum temperature of the loop is reached downward the Cold Trap. Liquid metal exits the component at 260 °C. The eutectic alloy experiences its minimum temperature (253.2 °C) in the pipeline connecting the cold trap to the storage tank, due to the heat losses through the walls. One of the main requirements for the loop design is to maintain a satisfactory margin from the PbLi melting point (237 °C) in any section of the circuit. The margin calculated by the code was considered acceptable. However, the pipeline can be equipped with heating cables to increase the minimum temperature to the required value.

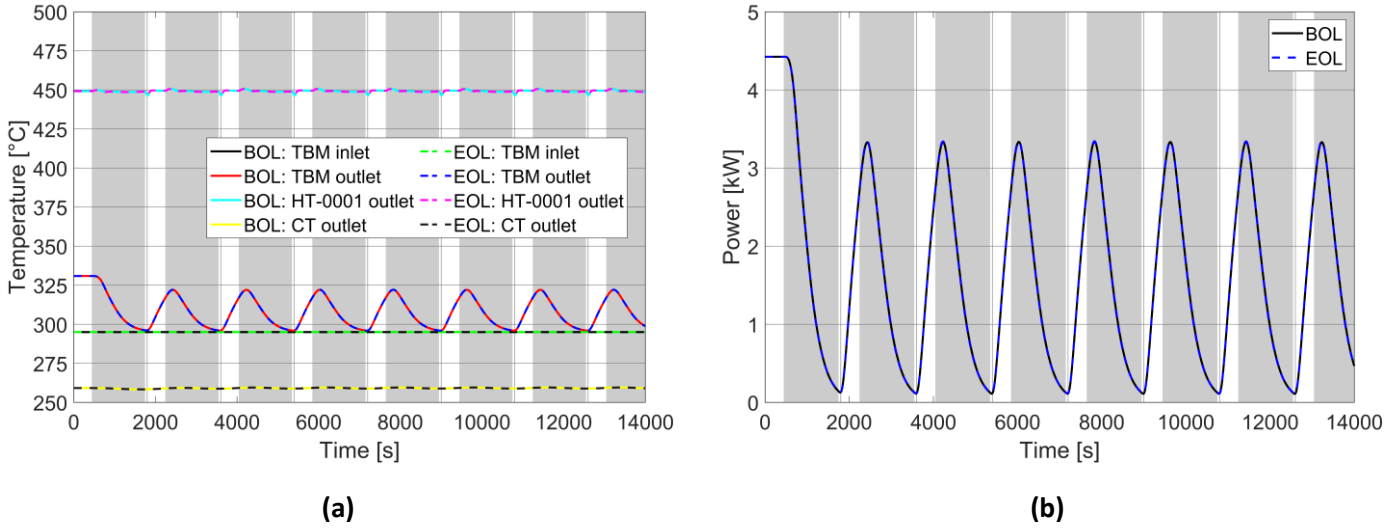

(a) **(b)**

Figure 6.7 – Normal Operation State, comparison between BOL and EOL conditions: **(a)** PbLi loop relevant temperatures; **(b)** Power delivered from TBM to PbLi loop.

Finally, Figure 6.8 and Figure 6.9 provide an insight into the TBM. It is important to remind that a deep analysis of the module behavior during NOS is out of the scope of the research activity presented in this PhD thesis. In addition, the RELAP5 model, given its coarse mesh, is not the best numerical tool to analyze such component. However, results obtained with the system code allow to underline some important features of the TBM performances during this operational transient. The main module characteristic, strongly highlighted by Figure 6.8a and Figure 6.8b, is the low thermal inertia. This is due to the reduced PbLi inventory within the component. The result is temperature trends for the breeder (Figure 6.8b) and the main EUROFER components (Figure 6.8a) that fastly respond to plasma power variations (Figure 6.5b). TBM Cooling/heating transients associated to plasma power ramp-down/ramp-up are quite short. Since dwell time lasts significantly more than the cooling transient, after this initial time window, water, PbLi and EUROFER within the TBM are nearly isothermal, with the first removing the residual decay heat. Instead, the flat-top phase is even shorter than the heating transient, preventing the system from reaching steady-state condition (see also the comment to Figure 6.5b). Thus, the TBM thermal-hydraulic state fully characterized in **§** 6.3 (related to full plasma power) is only an asymptotic scenario never actually reached by the system.

The detail of the PbLi temperatures within the breeding units is provided by Figure 6.9a and Figure 6.9b in two relevant moments also highlighted in Figure 6.8b. At the end of dwell time, PbLi is nearly isothermal within the box (Figure 6.9a), and its temperatures approach the inlet one (295 °C) that is kept constant by the PbLi loop control system (see Figure 6.7a). Instead, at the end of flat-top, the PbLi thermal field tends to the one already shown by Figure 6.4b.

The TBM thermal-hydraulic performances during NOS do not change from BOL to EOL, since, thanks to the control systems associated to WCS and PbLi loop, water coolant and liquid metal are provided at the module inlet with constant thermodynamic conditions and flow rate.

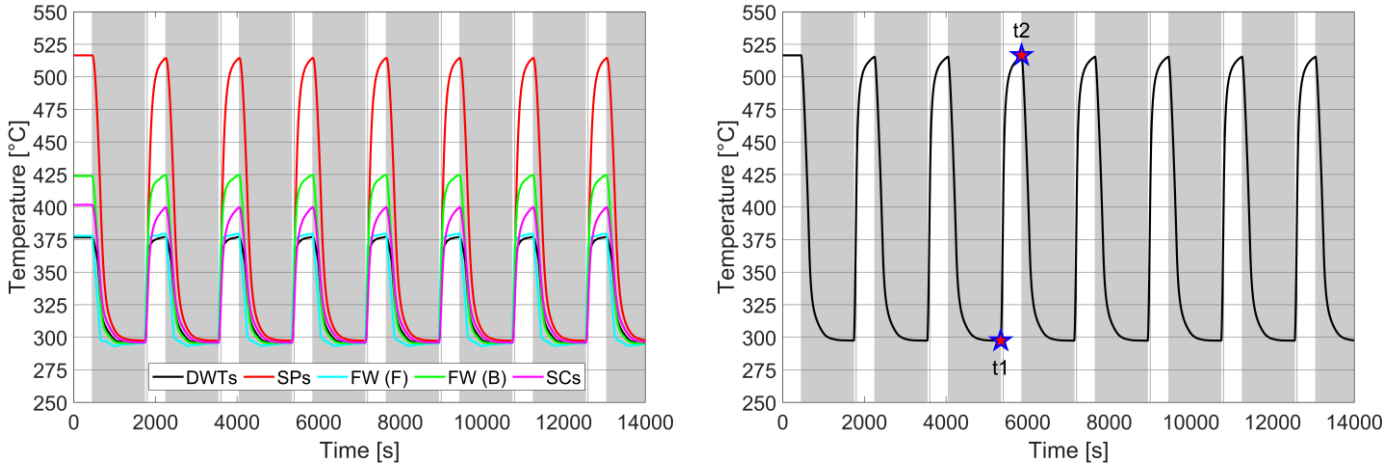

(a) **(b)**

Figure 6.8 – Normal Operation State, insight into TBM box: **(a)** maximum EUROFER temperatures in some relevant TBM components (for the FW both front (F) and back (B) temperatures are provided, see Table 6.4); **(b)** maximum PbLi temperature within breeding units.

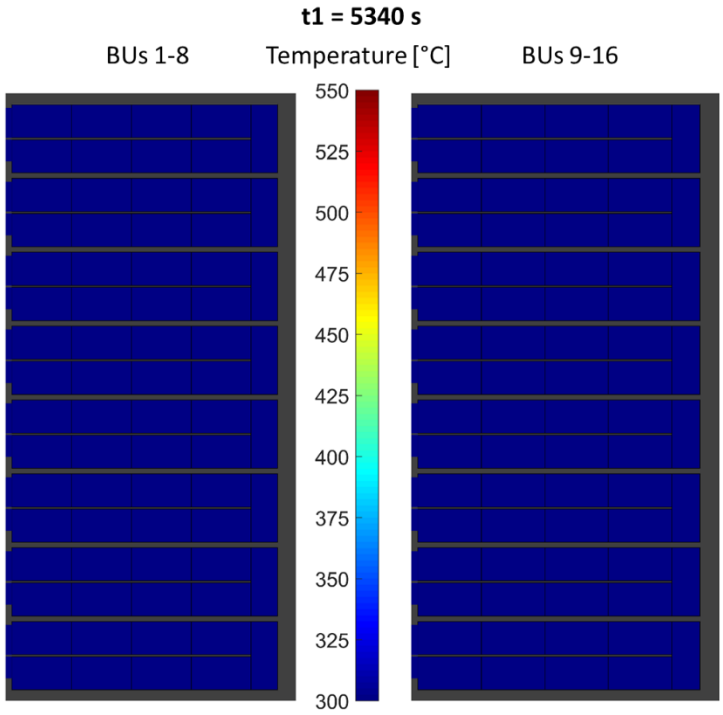

(a)

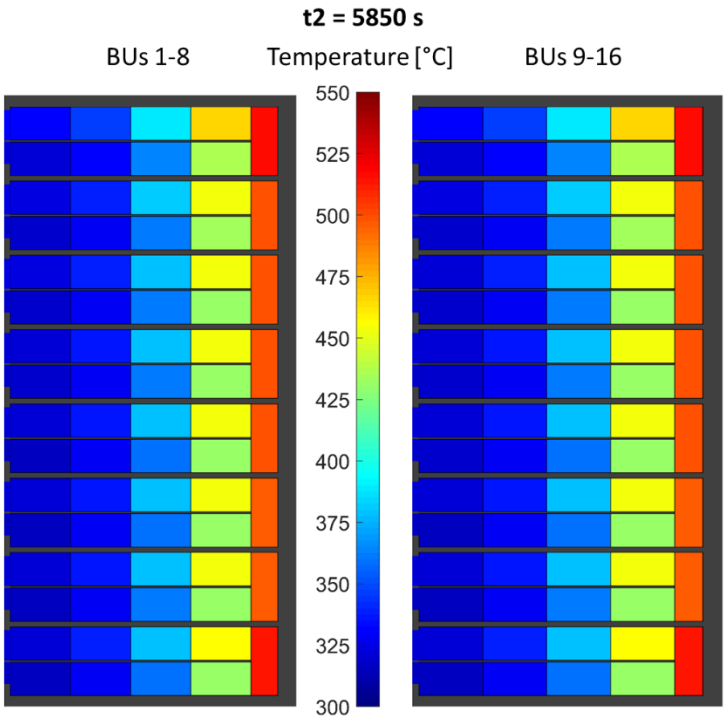

(b)

Figure 6.9 – Normal Operation State, insight into TBM: PbLi temperatures in breeding units at t1=5340 s **(a)** and t2=5850 s **(b)**. The two selected times are also highlighted in Figure 6.8b.

6.5 Selected abnormal conditions

In order to assess and verify the WCS design, two abnormal scenarios were selected and investigated. The aim was to evaluate the system capabilities under degraded conditions and to verify if the standard control strategies without any external action are capable to maintain the TBM cooling function for an entire plasma pulse. This last condition allows to avoid the triggering of the Fast Plasma Shutdown System (FPSS), demonstrating that a minor accident in the WCS does not interfere with the ITER global operation. The transients considered are: **i)** LOFA occurring in WCS secondary loop; **ii)** LOHS, i.e. loss of flow in the CCWS. The worst operative condition is supposed to be the EOL, since plugging and fouling limit the heat exchange. For this reason, NOS at EOL is imposed as an initial condition for both the transient analyses.

6.5.1 LOFA occurring in the WCS secondary loop

The initiating event consists in the blockage of the active secondary pump. The second one, foreseen by design for back-up (see **§** 5.4.2), is conservatively considered unavailable since under maintenance. PIE is assumed to occur at the beginning of the flat-top phase. Since the goal of these simulations is to prove that call the FPSS is unnecessary, the chosen one is the worst possible scenario. Indeed, from the start of transient, plasma is shutdown only at the end of the pulse, i.e. after 450 s. Later, TBM power decreases to the decay heat value. Simulation starts with two complete cycles of NOS pulsed regime, considering EOL operation. In the figures of this section, such time interval is associated to negative abscissa values. In particular, pulse phase is characterized by white background and dwell time by grey background. In the plots, the initiating event is identified with t = 0 s, while the red background stands for the following pulse. The temperature control system operates over the whole simulation. Pressure control system continues to actively work on the primary loop. Instead, in the secondary circuit, the pressurizer sprays are disabled when pump head drops to 80% of the nominal value (time-dependent junction #476 is turned off by means of a control trip). The PbLi loop draining is not assumed; it works over the whole transient. After the plasma shutdown, no further actions are considered, and WCS continues to remove power up to the end of the transient analysis (8000 s).

Figure 6.10a shows the mass flow through the secondary loop. After the pump trip, the system flow quickly decreases to the minimum value (0.2 kg/s at 25 s). Consequently, the HX-0002 power falls from 715 kW to the minimum of 156 kW (black line in Figure 6.10b). The loss of flow at the secondary side of HX-0002 leads to a temperature increase at the correspondent shell outlet (see the black line in Figure 6.10c). At the same time, a temperature decrease is observed at the HX-0003 primary side (tube) outlet, following the mass flow rate reduction (green line in Figure 6.10c). The correspondent control system reacts to the temperature drop by opening valve VC-0009 (#518 in Figure 6.1). The result is the trend reported in Figure 6.10d for the CCWS mass flow feeding the HX-0003 shell. In the first seconds after the initiating event, almost the total CCWS flow bypasses the HX-0003 and the power removed quickly decreases to 27 kW (red line in Figure 6.10b). The power unbalance in the secondary loop increases the density difference between cold and hot leg, promoting the natural circulation. The secondary flow rises over the whole pulse, reaching a maximum of 0.34 kg/s around 130 s after the plasma termination (see Figure 6.10a). At this time, saturated conditions occur within the HX-0002 shell side. The boiling rate leads to a fast increase of the system pressure, that reaches the PORV opening setpoint at 570 s (Figure 6.10e). From this moment up to 965 s, repeated PORV openings manage the overpressure transient in the secondary loop and contribute to the heat removal from the primary system. At 960 s, steam arrives to the inlet of HX-0003 tube bundle (see red line in Figure 6.10c) and condensation takes

place. Due to the high HTC associated to this heat transfer mode, the exchanged power in HX-0003 increases, matching the one of HX-0002 and returning the secondary loop to a power equilibrium condition (Figure 6.10b). In addition, steam condensation reduces the system pressure, which drops below 2 MPa (Figure 6.10e). Later, the loop power balance ensures quasi-steady state conditions. The power exchanged in HX-0002 and HX-0003 stabilizes to 265 kW. Such value coincides with the power supplied in the primary loop by HT-0001 to provide water to TBM with the required inlet conditions (see Figure 6.11a). Natural circulation completely establishes ensuring a secondary flow around 0.1 kg/s (Figure 6.10a). The temperature control system sets the HX-0003 shell flow to nearly 1 kg/s (Figure 6.10d). In the long term, secondary loop pressure shows a slowly increasing rate, stabilizing at 2.01 MPa at the end of the simulation (Figure 6.10e). Within the CCWS, subcooled conditions are kept over the whole transient. The maximum temperature is reached at the HX-0003 outlet (red line in Figure 6.10f). Then, hot water is mixed with cold water coming from the bypass line, and the requirement on the maximum CCWS return temperature is always verified (see green line in Figure 6.10f).

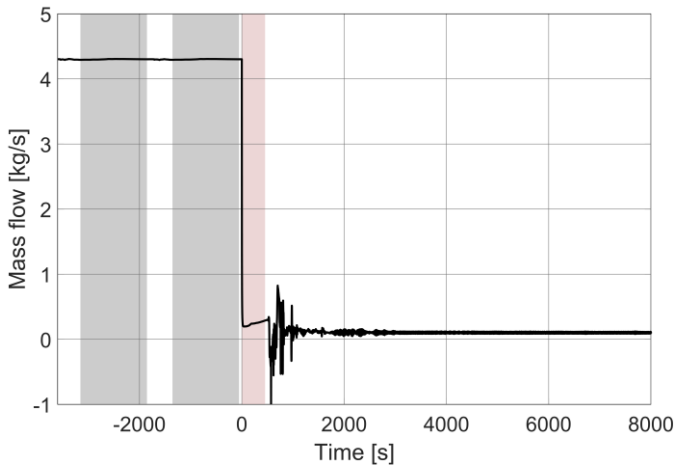

(a)

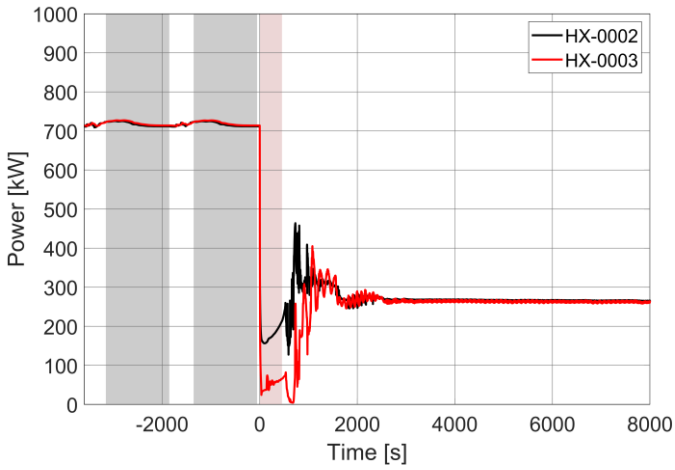

(b)

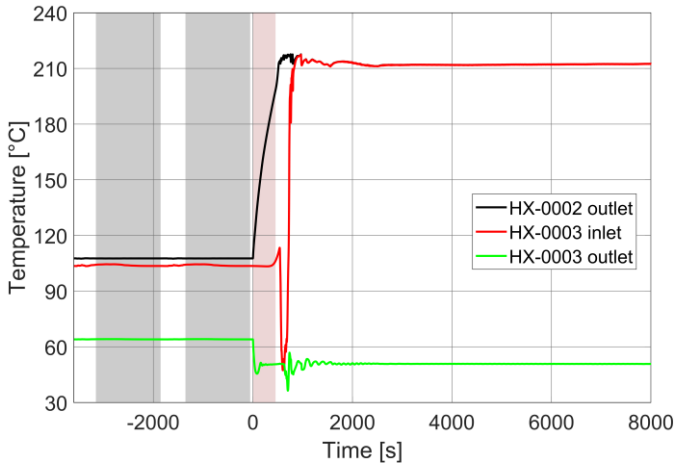

(c)

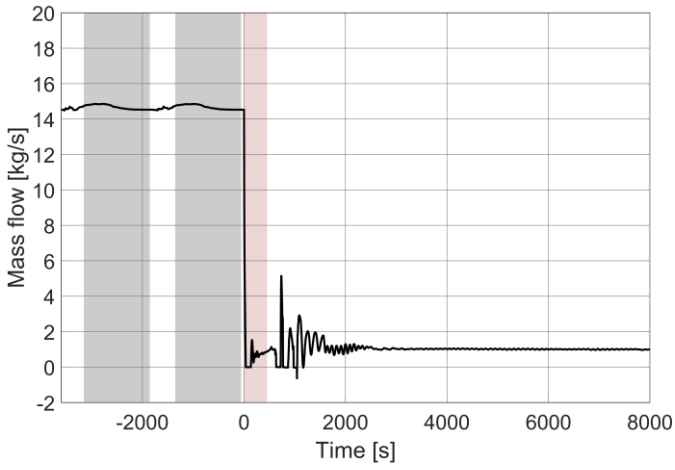

(d)

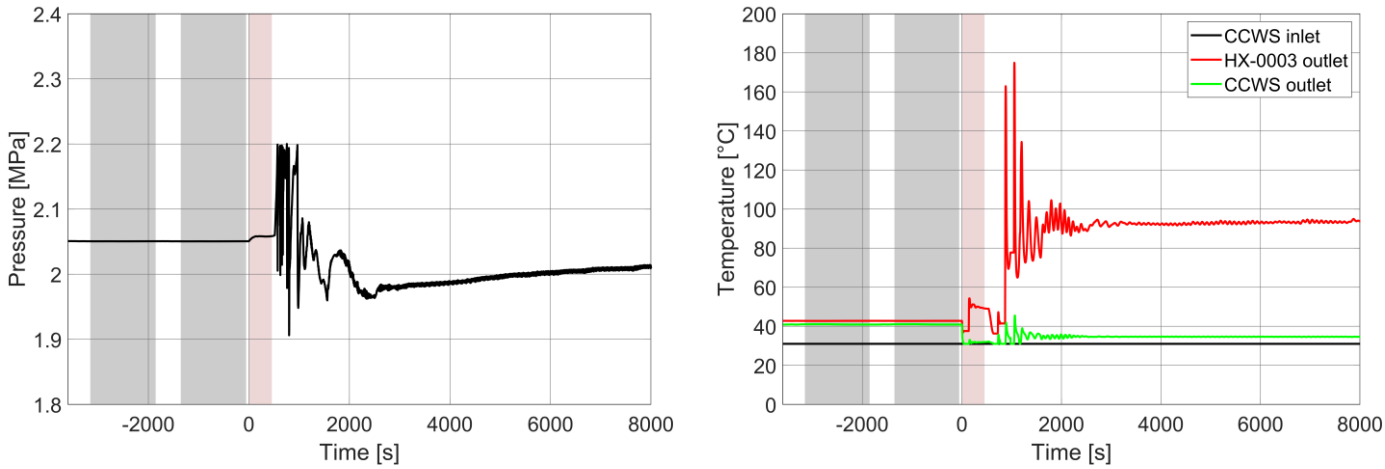

(e) **(f)**

Figure 6.10 – LOFA occurring in the WCS secondary loop: **(a)** WCS secondary loop mass flow; **(b)** WCS secondary loop power balance; **(c)** WCS secondary loop relevant temperatures; **(d)** CCWS mass flow through HX-0003 shell; **(e)** WCS secondary loop pressurizer pressure; **(f)** CCWS relevant temperatures.

The following plots present the figures of merit selected to assess the behavior of the primary loop. The pulse following the initiating event (red background) is characterized by a relevant power unbalance, detectable in the difference between the power supplied to the primary loop (TBM and HT-0001, black and green lines in Figure 6.11a) and the power removed from it (HX-0002, red line in Figure 6.11a). Following the decrease of HX-0002 power, due to the drop of secondary side flow rate, the temperature at tube (primary side) outlet increases, reaching the maximum of 220 °C after the plasma shutdown (see red line in Figure 6.11b). Before the accident occurrence, primary loop water exits HX-0002 at 111 °C and the control system regulate the HX-0001 shell flow to absorb temperature oscillations observed at the TMB outlet. After the secondary pump trip, hotter water feeds the HX-0001 shell, causing a temperature increase also at the tube (primary side) outlet (see the black line in Figure 6.11b). The control system reacts sending the whole system flow to the HX-0001 shell (i.e. closing VC-0010, #485 in Figure 6.1). This is witnessed by red line in Figure 6.11c. Anyway, the heat exchange within the component is degraded due to the low logarithmic mean temperature difference between primary and secondary sides (see Figure 6.11d). After the establishment of quasi-steady state conditions in the secondary loop, also the primary system stabilizes. The water exits the HX-0001 shell at 232 °C and a constant power of 265 kW is supplied by the HT-0001 to ensure 295 °C at the TBM inlet. Figure 6.11a shows that, in quasi-steady state conditions, the power supplied by the TBM is near to zero (residual decay heat is of the same order of magnitude of the total heat losses) and the HT-0001 compensate the power removed by the HX-0002. In the long term, the power exchanged in the HX-0001 is nearly 1140 kW (see Figure 6.11d). Figure 6.11e shows the water temperatures at TBM inlet and outlet. Around 100 s after the initiating event, two temperature peaks are observed in both the inlet and outlet sections. The peaks are due to a temporary reduction of the system flow (see black line in Figure 6.11c). The power unbalance at the transient beginning (Figure 6.11a) leads to the rise of primary loop average temperature. This causes the decrease of water density in the primary pump and also an increase of the circuit pressure drops. These two combined effects produce the reduction of the mass flow elaborated by pump. The PI controller acting on the circulator does not allow an instant regulation of the pump speed, leading to a temporary lower peak of the mass flow (3.55 kg/s). After that, nominal flow condition is re-

established nearly at 1400 s (Figure 6.11c). The primary flow decreasing trend explains the temperature peaks at TBM inlet. They propagate also to the module outlet section since plasma power remains in operation up to 450 s. In this initial time window, the increase of water temperature at TBM inlet produces the HT-0001 shut-off (Figure 6.11a). The WCS water temperature transient is managed by the TBM thermal inertia, i.e. absorbed by the breeder and EUROFER structures within the module. This is clear comparing the magnitude of water inlet (+ 10 °C) and water outlet (+ 2 °C) temperature spikes. Nevertheless, the temperature excursion experienced by PbLi and EUROFER components is negligible, as witnessed by trends reported in Figure 6.11f. As discussed in **§** 6.3, liquid breeder curve is valid also for the stiffening plates (vertical, horizontal and baffle). Such components, being completely immersed in the eutectic alloy, are nearly isothermal with it.

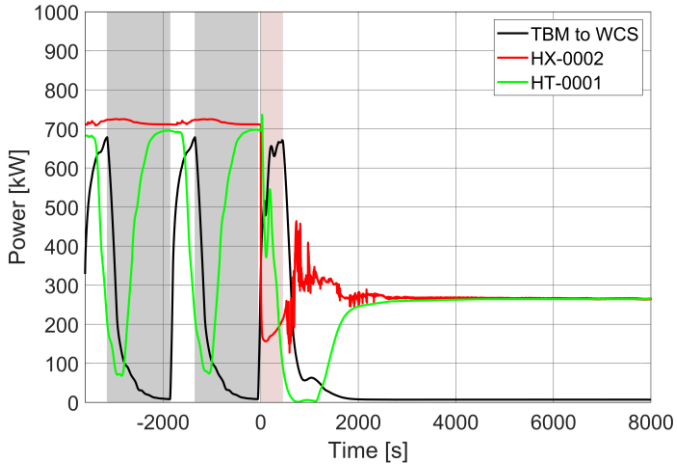

(a)

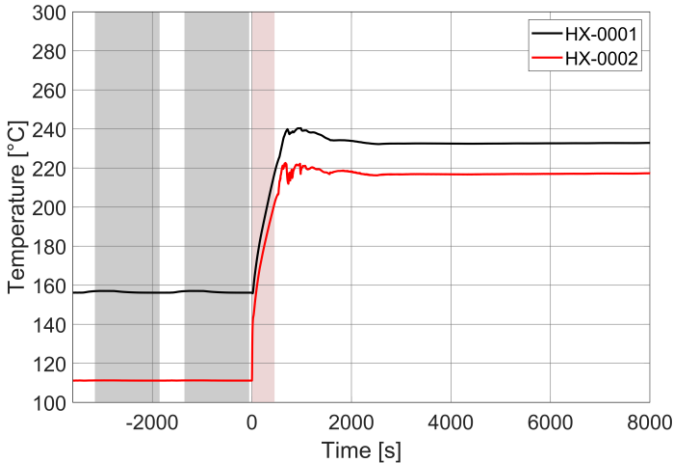

(b)

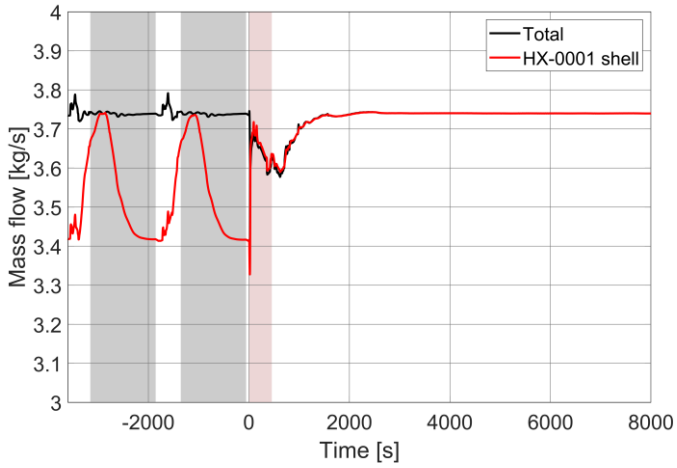

(c)

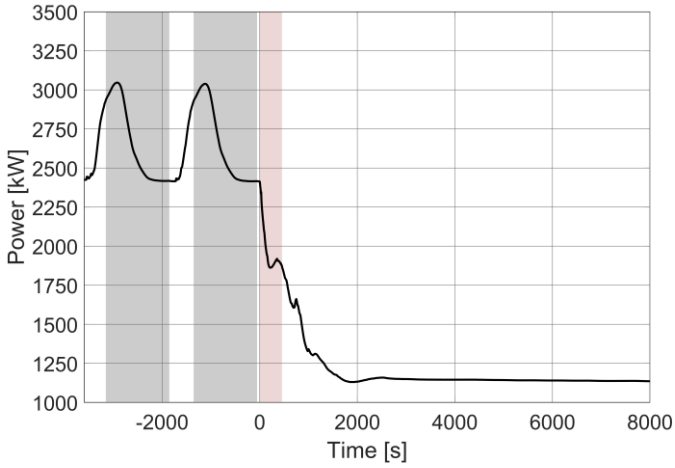

(d)

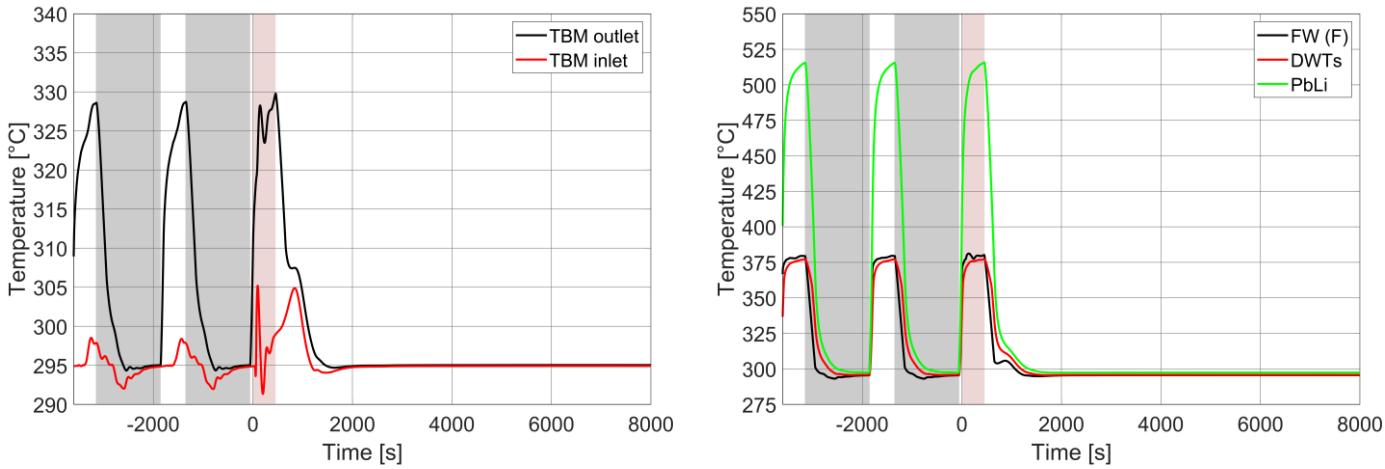

(e) **(f)**

Figure 6.11 – LOFA occurring in the WCS secondary loop: **(a)** WCS primary loop power balance; **(b)** WCS HX-0001 and HX-0002 tube side outlet temperatures; **(c)** WCS primary loop mass flows; **(d)** HX-0001 exchanged power; **(e)** WCS primary loop temperatures at TBM inlet/outlet; **(f)** Maximum temperature related to PbLi within breeding units, FW front (F) layer (see Table 6.4) and DWTs.

Conclusions

At the transient beginning, due to the loss of WCS secondary flow, the heat exchange capabilities of HX-0002 and HX-0003 are compromised. The power surplus coming from the primary loop (plasma is operated for an entire pulse) is managed by the secondary system pressure control function, in particular the pressurizer PORV. In the long term, natural circulation establishes in the secondary loop, the system temperature field significantly changes with respect to nominal conditions but the power equilibrium is restored in the circuit. At this time, the overall WCS operation results quasi-steady state, with the HT-0001 ensuring the required TBM inlet conditions and the HX-0002 and HX-0003 removing the power supplied. In conclusion, the WCS primary loop is kept in safety conditions over the whole accidental scenario. In addition, the safety margin from the PbLi freezing is ensured by keeping the reference water temperature at the TBM inlet. It guarantees to operate the PbLi loop at nearly nominal conditions for the overall transient.

6.5.2 LOHS, i.e. loss of flow in the CCWS

The initiating event consists in the blockage of the CCWS circulator (i.e. the time-dependent junction #502 is turned off). The current RELAP5 model does not include the overall CCWS system, but only its section located in TCWS Vault. Time dependent volumes and junctions are used to simulate the CCWS inlet/outlet. This modelling approach does not allow to model the natural circulation flow establishing in CCWS after the pump stop. For this, conservatively, the mass flow through the time-dependent junction #502 is linearly decreased from nominal value to zero in one second.

Also, the pressure at CCWS outlet is set as boundary condition. This is acceptable for simulations involving operational states, when the system reference pressure is imposed at the outlet and no

pressure transients are expected. Instead, for this scenario, such hypothesis could affect the computed results. In fact, the outlet pressure is kept constant for all the calculation and the pressure transient in the CCWS section considered is not simulated. Consequently, the HX-0003 heat exchange performances during the accidental evolution could be altered. For this, in the sequence simulated, after the occurrence of the initiating event, the isolation valve located at the outlet of HX-0003 CCWS side (VG-0018 in Figure 5.10) is conservatively closed. Actually, this action is not foreseen in the management of such scenario. Although, in this way, even if the transient simulated is more conservative, the simulation outcomes are more reliable. The valve closure occurs 5 s after the PIE.

WCS primary loop is kept in normal operation over the whole transient. The control system ensures the temperature and pressure regulation and the primary pump continues to operate. On the secondary loop, in order to avoid cavitation in the component, pump is disabled when the inlet water temperature rises above 10 degrees below the saturation temperature at the operative pressure. A control variable regulates the operation of the pump component #452. Consequently, pressurizer sprays are disabled when the pump head decreases to 80% of the nominal value. The PbLi is kept in operation over the whole transient. No further actions are foreseen up to the end of the simulation (8000 s).

Initiating event is assumed to occur at the beginning of the flat-top phase (worst possible scenario, see **§** 6.5.1). Plasma is shutdown only at the end of the pulse, i.e. after 450 s. Later, TBM power decreases to the decay heat value. Simulation starts with two complete cycles of NOS pulsed regime, considering EOL operation. In the following figures, this time window is associated to negative abscissa values. Pulse phase and dwell time are characterized by white/grey background, respectively. The initiating event is identified with t = 0 s, while the red background stands for the following pulse.

Figure 6.12a presents the mass flow feeding the HX-0003 shell. Initiating event occurs at 0 s, and the flow rate decreases to zero in 1 s. Water temperature at heat exchanger outlet starts to increase (see red line in Figure 6.12b). Following the closure of the outlet isolation valve, pressure within the isolated section of the CCWS rises. The first opening of the safety valve (#539 in Figure 6.1) occurs after 12 s from the start of transient, and it is followed by repeated opening and closing cycles (Figure 6.12c). Figure 6.12d shows the power exchanged in HX-0002 and HX-0003. HX-0003 power drops to 93 kW in 2 s. Then, the reduction rate decreases, due to the safety valve openings. The minimum value of the HX-0003 power in the first phase of the transient is reached at 720 s (around 50 kW). At this time, water within the HX-0003 secondary side reaches saturated conditions and starts to boil (Figure 6.12b), increasing HX-0003 power (see the first fluctuations of the red line in Figure 6.12d). Steam production leads to a further increase in the frequency of the safety valve opening/closing cycle (Figure 6.12c).

Figure 6.12e shows three relevant temperatures within the WCS secondary loop. The green line represents water temperature at the HX-0003 primary side (tube) outlet. The HX-0003 power decrease leads to an increase of the water temperature. At this time, secondary pump is still in operation. Immediately after the start of transient, a small step down can be observed in the secondary flow (see Figure 6.12f). It is due to the water density change. The secondary flow is kept at around 4.15 kg/s over the whole flat-top condition and the temperature rise is also detected within the HX-0002 (see black line in Figure 6.12e). At 1200 s, HX-0003 outlet temperature reaches the maximum temperature of 202 °C, which corresponds to secondary pump cut off setpoint. Thus, the component is stopped and the mass flow rate decreases to zero in 15 s (Figure 6.12f). A quick temperature decrease is observed in both the sides of HX-0003. As a consequence of the secondary pump trip, the power removed by the HX-0003 decreases, leading

to the reduction of the boiling rate within the isolated section of the CCWS. The correspondent system pressure decreases to the minimum value of 0.63 MPa (1282 s, Figure 6.12c) and remains below the safety valve opening setpoint up to 3200 s. The negative gradient of the pressure is due to the heat losses, which exceeds the HX-0003 power.

On the WCS secondary loop, as the pump is cut-off, pressure rises reaching the PORV opening set point at 1220 s (Figure 6.12g). It is followed by repeated opening and closing cycles up to 1774 S. After that, power removed from the system (HX-0003 power and heat losses) exceeds the supplied power (HX-0002 power and pressurizer heaters), explaining the negative gradient of the system pressure (up to 3120 s). HX-0002 continues to exchange power, increasing steam fraction within the shell side. The collapsed level referred to the component is reported in Figure 6.12h. At 2950 s almost the total amount of water within the HX-0002 shell reaches the vapor phase, causing a quick increase of the secondary pressure. The system PORV restarts to open (from 3175 s to 5125 s), causing the HX-0002 power and mass flow peaks observed in Figure 6.12d (black line) and Figure 6.12f. Also the HX-0003 power rises (red line in Figure 6.12d), leading to repeated opening and closing cycles of the CCWS safety valve (see pressure fluctuations between 3210 and 4920 s, Figure 6.12c). After that, HX-0003 power remains below the CCWS heat losses up to the end of the simulation. Consequently, the pressure in the CCWS isolated section returns to drop (final part of the trend in Figure 6.12c). In the WCS secondary loop, the vapor discharging operated by the PORV produces a decrease of the overall system quality, above all in the HX-0002. The same dynamic that leads to the PORV opening at 3175 s is repeated in the time interval between 5125 s and 6865 s. The power balance for the secondary circuit is negative (pressure drops in Figure 6.12g) but the heat exchange within HX-0002 increments the vapor fraction in the shell side (Figure 6.12h). A limited heat exchange in HX-0002 is always present due to the temperature difference between WCS primary and secondary circuits. Once the component is full of vapor, the secondary pressure experiences a new spike, producing the PORV intervention (Figure 6.12g) and the HX-0002 power and system flow peaks (Figure 6.12d and Figure 6.12f). Such long-term cycle of system operation does not end at 8000 s (final simulation time). This is well evidenced by Figure 6.12g and Figure 6.12h, where the final parts of the curves tend to repeat the same trend described for the previous time windows. Such behavior continues until the secondary loop water inventory is almost completely evacuated through the PORV. If simulation time were extended, this phenomenon would be observed.

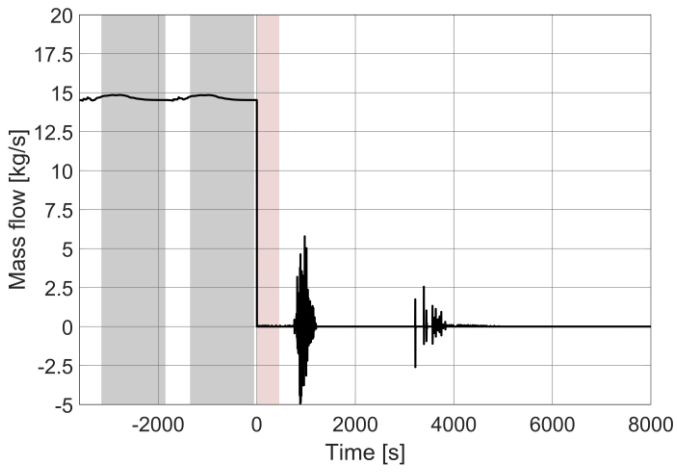

(a)

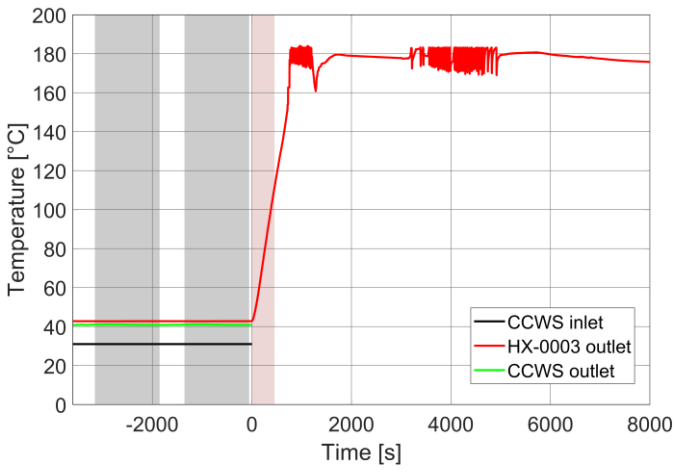

(b)

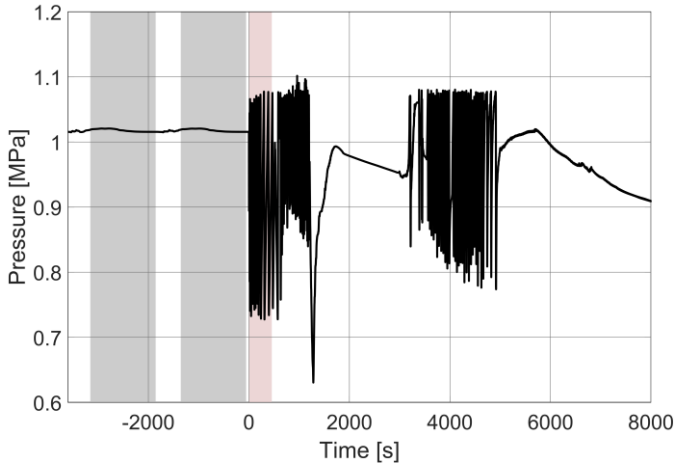
Pressure [MPa]
Time [s]

(c)

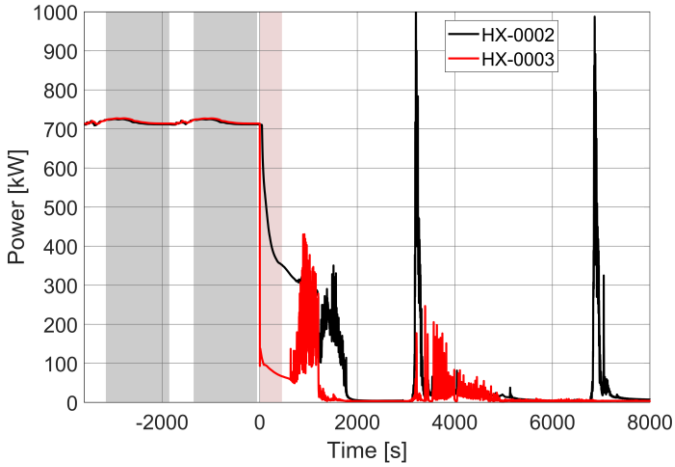
HX-0002
HX-0003
Power [kW]
Time [s]

(d)

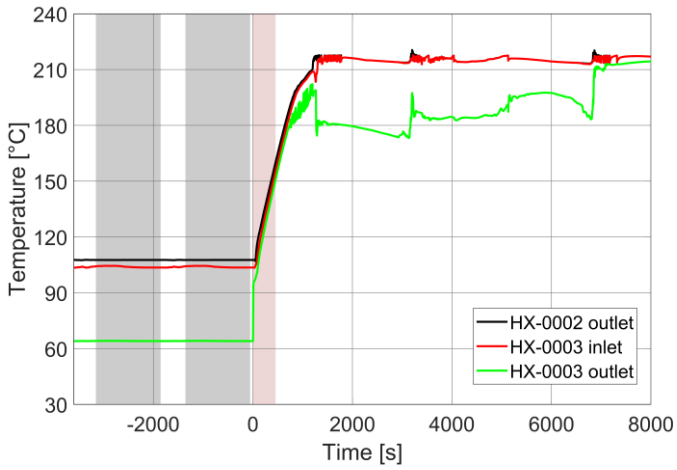
HX-0002 outlet
HX-0003 inlet
HX-0003 outlet
Temperature [°C]
Time [s]

(e)

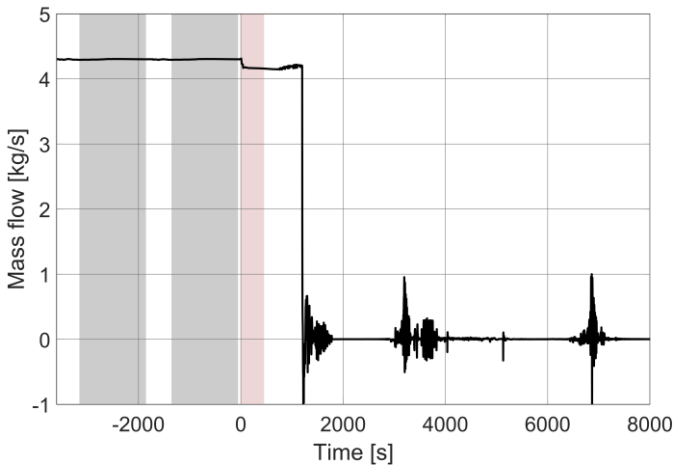
Mass flow [kg/s]
Time [s]

(f)

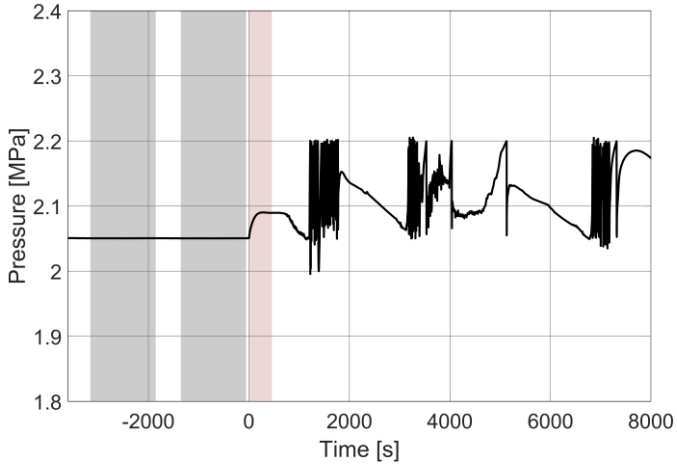
Pressure [MPa]
Time [s]

(g)

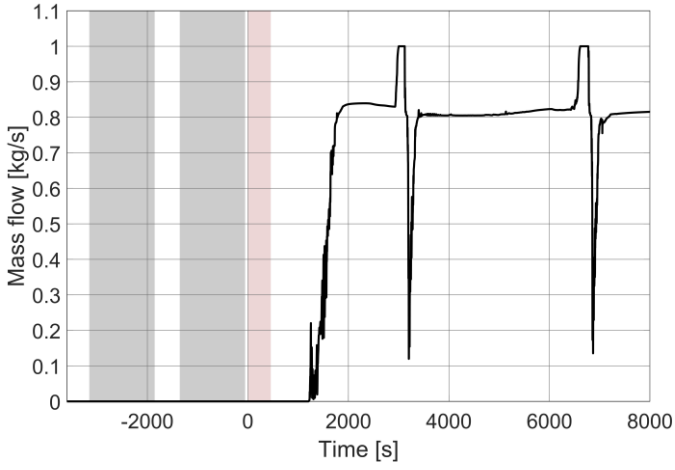
Mass flow [kg/s]
Time [s]

(h)

Figure 6.12 – Loss of flow in the CCWS: **(a)** CCWS mass flow through HX-0003 shell; **(b)** CCWS relevant temperatures; **(c)** CCWS pressure (in the section between isolation valves); **(d)** WCS secondary loop power balance; **(e)** WCS secondary loop relevant temperatures; **(f)** WCS secondary loop mass flow; **(g)** WCS secondary loop pressurizer pressure; (h) collapsed level in HX-0002 shell side.

Regarding the WCS primary loop, the main figures of merit are the HX-0001 and HX-0002 temperatures at tube side outlet (Figure 6.13a). These parameters are the most influenced by the behavior of the systems located downwards in the heat removal chain (i.e. WCS secondary loop and CCWS). Their trends reflect all the main events described above and shown by Figure 6.12. After the initiating event, the HX-0002 power strongly decreases (Figure 6.13b), leading to a significant temperature increase at the HX-0002 primary side (tube) outlet (red line in Figure 6.13a). The effect of such increasing on the HX-0001 tube side outlet temperature (black line in Figure 6.13a) and exchanged power (Figure 6.13c) is already discussed in **§** 6.5.1. When, at 1200 s, the secondary pump trip occurs, the HX-0002 exchange capability becomes negligible and the WCS cold branch becomes nearly isothermal (black and red lines in Figure 6.13a are overlapped). Gradually, the WCS cold branch temperature approaches the TBM inlet temperature (Figure 6.13d) and the power exchanged in the HX-0001 becomes null (Figure 6.13c). In the long-term, two cooling spikes are detectable in Figure 6.13a, due to the secondary PORV openings. The temperature control system regulates the power supplied by the HT-0001 (green line in Figure 6.13b), ensuring the almost constant temperature of 295 °C at the TBM inlet (Figure 6.13d). Three main interventions of the control system are detectable in Figure 6.13b. The first, before 2000 s, is related to the water boiling in the HX-0003 shell (propagated to HX-0002 since the secondary flow is still active). The following two are referred to the cooling transients provided by the PORV openings. In comparison with the previous scenario, temperature peaks at the TBM inlet and outlet sections are significantly lower (compare Figure 6.13d and Figure 6.12f). Such temperature transient is easily managed by the TBM thermal inertia. The effect on the PbLi and EUROFER structures is negligible. The maximum water temperature reached in WCS circuit after the PIE does not exceed the one characterizing the Normal Operation State (Figure 6.13d). In addition, the provision of water to TBM with the required inlet conditions also ensures the respect of a satisfactory margin from the PbLi freezing point.

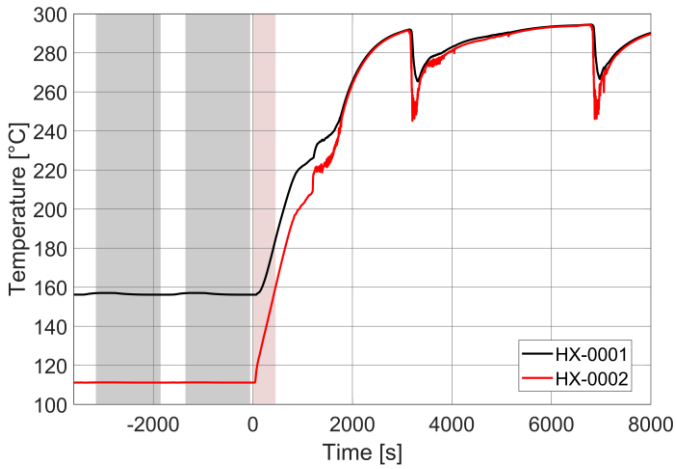

(a)

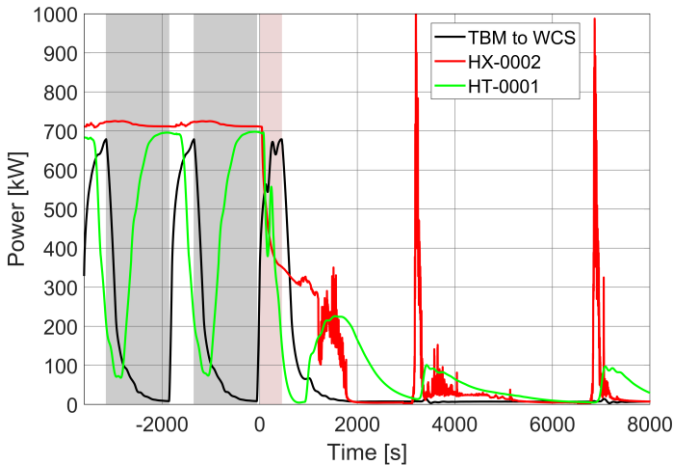

(b)

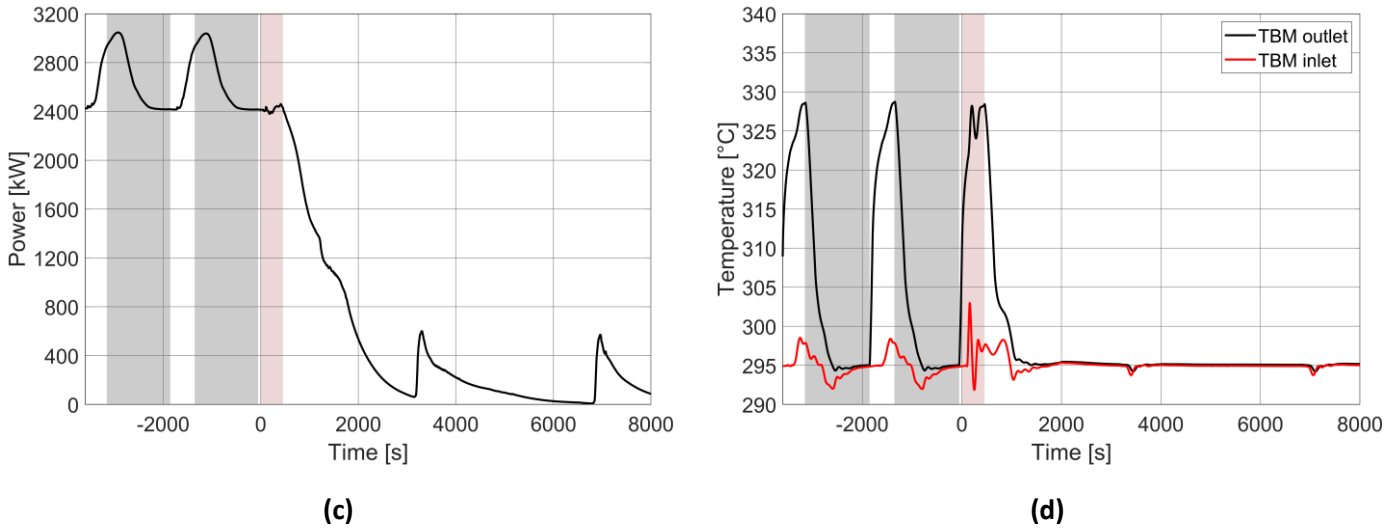

(c) **(d)**

Figure 6.13 – Loss of flow in the CCWS: **(a)** WCS HX-0001 and HX-0002 tube side outlet temperatures; **(b)** WCS primary loop power balance; **(c)** HX-0001 exchanged power; **(d)** WCS primary loop temperatures at TBM inlet/outlet.

Conclusions

The transient scenario simulated consists in the loss of heat sink for the WCS system. Due to the limits of the RELAP5 model prepared, after the initiating event, the CCWS section within the TCWS Vault is conservatively isolated. At the transient beginning, the power surplus coming from the primary loop (plasma is operated for an entire pulse) is evacuated by means of multiple openings of the safety valve whose this CCWS section is provided. Part of the energy is also used for the phase transition of the water present in the HX-0003 shell and upwards/downwards pipelines (circuit section between the isolation valves). The loss of the heat sink (HX-0003 heat exchange capability is immediately compromised after the start of transient) leads the WCS secondary loop to be gradually heated. Once reached the maximum allowable temperature at the pump inlet, the component is cut-off to avoid cavitation. Later, also the secondary system starts to evacuate energy in the form of vapor flow through the pressurizer PORV. The loss of the secondary flow disables the HX-0002, thermally isolating the primary loop. From this moment onwards, the primary loop is a nearly isothermal circuit. Indeed, neither power input (plasma is shut down and decay heat is of the same order of magnitude of the heat losses) nor power output (HX-0002 does not remove power) are present. In the long term, the system temperature is kept at the value required at TBM inlet by the HT-0001. By the end of simulation time (8000 s), the component must intervene only twice to compensate cooling transients provided by the secondary PORV openings. In fact, the evacuation of WCS secondary loop water inventory proceeds in a step-wise mode and it is not completed before the transient end. Instead, the water inventory in CCWS section is almost completely evacuated in 5000 s. In conclusion, the WCS primary loop is kept in safety conditions over the whole accidental scenario. In addition, the safety margin from the PbLi freezing is ensured by keeping the reference water temperature at the TBM inlet.

7 CONCLUSIONS AND FUTURE PERSPECTIVES

The work discussed in this PhD thesis was conducted between 2018 and 2021 within the framework of EUROfusion Consortium research activity. It profited from a collaboration between DIAEE of Sapienza University of Rome and the Experimental Engineering Division of ENEA at Brasimone. In the past years, R&D efforts focused on the investigation of one principal candidate option for EU-DEMO blanket: the Water-Cooled Lead-Lithium. For this concept, ENEA and its Italian related partners have been the principal investigators.

7.1 DIAEE version of RELAP5/Mod3.3 system code

System thermal-hydraulic codes are the reference numerical tools adopted for the nuclear reactor transient analysis. Most of them, such as RELAP5, were developed and validated to perform best-estimate transient simulations of Light Water Reactors. Once validated against experimental data coming from more than one-hundred facilities, they have been used throughout decades to perform the licensing of LWRs. Simulation results allowed to characterize the reactor transient behavior in the full range of operative and accidental conditions. The same approach to reactor transient analysis was envisaged also for fusion power plants.

Although, existing system codes lack of some specific features required to properly simulate the fusion reactor thermal-hydraulic performances. For this, during the last years, a modified version of the system code RELAP5/Mod3.3 was developed at DIAEE, in collaboration with ENEA, including some new upgrades needed to address the modelling issues arising from the simulation of tokamak fusion reactors. New implementations were presented in **§** 2 of this document and consist in:

- Lead-lithium and HITEC© working fluids, with their thermophysical properties;
- New heat transfer correlations;
- Helicoidally tubes dedicated heat transfer correlations and two-phase flow maps.

The effectiveness of the new features introduced was verified throughout the three years of research activity by performing transient simulations involving tokamak fusion reactors.

Referring to the helicoidally geometry, the new two-phase flow maps were also tested against experimental data coming from OSU-MASLWR facility, [54]. In particular, a power manoeuvring test (named ICSP Test SP3) was selected for benchmarking purposes. The aim of the experiment was to investigate the primary system natural circulation and secondary system superheating for a variety of core power levels and feedwater flow rates. The effects of the code modifications on the simulation outcomes were clearly visible at higher power levels when the heat transfer within the HCSG plays a more important role. Indeed, above a certain power threshold, the default version showed limited capabilities to reproduce the test. On the contrary, the trends related to the modified version fit quite well the experimental data.

The ones reported in this PhD thesis were only the first features implemented in the DIAEE version of RELAP5/Mod3.3 system code. Additional work is currently ongoing in this field, [104]. It is focused on enhancing the code modelling capabilities with respect to magnetohydrodynamic issues. However, this version of the code will be furtherly validated and integrated by exploiting the seven years of activities planned in the just began Horizon Europe research programme (2021-2027). An integrated water test facility is supposed to be built at the ENEA research center of Brasimone, [81]. Among the other expected outcomes, there is the validation of system-level

thermal-hydraulic codes, such as RELAP5/Mod3.3. Experimetal data coming from the facility will be an effective instrument to also evaluate the DIAEE version of the code. The main goal to be reached by the end of the Horizon Europe research programme is to have a full validated system-level thermal-hydraulic code suitable for transient analysis of tokamak fusion reactor, thus provided with all the features needed to simulate its specific thermal-hydraulic phenomena.

7.2 WCLL blanket primary cooling systems transient analysis

During last years, DIAEE played an important role in the conceptualization of the WCLL blanket and its related primary cooling systems. In addition, an extended transient analysis was carried out to assess their thermal-hydraulic performances in both normal operations and accidental conditions. Such work was carried out involving research activities related to both ITER and EU-DEMO tokamak fusion reactors.

7.2.1 DEMO WCLL

Referring to DEMO WCLL, in **§** 3, it was presented the outcome of the pre-conceptual design developed during the just finished Horizon 2020 reasearch programme. The design activity performed at DIAEE which the candidate took part to was mainly related to the BB PHTS layout, [64][65][66]. With the aim of the design improvement, system-level transient analyses were run involving the WCLL blanket component and related PHTS. The DIAEE version of RELAP5/Mod3.3 was used for this purpose. Such activity was related to EUROfusion Consortium Work Packages Breeding Blanket and Balance of Plant.

Firstly, a full DEMO WCLL thermal-hydraulic model was prepared (**§** 4.1), considering the BoP Indirect Coupling Design option. Blanket was simulated using equivalent components characterized by lumped parameters. The BZ and FW PHTS circuits were modelled including all the components within and outside the vacuum vessel. PCS nodalization starts from the main feedwater line and arrives up to the Turbine Stop Valves. Thus, only the BZ OTSGs secondary side was simulated. Regarding the IHTS, the same approach was adopted. Only the cold and hot legs upwards/downwards the FW HEX shell side were added to the input deck. PCS feedwater and IHTS molten salt conditions at the BZ OTSGs and FW HEXs secondary side inlet were provided by means of boundary conditions.

The model developed was tested against the design data by simulating the full plasma power state (**§** 4.3). Beginning of Life conditions were considered. PI controllers were implemented to: **i)** regulate the primary pump rotational velocity and set the required value of the system flow; **ii)** control the PCS feedwater and IHTS molten salt mass flows in order to obtain the required PHTS water temperature at blanket inlet (i.e. OTSG outlet, 295 °C). Simulation results were in good agreement with the nominal values, demonstrating the appropriateness of the nodalization scheme prepared and of the control system implemented. Blanket and PHTS thermal-hydraulic performances in this flat-top power state were fully characterized, including the calculation of the system pressure drops and heat losses.

Then, this steady-state calculation was used as initial condition to perform the DEMO WCLL transient analysis, including some operational and accidental transients. The DEMO reactor normal operations were simulated, including both pulse and dwell phases (§ 4.4.1). Reference plasma ramp-down and ramp-up curves were adopted for simulations purposes. Primary pumps were kept running at nominal velocity for the whole transient, as for DEMO requirement. In

addition, during dwell, PHTS circuits must be operated at the system average temperature (nearly 310 °C). Since no control strategies related to BZ OTSGs and FW HEXs were available, a preliminary management strategy for the PCS feedwater and IHTS molten salt mass flows were proposed and investigated. The BB PHTS parameters calculated by the code were analyzed to assess the circuit performances. The imposed trends proved to be effective in keeping the PHTS average temperature during dwell at the required value. From simulation outcomes arised an important issue to be addressed, consisting in the presence of oscillations in the BZ system. They were detected just after the ramp-up, lasting few hundreds seconds. Preliminary investigations were carried out varying the time step of the calculations but no results were obtained. Several source terms responsible for generating the oscillations were identified. A wider computational activity involving the BZ OTSG operational field was out of the scope of the calculations performed. However, a sensitivity on the BZ OTSG model will be performed in the future to assess if the nature of the oscillations is purely numerical. Furthermore, an extended experimental campaign is planned for the next years to address this aspect, [81]. One of the main goal of the STEAM facility is the design of a scaled OTSG mock-up to test the component performances during operational and accidental sequences. Data produced by the experimental campaign will deserve to validate the DIAEE version of RELAP5/Mod3.3 and improve its modelling capabilities with respect to this peculiar steam generator technology.

After, it was performed a benchmark exercise involving DEMO reactor power fluctuations (§ 4.4.2). System code results were compared with the more detailed ones obtained with ANSYS CFX. The aim was to evaluate the effectiveness of the thermal-hydraulic model developed for the blanket component, prepared using equivalent components characterized by lumped parameters. BZ and FW PHTS water temperatures at blanket outlet were selected as figures of merit. Their trends showed a good agreement between the simulation outcomes obtained with the system code and the FEM model. Results obtained from this benchmark exercise also indicated an effective way to perform simulations involving components, such as the breeding blanket, characterized by complex geometries and heat transfer phenomena. System code and 3D calculations can be externally coupled in an iterative process where CFX provides more accurate parameters to refine the RELAP5 model and the latter is used to update the inlet conditions for finite volume model computation. Such procedure will be furtherly investigated in the future developments of simulation activity related to WPBB and WPBoP.

Finally, the blanket primary cooling system response during accidental conditions was investigated. The selected transients to be studied belong to the category of “Decrease in reactor coolant system flow rate” (§ 4.5). This transient analysis was aimed at understanding the thermal-hydraulic response of the blanket component and related primary circuits. In this way, it was possible to evaluate the appropriateness of their pre-conceptual design and the eventual need of mitigation actions to withstand such accidental scenarios. Different faults that could result in a decrease of the BB PHTS primary flow were postulated and investigated. In particular:

- Partial loss of forced primary coolant flow, **§** 4.5.2, [84];
- Complete loss of forced primary coolant flow, **§** 4.5.2, [84];
- Primary pump shaft seizure (or locked rotor), **§** 4.5.3, [85];
- Inadvertent operation of a loop isolation valve, **§** 4.5.4.

Firstly, the most limiting of the above primary flow decrease event was chosen. It consisted in the complete loss of forced circulation in both FW and BZ PHTS. In this ‘worst case’ scenario, **§** 4.5.1, even if very unlikely, a sensitivity was performed on the flywheel to be added to the PHTS main coolant pumps in order to keep the system temperatures within acceptable ranges, [83]. The

proper moment of inertia values to be applied to BZ and FW primary pumps were selected according to the simulation outcomes. Later, they were also used in all the following transient calculations.

The initiating events mentioned above were all simulated when interesting either BZ or FW system components (i.e. pumps and loop isolation valves). Calculations were replicated also considering the influence of loss of off-site power, assumed to occur in combination with the PIE. An actuation logic, involving some components of the DEMO reactor, was proposed and preliminary investigated. It was inspired by the one used for Generation III + nuclear power plants.

In the short term after the start of transient, the inadvertent operation of a loop isolation valve is the initiating event leading to the worst possible accidental evolutions. When loss of off-site power is postulated, the system flow available to cope with the plasma power is the minimum among all the transients analyzed in **§** 4.5. Indeed, a loop is interrupted (the associated flow is zero) and the pump/pumps belonging to the other are cut-off at the transient beginning (due to the unavailability of off-site power). The correspondent blanket outlet temperatures are the maximum experienced by BZ and FW systems among all the cases considered. Void fraction spikes are detected at the outlet section of the FW channels belonging to the most stressed blanket sectors (the nearest to the failed loop). However, the associated Departure from Nucleate Boiling Ratio calculated by the code is >> 1. No thermal crisis is thus expected in the cooling channels. Nevertheless, it must be noted that the blanket model prepared for the current simulation activity is not able to investigate the local behavior of FW component since no poloidal differentiation is performed. In addition, the heat flux used as boundary condition is the average one related to the overall reactor. Although, this parameter varies significantly along the tokamak poloidal dimension, arriving at values far higher than the mean. In conclusion, the DNBR computed by the code is only an average parameter evaluated for the overall FW component. For this reason, more detailed analyses are planned for the future to evaluate the DNBR at different poloidal locations inside the blanket.

Results presented in **§** 4.5 highlighted how the type of circulation (natural or forced) characterizing each cooling system is the main element influencing the correspondent thermal-hydraulic performances. According to the considered case, BZ and FW systems can have the same kind of circulation or not. However, as a general rule, for the suitability of the forced circulation in a primary cooling circuit is mandatory the presence of the off-site power. If its loss is assumed in combination with the initiating event, at the occurrence of turbine trip forced circulation is lost in both systems, if not already missing in one of them according to the specific PIE considered. In fact, the turbine generator set is the only element ensuring the AC power needed for the pump operation and it is disconnected after the turbine trip. If forced circulation is available, the following thermal-hydraulic behavior can be observed in BZ and FW systems.

- Few seconds after the start of transient, the temperature spikes at blanket outlet characterizing the trend of both BZ and FW PHTS water are significantly smoothed.
- In FW system, the availability of forced circulation in both primary and secondary (only for the first 10 s) circuits limits the pressure increase and avoids the intervention of the pressurizer PORV in the short term.
- The OTSGs cooling capability lasts less. The presence of forced circulation in the primary cooling system enhances the steam generator heat transfer coefficient, increasing the thermal power transferred to the PCS. This reduces the time between two subsequent steam line SRVs openings and speeds up the evacuation of the water mass present in the

OTSGs secondary side. Once terminated, the steam generators are no more able to provide any cooling function to the BZ PHTS.

- For more or less two hours from PIE occurrence, the system pressure is controlled by the pressurizer sprays. The first PORV intervention in the long term is significantly delayed.
- The temperature slope characterizing both BZ and FW systems (thermally coupled) is higher since pumping power is added to the power balance. This is valid until the pump trip is triggered in each system.

Summarizing, forced circulation improves the BZ and FW TH performances in the short term, smoothing the temperature spikes, but reduces the ones in the mid-long term. In fact, it shortens the cooling interval provided to the BZ PHTS by the steam generators and increases the temperature slope experienced by BZ and FW systems, reducing the reactor grace time. The best management strategy for PHTS pumps is to use, at the SOT, the forced circulation they provide, in order to avoid excessive temperatures in the blanket, and then stop them, to increase the reactor grace time. The effectiveness of this control logic was proved by testing it against the case of partial LOFA in BZ PHTS without loss of off-site power. The obtained results showed how this new pump management strategy combines the benefits of forced circulation in the short term and of natural circulation in the long term.

In all the transient simulations, BZ and FW systems experienced a positive temperature drift in the mid-long term. It is due to the unbalance between decay heat produced in the blanket and system heat losses, with the former overwhelming the latter. The temperature slope is higher if the forced circulation is still active. In these cases, it must be added another source term to the power balance, represented by the pumping power. In the calculations performed, no Decay Heat Removal system was implemented in the input deck and the power surplus is managed by the pressurizer PORV. Power in excess produces a pressure increase and when this parameter reaches the PORV opening setpoint, PHTS water mass is discharged with its associated enthalpy content. This is the way adopted by BZ and FW system to dissipate the power surplus. In the future developments of this research activity, the impact of the DHR system will be also evaluated.

In conclusion, simulation outcomes highlighted the appropriateness of the current PHTS design and of the management strategy chosen for the selected accidental scenarios. In addition, it is important to note that the strategic objective of the planned STEAM facility is to have an experimental infrastructure capable to empirically investigate the BoP of DEMO based on water coolant technology. DIAEE will play an important role in supporting the design of the whole facility. The latter will host components simulating the DEMO WCLL blanket primary and secondary cooling systems. During testing, several management strategies involving these circuits will be studied, related to both operative states and accidental conditions. The experience gained thanks to this DEMO WCLL transient analysis will help in defining such management startegies. At their time, the experimental tests will provide an important feedback on the effectiveness of the systems and components proposed for DEMO WCLL PHTSs that were simulated in the calculations presented in this PhD thesis.

7.2.2 ITER WCLL

During the third ITER council (2008), it was established the so-called ITER Test Blanket Module program. Its objective is to provide the first experimental data on the performance of the breeding blankets in the integrated fusion nuclear environment. More recently, in 2018, the WCLL option was inserted among the selected blanket concepts to be investigated. From this time, an intense research activity was conducted within the EUROfusion Work Package WPPMI in order to

perform the pre-conceptual and conceptual design phases of ITER WCLL Test Blanket System. The overall work (i.e. TBS) was divided in 'Part A', related to TBM set and 'Part B', referring to its related ancillary systems. For the latter, R&D effort was led by ENEA and involved many European research institutions and universities, including DIAEE of Sapienza University of Rome. The work was supervised also by Fusion for Energy, the EU organization managing Europe's contribution to ITER reactor. By the fall of 2020, both design phases were concluded and the system successfully underwent its Conceptual Design Review. Among the TBM ancillary systems, the most relevant is the Water Cooling System, acting as primary cooling circuit of the TBM module. The design and thermal-hydraulic characterization of this circuit was up to DIAEE.

The TBS conceptual design was presented in **§** 5. A special focus was given to the WCS layout (**§** 5.4) whose DIAEE is responsible for (i.e. the candidate took part to), [89][90]. The Water Cooling System was designed to implement the following main functions: **i)** provide suitable operating parameters to the water flow cooling the TBM in any operational state; **ii)** transfer thermal power from WCLL-TBM to CCWS; **iii)** provide confinement for water and radioactive products; **iv)** ensure the implementation of the WCLL-TBS safety functions. In addition, ITER WCLL-TBM must be DEMO relevant. Such relevancy refers to the water thermodynamic conditions at the TBM (15.5 MPa, 295-328 °C) since the experimental program will deal with the test of this blanket reference concept. The reduced thermal power produced in the TBM set (near 700 kW) with respect to DEMO blanket (1923 MW), allows to use a single water-cooling system for both the FW and the BZ. The correspondent WCS primary flow was computed considering the TBM power balance. The ultimate heat sink for the WCLL-TBM WCS is the ITER CCWS. With the aim to include an additional barrier between the contaminated primary water and the CCWS coolant, the WCLL-WCS was split in a primary and a secondary loop. In such a way, the CCWS radioactive inventory is kept below the limit in any operative and accidental scenario (note that CCWS is a non-nuclear system). To simplify the WCLL-WCS management, liquid only condition was selected for the secondary coolant instead of the two-phase fluid, as in DEMO PCS. It is worth to emphasize that electricity generation is not a purpose of ITER and, thus, steam production is not required. CCWS provides water coolant at low pressure and temperature (0.8 MPa at 31 °C), and requires that return temperature must be limited to 41 °C. Hence, there is a considerable difference between the average TBM temperature and the average CCWS temperature. To avoid an excessive temperature excursion (i.e. thermal stresses) between the two sides of a single heat exchanger, an economizer was installed in the middle of the WCS primary loop, leading to the typical "eight" shape of this circuit. Therefore, a total of three heat exchangers were considered for the whole WCS, namely: HX-0001 (economizer), HX-0002 (intermediate heat exchanger between primary and secondary loops) and HX-0003 (heat sink delivering power to CCWS). Each heat exchanger was provided with a bypass line allowing the regulation of the exchanged power by tuning the shell side mass flow. Finally, an electrical heater was added to the WCS primary loop in order to compensate the power unbalance in the system. Most of the WCS equipment is installed in the TCWS Vault, at level four of the tokamak building. The rest of the components, including the TBM, is placed in the level one Port Cell #16. Both locations are linked by means of connection pipes hosted in a vertical shaft.

To support the WCS design a preliminary transient analysis was performed. For this purpose, a full thermal-hydraulic model of the system was developed by using the DIAEE version of RELAP5/Mod3.3. Since this circuit is directly connected to PbLi loop within the TBM, also these two systems were included in the overall TBS model. The nodalizations was described in detail in **§** 6.1. A preliminary control system was implemented for both WCS and PbLi loop. All the main circuit parameters (pressure, temperatures and mass flows) are controlled in order to ensure system stability in any operative scenario and to provide water coolant and breeder at TBM with the required inlet conditions.

Firstly, full plasma power state was simulated at both BOL and EOL conditions (**§** 6.3). Such calculations were needed to test and evaluate the appropriateness of the model prepared. Simulation outcomes demonstrated that control systems corresponding to WCS and PbLi loop are able to ensure the required values at TBM inlet in both the operative scenarios. For WCS, the main differences between BOL and EOL conditions were highlighted, mainly regarding the operation of the temperature control system (i.e., the mass flow through the heat exchangers bypass). WCS and PbLi loop performances in this flat-top states were fully characterized, including the calculation of pressure and temperature fields, as well as the system power balance. In addition, an insight into the TBM behavior during full plasma power condition was given. Its operation does not change from BOL to EOL since it is provided with water coolant and liquid metal at constant thermodynamic conditions and flow rate. It is important to note that a full thermal-hydraulic characterization of the component was out of the scope of the research activity carried out by DIAEE. Nevertheless, TBM box contains part of the WCS circuit and constitutes the system source term. Furthermore, thermal coupling between WCS and PbLi loop occurs inside the module. For this, it was mandatory to properly simulate the heat transfer phenomena taking place within the component. The TBM results obtained with the system code were compared with the more detailed ones produced by CEA using FEM methodologies. The latter were used to calibrate the component thermal-hydraulic model.

Then, the two steady-state calculations were used as initial condition to simulate operative scenarios and abnormal conditions. The Normal Operation State was the first to be analyzed (§ 6.4). The WCS and PbLi loop control systems were tested to demonstrate their effectiveness in ensuring stable operations against the pulsed regime characterizing the NOS. Preliminary investigations on this key issue were performed also during the pre-conceptual design phase [102]. They were reported in annex A3 since they provided important feedbacks for the subsequent (conceptual) design phase. In this framework, new calculations were carried out, [90]. They included both BOL and EOL conditions in order to assess the change in WCS thermal-hydraulic performances with the system aging. The reference ITER pulsed plasma regime was adopted for simulation purposes. The system code results demonstrated the appropriateness of the WCS and PbLi loop control systems. They are able to ensure water coolant and PbLi at the TBM with nearly constant inlet thermodynamic conditions and flow rate. For water inlet temperature, oscillations were limited to +/- 3 °C, acceptable for WCS and TBM operation. Moreover, it was verified that in any part of the PbLi loop an adequate margin (16 °C) from the freezing point is maintained. For WCS, what is interesting to be noted is that the economizer and the electrical heater control systems absorb the fluctuations present at the TBM outlet section, due to the pulsed plasma power. In such a way, they guarantee a quasi-steady state operation over the whole NOS to the WCS cold branch, as well as to WCS secondary loop and CCWS section in TCWS vault.

Finally, in order to assess and verify the WCS design, two abnormal scenarios were selected and investigated (**§** 6.5, [90]). The aim was to evaluate the system capabilities under degraded conditions and to verify if the standard control strategies without any external action are capable to maintain the TBM cooling function for an entire plasma pulse. This last condition allows to avoid the triggering of the Fast Plasma Shutdown System, demonstrating that a minor accident in the WCS does not interfere with the ITER global operation. The transients considered were: **i)** LOFA occurring in WCS secondary loop; **ii)** LOHS, i.e. loss of flow in the CCWS. The worst operative condition was supposed to be the EOL, since plugging and fouling limit the heat exchange. For this reason, NOS at EOL was imposed as an initial condition for both the transient analyses.

Regarding the first abnormal scenario (**§** 6.5.1), the initiating event consists in the blockage of the active secondary pump. The second one, foreseen by design for back-up is conservatively

considered unavailable since under maintenance. PIE is assumed to occur at the beginning of the flat-top phase. Since the goal of these simulations is to prove that call the FPSS is unnecessary, the chosen one is the worst possible scenario. Indeed, from the start of transient, plasma is shutdown only at the end of the pulse, i.e. after 450 s. The PbLi loop draining is not assumed; it works over the whole transient. After the plasma shutdown, no further actions are considered, and WCS continues to remove power up to the end of the simulation time. At the transient beginning, due to the loss of WCS secondary flow, the heat exchange capabilities of HX-0002 and HX-0003 are compromised. The power surplus coming from the primary loop (plasma is operated for an entire pulse) is managed by the secondary system pressure control function, in particular the pressurizer PORV. In the long term, natural circulation establishes in the secondary loop, the system temperature field significantly changes with respect to nominal conditions but the power equilibrium is restored in the circuit. At this time, the overall WCS operation results quasi-steady state, with the HT-0001 ensuring the required TBM inlet conditions and the HX-0002 and HX-0003 removing the power supplied. In conclusion, the WCS primary loop is kept in safety conditions over the whole accidental scenario. In addition, the safety margin from the PbLi freezing is ensured by keeping the reference water temperature at the TBM inlet. It guarantees to operate the PbLi loop at nearly nominal conditions for the overall transient.

The second abnormal scenario simulated consists in the loss of heat sink for the WCS system (**§** 6.5.2). Due to the limits of the RELAP5 model prepared, after the initiating event, the CCWS section within the TCWS Vault is conservatively isolated. At the transient beginning, the power surplus coming from the primary loop (plasma is operated for an entire pulse) is evacuated by means of multiple openings of the safety valve whose this CCWS section is provided. Part of the energy is also used for the phase transition of the water present in the HX-0003 shell and upwards/downwards pipelines (circuit section between the isolation valves). The loss of the heat sink (HX-0003 heat exchange capability is immediately compromised after the start of transient) leads the WCS secondary loop to be gradually heated. Once reached the maximum allowable temperature at the pump inlet, the component is cut-off to avoid cavitation. Later, also the secondary system starts to evacuate energy in the form of vapor flow through the pressurizer PORV. The loss of the secondary flow disables the HX-0002, thermally isolating the primary loop. From this moment onwards, the primary loop is a nearly isothermal circuit. Indeed, neither power input (plasma is shut down and decay heat is of the same order of magnitude of the heat losses) nor power output (HX-0002 does not remove power) are present. In the long term, the system temperature is kept at the value required at TBM inlet by the HT-0001. By the end of simulation time, the component intervenes only twice to compensate cooling transients provided by the secondary PORV openings. In fact, the evacuation of WCS secondary loop water inventory proceeds in a step-wise mode and it is not completed before the transient end. Instead, the water inventory in CCWS section is almost completely evacuated in 5000 s. In conclusion, the WCS primary loop is kept in safety conditions over the whole accidental scenario. In addition, the safety margin from the PbLi freezing is ensured by keeping the reference water temperature at the TBM inlet.

In conclusion, simulation outcomes highlighted the appropriateness of the current WCS design and of the control systems implemented in withstanding the selected accidental scenarios. Referring to the future developments of this activity, within the framework of Horizon Europe research programme, it is planned the construction of a facility, named ‘Water Loop’, reproducing the WCS with a 1:1 scale. The aim is investigating in detail the circuit thermal-hydraulic performances. The experimental setup is supposed to be built at the ENEA research centre of Brasimone. Thanks to the large experience maturated during the design and simulation activities discussed in this PhD thesis, DIAEE will play a primary role in the conceptualization of the facility.

A1. Thermal properties for fluids and materials used in RELAP5 thermal-hydraulic model.

For solid materials involved in the heat transfer problem, RELAP5 code prompts the user to enter the needed thermal properties. The required input consists of two tables collecting the thermal conductivity and heat capacity trends against temperature, [35]. These properties were used to solve the Fourier's law for heat conduction in solid layers, [75]. This annex contains the tables collecting the thermal properties for all the materials used in the RELAP5 input deck. Each subsection refers to a specific material. The references adopted are collected in Table A1.1.

Table A1.1 – References adopted for material properties.

Material	**References**
EUROFER97	[73][74]
Lead-lithium	[39]
Tungsten	[75]
AISI 316L(N)	[76]
Thermal insulator	[77]
INCONEL 690	[76]
Constantan	[78]
Ceramic	[78]
ALLOY 800	[76]

EUROFER-97:

Table A1.2 – EUROFER-97 thermal properties, [73][74].

T **[°C]**	**ρ** **[kgm^{-3}]**	**C_p** **[Jkg^{-1}K^{-1}]**	**λ** **[Wm^{-1}K^{-1}]**
20	7744	448.1	28.4
100	7740	488.7	29.9
200	7723	518.5	30.3
300	7691	543.8	29.9
400	7657	584.5	29.5
500	7625	660.8	29.7
600	7592	792.6	31.0
700	7559	999.9	34.3

T: temperature; **ρ**: density; **C_p**: specific heat; **λ**: thermal conductivity.

Lead-lithium:

Table A1.3 – Lead-lithium thermal properties, [39].

T [°C]	**ρ** [kgm^{-3}]	**C_p** [Jkg^{-1}K^{-1}]	**λ** [Wm^{-1}K^{-1}]
235	9916	190.4	11.90
300	9838	189.8	13.17
350	9778	189.3	14.15
400	9719	188.9	15.13
450	9659	188.4	16.11
500	9600	187.9	17.09
550	9540	187.5	18.07
600	9481	187.0	19.05
650	9421	186.6	20.03
700	9362	186.1	21.01
T: temperature; **ρ**: density; **C_p**: specific heat; **λ**: thermal conductivity.			

Tungsten:

Table A1.4 – Tungsten thermal properties, [75].

Parameter	**Unit**	**Value**
Density	kgm^{-3}	19300
Specific Heat	Jkg^{-1}K^{-1}	145
Thermal Conductivity	Wm^{-1}K^{-1}	125

AISI 316L:

Table A1.5 – AISI 316L thermal properties, [76].

T [°C]	**λ** [Wm^{-1}K^{-1}]	**α** [m^{2}s]	**C_v** [Jm^{3}K^{-1}]
20	14.10	3.57	3.95E+06
100	15.40	3.75	4.11E+06

200	16.80	3.98	4.22E+06
300	18.30	4.22	4.34E+06
400	19.70	4.44	4.44E+06
500	21.20	4.66	4.55E+06
600	22.60	4.90	4.61E+06
700	23.90	5.12	4.67E+06

T: temperature; **λ**: thermal conductivity; **α**: thermal diffusivity; **C_v**: volumetric heat capacity.

Thermal insulator:

Table A1.6 – Thermal insulator thermal properties, [77].

T [°C]	**ρ [kgm^{-3}]**	**C_p [Jkg^{-1}K^{-1}]**	**λ [Wm^{-1}K^{-1}]**
20	66	1000	0.038
50	66	1000	0.038
100	66	1000	0.045
150	66	1000	0.052
200	66	1000	0.062
300	66	1000	0.083
400	66	1000	0.110

T: temperature; **ρ**: density; **C_p**: specific heat; **λ**: thermal conductivity.

INCONEL 690:

Table A1.7 – INCONEL 690 thermal properties, [76].

T [°C]	**λ [Wm^{-1}K^{-1}]**	**α [m^{2}s]**	**C_v [Jm^{3}K^{-1}]**
20	11.80	3.23	3.65E+06
100	13.30	3.48	3.82E+06
200	15.10	3.78	3.99E+06
300	17.00	4.09	4.16E+06
400	18.90	4.41	4.29E+06
500	20.80	4.71	4.42E+06

600	22.80	4.97	4.59E+06
700	24.70	5.17	4.78E+06

T: temperature; **λ**: thermal conductivity; **α**: thermal diffusivity; $\mathbf{C_v}$: volumetric heat capacity.

Constantan:

Table A1.8 – Constantan thermal properties, [78].

T [°C]	**λ [$Wm^{-1}K^{-1}$]**	**C_v [Jm^3K^{-1}]**
20	22	3.66E+06
100	26	3.66E+06
200	35	3.66E+06
600	35	3.66E+06

T: temperature; **λ**: thermal conductivity; **α**: thermal diffusivity; $\mathbf{C_v}$: volumetric heat capacity.

Ceramic:

Table A1.9 – Ceramic thermal properties, [78].

T [°C]	**λ [$Wm^{-1}K^{-1}$]**	**C_v [Jm^3K^{-1}]**
20	2.15	2.86E+06
100	1.93	3.26E+06
200	1.67	3.53E+06
300	1.42	3.71E+06
400	1.30	3.81E+06
500	1.19	3.88E+06
600	1.09	3.95E+06
700	1.12	4.02E+06
800	1.15	4.07E+06
1000	1.39	4.15E+06
1200	1.50	4.24E+06

T: temperature; **λ**: thermal conductivity; **α**: thermal diffusivity; $\mathbf{C_v}$: volumetric heat capacity.

ALLOY 800:

Table A1.10 – ALLOY 800 thermal properties, [76].

T [°C]	**λ** [$Wm^{-1}K^{-1}$]	**α** [m^2s]	**C_v** [Jm^3K^{-1}]
20	11.50	3.14	3.66E+06
100	13.00	3.46	3.76E+06
200	14.70	3.78	3.89E+06
300	16.40	4.05	4.05E+06
400	17.90	4.30	4.16E+06
500	19.40	4.53	4.28E+06
600	21.10	4.73	4.46E+06
700	22.90	4.91	4.66E+06

T: temperature; **λ**: thermal conductivity; **α**: thermal diffusivity; **C_v**: volumetric heat capacity.

A2. Detail description of DEMO WCLL blanket nodalization

The most relevant issues concerning the blanket modelling approach were: preserving as much as possible the blanket components actual geometry, and maintaining the design material inventories. Combining these two factors allowed to best-estimate the overall blanket heat capacity, that is one of the most relevant parameters in transient simulations involving the BB PHTS. The BZ and FW cooling circuits were simulated with independent hydrodynamic systems but they were thermally coupled by means of RELAP5 heat structures. This approach permitted to simulate the heat transfer phenomena which take place inside the breeding cell between FW cooling channels and BZ DWTs.

For each PHTS, the cooling circuits within the five poloidal segments (three for OB and two for IB) associated to a single DEMO sector were collapsed in three equivalent pipe components, as follows: LOB and ROB; COB; LIB and RIB. Each pipe simulates the series of all the components belonging to the BZ or FW cooling circuit inside vacuum vessel: 1) inlet feeding pipe; 2) inlet spinal water manifold; 3) DWTs or FW channels; 4) outlet spinal water manifold; 5) outlet feeding pipe. The control volume hydraulic properties (flow area, hydraulic diameter, etc.) vary along the pipe length according to the different geometry associated with each component simulated. For the equivalent pipes corresponding to LOB/ROB and LIB/RIB, the control volume flow area and hydraulic diameter, as well as the water mass flow, were evaluated considering the reference data belonging to both segments. In this way, the pressure drops through these components were correctly modelled. The feeding pipes are connected to the PHTS sector collectors and distributors by means of inlet and outlet manifolds. Summarizing, for each PHTS (BZ and FW) and for each sector, the following hydraulic components were used:

- 1 pipe component for the BZ/FW sector distributor (BZ/FW-P1);
- 1 branch component for the BZ/FW inlet manifold (BZ/FW-B1);
- 1 pipe component to simulate the BZ/FW cooling circuit inside LOB and ROB segments (BZ/FW-P2);
- 1 pipe component to simulate the BZ/FW cooling circuit inside the COB segment (BZ/FW-P3);
- 1 pipe component to simulate the BZ/FW cooling circuit inside the LIB and the RIB segments (BZ/FW-P4);
- 1 branch component for the BZ/FW outlet manifold (BZ/FW-B2);
- 1 pipe component for the BZ/FW sector collector (BZ/FW-P5).

The total number of RELAP5 pipe and branch components used to model the blanket is shown in Table A2.11.

Design data for sector collectors and distributors (BZ/FW-P1, BZ/FW-P5) were taken from [67]. Pipeline routing was derived from the CAD model, differentiated for each segment. Pipeline features were maintained in the input deck.

BZ/FW-P2, BZ/FW-P3 and BZ/FW-P4 are the RELAP5 pipe components representing the BZ and FW cooling circuits inside vacuum vessel. They are respectively related to: LOB/ROB, COB, LIB/RIB. The water flow paths include: inlet feeding pipe; inlet spinal water manifold; DWTs or FW

channels; outlet spinal water manifold; outlet feeding pipe. Referring to these components the following modelling strategies were adopted:

- In the current design, inlet/outlet feeding pipes are straight vertical pipes (see Figure 3.2 and Figure 3.10). Their design data were available in [67], while pipeline routing was derived from CAD model. Actual pipeline features were kept in the RELAP5 model. Inlet and outlet feeding pipes represent the first and the last batch of hydrodynamic control volumes of each equivalent pipe component.
- DWTs and FW channels represent the central set of control volumes in each equivalent pipe component. DWTs are C-shaped pipes, split in three arrays along the radial direction. Each array is characterized by a different shape in the radial-toroidal plane. The reference layout adopted for the RELAP5 model was the one of the second array (the mid-one along the radial direction). It was considered enough representative of the average geometrical features of all the DWTs present in the breeding cell. The flow area entered for DWTs simulating-control volumes was calculated lumping all the cooling tubes belonging to the correspondent segment/segments (i.e. the flow area of a single DWT times the DWTs in a breeding cell (22) times the number of breeding cells in a segment (assumed 105) times the segment collapsed in each pipe component). Instead, the hydraulic diameter assumed was the one of the single DWT (8 mm). Similar approach permitted a correct evaluation of the pressure drops along these components. The same modelling choices were adopted also for the FW cooling channels. The only difference is that all the FW channels have the same shape in the radial-toroidal plane. Hence, the channel shape was strictly kept in the model.
- BZ and FW inlet/outlet water manifolds consist in spinal rectangular channels running along the back of the segment, radially inwards with respect to the BSS, as shown by Figure 3.3. They follow the segment curved profile. Manifold-simulating-control volumes are located before (inlet) and after (outlet) the ones modelling the DWTs/FW channels. For the equivalent pipe components related to IB segments (BZ/FW-P4), the manifold length was assumed equals to half the segment length along the external curved profile. Instead, for the pipes related to OB segments (BZ/FW-P2, BZ/FW-P3), the length adopted was the previous one minus the height difference between the top of the OB segments and the elevation where the OB feeding pipes are connected. This modelling approach allowed to locate, for all the segments, the control volumes representing the DWTs or the FW channels at the tokamak mid-quote. Assuming in first approximation a constant power source term along the poloidal direction, the tokamak mid-quote corresponds also to its thermal center. Hence, in the RELAP5 model, the design height difference between heat source (blanket breeding cells) and heat sink (the BZ OTSGs and the FW HEXs) thermal centers was maintained. This parameter is of primary importance in all the transients concerning natural circulation, such as in LOFA. For any segment, control volume flow area was calculated to keep the BZ and FW water manifold inventory. In first approximation, the COB design, described in [59], was used also for the pipes simulating LOB/ROB and LIB/RIB segments.

The geometrical input data adopted for the equivalent pipes representing the sector segments are collected in Table A2.12 and Table A2.13, respectively for BZ and FW. Table A2.14 offers a comparison between water inventories present in the model and their correspondent design values, derived from [59]-[62].

The RELAP5 heat structure components were used in the model to simulate: **i)** the inventories of the blanket solid materials (tungsten and EUROFER-97); **ii)** the liquid breeder; **iii)** the power

source terms (see Table 3.2); **iv)** the heat transfer phenomena which take place inside the breeding cell; **v)** the pipeline thermal insulation (sector collector and distributor, inlet/outlet FPs).

The PbLi circuit within the blanket was not modelled from a hydrodynamic point of view. This was decided to reduce the number of control volumes in the overall RELAP5 model and, thus, limit the calculation time. Because of the breeder low velocity inside the breeding cell (0.01 mm/s, [59]), the convective contribution to the overall heat transfer coefficient is negligible and the heat transfer is prevalently conductive. Hence, simulating the liquid metal as a material layer belonging to heat structure components was considered an acceptable approximation.

For each pair of BZ/FW equivalent pipe components related to a DEMO sector segment (BZ/FW-P2, BZ/FW-P3, BZ/FW-P4) the following heat structures were used:

- 1 heat structure for the FW front layer: BB-HS1;
- 1 heat structure for the FW radial segments: BB-HS2;
- 1 heat structure to model the heat transfer between FW channels and DWTs: BB-HS3;
- 1 heat structure to simulate the lasting heat transfer phenomena between DWTs and PbLi within the breeding cell: BB-HS4;
- 1 heat structure to simulate the EUROFER inventory in the water and PbLi manifold regions: BB-HS5;
- 1 heat structure for the back supporting structure: BB-HS6;

The summary of the heat structure components used in the RELAP5 model is contained in Table A2.15. For all the above heat structures, heat transfer problem in rectangular geometry was selected to be solved by the code. The needed input data to be entered in the input deck were: **i)** the solid layer thickness, distributed between the different materials; **ii)** the heat transfer surface; **iii)** the Left and Right Boundary conditions (LB and RB); **iv)** the internal source term (if any).

FW component was simulated through BB-HS1 and BB-HS2. The former refers to the front surface. A tungsten layer of 2 mm and an EUROFER thickness of 3 mm were modelled. The EUROFER thickness considered was the one between the plasma chamber and the FW cooling channels. The average heat flux reported in Table 3.2 was used as left boundary, while the FW cooling channels were entered as right boundary. BB-HS2 is related to FW radial segments. In this case, tungsten layer is not present and only the 3 mm-EUROFER thickness was modelled. A symmetry boundary condition was used as LB. Instead, FW cooling channels were still adopted as RB. The FW nuclear heating was distributed among these two heat structures considering the power density radial profiles presented in [62].

BB-HS3 models the thermal coupling between FW channels and BZ DWTs. In the radial-toroidal plane, DWTs are divided in three arrays with different layouts. The same DWT average layout chosen in the hydrodynamic model was selected for the thermal problem also. The radial distance between the FW cooling channels and the chosen DWT is composed by: 15 mm of EUROFER, representing the FW thickness between FW cooling channels and FW internal surface; 80 mm of PbLi, corresponding to the radial distance between the FW internal surface and the selected DWT external surface; 2.75 mm of EUROFER, modelling the DWTs thickness. As left and right boundary conditions FW cooling channels and BZ DWTs were used.

BB-HS4 was used to simulate the lasting heat transfer phenomena occurring in the breeding cell between DWTs and PbLi. The heat structure thickness is composed by two layers: the first of EUROFER-97 and the second of PbLi. The latter was computed to keep the breeder inventory

within the breeding cell. DWTs were used as LB and a symmetry boundary condition was adopted for RB.

BB-HS5 and BB-HS6 respectively represent the EUROFER inventory in the PbLi and water manifold region and in the back supporting structure. In the former, an average plate thickness of 20 mm was adopted. For the latter, the actual BSS thickness of 100 mm was used. Both heat structures have the control volumes corresponding to inlet/outlet spinal water manifolds as LB and a symmetry boundary condition as RB.

BZ nuclear heating was distributed among these heat structure components (BB-HS3 to BB-HS6) according to the power density radial profiles presented in [62] and by considering the actual material inventory distribution within the breeding cell, (see Figure 3.3). It was introduced in the input deck as an internal power source term, differentiated for each heat structure.

The main input parameters for the blanket heat structures are collected in Table A2.16. The comparison between RELAP5 model material inventories and design values, [59]-[62], is reported in Table A2.17.

Referring to Thermal Insulation (TI), for any sector, a dedicated heat structure was associated to: sector collector, sector distributor, inlet/outlet segment feeding pipes. The list of these heat structure components is contained in Table A2.15. The RB adopted for these heat structures was the tokamak building atmosphere, modelled with a constant temperature (30 °C) and a constant heat transfer coefficient (8 W/m^2K). The HTC considered is the sum of the convective and radiative contributions. For lower temperatures (< 50 °C), as in the case of the pipeline insulation external surface, the correlation for radiative HTC can be linearized, and this term can be sum to the convective one. The specific value adopted for the overall HTC derives from engineering judgement and experience. The data used for the thermal insulation heat structures are reported in Table A2.18 and Table A2.19. The comparison between RELAP5 model material inventories and design values, [67], is offered by Table A2.20.

Table A2.11 - RELAP5 hydrodynamic components used for BZ and FW cooling circuits inside vacuum vessel.

PHTS	Segment	Sector Collector	Inlet Manifold	Inlet FPs	BB Inlet Man.	DWTs/ FW Ch.	BB Outlet Man.	Outlet FPs	Outlet Manifold	Sector Distributor	Total		
											Sector	PHTS	Reactor
BZ	LOB/ROB	1 Pipe (**BZ-P1**)	1 Branch (**BZ-B1**)	1 Pipe (**BZ-P2**)					1 Branch (**BZ-B2**)	1 Pipe (**BZ-P5**)	7	112	**224**
	COB			1 Pipe (**BZ-P3**)									
	LIB/RIB			1 Pipe (**BZ-P4**)									
FW	LOB/ROB	1 Pipe (**FW-P1**)	1 Branch (**FW -B1**)	1 Pipe (**FW –P2**)					1 Branch (**BZ-B2**)	1 Pipe (**BZ-P5**)	7	112	
	COB			1 Pipe (**FW –P3**)									
	LIB/RIB			1 Pipe (**FW –P4**)									

Table A2.12 - Input parameters for hydrodynamic components simulating the BZ cooling circuit inside vacuum vessel.

Hyd. Comp. Type	CV N°			Length [m]			Flow Area [m^2]			Hyd. Diam. [m]		
	LOB/ROB (BZ-P2)	COB (BZ-P3)	LIB/RIB (BZ-P4)	LOB/ROB (BZ-P2)	COB (BZ-P3)	LIB/RIB (BZ-P4)	LOB/ROB (BZ-P2)	COB (BZ-P3)	LIB/RIB (BZ-P4)	LOB/ROB (BZ-P2)	COB (BZ-P3)	LIB/RIB (BZ-P4)
Inlet FPs	1-17	1-17	1-23	7.72	7.72	10.35	5.32E-02	2.66E-02	3.21E-02	0.184	0.184	0.143
Inlet Man.	18-28	18-28	24-41	4.81	4.81	8.24	4.35E-01	2.18E-01	2.26E-01	0.135	0.135	0.135
DWTs	29-37	29-37	42-50	1.78	1.78	1.78	2.32E-01	1.16E-01	2.32E-01	0.008	0.008	0.008
Outlet Man.	38-48	38-48	51-68	4.81	4.81	8.24	3.66E-01	1.83E-01	1.90E-01	0.133	0.133	0.133
Outlet FPs	49-65	49-65	69-91	7.72	7.72	10.35	5.32E-02	2.66E-02	3.20E-02	0.184	0.184	0.143

Table A2.13 - Input parameters for hydrodynamic components simulating the FW cooling circuit inside vacuum vessel.

Hyd. Comp. Type	CV N°			Length [m]			Flow Area [m^2]			Hyd. Diam. [m]		
	LOB/ROB (FW-P2)	COB (FW-P3)	LIB/RIB (FW-P4)	LOB/ROB (FW-P2)	COB (FW-P3)	LIB/RIB (FW-P4)	LOB/ROB (FW-P2)	COB (FW-P3)	LIB/RIB (FW-P4)	LOB/ROB (FW-P2)	COB (FW-P3)	LIB/RIB (FW-P4)
Inlet FPs	1-20	1-20	1-28	8.90	8.90	12.1	2.18E-02	1.09E-02	1.47E-02	0.118	0.118	0.097
Inlet Man.	21-31	21-31	29-44	5.58	5.58	8.24	4.83E-02	2.41E-02	3.03E-02	0.065	0.065	0.065
FW Ch.	32-41	32-41	45-53	2.55	2.55	2.55	1.03E-01	5.15E-02	1.03E-01	0.007	0.007	0.007
Outlet Man.	42-52	42-52	54-70	5.58	5.58	8.24	4.83E-02	2.41E-02	3.03E-02	0.065	0.065	0.065
Outlet FPs	53-72	53-72	71-98	8.90	8.90	12.1	2.18E-02	1.09E-02	1.47E-02	0.118	0.118	0.097

Table A2.14 - BZ and FW cooling circuits inside vacuum vessel: summary of water inventories.

PHTS	Segment (RELAP5 pipe)	Water Inv. [m^3]					
		Segment		Sector		Reactor	
		Inside BB	FPs	RELAP5	Design	RELAP5	Design
BZ	LOB/ROB (BZ-P2)	4.266	0.822	10.24 (BB Sector) 1.90 (FPs)	10.24 (BB Sector) 1.51 (FPs)	**163.90 (BB) 30.34 (FPs)**	**163.90 (BB) 24.1 (FPs)**
	COB (BZ-P3)	2.133	0.410				
	LIB/RIB (BZ-P4)	3.843	0.664				
FW	LOB/ROB (FW-P2)	0.802	0.388	1.97 (BB Sector) 0.94 (FPs)	1.97 (BB Sector) 0.76 (FPs)	**31.40 (BB) 15.01 (FPs)**	**31.40 (BB) 12.18 (FPs)**
	COB (FW-P3)	0.401	0.194				
	LIB/RIB (FW-P4)	0.762	0.356				

Table A2.15 - RELAP5 heat structures used for blanket thermal model.

PHTS	Segment	Sector Collector	Inlet FPs	DWTs/FW Channels	BB Inlet/Outlet Manifolds	Outlet FPs	Sector Distributor	Total	
								Sector	Blanket
BZ	LIB/RIB	1 HS: **BZ-TI-HS1**	1 HS: **BZ-TI-HS2**	2 HS: **BB-HS3[1]; BB-HS4**	2 HS **BB-HS5[2]**; **BB-HS6**	1 HS: **BZ-TI-HS3**	1 HS (**BZ-TI-HS8**)	34	544
	COB		1 HS: **BZ-TI-HS4**	2 HS: **BB-HS3; BB-HS4**	2 HS **BB-HS5**; **BB-HS6**	1 HS: **BZ-TI-HS5**			
	LOB/ROB		1 HS: **BZ-TI-HS6**	2 HS: **BB-HS3; BB-HS4**	2 HS **BB-HS5**; **BB-HS6**	1 HS: **BZ-TI-HS7**			
FW	LIB/RIB	1 HS: **FW-TI-HS1**	1 HS: **FW-TI-HS2**	2 HS: **BB-HS1; BB-HS2**	-	1 HS: **FW-TI-HS3**	1 HS (**FW-TI-HS8**)		
	COB		1 HS: **FW-TI-HS4**	2 HS: **BB-HS1; BB-HS2**	-	1 HS: **FW-TI-HS5**			
	LOB/ROB		1 HS: **FW-TI-HS6**	2 HS: **BB-HS1; BB-HS2**	-	1 HS: **FW-TI-HS7**			

[1]: BB-HS3 is the HS used to thermally couple the BZ DWTs and FW Channels. It can be considered in common between the two systems.

[2]: BB-HS5 and BB-HS6 are connected to both BZ and FW pipe components. For sake of clarity it has been reported in the table only once (for BZ system).

Table A2.16 - Input parameters for heat structure components simulating the heat transfer phenomena inside vacuum vessel.

HS Comp. Type	Segment Type	RELAP5 Geom. Type	Thickness [mm]	Tot. HT Surface [m^2]	Int. Power Source [yes/no]	LB	LB Heat. Diam. [m]	RB	RB Heat. Diam. [m]
BB-HS1	LOB/ROB	Rectangular	2 mm of EUROFER; 3 mm of PbLi	37.5	yes	Av. HF 0.22 MW/m2	-	FW Cooling Channels	0.007
	COB			21.2					
	LIB/RIB			31.7					
BB-HS2	LOB/ROB	Rectangular	5.79 mm of EUROFER	16.7	yes	Symm. BC	-	FW Cooling Channels	0.007
	COB			8.35					
	LIB/RIB			16.7					
BB-HS3	LOB/ROB	Rectangular	15 mm of EUROFER; 80 mm of PbLi; 2.75 mm of EUROFER	103.1	no	FW Cooling Channels	0.007	DWTs	0.008
	COB			51.5					
	LIB/RIB			103.1					
BB-HS4	LOB/ROB	Rectangular	2.75 mm of EUROFER; 20 mm of PbLi;	803.7	yes	DWTs	0.008	Symm. BC	-
	COB			448.5					
	LIB/RIB		2.75 mm of EUROFER; 15 mm of PbLi;	656.0					
BB-HS5	LOB/ROB	Rectangular	20 mm of EUROFER	176.4	no	SMS Water Man.	0.134	Symm. BC	-
	COB			93.8					
	LIB/RIB			158.8					
BB-HS6	LOB/ROB	Rectangular	100 mm of EUROFER	37.2	no	SMS Water Man.	0.134	Symm. BC	-
	COB			19.8					
	LIB/RIB			33.5					

Table A2.17 - Summary of blanket material inventories entered in the RELAP5 input deck.

Material	Inventory [m3]									
	Segment						Sector		Blanket	
	LOB/ROB		COB		LIB/RB					
	RELAP5	Design	RELAP5	Design	RELAP5	Design	RELAP5	Design	RELAP5	Design
Tungsten	0.088	0.088	0.047	0.047	0.098	0.098	0.233	0.233	**3.728**	**3.728**
EUROFER	11.49	11.49	6.112	6.112	10.35	10.35	27.95	27.95	**447.2**	**447.2**
PbLi	24.26	24.26	12.90	12.90	17.75	17.75	54.91	54.91	**878.6**	**878.6**

Table A2.18 - Input parameters for heat structures modelling the thermal insulation of BZ PHTS feeding pipes and sector collectors/distributors.

HS Comp. Type	RELAP5 Geom. Type	Thickness [mm]	Tot. HT Surface [m^2]	LB	LB Heat. Diam. [m]	RB
BZ-TI-HS1	Cylindrical	28 mm of AISI 316 L(N); 100 mm of ISOVER®.	45.9[1]	BZ-P1	0.300	Ext. Air[2]
BZ-TI-HS2	Cylindrical	17.5 mm of AISI 316 L(N); 100 mm of ISOVER®.	20.5	BZ-P2: CVs 1-17	0.184	Ext. Air
BZ-TI-HS3	Cylindrical	17.5 mm of AISI 316 L(N); 100 mm of ISOVER®.	20.5	BZ-P2: CVs 49-65	0.184	Ext. Air
BZ-TI-HS4	Cylindrical	17.5 mm of AISI 316 L(N); 100 mm of ISOVER®.	10.2	BZ-P3: CVs 1-17	0.184	Ext. Air
BZ-TI-HS5	Cylindrical	17.5 mm of AISI 316 L(N); 100 mm of ISOVER®.	10.2	BZ-P3: CVs 49-65	0.184	Ext. Air
BZ-TI-HS6	Cylindrical	12.7 mm of AISI 316 L(N); 100 mm of ISOVER®.	24.0	BZ-P4: CVs 1-23	0.143	Ext. Air
BZ-TI-HS7	Cylindrical	12.7 mm of AISI 316 L(N); 100 mm of ISOVER®.	24.0	BZ-P4: CVs 69-91	0.143	Ext. Air
BZ-TI-HS8	Cylindrical	28 mm of AISI 316 L(N); 120 mm of ISOVER®.	50.8	BZ-P5	0.300	Ext. Air

[1]: The total HT surface reported in the table is the external cylinder surface.

[2]: Tokamak Building atmosphere is simulated with a constant temperature (30 °C) and a constant HTC (8 W/m^2K).

Table A2.19 - Input parameters for heat structures modelling the thermal insulation of FW PHTS feeding pipes and sector collectors/distributors.

HS Comp. Type	RELAP5 Geom. Type	Thickness [mm]	Tot. HT Surface [m^2]	LB	LB Heat. Diam. [m]	RB
FW-TI-HS1	Cylindrical	17.5 mm of AISI 316 L(N); 100 mm of ISOVER®.	33.1[1]	FW-P1	0.184	Ext. Air[2]
FW-TI-HS2	Cylindrical	11 mm of AISI 316 L(N); 100 mm of ISOVER®.	18.7	FW-P2: CVs 1-20	0.118	Ext. Air
FW-TI-HS3	Cylindrical	11 mm of AISI 316 L(N); 100 mm of ISOVER®.	18.7	FW-P2: CVs 53-72	0.118	Ext. Air
FW-TI-HS4	Cylindrical	11 mm of AISI 316 L(N); 100 mm of ISOVER®.	9.4	FW-P3: CVs 1-20	0.118	Ext. Air
FW-TI-HS5	Cylindrical	11 mm of AISI 316 L(N); 100 mm of ISOVER®.	9.4	FW-P3: CVs 53-72	0.118	Ext. Air
FW-TI-HS6	Cylindrical	8.8 mm of AISI 316 L(N); 100 mm of ISOVER®.	23.9	FW-P4: CVs 1-28	0.097	Ext. Air
FW-TI-HS7	Cylindrical	8.8 mm of AISI 316 L(N); 100 mm of ISOVER®.	23.9	FW-P4: CVs 71-98	0.097	Ext. Air
FW-TI-HS8	Cylindrical	17.5 mm of AISI 316 L(N); 100 mm of ISOVER®.	28.9	FW-P5	0.184	Ext. Air

[1]: The total HT surface reported in the table is the external cylinder surface.

[2]: Tokamak Building atmosphere is simulated with a constant temperature (30 °C) and a constant HTC (8 W/m^2K).

Table A2.20 - Material inventories for BB PHTS integration pipelines (feeding pipes and sector collectors/distributors).

Material	PHTS	Inventory [m^3]									
		Sector					Reactor				
		Sector Distributors	Inlet FPs (OB)	Outlet FPs (OB)	Inlet FPs (IB)	Outlet FPs (IB)	Sector Collectors	Total (RELAP5)	Total (Design)	RELAP5	Design
AISI 316 L(N)	BZ	0.76	0.26	0.26	0.13	0.13	0.78	**2.31**	**2.31**	**36.96**	**36.96**
	FW	0.28	0.12	0.12	0.07	0.07	0.24	**0.90**	**0.90**	**14.4**	**14.4**
ISOVER®	BZ	3.76	2.34	2.34	1.74	1.74	4.87	**16.76**	**16.76**	**268.16**	**268.16**
	FW	2.52	1.98	1.98	1.63	1.63	2.20	**11.99**	**11.99**	**191.84**	**191.84**

A3. Preliminary investigation on the WCS thermal-hydraulic performances during NOS

This annex collects and discusses the main results obtained from the thermal-hydraulic analysis carried out during the pre-conceptual design phase. The aim was to verify the component design and to evaluate the system performances under steady state and transient scenarios. The outcomes of this study are also presented in [102].

In this first stage of the activity, the WCS design was different from the one described in **§** 5.4. No secondary loop was present and the HX-0002 was based on Shell and Tubes technology. The TBM power source was a little higher than the one reported in Table 6.1. It was assumed equals to 743 kW. Since the water thermodynamic conditions at TBM inlet/outlet sections were the same, the primary flow was set to 3.85 kg/s. Instead, the CCWS boundary conditions were unmodified, for both water provision and return. The delay and decay tanks at TBM outlet, as well as the control systems regulating the HX-0001 and HX-0002 were not yet implemented. The WCS thermal-hydraulic model prepared with RELAP5 reflected the design differences. It is shown in Figure A3.1. TBM was included in the input deck. Its model was the same described in **§** 6.1.3. Instead, PbLi loop was not yet simulated. It was substituted by constant boundary conditions at TBM inlet. In the pre-conceptual design, an inlet temperature of 330 °C and a nominal flow of 0.29 kg/s were assumed for the breeder, differently from what stated in **§** 5.5 . In order to verify the component layout, the simulations were focused on the EOL operation. The thermal power supplied by the HT-0001 was controlled with a general table.

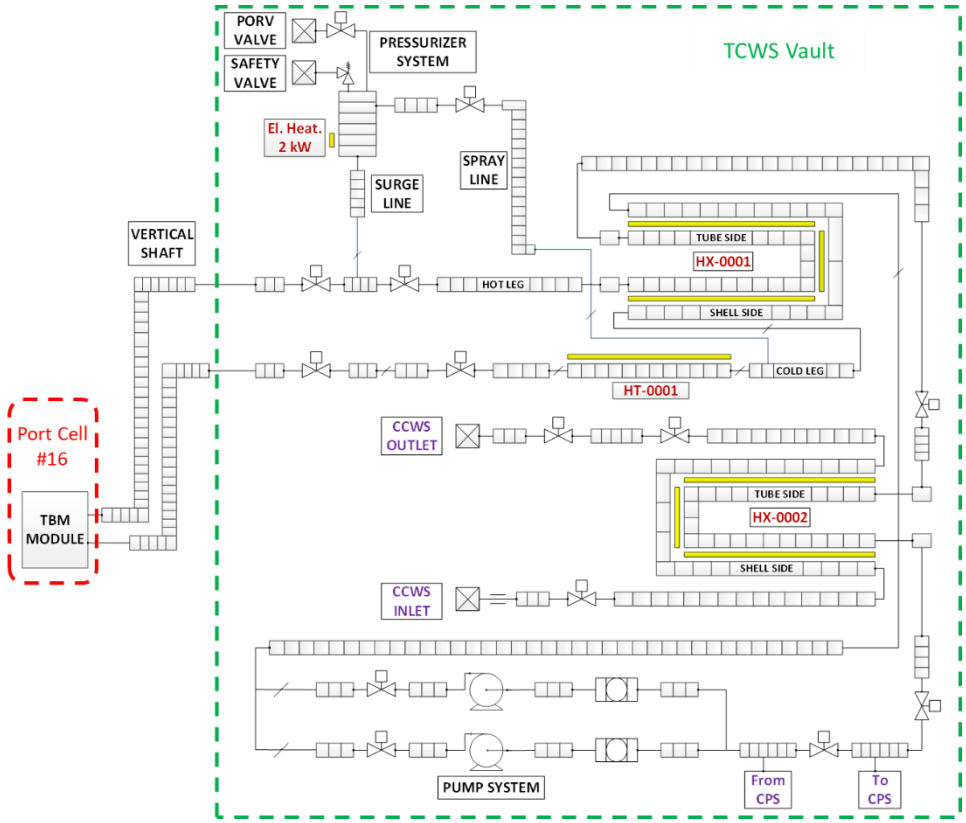

Figure A3.1 – Schematic view of the WCS nodalization adopted during pre-conceptual design phase.

A steady state calculation concerning the full plasma power state was run to qualify the thermal-hydraulic model. PbLi and CCWS inlet boundary conditions were set by means of time-dependent volumes (inlet temperature and outlet pressure) and time-dependent junctions (mass flow). Instead, WCS mass flow was calculated by the code from the balance between available pump head and loop pressure drops. The TBM rated power was supplied as constant boundary condition by the active heat structures composing the TBM model (see **§** 6.1.3). In such operative condition, the HT-0001 power was set to zero.

All the main system parameters were computed by RELAP5 and compared with the nominal values. Table A3.21 summarizes the simulation outcomes. Parameters indicated with "**(BC)**" were imposed as boundary conditions. WCS and CCWS temperatures are in good agreement with the reference data. As expected, PbLi is nearly isothermal between TBM inlet and outlet. WCS mass flow matches the design value. The HX-0001 exchanged power agrees with reference value and HX-0002 power is the sum of the TBM power delivered to the WCS (underestimated of a 0.4%) and the pumping power (nearly 3 kW).

Table A3.21 – Full plasma power state: simulation results related to WCS and CCWS.

System	Parameter	Unit	Nominal value	Simulation result	Relative difference [%]
WCS	TBM inlet temperature	°C	295	295.6	0.20%
	TBM outlet temperature	°C	328	328.3	0.09%
	HX-0001 outlet temperature	°C	157	157.4	0.25%
	HX-0002 outlet temperature	°C	111	111.8	0.72%
	Mass flow	kg/s	3.85	3.85	0.00%
	TBM power to WCS	kW	743	740	-0.40%
	HX-0001 exchanged power	kW	3200	3200	0.00%
	HX-0002 exchanged power	kW	743	743	0.00%
CCWS (section within the TCWS)	Inlet temperature **(BC)**	°C	31	31	-
	Mass Flow **(BC)**	kg/s	17.3	17.3	-
	Outlet temperature	°C	41	41	0.00%
PbLi loop (section within the TBM)	TBM inlet temperature **(BC)**	°C	330	330	-
	Mass Flow **(BC)**	kg/s	0.29	0.29	-
	TBM outlet temperature	°C	330	331.4	0.42%
	TBM power to PbLi	kW	~ 0	0.07	-

The above steady state results were used to carry out a transient analysis aimed at evaluating the WCS behavior during the Normal Operation State. The pulsed plasma regime adopted was the same discussed in **§** 6.4, even if scaled considering the different rated power. Starting with the flat-top phase, transient calculations were run for 9000 s, corresponding to five complete cycles of the pulsed regime. To investigate a DEMO relevant operational scenario, the WCS primary pump

was kept running at nominal velocity during the overall simulation, maintaining the system mass flow almost constant. Also PbLi and CCWS inlet boundary conditions did not vary during the calculation.

At the time of the analysis, no guidelines regarding the TBM conditions during NOS were available. For this reason, TBM outlet temperature was selected as control parameter, i.e. was kept almost constant over the whole simulation. This quantity was chosen since it is the maximum temperature in WCS and because, in the operational transient, the average loop temperature follows the same time trend of the selected parameter, as shown by the simulation results. Such temperature is used as figure of merit in Figure A3.2 to compare different cases.

A first calculation (case 1 in Figure A3.2a) was run setting to zero the HT-0001 power. In this scenario, after the initial flat-top, water temperature starts to decrease with a nearly sawtooth trend. During dwell time, there is no plasma power but the WCS nominal flow is maintained and the heat sink is still in operation. The availability of rated primary and secondary flows ensures a significant heat transfer (i.e. high HTCs) within the HX-0002. The low heat sink temperatures provoke an excessive cooling of the WCS system. When plasma power is ramped up, WCS restarts to be heated but the pulse phase is too short to allow the fluid to return at the original temperature values. As a result, cycle after cycle, the maximum, and consequently also the average, fluid temperature in WCS loop decreases. The same trend is valid also for the CCWS temperature at HX-0002 outlet. This simulation proves the need during dwell time to supply power with the HT-0001.

Since no control logic was implemented for the HT-0001 operation, as a first tentative (case 2 in Figure A3.2a), the HT-0001 sizing power was assumed equals to the TBM rated power and the heater duty cycle was reverted with respect to the pulsed plasma regime. In this case, the mean value of the TBM outlet temperature is kept constant during the overall transient, avoiding the loop overcooling. Although, there are significant negative and positive thermal spikes (-10/+15 °C) which constitute a relevant thermomechanical load for the TBM set. The fluctuations are caused by the relative timing between the plasma and the HT-0001 power figures. If HT-0001 is switched on exactly at the beginning of plasma power ramp down, water heated by the component must flow through the descendant shaft before reaching the TBM. The hot fluid arrives with a delay, resulting in a time window where the temperature at module outlet drops, provoking the negative spikes. On the other hand, switching off the HT-0001 at the beginning of plasma power ramp-up, leads to a time interval where WCS water is double-heated by the electric heater and the plasma power, producing the positive peaks at TBM outlet. Such time windows are equals to the water crossing time in the descendant shaft (slightly different between ramp-down and ramp-up due to the variation of the fluid density). In both cases, the low thermal inertia of the TBM set (due to its small PbLi and steel inventories) does not help in mitigating the thermal fluctuations. In conclusion, the location of TBM and HT-0001 at different levels of the tokamak building causes a relevant delay that determines the thermal fluctuations. Since HT-0001 cannot be installed within the Port Cell #16 (no space is available), the delay could be compensated by anticipating the chosen heater duty cycle.

A third simulation (case 3 in Figure A3.2a), was performed considering a time anticipation for the HT-0001 power figure of 60 s. This value was chosen after calculating the time needed to the water to flow from HT-0001 outlet to TBM inlet (nearly 45 m of pipelines with a fluid velocity of approximately 1 m/s) and considering the system inertia. This solution allows to strongly reduce the temperature oscillations at TBM outlet (-2/+5 °C) and to obtain a system more stable operation during the overall NOS.

In order to optimize the design solution adopted, a sensitivity was carried out on the HT-0001 anticipation time, in the range of 40 – 90 s. Figure A3.2b compares the TBM outlet temperature over the whole transient. A zoom of the single transition is shown in Figure A3.2c. When plasma power is ramped up, the magnitude of the positive spike decreases increasing the anticipation time. Although, if HT-0001 is switched-off too earlier, a time window occurs just before the restart of plasma power where no power sources are present and the WCS temperature at TBM outlet drops (see pink and black lines in Figure A3.2c, related to HT-0001 anticipation times of 80 and 90 s). The best compromise to reduce the positive spike, also avoiding the occurrence of a negative fluctuation just before it, is to select an anticipation time in the range of 65 – 70 s. The same is valid for the plasma power ramp down. This transition is smoother than the previous one since its time length is more than double (200 s with respect to 60 s).

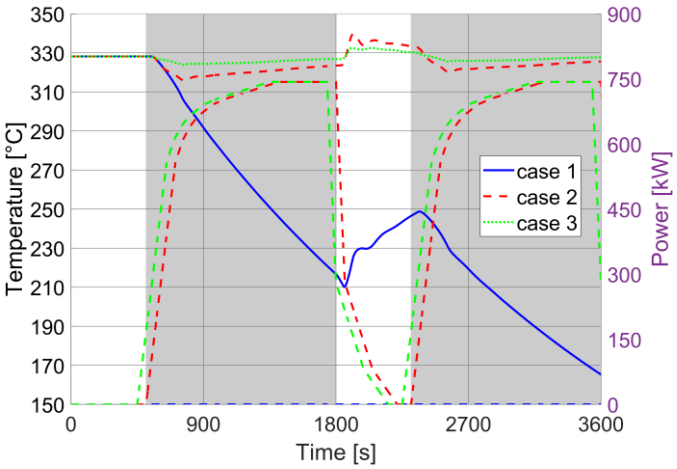

(a)

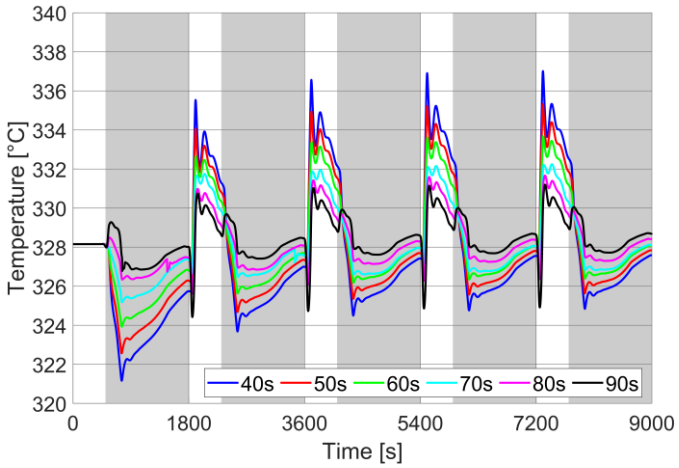

(b)

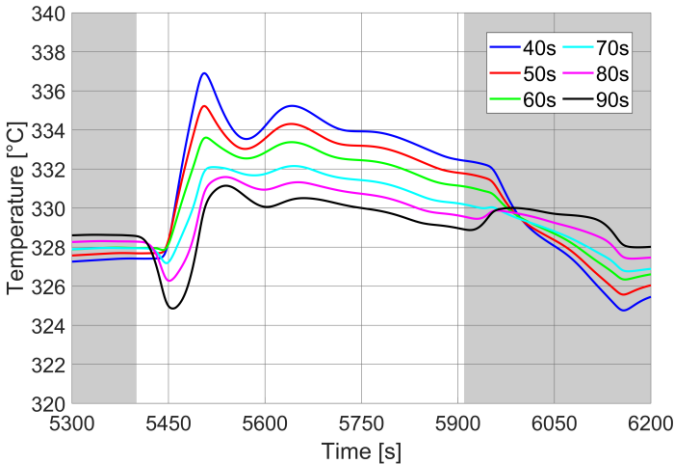

(c)

Figure A3.2 – Normal Operation State, WCS temperature at TBM outlet: **(a)** Comparison between case 1 (absence of HT-0001 heating), case 2 (presence of HT-0001 heating) and case 3 (presence of HT-0001 heating with power ramps anticipated of 60 s with respect to pulsed plasma regime); **(b)** Sensitivity on the HT-0001 heating anticipation time; **(c)** Sensitivity on the HT-0001 heating anticipation time (zoom on the single transition).

For the reference case (70 s of time advance) a deeper analysis of the TBS system behavior is discussed in the following. Figure A3.3 collects the time trends related to the main thermal-hydraulic parameters of WCS, CCWS and PbLi loop. Due to the management strategy selected for the electric heater, the temperatures at TBM outlet and HT-0001 inlet are characterized by low oscillations: the former in the range of 326-332 °C and the latter in the range of 294-299 °C (Figure A3.3a). Instead, TBM inlet temperature spans between the other two temperatures, increasing during dwell and decreasing during pulse (Figure A3.3a). Thus, also the TBM average temperature varies along the transient. This could lead to significant thermal stresses on the component. Further investigations in this field are required. Figure A3.3b shows that the fluctuations characterizing the water temperatures in the WCS hot branch nearly disappears in the cold branch and in the CCWS. Figure A3.3c compares the power input terms, TBM and HT-0001, with the output one, the power removed by HX-0002. The heater duty cycle adopted allows to operate the heat sink at nearly design conditions for the overall NOS. The PbLi temperature at TBM outlet, shown in Figure A3.3d, follows the same trend of the plasma power in Figure A3.3c. It must be noted that the power delivered to the eutectic alloy in the TBM is quite reduced, resulting in low thermal oscillations. Their amplitude around the mean value (330 °C) is limited in the range of +/- 3 °C. For the reference case a time step sensitivity was performed varying this parameter from 1.0 x 10^{-3} s to 5.0 x 10^{-3} s. No sensible differences in the simulation results were observed. The time trends reported in Figure A3.3 are for a time step of 5.0 x 10^{-3} s.

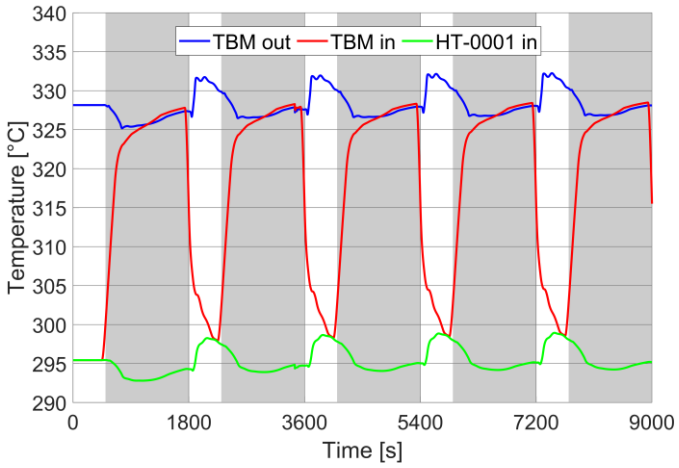

(a)

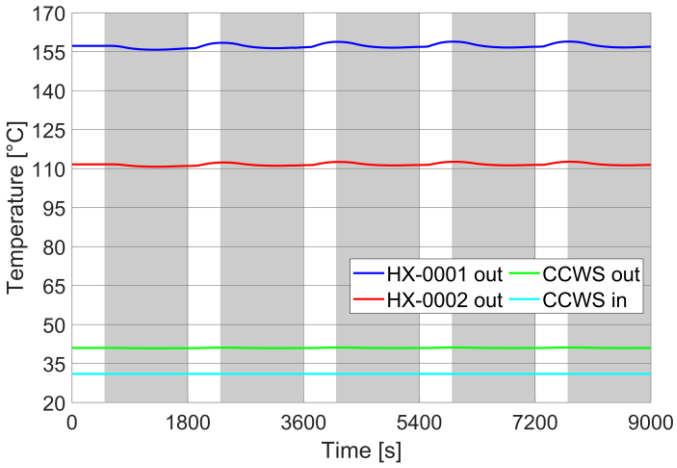

(b)

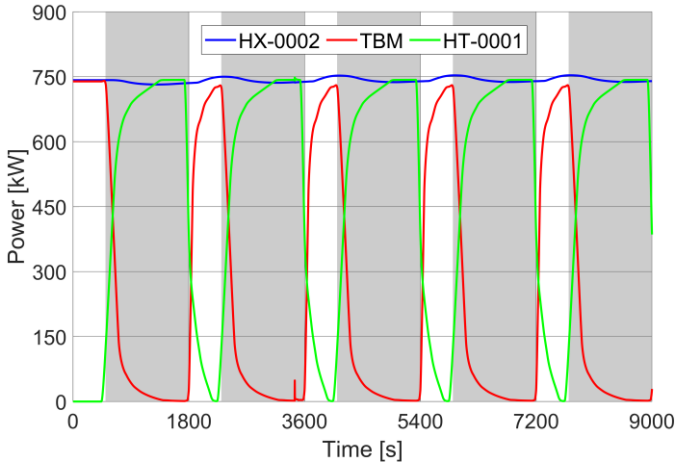

(c)

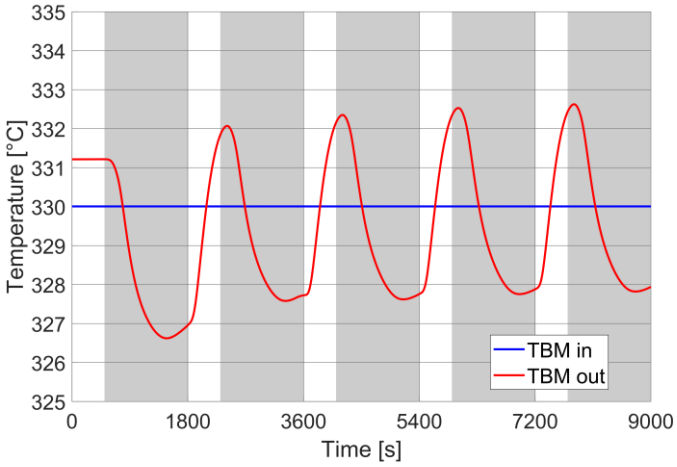

(d)

Figure A3.3 – Normal Operation State, reference case (70 s of HT-0001 heating anticipation time): **(a)** Relevant temperatures in WCS hot branch; **(b)** Relevant temperatures in WCS cold branch and CCWS; **(c)** WCS main power terms; **(d)** PbLi temperatures at TBM inlet/outlet.

Conclusions

The activity discussed in this annex, performed during the pre-conceptual design phase, was aimed at verifying the sizing of the main components belonging to the ITER WCLL-TBM WCS. Once qualified the system thermal-hydraulic model, the circuit behavior during the Normal Operation State was studied. Calculations were focused on finding a design solution to ensure system stable operation along the overall pulsed regime characterizing the NOS. The main feedback from the transient analysis is the need of an electrical heater to be installed in the circuit. It must supply power to WCS water when the plasma source is absent. In this way, the WCS overcooling due to low heat sink temperatures is avoided. Such lesson learned was of primary importance also in the subsequent (conceptual) design phase. The heater duty cycle was optimized to keep constant the water temperature at TBM outlet. By anticipating the heater power ramps of 70 s with respect to the pulsed plasma regime, the TBM outlet temperature was kept almost constant during the whole Normal Operation State.

Bibliography

[1] https://ec.europa.eu/clima/policies/international/negotiations/paris_en.

[2] J.D. Lawson., Some criteria for a power producing thermonuclear reactor, in Proc. Phys. Soc., vol. 70(B), pp. 6-10, 1957. DOI: 10.1088/0370-1301/70/1/303.

[3] F. Romanelli, et al., Fusion electricity – a roadmap to the realization of fusion energy, EFDA Report, 2012. ISBN 978-3-00-040720-8T.

[4] A.J.H. Donné et al., European roadmap to fusion energy, Presentation at 2018 Symposium On Fusion Technology (SOFT), Giardini Naxos, Italy, September 16-21 2018. Available online at: https://www.euro-fusion.org/fileadmin/user_upload/EUROfusion/Documents/180917.Donne.SOFT.Roadmap.v2.pdf.

[5] https://lasers.llnl.gov/science/icf

[6] J. Wesson, Tokamaks, 4th Ed., International Series of Monographs on Physics, vol. 149, Oxford Science Publications, Oxford, 2011. ISBN: 9780199592234.

[7] W.M. Stacey, An introduction to physics and technology of magnetic confinement fusion, 2nd Ed., Wiley-VCH Verlag GmbH &Co., Weinheim, 2010. ISBN: 978-3-527-40967-9.

[8] D. Maisonnier et al., A conceptual study of commercial fusion power plant, EFDA Report, EFDA-RP-RE-5.0, 2005. Available online at: https://www.euro-fusion.org/fileadmin/user_upload/Archive/wp-content/uploads/2012/01/PPCS_overall_report_final.pdf.

[9] G. Federici et al., An overview of the EU breeding blanket design strategy as an integral part of the DEMO design effort. Fusion Eng. Des., vol. 141, pp. 30-42, 2019. DOI: 10.1016/j.fusengdes.2019.01.141.

[10] www.iter.org

[11] www.eurofusion.org

[12] V. Narcisi, Validation of RELAP5-3D© for liquid metal reactor technologies, PhD thesis, Sapienza University of Rome, 2020. Available online at: https://phd.uniroma1.it/web/VINCENZO-NARCISI_nT1394736_IT.aspx.

[13] The US Nuclear Regulatory Commission (USNRC), RELAP5/MOD3.3 code manual volume 1: code structure, system models, and solution methods, NUREG/CR-5535; USNRC: Washington, DC, USA, 1995.

[14] P. Emonot et al., CATHARE-3: A new system code for thermal-hydraulics in the context of the NEPTUNE project. Nucl. Eng. Des., vol. 241, pp. 4476–4481, 2011. DOI: 10.1016/j.nucengdes.2011.04.049.

[15] The US Nuclear Regulatory Commission (USNRC), TRACE V5.0 theory manual: field equations, solution methods and physical models, USNRC: Washington, DC, USA, 2005.

[16] M. D'Onorio et al., Preliminary safety analysis of an in-vessel LOCA for the EU-DEMO WCLL blanket concept. Fusion Eng. Des., vol. 155, article ID 111560, 2020. DOI: 10.1016/j.fusengdes.2020.111560.

[17] M. D'Onorio et al., Preliminary sensitivity analysis for an ex-vessel LOCA without plasma shutdown for the EU DEMO WCLL blanket concept. Fusion Eng. Des., vol. 158, article ID 111745, 2020. DOI: 10.1016/j.fusengdes.2020.111745.

[18] R.O. Gauntt et al., MELCOR computer code manuals volume 1: primer and users; Guide Version 1.8.6., Revision 3, NUREG/CR-6119; Sandia National Laboratory: Albuquerque, NM, USA, 2005.

[19] M. D'Onorio et al., Pressure suppression system influence on vacuum vessel thermal-hydraulics and on source term mobilization during a multiple First Wall-Blanket pipe break. Fusion Eng. Des., vol. 164, article ID 112224, 2021. DOI: 10.1016/j.fusengdes.2020.112224.

[20] Idaho National Laboratory; The RELAP5-3D© Code Development Team, RELAP5-3D code manual volume 1: code structure, system models, and solution methods, Revision 4.3, INL-MIS-15-36723; Idaho National Laboratory: Idaho Falls, ID, USA, 2015.

[21] S. D'Amico et al., Preliminary thermal-hydraulic analysis of the EU-DEMO Helium-Cooled Pebble Bed fusion reactor by using the RELAP5-3D system code. Fusion Eng. Des. vol. 162, article ID 112111, 2021. DOI: 10.1016/j.fusengdes.2020.112111.

[22] X.Z. Jin et al., LOFA analysis for the FW of DEMO HCPB blanket concept. In Proceedings of the 1st IAEA Technical Meeting on the Safety, Design and Technology of Fusion Power Plants, Vienna, Austria, 3–5 May 2016.

[23] X.Z. Jin, BB LOCA analysis for the reference design of the EU DEMO HCPB blanket concept. Fusion Eng. Des., vol. 136(B), pp. 958–963, 2018. DOI: 10.1016/j.fusengdes.2018.04.046.

[24] X. Cheng et al., Steady states and LOFA analyses of the updated WCCB blanket for multiple fusion power modes of CFETR. Fusion Eng. Des. vol. 144, pp. 23-28, 2019. DOI: 10.1016/j.fusengdes.2019.04.075.

[25] X. Cheng et al., Loss of flow accident and loss of heat sink accident analyses of the WCCB primary heat transfer system for CFETR. Fusion Eng. Des. vol. 147, article ID 111247, 2019. DOI: 10.1016/j.fusengdes.2019.111247.

[26] S.B. Moon et al., Analysis of hydrogen and dust explosion after vacuum vessel rupture: Preliminary safety analysis of Korean fusion demonstration reactor using MELCOR. Int. J. Energy Res., vol. 42, pp. 104-116, 2018. DOI: 10.1002/er.3793.

[27] X. Cheng et al., Thermal dynamic analyses of the primary heat transfer system for the WCCB blanket of CFETR. Fusion Eng. Des. vol. 161, article ID 112067, 2020. DOI: 10.1016/j.fusengdes.2020.112067.

[28] G.-W. Kim et al., Development of thermal-hydraulic analysis methodology for multiple modules of water-cooled breeder blanket in fusion DEMO reactor. Fusion Eng. Des., vol. 103, pp. 98-109, 2016. DOI: 10.1016/j.fusengdes.2015.12.042.

[29] J.-J. Jeong et al., Development of a multi-dimensional thermal-hydraulic system code, MARS 1.3.1. Ann. Nucl. Energy, vol. 26, pp. 1611–1642, 1999. DOI: 10.1016/S0306-4549(99)00039-0.

[30] A. Ibarra and R. Kurtz, ITER-TBM and Blanket Programs toward DEMO, Presentation at 3rd IAEA DEMO Programme Workshop, Hefei, China, May 11-14 2015. Available online at:

https://nucleus.iaea.org/sites/fusionportal/Technical%20Meeting%20Proceedings/3rd%20DEMO/website/talks/May%2013%20Sessions/Ibarra_A%20Intro.pdf.

[31] L.M. Giancarli et al., Overview of the ITER TBM Program. Fusion Eng. Des., vol. 87, Issues 5-6, pp. 395-402, 2012. DOI: 10.1016/j.fusengdes.2011.11.005.

[32] L.M. Giancarli et al., Overview of recent ITER TBM Program activities. Fusion Eng. Des., vol. 158, article ID 111674, 2020. DOI: 10.1016/j.fusengdes.2020.111674.

[33] https://fusionforenergy.europa.eu.

[34] The US Nuclear Regulatory Commission (USNRC), RELAP5/MOD3.3 code manual volume 2: User's Guide and Input Requirements, NUREG/CR-5535; USNRC: Washington, DC, USA, 1995.

[35] The US Nuclear Regulatory Commission (USNRC), RELAP5/MOD3.3 code manual volume 2, appendix A: input requirements, NUREG/CR-5535; USNRC: Washington, DC, USA, 1995.

[36] The US Nuclear Regulatory Commission (USNRC), RELAP5/MOD3.3 code manual volume 4: models and correlations, NUREG/CR-5535; USNRC: Washington, DC, USA, 1995.

[37] F. Giannetti et al., Development of a RELAP5/Mod3.3 Version for FUSION Applications, Department of Astronautical, Electrical and Energy Engineering (DIAEE), Sapienza University of Rome, Technical Report No. D1902_ENBR_T01, Revision 1; Rome, 2019.

[38] Coastal Chemical Co., L.L.C. –HITEC® Heat Transfer Salt technical brochure. Available online at: https://pdf4pro.com/view/coastal-hitec-heat-transfer-salt-8ffaa.html.

[39] D. Martelli et al., Literature review of lead-lithium thermophysical properties, Fusion Eng. Des., vol. 138, pp. 183-195, 2019. DOI: 10.1016/j.fusengdes.2018.11.028.

[40] R. A. Seban and T. T. Shimazaki, Heat transfer to a fluid flowing, Trans. Am. Soc. Mech. Eng., vol. 73, pp. 803-809, 1951.

[41] X. Cheng et al., Turbulent Heat Transfer to Heavy Liquid Metals in Circular Tubes. Proceedings of HT-FED04, ASME Heat Transfer/Fluids Engineering Summer Conference, Volume 4, Charlotte, North Carolina, US, July 11-15, 2004. DOI: 10.1115/ht-fed2004-56562.

[42] B. Lubarsky and S. J. Kaufman, Review of experimental investigations of liquid-metal heat transfer, NACA technical note 3336, Lewis Flight Propulsion Laboratory, Washington (USA), 1955.

[43] A. Ushakov, Heat transfer to liquid metals in regular arrays of fuel elements, High Temperature, vol. 15, pp. 868-873, 1977. Translated from Teplofizika Vysokikh Temperatur vol. 15, No. 5, pp. 1027-1033, 1977.

[44] K. Mikityuk, Heat Transfer to Liquid Metal: Review of Data and Correlations for Tube Bundles, Nucl. Eng. Des., vol. 239, pp. 680-687, 2009. DOI: 10.1016/j.nucengdes.2008.12.014.

[45] M. S. Kazimi and M. D. Carelli, Clinch River Breeder Reactor Plant Heat Transfer Correlation for Analysis of CRBRP Assemblies, CRBRP-ARD-0034, Westinghouse technical report, 1976.

[46] W. T. Sha and B. E. Launder, A model for turbulent momentum and heat transport in large rod bundles, Technical report ANL-77-73, Argonne National Laboratory, IL (USA) 1979.

[47] E. N. Sieder and G. E. Tate, Heat transfer and pressure drop of liquids in tubes, J. Ind. Eng. Chem., vol. 28, pp. 1429-1435, 1936.

[48] Zukauskas A., Heat Transfer from Tubes in Crossflow, Adv. Heat Transf., vol. 8, pp. 93-160, 1972. DOI: 10.1016/S0065-2717(08)70038-8.

[49] Y. Mori and W. Nakayama, Study on Forced Convective Heat Transfer in Curved Pipes (1st Report, Laminar Region), Int. J. Heat Mass Transfer, vol. 8, pp. 67-82, 1965. DOI: 10.1016/0017-9310(65)90098-0.

[50] R. Roumy, Dryout in helically coiled tubes with boiling Freon-12, in European Two-phase Group Meeting, 1971.

[51] International Atomic Energy Agency (IAEA), Evaluation of Advanced Thermohydraulic System Codes for Design and Safety Analysis of Integral Type Reactor, IAEA-TECDOC-1733, IAEA, Vienna, Austria, 2014. Available online at: https://www.iaea.org/publications/10658/evaluation-of-advanced-thermohydraulic-system-codes-for-design-and-safety-analysis-of-integral-type-reactors.

[52] S. M. Modro et al., Multi-Application Small Light Water Reactor Final Report, INEEL/EXT-04-01626, Idaho National Engineering and Environmental Laboratory (INEEL), Idaho, USA, 2003. Available online at: https://digital.library.unt.edu/ark:/67531/metadc778608.

[53] F. Mascari et al., Analysis of the OSU-MASLWR 001 and 002 Tests by Using the TRACE Code, NUREG/IA-0466, U.S. NRC, Washington DC, USA, 2016. Available online at: https://www.nrc.gov/reading-rm/doc-collections/nuregs/agreement/ia0466/index.html.

[54] M. Molinari et al., Transient analysis of OSU-MASLWR with RELAP5, presented at 38th UIT International Conference, Gaeta, Italy, June 21-22, 2021. Submitted to J. Phys. Conf. Ser.

[55] G. Federici et al., DEMO design activity in Europe: Progress and updates, Fusion Eng. Des. vol. 136(A), pp. 729-741, 2018. DOI: 10.1016/j.fusengdes.2018.04.001.

[56] U. Fisher et al., Required, achievable and target TBR for the European DEMO, Fusion Eng. Des., vol. 155, article ID 111553, 2020. DOI: https://doi.org/10.1016/j.fusengdes.2020.111553.

[57] L. Barucca et al., Pre-conceptual design of EU DEMO balance of plant systems: objectives and challenges, Fusion Eng. Des., vol. 169, article ID 112504, 2021. DOI: 10.1016/j.fusengdes.2021.112504.

[58] M. D'Onorio, Safety Analyses with uncertainty quantification for fusion and fission nuclear power plants. Applications to EU DEMO fusion reactor and BWRs., PhD thesis, Sapienza University of Rome, 2020. Available online at: https://phd.uniroma1.it/web/MATTEO-D'ONORIO_nP1420584_IT.aspx.

[59] A. Del Nevo et al., Recent progress in developing a feasible and integrated conceptual design of the WCLL BB in EUROfusion project, Fusion Eng. Des., vol. 146, pp. 1805-1809, 2019. DOI: 10.1016/j.fusengdes.2019.03.040.

[60] E. Martelli et al., A Study of EU DEMO WCLL breeding blanket and primary heat transfer system integration, Fusion Eng. Des., vol. 136, pp. 828-833, 2018 DOI: 10.1016/j.fusengdes.2018.04.016A.

[61] F. Edemetti et al., Optimization of the first wall cooling system for the DEMO WCLL blanket, Fusion Eng. Des., vol. 161, article ID 111903, 2020. DOI: 10.1016/j.fusengdes.2020.111903.

[62] F. Edemetti et al., Thermal-hydraulic analysis of the DEMO WCLL elementary cell: BZ tubes layout optimization, Fusion Eng. Des., vol. 160, article ID 111956, 2020. DOI: 10.1016/j.fusengdes.2020.111956.

[63] A. Tassone, Study on liquid metal magnetohydrodynamic flows and numerical application to a water-cooled blanket for fusion reactors, PhD thesis, Sapienza University of Rome, 2019. Available online at: https://iris.uniroma1.it/handle/11573/1243658#.YTngi50zaUk.

[64] E. Martelli et al., Thermal-hydraulic modeling and analyses of the water-cooled EU DEMO using RELAP5 system code, Fusion Eng. Des., vol. 146, pp. 1121-1125, 2019. DOI: 10.1016/j.fusengdes.2019.02.021.

[65] L. Barucca et al., Maturation of Critical Technologies for the DEMO Balance of Plant Systems, submitted to Fusion Eng. Des., 2021.

[66] I. Moscato et al., Tokamak cooling systems and power conversion system options, submitted to Fusion Eng. Des., 2021.

[67] P. Lorusso et al., BB PHTS Data Sheets (Indirect Coupling), EUROfusion internal deliverable, EFDA_D_2NRKV7, 2020.

[68] European Committee for Standardization, Seamless and welded steel tubes - Dimensions and masses per unit length, EN 10220, 2002. Available online at: http://store.uni.com/catalogo/en-10220-2002/.

[69] U.S. Nuclear Regulatory Commission, Section 3.2—Reactor Coolant System. In Westinghouse Technology Systems Manual. 2012. Available online: https://www.nrc.gov/docs/ML1122/ML11223A213.

[70] The Babcock & Wilcox Company, Steam, its generation and use, 41st Ed., John B. Kitto and Steven C. Stultz, Barberton, Ohio, USA, 2005.

[71] U.S. Nuclear Regulatory Commission. Section 10.2—Pressurizer Pressure Control System. In Westinghouse Technology Systems Manual; 2012. Available online: https://www.nrc.gov/docs/ML1122/ML11223A287.

[72] F. Mascari et al., Sensitivity analysis of the MASLWR helical coil steam generator using TRACE, Nucl. Eng. Des., vol. 241 (4), pp. 1137-1144, 2011. DOI: 10.1016/j.nucengdes.2010.05.002.

[73] K. Mergia and N. Boukos, Structural, thermal electrical and magnetic properties of Eurofer 97 steel, J. Nucl. Mater., vol. 373, pp. 1-8, 2008. DOI: 10.1016/j.jnucmat.2007.03.267.

[74] F. Gillemot et al., Material Property Handbook; Pilot project on EUROFER97, EUROfusion internal deliverable, EFDA_D_2N5D9D, 2016.

[75] F. P. Incropera et al., Fundamentals of Heat and Mass Transfer, 7th Ed., John Wiley & Sons Inc., Hoboken, New Jersey, USA, 2011.

[76] The American Society of Mechanical Engineers (ASME), Boiler and Pressure Vessel Code, Section II, Part D, Properties (Metric), 2015 Edition, New York, New York, USA.

[77] ISOVER® Saint-Gobain Manufacturing Company, TECH Telisol 5.0 QN Technical Datasheet. ISOVER-TDS-Industry-INT-ENG-TECH Telisol 5.0 QN 2019-09. Available online at: https://www.isover-technical-insulation.com/products/tech-telisol-50-qn#children-attributes-table.

[78] Watlow® Electric Manufacturing Company, Datasheet for Pressurizer heaters, 2015. Available online at: https://www.watlow.com/resources-and-support/technical-library/specification-sheets.

[79] I. E. Idelchik, Handbook of Hydraulic Resistance, 2nd Ed., Hemisphere Publishing Corporation, Washington, DC, USA, 1986.

[80] G. A. Spagnuolo et al., Development of load specifications for the design of the breeding blanket system, Fusion Eng. Des. vol. 157, article ID 111657, 2020. DOI: 10.1016/j.fusengdes.2020.111657.

[81] P. Lorusso et al., STEAM: a novel experimental infrastructure for the development of the DEMO BoP water coolant technology, to be presented at 19th International Topical Meeting on Nuclear Reactor Thermal Hydraulics (NURETH 19), Brussels, Belgium, March 6-11 2022, under review.

[82] E. B. Wylie et al., Fluid transients in systems, Prentice Hall, Englewood Cliffs, New Jersey, USA, 1993.

[83] C. Ciurluini et al., Analysis of the thermal-hydraulic behavior of the EU-DEMO WCLL Breeding Blanket cooling systems during a Loss Of Flow Accident, Fusion Eng. Des. vol. 164, article ID 112206, 2021. DOI: 10.1016/j.fusengdes.2020.112206.

[84] C. Ciurluini et al., Study of the EU-DEMO WCLL Breeding Blanket Primary Cooling Circuits Thermal-Hydraulic Performances during Transients Belonging to LOFA Category, Energies, vol. 14(6), article ID 1541, 2021. DOI: 10.3390/en14061541.

[85] C. Ciurluini et al., Transient analysis of a locked rotor/shaft seizure accident involving the EU-DEMO WCLL breeding blanket primary cooling circuits, to be presented at 19th International Topical Meeting on Nuclear Reactor Thermal Hydraulics (NURETH 19), Brussels, Belgium, March 6-11 2022, under review.

[86] J. F. Salavy et al., Must we use ferritic steel in TBM?, Fusion Eng. Des., vol. 85, pp. 1896-1902, 2010. DOI: 10.1016/j.fusengdes.2010.06.017.

[87] M. A. Abdou et al., Results of an International Study on a High-Volume Plasma-Based Neutron Source for Fusion Blanket Development, Fusion Technol., vol. 29(1), pp. 1-57, 1996. DOI: 10.13182/FST96-3.

[88] Julien Aubert et al., Design and Preliminary Analyses of the New Water Cooled Lithium Lead TBM for ITER, Fusion Eng. Des., vol. 160, article ID 111921, 2020. DOI: 10.1016/j.fusengdes.2020.111921.

[89] A. Tincani et al., Conceptual design of the main Ancillary Systems of the ITER Water Cooled Lithium Lead Test Blanket System, Fusion Eng. Des., vol. 167, article ID 112345, 2021. DOI: 10.1016/j.fusengdes.2021.112345.

[90] C. Ciurluini et al., Conceptual design overview of the ITER WCLL Water Cooling System and supporting thermal-hydraulic analysis, Fusion Eng. Des., vol. 171, article ID 112598, 2021. DOI: 10.1016/j.fusengdes.2021.112598.

[91] I. Ricapito et al., European TBM programme: First elements of RoX and technical performance assessment for DEMO breeding blankets, Fusion Eng. Des., vol. 156, article ID 111584, 2020. DOI: 10.1016/j.fusengdes.2020.111584.

[92] Promat International N.V., Technical datasheet for MICROTHERM® MPS Insulator Material, 2017. Available online at: https://www.promat.com/en/industry.

[93] The American Society of Mechanical Engineers (ASME), Boiler and Pressure Vessel Code, Section III, Division 1, Subsection NC, 3324.3, 2015 Edition, New York, New York, USA.

[94] M. A. Kreider et al., A global fouling factor methodology for analyzing steam generator thermal performance degradation, Proceedings of 3rd International Steam Generator and Heat Exchanger Conference, Toronto, Canada, June 21-24, 1998. Available online at: https://inis.iaea.org/search/search.aspx?orig_q=RN:30031799.

[95] T. Prusek et al., A methodology to simulate the impact of tube fouling on steam generator performance with a thermal-hydraulic code, Proceedings of XI International Conference on Heat Exchanger Fouling and Cleaning, Enfield (Dublin), Ireland, 07-12 June 2015. Available online at: http://www.heatexchanger-fouling.com/papers/papers2015/17_Prusek_F.pdf.

[96] The American Society of Mechanical Engineers (ASME), Welded and Seamless Wrought Steel Pipe, Section B36.10M, 1995 Edition, New York, New York, USA.

[97] N. E. Todreas and M. S. Kazimi, Nuclear Systems Volume I. Thermal Hydraulic Fundamentals, 2nd Ed., Taylor & Francis Inc, Howick Place, London, UK, 2011. ISBN:1439808872.

[98] D. Q. Kern, Process Heat Transfer, 21st Ed., McGraw-Hill International Book Company, New York, New York, USA, 1983. ISBN 0-07-085353-3.

[99] P. Sauvan and B. De Gentile, Report on the MCNP Model and mode-0 Nuclear Analysis of EP#16 for PBS.56.F1.TB, EUROfusion internal deliverable, EFDA_D_2NGJJV v1.1, 2020.

[100] I. Ricapito, Pb-16Li flow-rate in WCLL-TBS: selection of the operational domain and reference value in nominal conditions, EUROfusion internal deliverable, EFDA_D_2GDTP7 v1.0, 2020.

[101] G. Aiello et al., Assessment of design limits and criteria requirements for Eurofer structures in TBM components, J. Nucl. Mater., vol. 414, pp. 53-68, 2011. DOI: 10.1016/j.jnucmat.2011.05.005.

[102] C. Ciurluini et al., Thermal-hydraulic modeling and analysis of the Water Cooling System for the ITER Test Blanket Module, Fusion Eng. Des., vol. 158, article ID 111709, 2020. DOI: 10.1016/j.fusengdes.2020.111709.

[103] C. Ortiz et al., TBM Port Plug (TBM PP) System Load Specifications, EUROfusion internal deliverable, EFDA_D_2NMHZ4 v1.0, 2019.

[104] L. Melchiorri et al., Development of a RELAP5/MOD3.3 module for MHD pressure drop analysis in liquid metals loops. Verification and validation, Energies, vol. 14(17), article ID 5538, 2021. DOI: 10.3390/en14175538.